Stochastic Geometry and Wireless Networks, Volume II - Applications

François Baccelli, Bartlomiej Blaszczyszyn

Stochastic Geometry and Wireless Networks

Volume II

APPLICATIONS

François Baccelli and Bartłomiej Błaszczyszyn
INRIA & Ecole Normale Supérieure, 45 rue d'Ulm, Paris.

Paris, December, 2009.

This monograph is based on the lectures and tutorials of the authors at Université Paris 6 since 2005, Eurandom (Eindhoven, The Netherlands) in 2005, Performance 05 (Juan les Pins, France), MIRNUGEN (La Pedrera, Uruguay) and Ecole Polytechnique (Palaiseau, France) in 2007. This working version was compiled December 4, 2009.

To Béatrice and Mira

Preface

A wireless communication network can be viewed as a collection of nodes, located in some domain, which can in turn be transmitters or receivers (depending on the network considered, nodes may be mobile users, base stations in a cellular network, access points of a WiFi mesh etc.). At a given time, several nodes transmit simultaneously, each toward its own receiver. Each transmitter–receiver pair requires its own wireless link. The signal received from the link transmitter may be jammed by the signals received from the other transmitters. Even in the simplest model where the signal power radiated from a point decays in an isotropic way with Euclidean distance, the geometry of the locations of the nodes plays a key role since it determines the *signal to interference and noise ratio* (SINR) at each receiver and hence the possibility of establishing simultaneously this collection of links at a given bit rate. The interference seen by a receiver is the sum of the signal powers received from all transmitters, except its own transmitter.

Stochastic geometry provides a natural way of defining and computing macroscopic properties of such networks, by averaging over all potential geometrical patterns for the nodes, in the same way as queuing theory provides response times or congestion, averaged over all potential arrival patterns within a given parametric class.

Modeling wireless communication networks in terms of stochastic geometry seems particularly relevant for large scale networks. In the simplest case, it consists in treating such a network as a snapshot of a stationary random model in the whole Euclidean plane or space and analyzing it in a probabilistic way. In particular the locations of the network elements are seen as the realizations of some point processes. When the underlying random model is ergodic, the probabilistic analysis also provides a way of estimating *spatial averages* which often capture the key dependencies of the network performance characteristics (connectivity, stability, capacity, etc.) as functions of a relatively small number of parameters. Typically, these are the densities of the underlying point processes and the parameters of the protocols involved. By spatial average, we mean an empirical average made over a large collection of 'locations' in the domain considered; depending on the cases, these locations will simply be certain points of the domain, or nodes located in the domain, or even nodes on a certain route defined on this domain. These various kinds of

spatial averages are defined in precise terms in the monograph. This is a very natural approach e.g. for ad hoc networks, or more generally to describe user positions, when these are best described by random processes. But it can also be applied to represent both irregular and regular network architectures as observed in cellular wireless networks. In all these cases, such a space average is performed on a large collection of nodes of the network executing some common protocol and considered at some common time when one takes a snapshot of the network. Simple examples of such averages are the fraction of nodes which transmit, the fraction of space which is covered or connected, the fraction of nodes which transmit their packet successfully, and the average geographic progress obtained by a node forwarding a packet towards some destination. This is rather new to classical performance evaluation, compared to time averages.

Stochastic geometry, which we use as a tool for the evaluation of such spatial averages, is a rich branch of applied probability particularly adapted to the study of random phenomena on the plane or in higher dimension. It is intrinsically related to the theory of point processes. Initially its development was stimulated by applications to biology, astronomy and material sciences. Nowadays, it is also used in image analysis and in the context of communication networks. In this latter case, its role is similar to that played by the theory of point processes on the real line in classical queuing theory.

The use of stochastic geometry for modeling communication networks is relatively new. The first papers appeared in the engineering literature shortly before 2000. One can consider Gilbert's paper of 1961 (Gilbert 1961) both as the first paper on continuum and Boolean percolation and as the first paper on the analysis of the connectivity of large wireless networks by means of stochastic geometry. Similar observations can be made on (Gilbert 1962) concerning Poisson–Voronoi tessellations. The number of papers using some form of stochastic geometry is increasing fast. One of the most important observed trends is to take better account in these models of specific mechanisms of wireless communications.

Time averages have been classical objects of performance evaluation since the work of Erlang (1917). Typical examples include the random delay to transmit a packet from a given node, the number of time steps required for a packet to be transported from source to destination on some multihop route, the frequency with which a transmission is not granted access due to some capacity limitations, etc. A classical reference on the matter is (Kleinrock 1975). These time averages will be studied here either on their own or in conjunction with space averages. The combination of the two types of averages unveils interesting new phenomena and leads to challenging mathematical questions. As we shall see, the order in which the time and the space averages are performed matters and each order has a different physical meaning.

This monograph surveys recent results of this approach and is structured in two volumes.
Volume I focuses on the theory of spatial averages and contains three parts. Part I in Volume I provides a compact survey on *classical* stochastic geometry models. Part II in Volume I focuses on *SINR* stochastic geometry. Part III in Volume I is an appendix which contains mathematical tools used throughout the monograph. Volume II bears on more practical wireless network modeling and performance analysis. It is in this volume that the interplay between wireless communications and stochastic geometry is deepest and that the time–space framework alluded to above is the most important. The aim is to show how stochastic geometry can be used in a more or less systematic way to analyze the phenomena that arise in this context. Part IV in Volume II is focused on medium access control (MAC). We study MAC protocols used in ad hoc networks and in cellular networks. Part V in Volume II discusses the use of stochastic geometry for the

quantitative analysis of routing algorithms in MANETs. Part VI in Volume II gives a concise summary of wireless communication principles and of the network architectures considered in the monograph. This part is self-contained and readers not familiar with wireless networking might either read it before reading the monograph itself, or refer to it when needed.

Here are some comments on what the reader will obtain from studying the material contained in this monograph and on possible ways of reading it.

For readers with a background in applied probability, this monograph provides direct access to an emerging and fast growing branch of spatial stochastic modeling (see e.g. the proceedings of conferences such as IEEE Infocom, ACM Sigmetrics, ACM Mobicom, etc. or the special issue (Haenggi, Andrews, Baccelli, Dousse, and Franceschetti 2009)). By mastering the basic principles of wireless links and of the organization of communications in a wireless network, as summarized in Volume II and already alluded to in Volume I, these readers will be granted access to a rich field of new questions with high practical interest. SINR stochastic geometry opens new and interesting mathematical questions. The two categories of objects studied in Volume II, namely medium access and routing protocols, have a large number of variants and of implications. Each of these could give birth to a new stochastic model to be understood and analyzed. Even for classical models of stochastic geometry, the new questions stemming from wireless networking often provide an original viewpoint. A typical example is that of route averages associated with a Poisson point process as discussed in Part V in Volume II. Reader already knowledgeable in basic stochastic geometry might skip Part I in Volume I and follow the path:

$$\text{Part II in Volume I} \;\Rightarrow\; \text{Part IV in Volume II} \;\Rightarrow\; \text{Part V in Volume II},$$

using Part VI in Volume II for understanding the physical meaning of the examples pertaining to wireless networks.

For readers whose main interest in wireless network design, the monograph aims to offer a new and comprehensive methodology for the performance evaluation of large scale wireless networks. This methodology consists in the computation of both time and space averages within a unified setting. This inherently addresses the scalability issue in that it poses the problems in an infinite domain/population case from the very beginning. We show that this methodology has the potential to provide both qualitative and quantitative results as below:

- Some of the most important qualitative results pertaining to these infinite population models are in terms of *phase transitions*. A typical example bears on the conditions under which the network is spatially connected. Another type of phase transition bears on the conditions under which the network delivers packets in a finite mean time for a given medium access and a given routing protocol. As we shall see, these phase transitions allow one to understand how to tune the protocol parameters to ensure that the network is in the desirable "phase" (i.e. well connected and with small mean delays). Other qualitative results are in terms of scaling laws: for instance, how do the overhead or the end-to-end delay on a route scale with the distance between the source and the destination, or with the density of nodes?
- Quantitative results are often in terms of closed form expressions for both time and space averages, and this for each variant of the involved protocols. The reader will hence be in a position

to discuss and compare various protocols and more generally various wireless network organizations. Here are typical questions addressed and answered in Volume II: is it better to improve on Aloha by using a collision avoidance scheme of the CSMA type or by using a channel-aware extension of Aloha? Is Rayleigh fading beneficial or detrimental when using a given MAC scheme? How does geographic routing compare to shortest path routing in a mobile ad hoc network? Is it better to separate the medium access and the routing decisions or to perform some cross layer joint optimization?

The reader with a wireless communication background could either read the monograph from beginning to end, or start with Volume II i.e. follow the path

$$\text{Part IV in Volume II} \Rightarrow \text{Part V in Volume II} \Rightarrow \text{Part II in Volume I}$$

and use Volume I when needed to find the mathematical results which are needed to progress through Volume II.

We conclude with some comments on what the reader will *not* find in this monograph:

- We do not discuss statistical questions and give no measurement based validation of certain stochastic assumptions used in the monograph: e.g. when are Poisson-based models justified? When should one rather use point processes with some repulsion or attraction? When is the stationarity/ergodicity assumption valid? Our only aim is to show what can be done with stochastic geometry when assumptions of this kind can be made.
- We will not go beyond SINR models either. It is well known that considering interference as noise is not the only possible option in a wireless network. Other options (collaborative schemes, successive cancellation techniques) can offer better rates, though at the expense of more algorithmic overhead and the exchange of more information between nodes. We believe that the methodology discussed in this monograph has the potential of analyzing such techniques but we decided not to do this here.

Here are some final technical remarks. Some sections, marked with a * sign, can be skipped at the first reading as their results are not used in what follows; The index, which is common to the two volumes, is designed to be the main tool to navigate within and between the two volumes.

Acknowledgments

The authors would like to express their gratitude to Dietrich Stoyan, who first suggested them to write a monograph on this topic, as well as to Daryl Daley and Martin Haenggi for their very valuable proof-reading of the manuscript. They would also like to thank the anonymous reviewer of NOW for his suggestions, particularly so concerning the two volume format, as well as Paola Bermolen, Pierre Brémaud, Srikant Iyer, Mohamed Karray, Omid Mirsadeghi, Paul Muhlethaler, Barbara Staehle and Patrick Thiran for their useful comments on the manuscript.

Preface to Volume II

The two first parts of volume II (Part IV and Part V) are structured in terms of the key ingredients of wireless communications, namely medium access and routing. The general aim of this volume is to show how stochastic geometry can be used in a more or less systematic way to analyze the key phenomena that arise in this context. We limit ourselves to simple (yet not simplistic) models and to basic protocols. This volume is nevertheless expected to convince the reader that much more can be done for improving the realism of the models, for continuing the analysis and for extending the scope of the methodology.

Part IV is focused on medium access control (MAC). We study MAC protocols used both in mobile ad hoc networks (MANETs) and in cellular networks. We analyze spatial Aloha schemes in terms of Poisson shot-noise processes in Chapters 16 and 17 and carrier sense multiple access (CSMA) schemes in terms of Matérn point processes in Chapter 18. The analytical results are then used to perform various optimizations on these schemes. For instance, we determine the tuning of the protocol parameters which maximizes the number of successful transmissions or the throughput per unit of space. We also determine the protocol parameters for which end-to-end delays have a finite mean, etc. Chapter 19 is focused on the Code Division Multiple Access (CDMA) schemes with *power control* which are used in cellular networks. The terminal nodes associated with a given concentration node (base station, access point) are those located in its Voronoi cell w.r.t. the point process of concentration nodes. For analyzing these systems, we use both shot noise processes and tessellations. When the terminal nodes require a fixed bit rate, and power is controlled so as to maximize the number of terminal nodes that can be served by such a cellular network, powers become functionals of the underlying point processes. We study admission control and capacity within this context.

Part V discusses the use of stochastic geometry for the qualitative and quantitative analysis of routing algorithms in a MANET where the nodes are some realization of a Poisson point process (p.p.) of the plane. In the point-to-point routing case, the main object of interest is the path from some source to some destination node. In the point-to-multipoint case, this is the tree rooted in the source node and spanning a set of destination nodes. The motivations are multihop diffusion in MANETs. We also analyze the multipoint-to-point case, which is used for instance for concentration in wireless sensor communication

networks where information has to be gathered at some central node. These random geometric objects are made of a set of wireless links, which have to be either simultaneously of successively feasible. Chapter 20 is focused on optimal routing, like e.g. shortest path and minimal weight routing. The main tool is subadditive ergodic theory. In Chapter 21, we analyze various types of suboptimal (greedy) geographic routing schemes. We show how to use stochastic geometry to analyze local functionals of the random paths/tree such as the distribution of the length of its edges or the mean degree of its nodes. Chapter 22 bears on time-space routing. This class of routing algorithms leverages the interaction between MAC and routing and belongs to the so called *cross-layer* framework. More precisely, these algorithms take advantage of the time and space diversity of fading variables and MAC decisions to route packets from source to destination. Typical qualitative results bear on the 'convergence' of these routing algorithms or on the fact that the velocity of a packet on a route is positive or zero. Typical quantitative results are in terms of the comparison of the mean time it takes to transport a packet from some source node to some destination node.

Part VI is an appendix which contains a concise summary of wireless communication principles and of the network architectures considered in the monograph. Chapter 23 is focused on propagation issues and on statistical channel models for fading such as Rayleigh or Rician fading. Chapter 24 bears on detection with a special focus on the fundamental limitations of wireless channels. As for architecture, we describe both MANETs and cellular networks in Chapter 25. MANETs are "flat" networks, with a single type of nodes which are at the same time transmitters, receivers and relays. Examples of MAC protocols used within this framework are described as well as multihop routing principles. Cellular networks have two types of network elements: base stations and users. Within this context, we discuss power control and its feasibility as well as admission control. We also consider other classes of heterogeneous networks like WiFi mesh networks, sensor networks or combinations of WiFi and cellular networks.

Let us conclude with a few general comments on the wireless channels and the networks to be considered throughout the volume. [1]

Two basic communication models are considered:

- A *digital communication model*, where the throughput on a link (measured in bits per seconds) is determined by the SINR at the receiver through a Shannon-like formula;
- A *packet model*, where the SINR at the receiver determines the probability of reception (also called probability of capture) of the packet and where the throughput on a link is measured in packets per time slot.

In most models, time is slotted and the time slot is assumed to be such that fading is constant over a time slot (see Chapter 23 for more on the physical meaning of this assumption). There are hence at least three time scales:

- The time scale of *symbol transmissions*. In this volume, this time scale is considered small compared to the time slot, so that many symbols are sent during one slot. At this time scale, the additive noise is typically assumed to be a Gaussian white noise and spreading techniques can be invoked to justify the representation of the interference on each channel as a Gaussian addi-

[1] For those not familiar with wireless networks, a full understanding of these comments might require a preliminary study of Part VI

tive white noise (see § 24.3.3). Shannon's formula can then in turn be invoked to determine the bit-rate of each channel over a given time slot in terms of the ratio of the mean signal power to the mean interference-and-noise power seen on the channel; the latter mean is the sum of the variance of noise and of the variance of the Gaussian representation of interference; the bit rate is an ergodic average over the many symbols sent in one slot.

- The time scale of *slots*. At this time scale, only the mean interference and noise powers for each channel and each time slot are retained from the symbol transmission time scale. These quantities change from a time slot to the next due to the fact that MAC decisions and fading may change. For example, with Aloha, the MAC decisions are resampled at each time slot; as for fading, we consider a *fast fading* scenario, [2] where the fading between a transmitter and a receiver changes (e.g. is resampled) from a time slot to the next (for instance do the motion of reflectors – see § 23) and a *slow fading* scenario, where it remains unchanged over time slots. At this time scale, the interference powers are hence again random processes, fully determined by the fading scenario and the MAC. As we shall see, their laws (which are not Gaussian anymore) can be determined using the Shot-Noise theory of Chapter 2 in Volume I.
- The time scale of *mobility*. In this monograph, this time scale is considered large compared to time slots. In particular in the part on routing, we primarily focus on scenarios where all nodes are static and where routes are established on this static network. The rationale is that the time scale of packet transmission on a route is smaller than that of node mobility. Stated differently, we do not consider here the class of delay tolerant networks which leverage node mobility for the transport of packets.

[2] Notice that this definition of fast fading differs from the definition used in many papers of literature, where fast fading often means that the channel conditions fluctuate much over a given time slot.

Contents of Volume II

Part IV

Medium Access Control

In this part, we analyze various kinds of medium access control (MAC) protocols using stochastic geometry tools. The reader not familiar with MAC should refer to §25.1 in the appendix in case what is described in the chapters is not self-sufficient.

We begin with Aloha, which is analyzed in detail in Chapters 16 and 17 (Aloha is also central in Chapter 22). We then analyze CSMA in Chapter 18, both in the context of MANETs. We then study CDMA in cellular networks in Chapter 19. In all three cases, we develop a whole-plane snapshot analysis which yields estimates of various instantaneous spatial or time-space performance metrics. This whole-plane analysis is meant to address the scalability of protocols since it focuses on results which are pertinent for very large networks.

For MANETs using Aloha and CSMA, we analyze:

- The spatial density of nodes authorized to transmit by the MAC;
- The probability of success of a typical transmission, which leads to formulas for the *density of successful transmissions* whenever a target SINR is prescribed;
- The distribution of the throughput obtained by an authorized node in case of elastic traffic, namely when no target SINR is given, which leads to estimates for the *density of throughput* in the network, where the throughput is defined in terms of a Shannon-like formula. In addition to this digital communication view point, we also discuss the packet transmission model, where the throughput is defined in terms of the number of time slots required to successfully transmit a packet.

For the CDMA case, we incorporate the key concept of power control (see § 25.2 in the appendix for the algebraic formulation of the power control problem). In this case, the spatial performance metrics are:

- For the case where a target SINR is prescribed, the spatial intensity of cells where some admission control has to be enforced in order to make the global power control problem feasible and the resulting density of users accepted in the access network;
- For the case where no target SINR is prescribed, the density of throughput in the network.

A key paradigm throughout this part is that of the 'social optimization' of the protocol, which consists in determining the tuning of the protocol parameters which maximizes the density of successful transmissions or the density of throughput or the spatial reuse (to be defined) in such a network.

Let us stress that the analysis of Aloha is by far the most comprehensive and that the aim of the CSMA and the CDMA chapters is primarily to introduce features (spatial contention for the former and power control for the latter) which are not present in Aloha. As we shall see, these new features lead to technical difficulties and more research will be required to extend all types of results available for Aloha to these more complex (and more realistic) MAC protocols.

16

Spatial Aloha: the Bipole Model

16.1 Introduction

In this chapter we consider a simplified MANET model called the *bipolar model*, where we do not yet address routing issues but do assume that each transmitter has its receiver at some fixed or random distance. We study a slotted version of Aloha. As explained in Section 25.1.2, under the Aloha MAC protocol, at each time slot, each potential transmitter independently tosses a coin with some bias p which will be referred to as the medium access probability (MAP); it accesses the medium if the outcome is heads and it delays its transmission otherwise.

It is important to tune the value of the MAP p so as to realize a compromise between the two contradicting wishes to have a large average number of concurrent transmissions per unit area and a high probability that authorized transmissions be successful: large values of p allow more concurrent transmissions but (statistically) smaller exclusion zones, making these transmissions more vulnerable; smaller values of p give fewer transmissions with higher probability of success.

Another important tradeoff concerns the typical one-hop distance of transmissions. A small distance makes the transmissions more secure but involves more relaying nodes to communicate packets between origin and destination. On the other hand, a larger one-hop distance reduces the number of hops but might increase the number of failed transmissions and hence that of retransmissions at each hop.

We define and study the following performance metrics: the probability of success (high enough SINR) for a typical transmission and the mean throughput (bit-rate) for a typical transmission at this distance. The mean number of successful transmissions and the mean throughput per unit area, the mean distance of progress per unit area, the transport density, etc. are studied in § 16.3, together with the notion of *spatial reuse* which is quite useful to compare scenarios and policies. Let us stress that the definitions of § 16.3 extend to other MAC than Aloha and will be used throughout the present volume. In § 16.4, this simplified setting is also used to study variants of Aloha such as *opportunistic Aloha*, which leverages the channels fluctuations due to fading.

16.2 Spatial Aloha

16.2.1 The Poisson Bipolar MANET Model with Independent Fading and Aloha MAC

Below, we consider a *Poisson bipolar network model* in which each point of the Poisson pattern represents a node of the MANET (a potential transmitter) and has an infinite backlog of packets to transmit to its associated receiver; the latter is *not part of the Poisson pattern of points* and is located at distance r. [1] This model can be used to represent a snapshot of a multi-hop MANET: the transmitters are some relay nodes and are not necessarily the sources of the transmitted packets; similarly, the receivers need not be the final destinations.

More precisely, we assume that the MANET snapshot can be represented by an independently marked (i.m.) Poisson p.p. (cf. Sections 1.1.1 and 2.1.1 in Volume I), where the Poisson p.p. is homogeneous on the Euclidean plane, with intensity λ, and where the multidimensional mark of a point carries information about the MAC status of the point (allowed to transmit or delayed; cf. Section 25.1) at the current time slot and about the fading conditions of the channels to all receivers (cf. Section 23.2 and also Section 2.3 in Volume I). This marked Poisson p.p. is denoted by $\widetilde{\Phi} = \{(X_i, e_i, y_i, \mathbf{F}_i)\}$, where

(1) $\Phi = \{X_i\}$ denotes the locations of the points (the potential transmitters); Φ is always assumed Poisson with positive and finite intensity λ;

(2) $\{e_i\}$ is the medium access indicator of node i; ($e_i = 1$ if node i is allowed to transmit in the considered time slot and 0 otherwise). The random variables e_i are hence i.i.d. and independent of everything else, with $\mathbf{P}(e_i = 1) = p$ (p is the MAP).

(3) $\{y_i\}$ denotes the location of the receiver for node X_i (we assume here that no two transmitters have the same receiver). We assume that the random vectors $\{X_i - y_i\}$ are i.i.d with $|X_i - y_i| = r$; i.e. each receiver is at distance r from its transmitter (see Figure 16.1). There is no difficulty extending what is described below to the case where these distances are independent and identically distributed random variables, independent of everything else.

(4) $\{\mathbf{F}_i = (F_i^j : j)\}$ where F_i^j denotes the *virtual power* emitted by node i (provided $e_i = 1$) towards receiver y_j. By virtual power F_i^j, we understand the product of the effective power of transmitter i and of the random fading from this node to receiver y_j (cf. Remark 2.3.1 in Volume I). The random vectors $\{\mathbf{F}_i\}$ are assumed to be i.i.d. and the components (F_i^j, j) are assumed to be identically distributed (distributed as a generic random variable (r.v.) denoted by F) with mean $1/\mu$ assumed finite. In the case of constant effective transmission power $1/\mu$ and Rayleigh fading, F is exponential with mean $1/\mu$ (see Section 23.2.4). In this case, it is reasonable to assume that the components of $(F_i^j : j)$ are independent, which is the default option in what follows. This is justified if the distance between two receivers is larger than the coherence distance of the wireless channel (cf. Section 23.3), which is a natural assumption here. Below, we also consider non-exponential cases which allow one to analyze other types of fading scenarios such as e.g. Rician or Nakagami (see Section 23.2.4) or simply the case without fading (when $F \equiv 1/\mu$ is deterministic).

In addition, we consider a non-negative random variable W independent of $\widetilde{\Phi}$ modeling the power of the thermal noise. A natural extension consists in considering a random field rather than a random variable.

Since we assume that Aloha is used, the set of nodes that transmit in the reference time slot $\Phi^1 =$

[1] The fact that all receivers are at the same distance from their transmitter is a simplification that will be relaxed in Chapter 16.

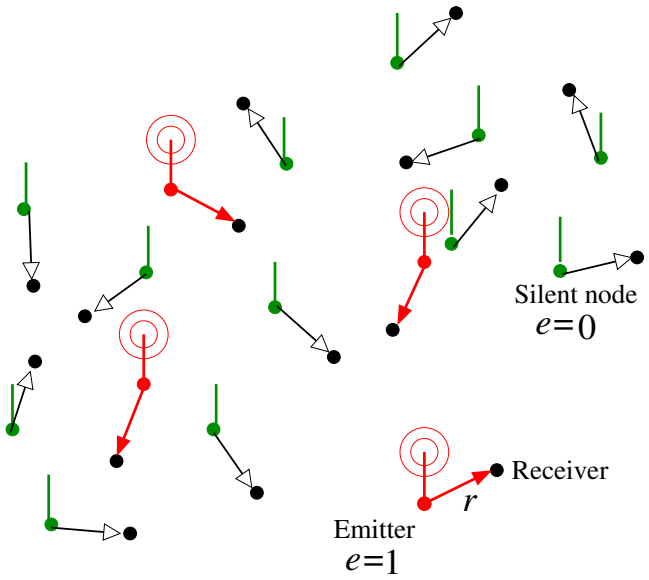

Fig. 16.1 A snapshot of bipolar MANET with Aloha MAC.

$\{X_i : e_i = 1\}$ is an independent thinning of Φ; By the corresponding property of the Poisson p.p. (cf. Proposition 1.3.5 in Volume I), Φ^1 is a Poisson p.p. with intensity $\lambda_1 = \lambda p$.

Select some omni-directional path-loss (OPL) model $l(\cdot)$ (see Section 23.1.2). An important special case consists in taking

$$l(u) = (Au)^\beta \quad \text{for } A > 0 \text{ and } \beta > 2, \tag{16.1}$$

which we call OPL 3. Note that $1/l(u)$ has a pole at $u = 0$, and thus OPL 3 *is not* appropriate for small distances (and hence in particular for u small compared to the mean distance to the nearest neighbor in the Poisson p.p., namely $1/2\sqrt{\lambda}$ — see Example 1.4.7 in Volume I). Another consequence of this path-loss model is that the total power received at a given location from an infinite Poisson pattern of transmitters has an *infinite mean* (where the averaging is taken over all configurations of transmitters); cf. Remark 2.3.5 in Volume I. In spite of these drawbacks, the OPL 3 path-loss model (16.1), will be used as the default model in what follows, because it is precise enough for large enough values of u, it simplifies many calculations and it reveals important scaling laws (see Section 16.2.4).

Other possible choices of path-loss function, OPL 1, OPL 2, avoiding the pole at at $u = 0$ are considered in Example 23.1.3.

Note that the power received from transmitter (node) j by the receiver of node i is then equal to $F_i^j / l(|X_j - y_i|)$, where $|\cdot|$ denotes the Euclidean distance on the plane.

16.2.2 Coverage (Non-Outage) Probability for a Typical Node

In what follows we present the basic analysis of the performance of the bipolar MANET model. This analysis uses the shot-noise (SN) interference model of Section 2.3 in Volume I and in particular the random cross-fading model model of Example 2.3.9 in Volume I. We assume that a connection between a transmitter and its receiver is successful (or that the formet covers the latter) when the signal to interference and noise ratio (SINR) at the receiver is larger than some threshold T:

Definition 16.2.1. Transmitter $\{X_i\}$ *covers* its receiver y_i in the reference time slot if

$$\text{SINR}_i = \frac{F_i^i / l(|X_i - y_i|)}{W + I_i^1} \geq T\,, \tag{16.2}$$

where the *interference* I_i^1 is the SN associated with $\widetilde{\Phi}^1$, namely, $I_i^1 = \sum_{X_j \in \widetilde{\Phi}^1, j \neq i} F_j^i / l(|X_j - y_i|)$ and where T is some SINR threshold.

The last condition might be required in practice for x_i to be successfully received by y_i due to the use of a particular coding scheme associated with a given bit-rate (cf. Section 24.3.4). It is also called the non-outage or the capture condition depending on the framework.

Remark: Later, in Section 16.2.3, we shall also consider *adaptive coding schemes* in which the appropriate choice of coding scheme is selected for each observed SINR level, which allows one to obtain a bit-rate close to that given by Shannon's law for all such SINR.

In what follows we focus on the probability that this property holds true for the *typical node* of the MANET, given it is a transmitter. This notion can be formalized using Palm theory for stationary marked point processes (cf. Section 2.1.2 in Volume I).

Denote by δ_i the indicator that (16.2) holds, namely, that location y_i is covered by transmitter X_i. We can consider δ_i as a new mark of X_i. The marked point process $\widetilde{\Phi}$ enriched with these marks is still stationary (cf. Definition 2.1.4 in Volume I). However, in contrast to the original marks $e_i, y_i, \mathbf{F}_i$, given the points of Φ, the random variables $\{\delta_i\}$ are neither independent nor identically distributed. Indeed, the points of Φ lying in dense clusters have a smaller probability of coverage than more isolated points due to interference; in addition, because of the shot noise variables I_i^1, the random variables $\{\delta_i\}$ are dependent.

By probability of coverage of a typical node given it is a transmitter, we understand

$$\mathbf{P}^0\{\, \delta_0 = 1 \,|\, e_0 = 1\} = \mathbf{E}^0[\delta_0 \,|\, e_0 = 1],$$

where $\mathbf{P}^0$ is the Palm probability associated to the (marked) stationary point process $\widetilde{\Phi}$ and where δ_0 is the mark of the point $X_0 = 0$ a.s. located at the origin 0 under $\mathbf{P}^0$. This Palm probability $\mathbf{P}^0$ is derived from the original (stationary) probability $\mathbf{P}$ by the following relation (cf. Definition 2.1.5 in Volume I)

$$\mathbf{P}^0\{\, \delta_0 = 1 \,|\, e_0 = 1\} = \frac{1}{\lambda_1 |B|} \mathbf{E}\left[\sum_i \delta_i \mathbb{1}(X_i \in B) \right],$$

where B is an arbitrary subset of the plane and $|B|$ is its surface. Thus, knowing that $\lambda_1 |B|$ is the expected number of transmitters in B, the typical node coverage probability is the mean number of transmitters which cover their receivers in any given window B in which we observe our MANET. Note that this mean is based on a *double averaging*: a *mathematical expectation* – over all possible realizations of the MANET and, for each realization, a spatial averaging – over all nodes in B.

If the underlying point process is ergodic (as it is the case for our i.m. Poisson p.p. $\tilde{\Phi}$) the typical node coverage probability can also be interpreted as a *spatial average of the number of transmitters which cover their receiver* in almost every given realization of the MANET and large B (tending to the whole plane; cf. Proposition 1.6.10 in Volume I).

For a stationary i.m. Poisson p.p., the probability $\mathbf{P}^0$ can easily be constructed using Slivnyak's theorem (cf. Theorem 1.4.5 in Volume I): under $\mathbf{P}^0$, the nodes of the Poisson MANET and their marks follow the

distribution $\widetilde{\Phi} \cup \{(X_0 = 0, e_0, y_0, \mathbf{F}_0)\}$, where $\widetilde{\Phi}$ is the original stationary i.m. Poisson p.p. (i.e. that seen under the original probability $\mathbf{P}$) and $(e_0, y_0, \mathbf{F}_0)$ is a new copy of the mark independent of everything else and distributed like all other i.i.d. marks $(e_i, y_i, \mathbf{F}_i)$ of $\widetilde{\Phi}$ under $\mathbf{P}$. (cf. Remark 2.1.7 in Volume I).

Note that, under $\mathbf{P}^0$, the node at the origin (the typical node), is not necessarily a transmitter; e_0 is equal to 1 or 0 with probability p and $1-p$ respectively.

Denote by $p_c(r, \lambda_1, T) = \mathbf{E}^0[\delta_0 \,|\, e_0 = 1]$ the probability of coverage of the typical MANET node given it is a transmitter. It follows from the above construction that this probability only depends on the density of effective transmitters $\lambda_1 = \lambda p$, on the distance r and on the SINR threshold T; it can be expressed using three independent generic random variables F, I^1, W by the following formula:

$$p_c(r, \lambda_1, T) = \mathbf{P}^0\{\, F_0^0 > l(r)T(W + I_0^1) \mid e_0 = 1 \,\} = \mathbf{P}\{\, F \geq Tl(r)(I^1 + W) \,\}\,. \tag{16.3}$$

Note also that this probability is equal to the one-point coverage probability $p_0(y_0)$ in the $\frac{\text{GI}}{W+\text{M/GI}}$ SINR cell model of Section 5.3.1 in Volume I associated with the Poisson p.p. intensity λ_1. (see the meaning of this Kendall-like notation in Section 5.3 in Volume I). For this reason, our Aloha MANET model is of the $\frac{\text{GI}}{W+\text{M/GI}}$ type, where the GI in the numerator indicates a general distribution for the virtual power of the signal F and where the M/GI in the denominator indicates that the SN interference is generated by a Poisson pattern of interferers (M), with a general distribution (G) for their virtual powers. Special cases of distributions marks are deterministic (D) and exponential (M). We recall that M/· denotes a SN model with a Poisson point process.

In what follows, we often use the following explicit formula for the Laplace transform of the generic shot-noise $I^1 = \sum_{X_j \in \widetilde{\Phi}^1} F_j / l(|X_j|)$, which is valid in the Poisson p.p. case whenever the random variables F_j are independent copies of the generic fading variable F (cf. Corollary 2.3.8 in Volume I):

$$\mathcal{L}_{I^1}(s) = \mathbf{E}[e^{-I^1 s}] = \exp\left\{ -\lambda_1 2\pi \int_0^\infty t\Big(1 - \mathcal{L}_F(s/l(t))\Big)\, \mathrm{d}t \right\}, \tag{16.4}$$

where $\mathcal{L}_F$ is the Laplace transform of F. This can be derived from the formula for the Laplace functional of the Poisson p.p. (see Propositions 1.2.2 and 2.2.4 in Volume I).

16.2.2.1 Rayleigh Case

The next result bears on the Rayleigh fading case (F exponential with mean $1/\mu$). Using the independence assumptions, it is easy to see that the right-hand side of (16.3) can be rewritten as

$$p_c(r, \lambda) = p_c(r, \lambda, T) = \mathbf{E}\left[e^{-\mu(Tl(r)(I^1+W)}\right] = \mathcal{L}_{I^1}(\mu T l(r))\mathcal{L}_W(\mu T l(r))\,, \tag{16.5}$$

where $\mathcal{L}_W$ is the Laplace transform of W and where $\mathcal{L}_{I^1}$ can be expressed as follows from (16.4) when using the fact that F is exponential:

$$\mathcal{L}_{I^1}(s) = \exp\left(-2\pi\lambda_1 \int_0^\infty \frac{t}{1 + \mu l(t)/s} \mathrm{d}t \right)\,. \tag{16.6}$$

Using this observation, one immediately obtains (cf. also Proposition 5.3.3 and Example 5.3.4 in Volume I):

Proposition 16.2.2. For the $\frac{\text{M}}{W+\text{M/M}}$ bipolar model,

$$p_c(r,\lambda_1,T) = \mathcal{L}_W(\mu T l(r)) \exp\left\{ -2\pi\lambda_1 \int_0^\infty \frac{u}{1+l(u)/(Tl(r))}\,\mathrm{d}u \right\}. \tag{16.7}$$

In particular if $W \equiv 0$ and that the path-loss model (16.1) is used then

$$p_c(r,\lambda_1,T) = \exp(-\lambda_1 r^2 T^{2/\beta} K(\beta))\,, \tag{16.8}$$

where

$$K(\beta) = \frac{2\pi\Gamma(2/\beta)\Gamma(1-2/\beta)}{\beta} = \frac{2\pi^2}{\beta\sin(2\pi/\beta)}\,. \tag{16.9}$$

Example 16.2.3. The above result can be used in the following context: assume one wants to operate a MANET in a regime where each transmitter is guaranteed a SINR at least T with a probability larger than $1-\varepsilon$, where ε is a predefined quality of service, or equivalently, where the probability of outage is less then ε. Then, if the transmitter-receiver distance is r, the MAP p should be such that $p_c(r,\lambda p,T) = 1-\varepsilon$. In particular, assuming the path-loss setting (16.1), one should take

$$p = \min\left(1, \frac{-\ln(1-\varepsilon)}{\lambda r^2 T^{2/\beta} K(\beta)}\right) \approx \min\left(1, \frac{\varepsilon}{\lambda r^2 T^{2/\beta} K(\beta)}\right)\,. \tag{16.10}$$

For example, for $T = 10$dB [2] and OPL 3 model with $\beta = 4$, $r = 1$, one should take $p \approx \min\left(1, 0.064\,\varepsilon/\lambda\right)$.

16.2.2.2 General Fading

In what follows, we consider a $\frac{\text{GI}}{W+\text{M/GI}}$ bipolar Aloha MANET model. In this case one can get integral representations for the probability of coverage on the basis of the results of Section 5.3.1 in Volume I.

Proposition 16.2.4. Consider a $\frac{\text{GI}}{W+\text{M/GI}}$ bipolar model with general fading variables F such that

- F has a finite first moment and admits a square integrable density;
- Either I^1 or W admit a density which is square integrable.

Then the probability of a successful transmission is equal to

$$p_c(r,\lambda_1,T) = \int_{-\infty}^{\infty} \mathcal{L}_{I^1}(2i\pi l(r)Ts)\,\mathcal{L}_W(2i\pi l(r)Ts)\,\frac{\mathcal{L}_F(-2i\pi s)-1}{2i\pi s}\mathrm{d}s\,. \tag{16.11}$$

[2] A positive real number x is $10\log_{10}(x)$ dB.

Remark: Sufficient conditions for I^1 to admit a density are given in Proposition 2.2.6 in Volume I. Roughly speaking these conditions require that F be non-null and that the path-loss function l be not constant in any interval. This is satisfied e.g. for the OPL 3 and OPL 2 model, but not for OPL 1 – see Example 23.1.3. Concerning the square integrability of the density, which is equivalent to the integrability of $|\mathcal{L}_{I^1}(is)|^2$ (see (Feller 1971, p. 510) and also (2.20 in Volume I)), using (16.4), one can easily check that it is satisfied for the OPL 3 model provided $\mathbf{P}\{F > 0\} > 0$. Moreover, under the same conditions $|\mathcal{L}_{I^1}(is)|$ is integrable (and so is $|\mathcal{L}_{I^1}(is)|/|s|$ for large $|s|$).

Proof. (*of Proposition 16.2.4*) By the independence of I^1 and W in (16.3), the second assumption of Proposition 16.2.4 implies that $I^1 + W$ admits a density $g(\cdot)$ that is square integrable. The result then follows from

$$p_c(r, \lambda_1, T) = \mathbf{P}\{\, (I^1 + W)Tl(r) < F \,\},$$

by the Plancherel-Parseval theorem; see e.g. (Brémaud 2002, Th. C3.3, p.157)) and for more details Corollary 12.2.2 in Volume I. □

16.2.3 Shannon Throughput of a Typical Node

In Section 16.2.2 we assumed that a channel could be sustained if the SINR was above some fixed threshold T, which corresponds to the case where some minimum bit rate is required (like in e.g. voice). In this section we consider the situation where there is no minimal requirement on the bit rate $\mathcal{T}$ and where the latter depends on the SINR through some Shannon like formula. This is possible with adaptive coding, where a coding with a high bit-rate is used if the SINR is high, whereas a coding with a low bit-rate is used in case of lower SINR. We adopt the following definition.

Definition 16.2.5. We define the *(Shannon) throughput* (bit-rate) of the channel from transmitter X_i to its receiver y_i to be

$$\mathcal{T}_i = \log(1 + \mathrm{SINR}_i)\,, \tag{16.12}$$

where SINR_i is as in Definition 16.2.1.

One can then ask about the throughput of a typical transmitter (or equivalently about the spatial average of the rate obtained by the transmitters), namely

$$\tau = \tau(r, \lambda_1) = \mathbf{E}^0[\mathcal{T}_0 \,|\, e_0 = 1] = \mathbf{E}^0[\log(1 + \mathrm{SINR}_0) \,|\, e_0 = 1]$$

and also about its Laplace transform

$$\mathcal{L}_{\mathcal{T}}(s) = \mathbf{E}^0[e^{-s\mathcal{T}_0} \,|\, e_0 = 1] = \mathbf{E}^0[(1 + \mathrm{SINR}_0)^{-s} \,|\, e_0 = 1]\,.$$

Let us now make the following simple observations:

$$\begin{aligned}\tau(r,\lambda_1) &= \mathbf{E}^0[\log(1+\mathrm{SINR}_0)\,|\,e_0=1]\\ &= \int_0^\infty \mathbf{P}^0\{\,\log(1+\mathrm{SINR}_0)>t\,|\,e_0=1\,\}\,\mathrm{d}t\\ &= \int_0^\infty \mathbf{P}^0\{\,\mathrm{SINR}_0>e^t-1\,|\,e_0=1\,\}\,\mathrm{d}t\\ &= \int_0^\infty p_c(r,\lambda_1,e^t-1)\,\mathrm{d}t=\int_0^\infty \frac{p_c(r,\lambda_1,v)}{v+1}\,\mathrm{d}v \end{aligned} \tag{16.13}$$

and similarly

$$\begin{aligned}\mathcal{L}_{\mathcal{T}}(s) &= \mathbf{E}^0[(1+\mathrm{SINR}_0)^{-s}\,|\,e_0=1]\\ &= 1-\int_0^1 p_c(r,\lambda_1,t^{-1/s}-1)\,\mathrm{d}t = 1-s\int_0^\infty \frac{p_c(r,\lambda_1,v)}{(1+v)^{1+s}}\mathrm{d}v\,, \end{aligned} \tag{16.14}$$

provided $\mathbf{P}\{\mathrm{SINR}_0=T\}=0$ for all $T\geq 0$, which is true e.g. when F admits a density (cf. (16.3)). This, together with Propositions 16.2.2 and 16.2.4, lead to the following results:

Corollary 16.2.6. Under the assumptions of Proposition 16.2.2 (namely for the model with Rayleigh fading) and for the OPL 3 path-loss model (16.1)

$$\tau=\frac{\beta}{2}\int_0^\infty e^{-\lambda_1 K(\beta) r^2 v}\frac{v^{\frac{\beta}{2}-1}}{1+v^{\frac{\beta}{2}}}\mathcal{L}_W\left(\mu(Ar)^\beta v^{\beta/2}\right)\mathrm{d}v \tag{16.15}$$

and

$$\mathcal{L}_{\mathcal{T}}(s)=\frac{\beta s}{2}\int_0^\infty\left(1-e^{-\lambda_1 K(\beta) r^2 v}\mathcal{L}_W\left(\mu(Ar)^\beta v^{\beta/2}\right)\right)\frac{v^{\frac{\beta}{2}-1}}{\left(1+v^{\frac{\beta}{2}}\right)^{1+s}}\mathrm{d}v\,, \tag{16.16}$$

where $K(\beta)$ is defined in (16.9).

Corollary 16.2.7. Under the assumptions of Proposition 16.2.4 (namely in the model with general fading F),

$$\tau=\int_0^\infty\int_{-\infty}^\infty \mathcal{L}_{I^1}\left(2i\pi v s l(r)\right)\mathcal{L}_W\left(2i\pi v s l(r)\right)\frac{\mathcal{L}_F(-2i\pi s)-1}{2i\pi s(1+v)}\mathrm{d}s\mathrm{d}v \tag{16.17}$$

and

$$\mathcal{L}_{\mathcal{T}}(s)=1-s\int_0^\infty\int_{-\infty}^\infty \mathcal{L}_{I^1}\left(2i\pi v s l(r)\right)\mathcal{L}_W\left(2i\pi v s l(r)\right)\frac{\mathcal{L}_F(-2i\pi s)-1}{2i\pi s(1+v)^{1+s}}\,\mathrm{d}s\mathrm{d}v\,. \tag{16.18}$$

Here is a direct application of the last results.

	$r = .25$	$r = .37$	$r = .5$	$r = .65$	$r = .75$	$r = .9$	$r = 1$
Rayleigh	1.52	.886	.480	.250	.166	.0930	.0648
Erlang (8)	1.71	.942	.495	.242	.155	.0832	.0571

Table 16.1 Impact of the fading on the mean throughput τ for varying distance r. The Erlang distribution of order 8 mimics the no-fading case; we use OPL3 3 with $A = 1$, $\beta = 4$ and Rayleigh (exponential) thermal noise W with mean 0.01.

Example 16.2.8. Table 16.1 shows how Rayleigh fading compares to the situation with no fading. The OPL 3 model is assumed with $A = 1$ and $\beta = 4$. We assume W to be exponential with mean 0.01. We use the formulas of the last corollaries; the Rayleigh case is with F exponential of parameter 1; to represent the no fading case within this framework we take F Erlang of high order (here 8) with the same mean 1 as the exponential. The reason for using Erlang rather than deterministic is that the latter does not satisfy the first technical condition of Proposition 16.2.4. We see that the presence of fading is beneficial in the far-field, and detrimental in the near-field.

16.2.4 Scaling Properties

We show below that in the Poisson bipolar network model of Section 16.2.1, when using the OPL 3 model (16.1) and when $W = 0$, some interesting scaling properties can be derived.

Denote by $\bar{p}_c(r) = p_c(r, 1, 1)$ the value of the probability of coverage calculated in this model with $T \equiv 1, \lambda_1 = 1, W \equiv 0$ and with normalized virtual powers $\bar{F}_i^j = \mu F_i^j$. Note that $\bar{p}_c(r)$ does not depend on any parameter of the model other than the distribution of the normalized virtual power $\bar{F}$.

Proposition 16.2.9. In the Poisson bipolar network model of Section 16.2.1 with path-loss model (16.1) and $W = 0$

$$p_c(r, \lambda_1, T) = \bar{p}_c(rT^{1/\beta}\sqrt{\lambda_1})\,.$$

Proof. The Poisson point process Φ^1 with intensity $\lambda_1 > 0$ can be represented as $\{X_i'/\sqrt{\lambda_1}\}$, where $\Phi' = \{X_i'\}$ is Poisson with intensity 1 (cf. Example 1.3.12 in Volume I). Because of this, under (16.1), the Poisson shot-noise interference variable I^1 admits the following representation: $I^1 = \lambda_1^{\beta/2} I'^1$, where I'^1 is defined in the same manner as I^1 but with respect to Φ'. Thus for $W = 0$,

$$\begin{aligned} p_c(r, \lambda_1, T) &= \mathbf{P}(F \geq T(Ar)^\beta I^1) \\ &= \mathbf{P}\Big(\mu F \geq \mu(ArT^{1/\beta}\lambda_1^{1/2})^\beta I'^1\Big) \\ &= \bar{p}_c(rT^{1/\beta}\sqrt{\lambda_1})\,. \end{aligned}$$

□

Remark 16.2.10. The scaling of the coverage probability presented in Proposition 16.2.9 is the first of several examples of scaling in $\sqrt{\lambda}$. Recall that this is also how the transport capacity scales in the well-known Gupta and Kumar law. There are three fundamental ingredients for obtaining this scaling in the present context:

- the scale invariance property of the Poisson p.p. (cf. Example 1.3.12 in Volume I),
- the power-law form of OPL 3,
- the fact that thermal noise was neglected.

Note however the following important limitations concerning this scaling. First, when $\lambda \to \infty$, the nodes are closer to each other and one may challenge the use of OPL 3 (the pole at the origin is not adequate for representing the path loss on small distances). On the other hand, when $\lambda \to 0$, the transmission distances are very long; communications become noise limited and the assumption $W = 0$ may no longer be justified.

16.3 Spatial Performance Metrics

When trying to maximize the coverage probability $p_c(r, \lambda_1, T)$ or the throughput $\tau(r, \lambda_1)$, one obtains degenerate maxima at $r = 0$. Assuming that our MANET features packets which have to reach some distant destination nodes, a more meaningful optimization consists in maximizing some distance-based characteristics. In the coverage scenario, we for instance consider the mean progress made in a typical transmission:

$$prog(r, \lambda_1, T) = r\mathbf{E}^0[\delta_0] = rp_c(r, \lambda_1, T)\,. \tag{16.19}$$

Similarly, in the digital communication (or Shannon-throughput) scenario, we define the mean transport of a typical transmission as

$$trans(r, \lambda_1, T) = r\mathbf{E}^0[\mathcal{T}_0] = r\tau(r, \lambda_1)\,. \tag{16.20}$$

These characteristics might still not lead to pertinent optimizations of the MANET, as they are concerned with one (typical) transmission. In particular, they are trivially maximized when $p \to 0$, when transmissions are very efficient but very rare in the network. In fact, we need some network (social) performance metrics.

Definition 16.3.1. We call

- *(spatial) density of successful transmissions,* d_{suc}, the mean number of successful transmissions per surface unit;
- *(spatial) density of progress,* d_{prog}, the mean number of meters progressed by all transmissions taking place per surface unit;
- *(spatial) density of throughput,* d_{throu}, the mean throughput per surface unit;
- *(spatial) density of transport,* d_{trans}, the mean number of bit-meters transported per second and per unit of surface.

The knowledge of $p_c(r, \lambda_1, T)$ or $\tau(r, \lambda_1)$ allows one to estimate these spatial network performance metrics. The link between individual and social characteristics is guaranteed by Campbell's formula (cf. (2.9 in Volume I)).

In what follows we make precise the meaning of the characteristics proposed in Definition 16.3.1 for Poisson bipolar MANETs.

The density of successful transmissions can formally be seen as the mean number of successful transmissions in some arbitrary subset B of the plane:

$$d_{suc}(r, \lambda_1, T) = \frac{1}{|B|}\mathbf{E}\left[\sum_i e_i\delta_i \mathbb{1}(X_i \in B)\right].$$

By stationarity, the last quantity does not depend on the particular choice of set B. Let $g(x, \tilde{\Phi}) = \mathbb{1}(x \in B) e_0 \delta_0$. The right hand side of the above equation can be expressed as

$$\frac{1}{|B|} \mathbf{E}\Big[\int_{\mathbb{R}^2} g(x, \tilde{\Phi} - x)\, \Phi(\mathrm{d}x) \Big] ,$$

and by Campbell's formula (2.9 in Volume I) is equal to

$$\frac{\lambda}{|B|} \int_{\mathbb{R}^2} \mathbf{E}^0[g(x, \tilde{\Phi})]\, \mathrm{d}x = \lambda \mathbf{E}^0[e_0 \delta_0] ,$$

which gives the following result

$$d_{suc}(r, \lambda_1, T) = \lambda_1 p_c(r, \lambda_1, T) = \lambda p p_c(r, \lambda p, T). \tag{16.21}$$

Similarly, the density of progress can be defined as the mean distance progressed by all transmissions taking place in some arbitrary subset B of the plane

$$d_{prog}(r, \lambda_1, T) \;=\; \frac{1}{|B|} \mathbf{E}\Big[\sum_i r e_i \delta_i \mathbb{1}(X_i \in B) \Big] = r \lambda_1 p_c(r, \lambda_1, T) , \tag{16.22}$$

by the same arguments as for (16.21).

The spatial density of throughput is equal to

$$d_{throu}(r, \lambda_1) \;=\; \frac{1}{|B|} \mathbf{E}\Big[\sum_i e_i \mathbb{1}(X_i \in B) \log(1 + \mathrm{SINR}_i) \Big] = \lambda_1 \tau(r, \lambda_1) \tag{16.23}$$

and the density of transport to

$$d_{trans}(r, \lambda_1) \;=\; \frac{1}{|B|} \mathbf{E}\Big[\sum_i e_i r \mathbb{1}(X_i \in B) \log(1 + \mathrm{SINR}_i) \Big] = \lambda_1 r \tau(r, \lambda_1). \tag{16.24}$$

In the following sections we focus on the optimization of the spatial performance of an Aloha MANET.

16.3.1 Optimization of the Density of Progress

16.3.1.1 Best MAP Given Some Transmission Distance

We already mentioned that a good tuning of p should find a compromise between the average number of concurrent transmissions per unit area and the probability that a given authorized transmission is successful. To find such a compromise, one ought to maximize the density of progress, or equivalently the density of successful transmissions, $d_{suc}(r, \lambda p, T) = \lambda p\, p_c(r, \lambda p, T)$, w.r.t. p, for a given r and λ. This can be done explicitly for the Poisson bipolar network model with Rayleigh fading. For this we first optimize w.r.t. λ assuming p fixed and then deduce from this the optimal MAP for some fixed λ.

Define

$$\lambda_{\max} = \arg\max_{0 \le \lambda < \infty} d_{suc}(r, \lambda, T) ,$$

whenever such a value of λ exists and is unique. The following result follows from Proposition 16.2.2.

Proposition 16.3.2. Under the assumptions of Proposition 16.2.2 (namely for the $\frac{\text{M}}{W+\text{M/M}}$ model), if $p = 1$, the unique maximum of the density of successful transmissions $d_{suc}(r, \lambda, T)$ is attained at

$$\lambda_{\max} = \left(2\pi \int_0^\infty \frac{u}{1 + l(u)/(Tl(r))} \, \mathrm{d}u \right)^{-1} ,$$

and the maximal value is equal to

$$d_{suc}(r, \lambda_{\max}, T) = e^{-1} \lambda_{\max} \, \mathcal{L}_W(\mu T l(r)) \, .$$

In particular, assuming $W \equiv 0$ and OPL 3 model (16.1)

$$\lambda_{\max} = \frac{1}{K(\beta) r^2 T^{2/\beta}} , \tag{16.25}$$

$$d_{suc}(r, \lambda_{\max}, T) = \frac{1}{eK(\beta) r^2 T^{2/\beta}} . \tag{16.26}$$

with $K(\beta)$ defined in (16.9).

Proof. The result follows from (16.7) by differentiation of the function $\lambda p_c(r, \lambda, T)$ with respect to λ. □

The above result yields the following corollary concerning the tuning of the MAC parameter when λ is fixed.

Corollary 16.3.3. Under assumptions of Proposition 16.2.2 with given r, the value of the MAP p that maximizes the density of successful transmissions is

$$p_{\max} = \min(1, \lambda_{\max}/\lambda) \, .$$

In order to extend our observations to general fading (or equivalently to a general distribution for virtual power), let us assume that $W = 0$ and let us adopt model OPL 3. Then, for Rayleigh fading, using Lemma 16.2.9, we can easily show that $\lambda_{\max}$ and $d_{suc}(r, \lambda_{\max})$ exhibit, up to some constant, the same dependence on the model parameters (namely r, T and μ) as that given in (16.25) and (16.26).

Proposition 16.3.4. In the $\frac{\text{GI}}{0+\text{M/GI}}$ bipolar model with OPL 3 and $W = 0$,

$$\lambda_{\max} = \frac{\text{const}_1}{r^2 T^{2/\beta}} , \quad \text{and} \quad d_{suc}(r, \lambda_{\max}) = \frac{\text{const}_2}{r^2 T^{2/\beta}} , \tag{16.27}$$

where the constants const_1 and const_2 do not depend on r, T, μ, provided $\lambda_{\max}$ is well defined.

Proof. Assume that $\lambda_{\max}$ is well defined. [3] By Lemma 16.2.9, $\text{const}_1 = \arg\max_{\lambda \geq 0} \{\lambda \bar{p}_c(\sqrt{\lambda})\}$ and $\text{const}_2 = \max_{\lambda \geq 0} \{\lambda \bar{p}_c(\sqrt{\lambda})\}$. □

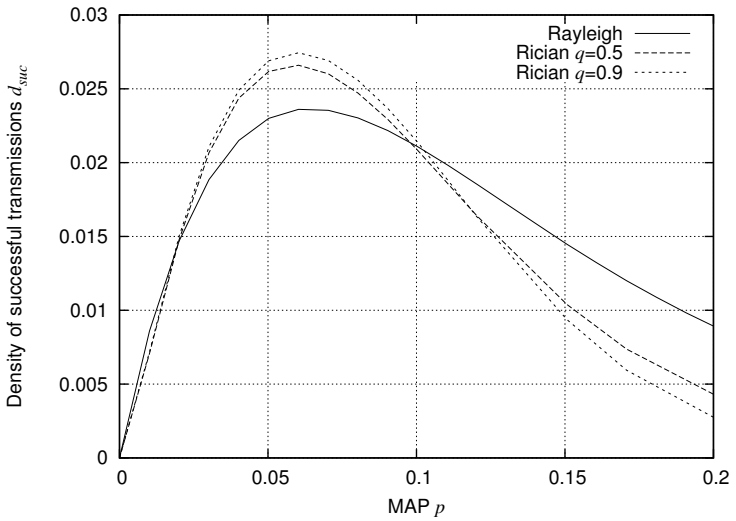

Fig. 16.2 Density of successful transmissions d_{suc} for Aloha in function of p in the Rayleigh and the Rician (with $q = 1/2$ and $q = .9$) fading cases; $\lambda = r = 1$, $W = 0$, and $T = 10$dB; we use OPL 3 with $A = 1$ and $\beta = 4$.

Example 16.3.5 (Rayleigh versus Rician fading). Figure 16.2 compares the density of success for Rayleigh and Rician fading. For this, we use the representations of Propositions 16.2.2 and Proposition 16.2.4, respectively. In the Rayleigh case, F is exponential with mean 1. In the Rician case $F = q+(1-q)F'$, with $0 \leq q \leq 1$, where F' is exponential with mean 1 and q represents the part of the energy received on the line-of-sight. The density of success is plotted in function of p. We again observe that higher variances are beneficial for high densities of transmitters (which is here equivalent to the far field case) and detrimental for low densities. However here, in each case, there is an optimal MAP, and when properly optimized, Spatial Aloha does better for lower variances (i.e. for Rician fading with higher q).

16.3.1.2 *General Definition of $\lambda_{\max}$

In this section, we show that under some mild conditions, $\lambda_{\max}$ is well defined and not degenerate (i.e. $0 < \lambda_{\max} < \infty$) for a general $\frac{\text{GI}}{W+\text{M/GI}}$ model. Assume $T > 0$. Note that $d_{suc}(r, 0, T) = 0$; so under some natural non-degeneracy assumptions, the maximum is certainly not attained at $\lambda = 0$.

Proposition 16.3.6. Consider the $\frac{\text{GI}}{W+\text{M/GI}}$ bipolar model with $p = 1$ and general fading with a finite mean. Assume that $l(r) > 0$ and is such that the generic SN $I(\lambda) = \sum_{X_j \in \widetilde{\Phi}} F_j / l(|X_j|)$ admits a density for all $\lambda > 0$. Then

(1) If $\mathbf{P}\{ F > 0 \} > 0$, then $p_c(r, x, T)$ (and so $d_{suc}(r, x, T)$) is continuous in x, so that the maximum of the function $x \to d_{suc}(r, x, T)$ in the interval $[0, \lambda]$ is attained for some $0 < \lambda_{\max} \leq \lambda$;
(2) If for all $a > 0$, the following modified SN:

$$I'(\lambda) = \sum_{X_j \in \widetilde{\Phi}} \mathbb{1}(|X_j| > a) F_j / l(|X_j|)$$

[3]The question of the definition of $\lambda_{\max}$ is addressed in § 16.3.1.2.

has finite mean for all $\lambda > 0$, then $\lim_{x\to\infty} d_{suc}(r,x,T) = 0$ and consequently, for sufficiently large λ, this maximum is attained for some $\lambda_{\max} < \lambda$.

The statement of the last proposition means that for a sufficiently large density of nodes λ, a nontrivial MAP $0 < p_{\max} < 1$ equal to $p_{\max} = \lambda_{\max}/\lambda$ optimizes the density of successful transmissions.

Proof. (of Proposition 16.3.6) Recall that $p_c(r,\lambda,T) = \mathbf{P}\{\, I(\lambda) \le F/(l(r)T - W)\,\}$, where the dependence of the SN variable $I(\lambda) = I^1 = I$ (note that $p = 1$) on the intensity of the Poisson p.p. was made explicit. By the thinning property of the Poisson p.p. (stated in Proposition 1.3.5 in Volume I) we can split the SN variable into two independent Poisson SN terms $I(\lambda+\epsilon) = I(\lambda) + I(\epsilon)$. Moreover, we can do this in such a way that $I(\epsilon)$, which is finite by assumption, almost surely converges to 0 when $\epsilon \to 0$. Consequently,

$$0 \le p_c(r,\lambda,T) - p_c(r,\lambda+\epsilon,T) = \mathbf{P}\Big\{\, \frac{F}{l(r)T-W} - I(\epsilon) < I(\lambda) \le \frac{F}{l(r)T-W} \,\Big\}\,,$$

and

$$\lim_{\epsilon\to 0}\big(p_c(r,\lambda,T) - p_c(r,\lambda+\epsilon,T)\big) = \mathbf{P}\Big\{\, I(\lambda) = \frac{F}{l(r)T-W} \,\Big\} = 0\,,$$

where the last equation is due to the fact that $I(\lambda)$ is independent of F, W and admits a density. Splitting the Poisson p.p. of intensity λ into two Poisson p.p.s with intensity $\lambda-\epsilon$ and ϵ respectively, and considering the associated SN variables $I(\lambda-\epsilon)$ and $I(\epsilon)$, with $I(\lambda)$ defined as their sum, one can show in a similar manner that $\lim_{\epsilon\to 0} p_c(r,\lambda-\epsilon,T) - p_c(r,\lambda,T) = 0$. This concludes the proof of the first part of the proposition.

We now prove the second part. Let $\overline{G}(s) = \mathbf{P}\{\, F \ge s\,\}$. Take $\epsilon > 0$ and such that $\epsilon < \mathbf{E}[I'(1)] = \overline{I}'(1) < \infty$. By independence we have

$$d_{suc}(r,\lambda,T) = \lambda p_c(r,\lambda,T) \le \lambda \mathbf{E}\Big[\mathbf{P}\Big\{\, F \ge I'(\lambda) T l(r) | I'(\lambda)\,\Big\}\Big] \le J_1 + J_2\,,$$

where

$$\begin{aligned} J_1 &= \mathbf{E}\Big[\frac{\lambda}{I'(\lambda)} \mathbb{1}\Big(I'(\lambda) \ge \lambda(\overline{I}'(1) - \epsilon)\Big) I'(\lambda)\overline{G}\big(I'(\lambda)Tl(r)\big)\Big] \\ J_2 &= \lambda \mathbf{E}\Big[\mathbb{1}\Big(I'(\lambda) < \lambda(\overline{I}'(1) - \epsilon)\Big)\Big]\,. \end{aligned}$$

Since $\mathbf{E}[F] = \int_0^\infty \overline{G}(s)\,\mathrm{d}s < \infty$, $I'(\lambda)\overline{G}\big(I'(\lambda)Tl(r)\big)$ is uniformly bounded in $I'(\lambda)$ and $I'(\lambda)\overline{G}\big(I'(\lambda)Tl(r)\big) \to 0$ when $I'(\lambda) \to \infty$. Moreover, one can construct a probability space such that $I'(\lambda) \to \infty$ almost surely as $\lambda \to \infty$. Thus, by Lebesgue's dominated convergence theorem, we have $\lim_{\lambda\to\infty} J_1 = 0$.

For J_2 and $t > 0$ we have

$$\begin{aligned} J_2 &\le \lambda \mathbf{P}^0\{\, e^{-tI'(\lambda)} \ge e^{-\lambda t(\overline{I}'(1)-\epsilon)}\,\} \\ &\le \lambda \mathbf{E}^0\big[e^{-tI'(\lambda)+\lambda t(\overline{I}'(1)-\epsilon)}\big] \\ &= \lambda \exp\Big\{\lambda\Big(t(\overline{I}'(1)-\epsilon) - 2\pi\int_a^\infty s\big(1-\mathcal{L}_F(t/l(s))\big)\,\mathrm{d}s\Big)\Big\}\,. \end{aligned}$$

Note that the derivative of $t(\overline{I}'(1)-\epsilon) - 2\pi\int_a^\infty s\big(1-\mathcal{L}_F(t/l(s))\big)\,\mathrm{d}s$ with respect to t at $t = 0$ is equal to $\overline{I}'(1) - \epsilon - \overline{I}'(1) < 0$. Thus, for some small $t > 0$, $J_2 \le \lambda e^{-\lambda C}$ for some constant $C > 0$. This shows that $\lim_{\lambda\to\infty} J_2 = 0$, which concludes the proof. □

16.3.1.3 Best Transmission Distance Given Some Transmitter Density

Assume now some given intensity λ_1 of transmitters. We look for the distance r which maximizes the mean density of progress, or equivalently the mean progress $prog(r, \lambda_1, T) = r\, p_c(r, \lambda_1, T)$. We denote by

$$r_{\max} = r_{\max}(\lambda) = \arg\max_{r \geq 0} prog(r, \lambda, T)$$

the best transmission distance for the density of transmitters λ whenever such a value exists and is unique. Let

$$\rho = \rho(\lambda) = prog(r_{\max}(\lambda), \lambda, T)$$

be the optimal mean progress.

Proposition 16.3.7. In the $\frac{\text{GI}}{0+\text{M/GI}}$ bipolar model with OPL 3 function and $W = 0$,

$$r_{\max}(\lambda) = \frac{\text{const}_3}{T^{1/\beta}\sqrt{\lambda}}, \quad \text{and} \quad \rho(\lambda) = \frac{\text{const}_4}{T^{1/\beta}\sqrt{\lambda}}, \tag{16.28}$$

where the constants const_3 and const_4 do not depend on R, T, μ, provided $r_{\max}$ is well defined. If F is exponential (i.e. for Rayleigh fading) and $l(r)$ given by (16.1) then $\text{const}_3 = 1/\sqrt{2K(\beta)}$ and $\text{const}_4 = 1/\sqrt{2eK(\beta)}$.

Proof. The result for general fading follows from Lemma 16.2.9. The constants for the exponential case can be evaluated by (16.8). □

Remark 16.3.8. We see that the optimal distance $r_{\max}(\lambda)$ from transmitter to receiver is of the order of the distance to the nearest neighbor of the transmitter, namely $1/(2\sqrt{\lambda})$, when $\lambda \to \infty$. Notice also that for Rayleigh fading and $l(r)$ given by (16.1) we have the general relation:

$$2r^2\lambda_{\max}(r) = r_{\max}(\lambda)^2\lambda. \tag{16.29}$$

As before, one can show that for a general model, under some regularity conditions, $prog(r, \lambda, T)$ is continuous in r and that the maximal mean progress is attained for some positive and finite r. We skip these technicalities.

16.3.1.4 Degeneracy of Two Step Optimization

Assume for simplicity a $W = 0$ and OPL 3 path-loss (16.1). In Section 16.3.1.1, we found that for fixed r, the optimal density of successful transmissions d_{suc} is attained when the density of transmitters is equal to $\lambda_1 = \lambda_{\max} = \text{const}_1/(r^2T^{2/\beta})$. It is now natural to look for the distance r maximizing the mean progress for the network with this optimal density of transmitters. But by Proposition 16.3.4

$$\begin{aligned}
\sup_{r \geq 0} prog(r, \lambda_{\max}, T) &= \sup_{r \geq 0} r\, p_c(r, \lambda_{\max}, T) \\
&= \sup_{r \geq 0} r \frac{d_{suc}(r, \lambda_{\max}, T)}{\lambda_{\max}} \\
&= \sup_{r \geq 0} r \frac{\text{const}_2}{\text{const1}} = \infty,
\end{aligned}$$

and thus the optimal choice of r consists in taking $r = \infty$, and consequently $\lambda_{\max} = 0$. From a practical point of view, this is not of course an acceptable answer. The fact that the optimal value is $r = \infty$ might be a consequence of the fact that we took $W = 0$. But even if this is the case, the above observation suggests that for a small $W > 0$, a (possibly) finite optimal value of r would be too large from a practical point of view.

In a network-perspective, one might better optimize a more "social" characteristic of the MANET like e.g. the density of progress $d_{prog} = \lambda r p_c(r, \lambda, T)$ first in λ and then in r. However in this case one obtains the opposite degenerate answer:

$$\sup_{r \geq 0} d_{prog}(r, \lambda_{\max}, T) \quad = \quad \sup_{r \geq 0} r\, d_{suc}(r, \lambda_{\max}, T) = \sup_{r \geq 0} r \frac{\text{const}_2}{r^2 T^{2/\beta}} = 0\,,$$

which is attained for $r = 0$ and $\lambda_{\max} = \infty$.

The above analysis shows that a better receiver model is needed to study the joint optimization in the transmission distance and in λ. We propose such models in Chapter 17, where the receivers are no longer sampled as independent marks of the Poisson p.p. of potential transmitters, but belong to the point process of potential transmitters; more precisely, they are chosen among the nodes which are silenced by Aloha during the considered time slot. As we shall see in Section 17.4 these degeneracies may then vanish.

16.3.2 Optimization of the Density of Transport

16.3.2.1 Best MAP Given Some Transmission Distance

Define

$$\lambda_{\max}^{trans} = \arg\max_{0 \leq \lambda < \infty} d_{trans}(r, \lambda)$$

whenever such a value of λ exists and is unique. We have the following result.

Proposition 16.3.9. In the $\frac{\text{M}}{0+\text{M/M}}$ bipolar model with OPL 3 and $W = 0$, the unique maximum $\lambda_{\max}^{trans}$ of the density of transport $d_{trans}(r, \lambda)$ is attained at

$$\lambda_{\max}^{trans} = \frac{x^*(\beta)}{r^2 K(\beta)}, \tag{16.30}$$

where $x^*(\beta)$ is the unique solution of the integral equation

$$\int_0^\infty e^{-xv} \frac{v^{\frac{\beta}{2}-1}}{1+v^{\frac{\beta}{2}}} \mathrm{d}v = x \int_0^\infty e^{-xv} \frac{v^{\frac{\beta}{2}}}{1+v^{\frac{\beta}{2}}} \mathrm{d}v\,. \tag{16.31}$$

Proof. One obtains this characterization by differentiating (16.15) w.r.t. λ_1. □

Example 16.3.10. Consider the following model: $r = 1$, fading is Rayleigh with parameter $\mu = 1$; attenuation is OPL 3 with $A = 1$ and $\beta = 4$. One finds a unique positive solution to (16.31) which gives $\lambda_{\max}^{trans} \approx 0.157$. The associated mean throughput per node is $\tau(r, \lambda_{\max}^{trans}) \approx 0.898$. If one defines T^* by the Shannon-like formula $\tau(r, \lambda_{\max}^{trans}) = \log(1 + T^*)$, one finds $T^* \approx 0.8635$, which is a much lower SINR target than what is usually retained within this setting.

16.3.2.2 Best Transmission Distance Given a Density of Transmitters

Assume now some given intensity $\lambda_1 = \lambda p$ of transmitters. We look for the distance r which maximizes the mean density of transport, or equivalently the mean throughput $\tau(r, \lambda_1)$. We denote by

$$r_{\max}^{trans} = r_{\max}^{trans}(\lambda) = \arg\max_{r \geq 0} r\tau(r, \lambda)$$

the best transmission distance for this criterion, whenever such a value of r exists and is unique.

Proposition 16.3.11. In the $\frac{\text{M}}{0+\text{M/M}}$ bipolar model with OPL 3, the unique maximum of the density of transport $d_{trans}(r, \lambda)$ is attained at

$$r_{\max}^{trans} = \sqrt{\frac{y^*(\beta)}{\lambda K(\beta)}}\,, \tag{16.32}$$

where $y^*(\beta)$ is the unique solution of the integral equation

$$\int_0^\infty e^{-yv} \frac{v^{\frac{\beta}{2}-1}}{1+v^{\frac{\beta}{2}}} \mathrm{d}v = 2y \int_0^\infty e^{-yv} \frac{v^{\frac{\beta}{2}}}{1+v^{\frac{\beta}{2}}} \mathrm{d}v\,. \tag{16.33}$$

Proof. One obtains this characterization by differentiating (16.15) w.r.t. r. □

We do not pursue this line of thought any further. Let us nevertheless point out that the last results can be extended to more general fading models and also that the same degeneracies as those mentioned above take place.

16.3.3 Spatial Reuse in Optimized Poisson MANETs

In wireless networks, the MAC algorithm is supposed to prevent simultaneous neighboring transmissions from occurring, as often as possible, since such transmissions are likely to produce collisions. Some MAC protocols (as e.g. CSMA considered in Section 18.1) create exclusion zones to protect scheduled transmissions. Aloha creates a *random* exclusion disc around each transmitter. By this we mean that for an arbitrary radius there is some non-null probability that all the nodes in the disk with this radius do not transmit at a given time slot.

Definition 16.3.12. We define the *mean exclusion radius* as the mean distance from a typical transmitter to its nearest concurrent transmitter

$$R_{excl} = \mathbf{E}^0\Big[\min_{i \neq 0}\{|X_i| : e_i = 1\}\Big]\,.$$

Proposition 16.3.13. For the $\frac{\text{GI}}{W+\text{M/GI}}$ bipolar model, we have

$$R_{excl} = R_{excl}(\lambda_1) = \frac{1}{2\sqrt{\lambda_1}} = \frac{1}{2\sqrt{\lambda p}}\,. \tag{16.34}$$

Proof. The probability that the distance from the origin to the nearest point in the Poisson p.p. Φ^1 of intensity $\lambda_1 = \lambda p$ is larger than s is equal to $e^{-\lambda_1 \pi s^2}$ (cf. Example 1.4.7 in Volume I). Thus we have $R_{excl} = \int_0^\infty e^{-\lambda_1 \pi s^2}\, \mathrm{d}s$. □

Here are two questions pertaining to an optimized scenario and which can be answered using the results of the previous sections:

- If r is given and p is optimized, how does the resulting R_{excl} compare to r?
- If λ is given and r is optimized, how does the resulting r compare to R_{excl}?

We address these questions in a unified way using a notion of spatial reuse analogous to the concept of spectral reuse used in cellular networks.

Definition 16.3.14. The *spatial reuse factor* of the bipolar Aloha MANET is the ratio of the distance r between the transmitter and the receiver and the mean exclusion radius R_{excl}.

So if the spatial density of transmitters in this Aloha MANET is λ_1, then

$$S_{reuse} = S_{reuse}(\lambda_1, r) = \frac{r}{R_{excl}} = 2r\sqrt{\lambda_1}. \tag{16.35}$$

Here are a few illustrations.

Example 16.3.15. Consider the $\frac{\text{GI}}{W+\text{M/GI}}$ bipolar model of Section 16.2.1. Assume that the path-loss model is OPL 3 and that $W = 0$. Assume the fixed coding scenario of Section 16.2.2 i.e., the success of a transmission requires a SINR larger than or equal to T. We deduce from Proposition 16.3.4 that the spatial intensity of transmitters that maximizes the density of successful transmissions is $\lambda_{\max} = \text{const}_1/(r^2 T^{2/\beta})$. Hence by (16.34)

$$R_{excl}(\lambda_{\max}) = \frac{1}{2\sqrt{\lambda_{\max}}} = r\frac{T^{1/\beta}}{2\sqrt{\text{const}_1}}, \tag{16.36}$$

so that at the optimum, the spatial reuse

$$S_{reuse} = \frac{2\sqrt{\text{const}_1}}{T^{1/\beta}}, \tag{16.37}$$

is independent of r. For example, for $\beta = 4$ and Rayleigh fading, we can use the fact that $\text{const}_1 = 1/K(\beta)$ to evaluate the last expressions. For a SINR target of $T = 10$dB, $R_{excl}(\lambda_{\max}) \approx 1.976r$. Equivalently $S_{reuse} \approx 0.506$. In order to have a spatial reuse larger than 1, one needs a SINR target less than $\left(2\sqrt{2}/\pi\right)^4 = 0.657$, that is less than -1.82 dB.

Example 16.3.16. Consider the Poisson bipolar network model of Section 16.2.1 with general fading, path-loss model (16.1) and $W = 0$ and target SINR T. Assume that the spatial density of transmitters is fixed and equal to λ. Let $r_{\max}(\lambda)$ denote the transmitter-receiver distance which maximizes the mean progress. We get from Proposition 16.3.7 that at the optimum r,

$$S_{reuse} = \frac{\text{const}_3}{2T^{1/\beta}}\,, \tag{16.38}$$

for all values of λ. For $\beta = 4$ and Rayleigh fading, if we pick a SINR target of 10 dB, then $S_{reuse} \approx 0.358$ only. Similarly, $S_{reuse} > 1$ iff $T < (2/K(\beta))^{\beta/2}$. For $\beta = 4$, this is iff $T < 0.164$ or equivalently T less than -7.84 dB.

Example 16.3.17. Assume the Poisson bipolar network model of Section 16.2.1 with Rayleigh fading, path-loss model (16.1) and $W = 0$. Consider the optimal coding scenario with Shannon throughput of Section 16.2.3. The distance between transmitter and receiver is r. We deduce from Proposition 16.3.9 that in terms of density of transport, the best organization of the MANET is that where the spatial intensity of transmitters is $\lambda_{\max}^{trans} = x(\beta)/r^2K(\beta)$. Hence, at the optimum,

$$R_{excl} = r\frac{1}{2}\sqrt{\frac{K(\beta)}{x^*(\beta)}}\,, \tag{16.39}$$

so that

$$S_{reuse} = 2\sqrt{\frac{x^*(\beta)}{K(\beta)}}\,, \tag{16.40}$$

a quantity that again does not depend on r. For $\beta = 4$, one gets $x^*(\beta) \approx 0.771$, so that $R_{excl} \approx 1.27r$ and $S_{reuse} \approx 0.790$.

Example 16.3.18. Consider the same scenario as in the last example but assume now that the intensity of transmitter is λ fixed. Proposition 16.3.11 shows that in order to maximize the mean throughput, in the optimal scenario, the transmitter-receivers distance $r_{\max}^{trans}$ is such that

$$S_{reuse} = 2\sqrt{\frac{y^*(\beta)}{K(\beta)}}\,. \tag{16.41}$$

For $\beta = 4$, $y^*(\beta) \approx 0.122$ and $S_{reuse} \approx 0.314$.

16.4 Opportunistic Aloha

In the basic Spatial Aloha scheme, each node tosses a coin to access the medium independently of the fading variables. It is clear that something more clever can be done by combining the random selection of transmitters with the occurrence of good channel conditions. The general idea of *opportunistic Aloha* is to select the nodes with the channel fading larger than a certain threshold as transmitters in the reference time slot. This threshold may be deterministic or random (we assume fading variables to be observable which is needed for this scheme to be implementable; for more details on implementation issues see (Baccelli, Blaszczyszyn, and Mühlethaler 2009a)).

16.4.1 Model Definition

More precisely, in a Poisson MANET, opportunistic Aloha with random MAC threshold can be described by an i.m. Poisson p.p. $\widetilde{\Phi} = \{(X_i, \theta_i, y_i, \mathbf{F}_i)\}$, where $\{(X_i, y_i, \mathbf{F}_i)\}$ is as described in items (1)–(4) on the enumerated list in Section 16.2, with item (2) replaced by:

(2') The medium access indicator e_i of node i ($e_i = 1$ if node i is allowed to transmit and 0 otherwise) is the following function of the virtual power F_i^i: $e_i = \mathbb{1}(F_i^i > \theta_i)$, where $\{\theta_i\}$ are new random i.i.d. marks, with a generic mark denoted by θ. Special cases of interest are

- that where θ is constant,
- that where θ is exponential with parameter ν.

In this latter case one can obtain a closed-form expression for the coverage probability.

We still assume that for each i, the components of (F_i^j, j) are i.i.d. Note that $\{e_i\}$ are again i.i.d. marks of the point process $\widetilde{\Phi}$ (which of course depend on the marks $\{\theta_i, F_i^i\}$).

In what follows, we also assume that for each i, the coordinates of (F_i^j, j) are i.i.d. (cf. assumption (4) of the plain Aloha model of Section 16.2).

The set of transmitters is hence a Poisson p.p. Φ^1 (different from that in Section 16.2) with intensity $\lambda \mathbf{P}(F > \theta)$ (where F is a typical F_i^i and θ a typical θ_i, with (F, θ) independent). Thus in order to compare opportunistic Aloha to the plain Aloha described in Section 16.2, one can take $p = \mathbf{P}\{\, F > \theta \,\}$, where p is the MAP of plain Aloha, which guarantees the same density of (selected) transmitters at a given time slot.

16.4.2 Coverage Probability

Note that the virtual power emitted by any node to its receiver, given it is selected by opportunistic Aloha (i.e. given $e_i = 1$) has for law the distribution of F conditional on $F > \theta$. Below, we denote by F_θ a random variable with this law.

By the independence of (F_i^j, j), the virtual powers F_i^j, $j \neq i$, toward other receivers are still distributed as F. Consequently, the *interference I_i^1 experienced at any receiver has exactly the same distribution as in plain Aloha*. Hence, the probability for a typical transmitter to cover its receiver can be expressed by the following three independent generic random variables

$$\widehat{p}_c(r, \lambda_1, T) = \mathbf{P}\{\, F_\theta > Tl(r)(I^1 + W) \,\}\,, \tag{16.42}$$

where I^1 is the generic SN generated by Poisson p.p. with intensity $\lambda_1 = \mathbf{P}\{F > \theta\}\lambda$ and (non-conditioned) fading variables F_j (as in (16.3)). Using the Kendall-like notation of Section 5.3 in Volume I, we can see $\widehat{p}_c(r, \lambda_1, T)$ as the coverage probability in some $\frac{\mathrm{GI}_1}{W+\mathrm{M/GI}_2}$ model in which the distribution of interfering virtual powers (GI_2) is different from that of the useful signal (GI_1).

16.4.2.1 Rayleigh Fading and Exponential Threshold Case

We begin our analysis of opportunistic Aloha by a comparison of $\widehat{p}_c(r, \lambda_1, T)$ and $p_c(r, \lambda_1, T)$ of plain Aloha when all parameters (T, W, r, etc.) are the same. To get more insight we assume first Rayleigh fading. In this case, F is exponential with parameter μ and since θ is independent of F, by the lack of memory property of the exponential variable, given that $F > \theta$, the variables θ and $F - \theta$ are independent. Moreover, the conditional distribution of $F - \theta$ given $F > \theta$ is also exponential with parameter μ. Denote

by $\widetilde{\theta}$ the conditional law of θ given that $F > \theta$. Consequently in the Rayleigh fading case (16.42) can be rewritten as

$$\widehat{p}_c(r, \lambda_1, T) = \mathbf{E}\left[e^{-\mu\left(Tl(r)(I^1+W)-\widetilde{\theta}\right)^+}\right], \tag{16.43}$$

where $I^1, W, \widetilde{\theta}$ are independent random variables with distributions described above and $a^+ = \max(a, 0)$. Comparing (16.43) to the middle expression in (16.5) it is clear that the opportunistic scheme does better than plain Aloha with MAP p such that $p = \mathbf{P}(F > \theta) = \mathbf{E}\left(e^{-\mu\theta}\right) = \mathcal{L}_\theta(\mu)$. This follows from the fact that the intensity of transmitters is the same in both cases, which implies that the laws of interference coincide in both formulas.

In order to evaluate how much better opportunistic Aloha does in the Rayleigh case, we now focus on the case when θ is exponential (of parameter ν). Note that in this case, $\widetilde{\theta}$ is also exponential of parameter $\mu + \nu$. This is thus a $\frac{\mathrm{M}_1}{W+\mathrm{M}/\mathrm{M}_2}$ model.

Proposition 16.4.1. Assume the Poisson bipolar network model of Section 16.2.1 with opportunistic Aloha MAC given by (2') in Section 16.4.1. Assume Rayleigh fading (exponential F with parameter μ) and exponential distribution of θ with parameter ν. Then

$$\widehat{p}_c(r, \lambda_1, T) = \frac{\mu+\nu}{\nu}\mathcal{L}_{I^1}(\mu Tl(r))\mathcal{L}_W(\mu Tl(r)) - \frac{\mu}{\nu}\mathcal{L}_{I^1}((\mu+\nu)Tl(r))\mathcal{L}_W((\mu+\nu)Tl(r)),$$

where $\mathcal{L}_{I^1}$ is given by (16.6) with $\lambda_1 = \lambda\nu/(\mu+\nu)$. If moreover $W \equiv 0$ and the OPL 3 model (16.1) is assumed, then

$$\widehat{p}_c(r, \lambda_1, \nu) = \frac{\mu+\nu}{\nu}\exp\{-\lambda_1 T^{2/\beta} r^2 K(\beta)\} - \frac{\mu}{\nu}\exp\left\{-\lambda_1\left(\frac{(\mu+\nu)T}{\mu}\right)^{2/\beta} r^2 K(\beta)\right\},$$

with λ_1 as above.

Proof. Note that Φ^1 is a Poisson p.p. of intensity $\lambda\nu/(\nu+\mu)$ and $\widetilde{\theta}$ is exponential of parameter $\mu+\nu$. Using (16.43) we have hence

$$\begin{aligned}
&\widehat{p}_c(r, \lambda_1, T)\\
&= \mathbf{E}\Big[\int_0^{Tl(r)(I^1+W)} (\mu+\nu)e^{-(\mu+\nu)x}e^{-\mu\left(Tl(r)(I^1+W)-x\right)}\mathrm{d}x\Big] + \mathbf{E}\Big[\int_{Tl(r)(I^1+W)}^{\infty} (\mu+\nu)e^{-(\mu+\nu)x}\mathrm{d}x\Big]\\
&= \frac{\mu+\nu}{\nu}\mathbf{E}\Big[e^{-\mu Tl(r)(I_1+W)} - e^{-(\mu+\nu)Tl(r)(I_1+W)}\Big] + \mathbf{E}\Big[e^{-(\mu+\nu)Tl(r)(I^1+W)}\Big],
\end{aligned}$$

which completes the proof. □

Note that, as expected, when letting ν tend to infinity, under mild conditions, the first expression of the last proposition tends to $\mathcal{L}_{I^1}(\mu Tl(r))\mathcal{L}_W(\mu Tl(r))$, namely the formula (16.7) of plain Aloha with $\lambda_1 = \lambda$ or equivalently $p = 1$.

16.4.2.2 General Case

For a general fading and distribution of θ (for instance deterministic θ, in which case obviously $\widetilde{\theta} = \theta$), the following result can be proved along the same lines as Proposition 16.2.4.

Proposition 16.4.2. Assume the Poisson bipolar network model of Section 16.2.1 with opportunistic Aloha MAC given by (2') in Section 16.4.1 for some general distribution of F and θ. Take the same assumptions as in Proposition 16.2.4 except that the condition on F is replaced by the following one

- $\mathbf{E}[F_\theta] < \infty$ and F_θ admits a square integrable density.

Then

$$\widehat{p}_c(r, \lambda_1, T) = \int_{-\infty}^{\infty} \mathcal{L}_{I^1}\left(2i\pi l(r)Ts\right) \mathcal{L}_W\left(2i\pi l(r)Ts\right) \frac{\mathcal{L}_{F_\theta}(-2i\pi s) - 1}{2i\pi s} \mathrm{d}s\,. \tag{16.44}$$

Proof. It follows immediately from Equation (16.42) and Corollary 12.2.2 in Volume I. □

In the case of Rayleigh fading and deterministic θ, the last theorem can be used since F_θ is then the convolution of a deterministic distribution (with mean θ) and an exponential one (with parameter μ); this satisfies the assumptions of the proposition. In this case, $\mathcal{L}_{F_\theta}(s) = e^{-s\theta}\frac{\mu}{\mu+s}$. Obviously it can also be used when θ is exponentially distributed with intensity ν. In particular, for Rayleigh fading, we have $\mathcal{L}_{F_\theta}(s) = \frac{\mu+\nu}{\mu+\nu+s}\frac{\mu}{\mu+s}$.

Example 16.4.3. Assume Rayleigh fading. In Figure 16.3 we plot the density of successful transmissions d_{suc} in function of the parameter ν for three different scenarios:

(1) Opportunistic Aloha with a deterministic threshold θ with value $1/\nu$, where $d_{suc} = \lambda_1 \widehat{p}_c(r, \lambda_1, \nu)$, with $\lambda_1 = \lambda e^{-\frac{\mu}{\nu}}$ and $\widehat{p}_c(r, \lambda_1, \nu)$ given by Proposition 16.4.2;
(2) Opportunistic Aloha with a random exponential threshold with parameter ν, where $d_{suc} = \lambda_1 \widehat{p}_c(r, \lambda_1, \nu)$, with $\lambda_1 = \frac{\lambda\nu}{\mu+\nu}$ and $\widehat{p}_c(r, \lambda, \nu)$ given by Proposition 16.4.1;
(3) Plain Aloha where $d_{suc} = 1/(eK(\beta)r^2T^{2/\beta})$ is the optimal density of successful transmissions as obtained in Proposition 16.3.2 (this is of course a constant in ν).

In the particular case considered in this figure, the density of transmitters covering their target receiver is approx. 56% larger in the optimal opportunistic scheme with exponential threshold than in plain Aloha and 134% larger in the deterministic case.

It may look surprising that the curves for the random exponential and the deterministic threshold cases (1 and 2 above) differ so much. One should bear in mind the fact that the two associated MAPs are quite different: $p = \frac{\nu}{\mu+\nu}$ in the former case and $p = e^{-\frac{\mu}{\nu}}$ in the latter.

Example 16.4.4 (Rayleigh versus Rician fading). (Example 16.3.5 continued).

Figure 16.4 compares the density of success of opportunistic Aloha for Rayleigh and Rician ($q = 1/2$) fading. (The Rician case with $q = .9$ has thresholds θ larger than .9 and leads to very small densities of success; it is not displayed). The two curves are based on Proposition 16.4.2. Note first that for the two considered cases the density of transmitters are quite different: $(\exp(-\theta)$ in the Rayleigh case and $\exp(-2\theta)$ in the Rician case, for $\theta > 1/2)$, which explain why the shapes of the curves are so different. Here, we see

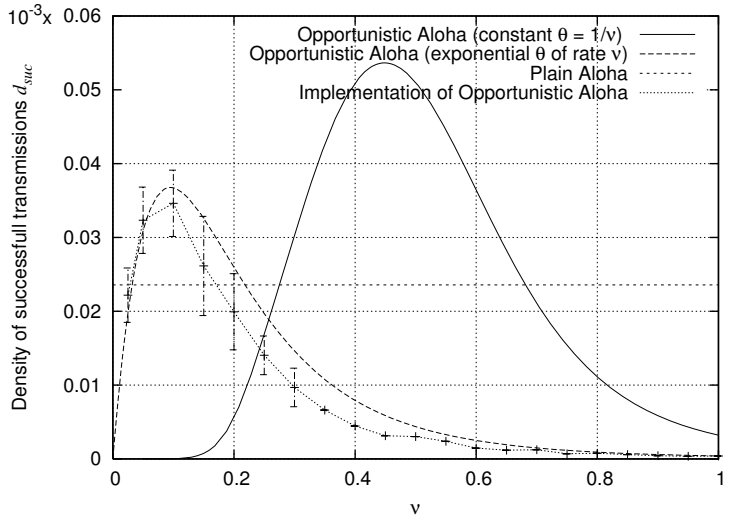

Fig. 16.3 The density of successful transmissions d_{suc} of opportunistic Aloha for various choices of θ. The propagation model is (16.1). We assume Rayleigh fading with mean 1, $W = 0$, $\lambda = 0.001$, $T = 10$dB, $r = \sqrt{1/\lambda}$ and $\beta = 4$. For comparison the constant value $\lambda_{\max} p_c(r, \lambda_{\max})$ of plain Aloha is plotted.

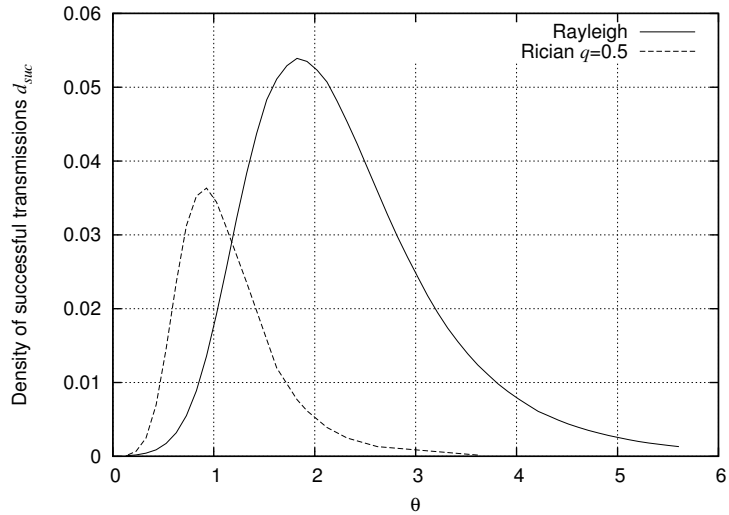

Fig. 16.4 Density of successful transmissions d_{suc} for opportunistic Aloha in function of the deterministic threshold θ in the Rayleigh and Rician (with $q = 1/2$) fading cases; other parameters as in Figure 16.2.

the opposite phenomenon compared to what was observed above: when properly optimized, opportunistic Aloha does better when the fading variance increases, namely does much better for Rayleigh fading than for Rician fading with $q = 1/2$. This is in fact quite natural since the aim of opportunistic Aloha is to leverage diversity: more fading diversity/variance is hence beneficial to this protocol when properly tuned.

16.4.3 Shannon Throughput

We consider now the adaptive coding scenario and the Shannon throughput introduced in Section 16.2.3. The following result on the throughput of opportunistic Aloha is a corollary of Proposition 16.4.2 and for-

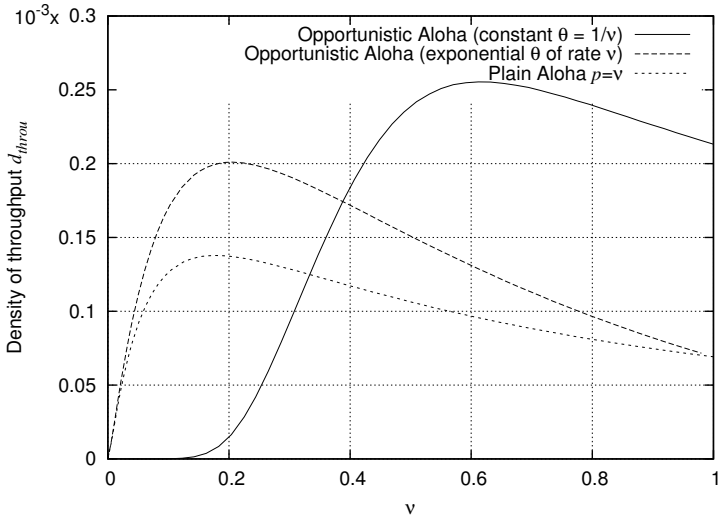

Fig. 16.5 The density of throughput of opportunistic Aloha as a function of its parameter ν and that of plain Aloha. Assumptions are as in Figure 16.3.

mula (16.13).

Corollary 16.4.5. Under the assumptions of Proposition 16.4.2, the mean Shannon throughput of the typical transmitting node is

$$\widehat{\tau} = \int_0^{\infty} \int_{-\infty}^{\infty} \mathcal{L}_{I^1}\left(2i\pi vsl(r)\right) \mathcal{L}_W\left(2i\pi vsl(r)\right) \frac{\mathcal{L}_{F_\theta}(-2i\pi s) - 1}{2i\pi s(1+v)} \, \mathrm{d}s\mathrm{d}v \, . \tag{16.45}$$

Since the assumptions of the last result hold in both deterministic and exponential θ case for Rayleigh fading, we can use (16.45) to evaluate the density of throughput in both cases.

Example 16.4.6. Figure 16.5 plots the density of throughput d_{throu} for Rayleigh fading and the same three cases of θ as in Example 16.4.3. In the particular case considered in this figure, the density of throughput is approx. 48% larger in the optimal opportunistic scheme with exponential threshold than in plain Aloha and 93% larger in the deterministic case.

Remark: The deterministic threshold case seems to always outperform the exponential threshold case when both are tuned optimally.

16.5 Conclusion

The two main assumptions of the chapter are that time is slotted and that the receivers are at some predefined from their transmitters. The last assumption is relaxed in the next chapter. Let us conclude with a few comments on how to relax the slotted time assumption.

Time–slots are required in e.g. TDMA (Time Division Multiple Access) and one of the well known advantages of Aloha is that it does not require slotted time. In order to model non-slotted Aloha, one has to

take into account the fact that interference (and thus SINR) can vary during a given transmission as some other transmissions may start or terminate. A more detailed packet reception model is hence needed. For example, if one assumes a coding with sufficient interleaving, then one can consider that it is the *averaged SINR*, where the averaging is over the whole packet reception period, that determines the success of reception. In this case a mathematical analysis of non-slotted Aloha is possible e.g. along the lines presented in (Błaszczyszyn and Radunović 2007; Błaszczyszyn and Radunović 2008); see also a forthcoming paper (Błaszczyszyn and Mühlethaler 2010).

17

Receiver Selection in Spatial Aloha

17.1 Introduction

In this chapter, we consider a few possible scenarios where the receiver of a given transmitter is not necessarily at distance r, as in the Poisson bipolar model (cf. Section 16.2.1) considered so far. In a MANET, some routing algorithm (cf. Section 25.3.1.2) specifies the receivers(s) (relay node(s)) of each given transmitter. The joint analysis and the joint design of MAC and routing are difficult tasks even if we assume the simplest MAC (Aloha). We shall come back to such cross-layer routing schemes in Chapter 22. In this chapter, we make a first step in this direction by proposing receiver models based on simplifying assumptions on the routing layer. Specifically, we assume one of the following *routing principles*:

- *Each transmitter selects its receiver as close by as possible.* We saw in Section 16.3.1.4, in one of the two-step optimizations (with respect to λ and then r), that it is in some sense best for a transmitter to select his receiver as close by as possible. This justifies the class of routing models which is considered in Section 17.2 and which consist in making as small as possible hops.
- *Each transmitter targets all available (potential) receivers.* This assumption, of interest in multicast scenarios, is considered in Section 17.3.
- *Each transmitter targets the most distant successful receiver.* In this scenario, as in the previous one, each transmitter targets all available receivers; however, some selection policy is applied among the nodes which successfully receive the packet. One selects the node optimizing the packet progress in a given direction as the relay node. All other nodes discard the packet (this is not a broadcast scheme). This *opportunistic* scenario, in which no specific receiver is prescribed in advance by the routing algorithm, and where one selects the best hop at the given time step, is considered in Section 17.4.

The above routing principles are considered in conjunction with the following models regarding receiver locations:

- The *independent receiver model*, where the *potential receivers* form a stationary p.p. Φ_0 with intensity λ_0, independent of the transmitter p.p. Φ. This model, considered in Section 17.2.1,

corresponds to the situation where the nodes of Φ transmit to randomly located nodes (access points or relay stations) which are external to the MANET. Several further specifications of this model are of interest. For example:

  - The *independent Poisson receiver model*, where Φ_0 is some homogeneous Poisson p.p.
  - The *independent honeycomb receiver model*, where Φ_0 is some stationary hexagonal grid; cf. Example 4.2.5 in Volume I.
  - The *independent Poisson + periodic receiver model*, where Φ_0 is the superposition of two independent p.p.s, a Poisson p.p. of intensity $\lambda_0 - \epsilon > 0$, and a stationary grid (e.g. the hexagonal one) of intensity $\epsilon > 0$. The presence of the periodic stations provides an upper-bound on the distance to the nearest neighbor, which can be arbitrarily large in the pure Poisson receiver model. The advantages of this solution will be discussed in Section 17.5.

- The *MANET receiver model*, where the transmitters of the MANET Φ choose their receivers in the original set Φ of nodes of the MANET. Two scenarios are considered in Section 17.2.2.
  - The nodes of Φ not allowed to access the shared medium form the set of potential receivers; i.e., we have $\Phi_0 = \Phi^0 = \Phi \setminus \Phi^1$. Note that this scenario assumes some kind of MAC-aware routing, since the pattern of actual receivers depends on the current MAC status of the nodes in MANET.
  - All the nodes of the MANET are considered as potential receivers; i.e. $\Phi_0 = \Phi$. In this case each transmitter targets some nodes in the MANET without knowing their MAC status. This assumption requires additional specification of what happens if the picked receiver is also transmitting.

The last section of the chapter (§ 17.5) is devoted to time–space scenarios and to the evaluation of the *local delays*, which are the random numbers of slots required to transmit a packet in the packet model. In most practical cases, these local delays are finite random variables but they have unexpected properties: in many cases, their mean value is infinite; in certain cases, they exhibit an interesting phase transition phenomenon which we propose to call the *wireless contention phase transition* and which has several incarnations. All this is central for the analysis of time–space routing in Part V.

17.2 Nearest Receiver Models

Assume that the potential receivers form some stationary p.p. Φ_0, which is either external to Φ, as in the independent receiver model, or a subset of Φ, as in the MANET receiver model.

The common assumption of the present section is that each transmitter selects the *nearest point* of Φ_0 as its receiver.

Formally, this consists in replacing the assumption concerning the distribution of $\{y_i\}$ in (3) of the definition of the Poisson bipolar model of Section 16.2.1 by:

(3') The receiver y_i of the transmitter $X_i \in \Phi$ is the point $y_i = Y_i^* = \arg\min_{Y_i \in \Phi_0, Y_i \neq X_i} \{|Y_i - X_i|\}$.

In such a generic nearest receiver (NR) routing, we have to assume that the arg min is almost surely well defined. The (technical) condition $Y_i \neq X_i$ that the receiver is not located at the same place as its transmitter is automatically satisfied for all the examples considered in what follows, except the model of Section 17.2.2.

Note that $\widetilde{\Phi}' = \{X_i, e_i, y_i = Y_i^*, \mathbf{F}_i\}$ is no longer an independently marked p.p., since the marks $\{Y_i^*\}$ jointly depend on Φ_0. By specifying the joint distribution of Φ and Φ_0, we have particular incarnations of this generic model.

NR routing also requires some additional specifications on what happens if two or more transmitters pick the same receiver. Our analysis applies to the following two situations: either the receivers are capable of receiving more than one (in fact, an arbitrarily large) number of transmissions at the same time, or the target SINR T is such that $T > 1$, which excludes such multiple receptions (cf. Remark 17.3.2).

17.2.1 Independent Receiver Models

In the independent receiver model, the nearest receiver y_i is almost surely well defined for all i (cf. Lemma 4.2.2 in Volume I).

It is easy to calculate the probability of successful reception $p_c(\text{INR}, \lambda_1, T)$ in this Independent Nearest Receiver (INR) model, provided one knows the distribution of the distance from the orign to the nearest point of Φ_0. For example:

Proposition 17.2.1. The coverage probability in the Poisson INR model of intensity λ_0 is equal to

$$p_c(\text{Poisson INR}, \lambda_1, T) = 2\pi\lambda_0 \int_0^\infty r \exp(-\lambda_0 \pi r^2) p_c(r, \lambda p, T)\, \mathrm{d}r\,, \tag{17.1}$$

where $p_c(r, \lambda p, T)$ is the probability of coverage at distance r, evaluated for the Poisson bipolar model under the same assumptions except for the receiver location.

Proof. One can easily evaluate the (tail of the) distribution function of the distance from the transmitter $X_0 = 0$ to its receiver Y_0^* under $\mathbf{P}^0$ (recall, $\mathbf{P}^0$ is the Palm probability associated to the p.p. Φ of the nodes in MANET; cf. Section 16.2.2)

$$\begin{aligned} \mathbf{P}^0\{\, |Y_0^*| > r \mid e_0 = 1\,\} &= \mathbf{P}^0\{\, \min_{Y_i \in \Phi_0} \{|Y_i|\} > r \mid e_0 = 1\,\} \\ &= \mathbf{P}^0\{\, \Phi_0\{B_0(r)\} = 0 \mid e_0 = 1\,\} \\ &= \mathbf{P}\{\, \Phi_0\{B_0(r)\} = 0\,\} = e^{-\lambda_0 \pi r^2}\,, \end{aligned} \tag{17.2}$$

where $B_x(r)$ is the ball of radius r centered at x and where the last but one equality is due to the independence of Φ_0 and Φ (cf. also Example 1.4.7 in Volume I). Thus the result follows when conditioning on $|Y_0^*|$ and using the independence of Φ_0 and Φ. □

In the same vein, for the independent honeycomb receiver model,

$$p_c(\text{Hex INR}, \lambda_1, T) = \int_{\mathcal{C}} p_c(|x|, \lambda p, T)\, \mathrm{d}x\,, \tag{17.3}$$

where $\mathcal{C}$ is the hexagon centered at the origin of the plane of side length $\Delta = \sqrt{(2\pi\sqrt{3})/\lambda_0}$ (see Example 4.2.5 in Volume I).

The other MANET performance metrics considered for the bipolar network model can be evaluated as well. The general formulas (16.13), (16.14) for the mean Shannon throughput and its Laplace transforms

remain true with the appropriate coverage probabilities. Similarly the expressions (16.21) and (16.23), for the spatial density of success and of throughput, remain valid. However, the evaluation of the mean progress and transport, as well as their densities have to be modified, due to the fact that the distance to the receiver is now a random variable. For example, for the Poisson INR model, we get the following corollary from the proof of Proposition 17.2.1.

Proposition 17.2.2. In the Poisson INR model of intensity λ_0, the mean progress and the mean transport are respectively equal to:

$$prog(\text{Poisson INR}, \lambda_1, T) \quad = \quad 2\pi\lambda_0 \int_0^\infty r^2 \exp(-\lambda_0 \pi r^2) p_c(r, \lambda p, T)\, \mathrm{d}r\,, \tag{17.4}$$

and

$$trans(\text{Poisson INR}, \lambda_1) \quad = \quad 2\pi\lambda_0 \int_0^\infty r^2 \exp(-\lambda_0 \pi r^2) \tau(r, \lambda_1)\, \mathrm{d}r\,. \tag{17.5}$$

With such modified mean progress and transport, the formulas for the spatial densities can be obtained by multiplication by λ_1 (cf. formulas (16.22) and (16.24) for the original bipolar model).

17.2.2 MANET Receiver Models

In the MANET receiver model, the following two situations aiming at making the smallest possible hops are of particular interest:

- In the *MANET Nearest Receiver* (MNR) model, each transmitter picks the nearest node of Φ which is a receiver at the considered time slot as its next relay.
- In the *MANET Nearest Neighbor* (MNN) model, we assume that each transmitter picks the nearest node of Φ (other than itself) as its receiver, regardless of whether the latter is authorized to transmit or not at the considered time slot. As already mentioned, this requires additional specification of what happens if
  - (a) a node is chosen as the receiver of two or more different transmitters;
  - (b) a node which is chosen as receiver by some transmitter is itself a transmitter (i.e. $y_i \in \Phi^1$).

  For simplicity, in what follows we suppose that $T > 1$, so that if (a) happens, then at most one of the transmitters is successful and the others fail (cf. Remark 17.3.2). If (b) happens we assume that the transmission fails.[1]

From the properties of independent thinnings of Poisson p.p. (cf. Proposition 1.3.5 in Volume I), for the Aloha MAC, at a given time slot, the transmitters Φ^1 and the nodes which are not authorized to transmit,

[1] In practice the transmitted signal power exceeds the received signal power by at least 40dB, often about 100dB, so T would have to be extremely small for (b) to lead to a successful transmission.

denoted by Φ^0, form two independent Poisson p.p.s. Thus, the probability of successful reception in the MNR model is equal to that for the Poisson INR model:

$$p_c(\text{MNR}, \lambda_1, T) = p_c(\text{Poisson INR}, \lambda_1, T)\,, \tag{17.6}$$

with $\lambda_0 = (1-p)\lambda$. This extends to other characteristics (mean progress, mean transport, spatial densities) considered in Section 17.2.1.

In order to evaluate the probability of successful reception in the MNN model, we also condition on the location of the nearest neighbor $y_0 = Y_0^*$. However this conditioning modifies the distribution of the interferers.

Proposition 17.2.3. The coverage probability in the MNN model is equal to

$$p_c(\text{MNN}, \lambda_1, T) = 2\pi\lambda p(1-p) \int_0^\infty r \exp(-\lambda\pi r^2) p_c^*(r, \lambda p, T)\, \mathrm{d}r\,,$$

where the conditional coverage probability $p_c^*(r, \lambda p, T)$, given the nearest node is at distance r and is a receiver, can be expressed using independent random variables $F, W, I^{*1}(r)$ as

$$p_c^*(r, \lambda p, T) = \mathbf{P}\{\, F \geq Tl(r)(I^{*1}(r) + W)\,\}\,.$$

In this formula, the SN $I^{*1}(r)$ has for Laplace transform

$$\mathcal{L}_{I^{*1}(r)}(s) = \exp\Big\{-\lambda_1\pi \int_0^\infty t\Big(1 - \mathcal{L}_F(s/l(t))\Big)\,\mathrm{d}t + \lambda_1 \int_{-\pi/2}^{\pi/2} \int_{2r\cos(\theta)}^\infty t\Big(1 - \mathcal{L}_F(s/l(t))\Big)\,\mathrm{d}t\mathrm{d}\theta\Big\}\,. \tag{17.7}$$

Proof. We condition on the location of the nearest neighbor $y_0 = Y_0^*$ of $X_0 = 0$ under $\mathbf{P}^0$. By Slivnyak's theorem (cf. Theorem 1.4.5 in Volume I and also Remark 2.1.7 in Volume I), we know that, under $\mathbf{P}^0$, the nodes of $\Phi \setminus \{X_0\}$ are distributed as those of the homogeneous Poisson p.p. Thus the distance $|Y_0^* - X_0| = |Y_0^*|$ has the same distribution as in the Poisson INR model with $\lambda_0 = \lambda$; see (17.2). However, in the MNN model, given some particular location of $y_0 = Y_0^*$, one has to take the following fact into account: there are *no MANET nodes* (thus, in particular, no interferers) in $B_0(|y_0|)$. Consequently, under $\mathbf{P}^0$, given $Y_0^* = y_0$, the value of I_0^1 in (16.2) is no longer distributed as the generic SN I^1 of Section 16.2.2, which was driven by the stationary Poisson p.p. of intensity λ_1, but as the SN of Φ^1 given that there are no nodes of Φ in $B_0(|y_0|)$. Note that the location y_0 at which we evaluate this last SN is on the boundary (and not in the center) of the empty ball. By the strong Markov property of Poisson p.p. (cf. Example 1.5.2 and Proposition 1.5.3 in Volume I), the distribution of a Poisson p.p. given that $B_0(|y_0|)$ is empty is equal to the distribution of the (non-homogeneous) Poisson p.p. with intensity equal to 0 in $B_0(|y_0|)$ and λ_1 outside this ball. Putting these arguments together and exploiting the rotation invariance of the picture, we conclude the proof. □

Other characteristics can be evaluated in a way similar to what was done for the Poisson INR model in Section 17.2.1.

In what follows we focus on the MNR model. In particular, we want to optimize the density of successful transmissions $d_{suc}(\text{MNR}, \lambda p, T)$ and the density of progress $d_{prog}(\text{MNR}, \lambda p, T)$ w.r.t. the MAP p. Recall from Section 16.3.1.4, that the joint optimization of $d_{prog}(\text{MNR}, \lambda p, T)$ in r and λ (or in p given λ) is degenerate in the Poisson bipolar model. For simplicity we consider only Rayleigh fading. The next result follows from (16.8):

Proposition 17.2.4. Consider the MNR model with Rayleigh fading, OPL 3 path loss model and no noise ($W = 0$). The density of successful transmission and the density of progress in this model are equal to

$$d_{suc}(\text{MNR}, \lambda p, T) = \frac{\lambda p(1-p)}{(1-p) + pT^{2/\beta}K(\beta)/\pi}\,, \tag{17.8}$$

$$d_{prog}(\text{MNR}, \lambda p, T) = \frac{\sqrt{\lambda}p(1-p)}{2\Big((1-p) + pT^{2/\beta}K(\beta)/\pi\Big)^{3/2}}\,. \tag{17.9}$$

It is easy to see that both densities d_{suc} and d_{prog} attain their maximal values for some $0 < p < 1$ that does not depend on λ. For example the density of success admits the following optimal tuning of the parameter p.

Corollary 17.2.5. Under the assumptions of Proposition 17.2.4, we have

$$\begin{aligned}
\arg\max_{0\le p\le 1} d_{suc}(\text{MNR}, \lambda p, T) &= \frac{1}{1 + T^{1/\beta}\sqrt{K(\beta)/\pi}}\,,\\
\max_{0\le p\le 1} d_{suc}(\text{MNR}, \lambda p, T) &= \frac{\lambda}{\Big(1 + \frac{1}{T^{1/\beta}\sqrt{K(\beta)/\pi}}\Big)\Big(1 + T^{1/\beta}\sqrt{K(\beta)/\pi}\Big)}\,.
\end{aligned}$$

17.3 Multicast Mode

In this section we consider the situation where each transmitter broadcasts some common data to many receiving nodes (see Chapter 25). More precisely, as in the MNR model considered above, we assume that the potential receivers $\Phi_0 = \Phi^0 = \Phi \setminus \Phi^1$ are those nodes of the MANET Φ which are not authorized to transmit at the considered time slot (a similar analysis can be done for other receiver models) and that each transmitter of this time slot targets *all* the potential receivers of Φ^0.

The model features an i.m. p.p. $\tilde{\Phi} = \{X_i, e_i, \mathbf{F}_i\}$ with Poisson nodes $\Phi = \{X_i\}$ and their MAC indicators $\{e_i\}$ as in Section 16.2.1, except that no prescribed receivers $\{y_i\}$ are considered; the virtual powers F_i^j have the following modified interpretation:

(4') F_i^j denotes the *virtual power* emitted by node i (provided $e_i = 1$) towards node j in Φ^0.

17.3.1 SINR-neighbors

Let us consider the coverage scenario of Section 16.2.2 in which a successful transmission requires a SINR not smaller than some threshold T. More precisely, adapting Definition 16.2.1 to the present scenario, we say that X_j successfully captures the signal from X_i if

$$\text{SINR}_{ij} = \frac{F_i^j / l(|X_i - X_j|)}{W + I_{ij}^1} \ge T\,, \tag{17.10}$$

where $I_{ij}^1 = \sum_{X_k \in \Phi^1, k \ne i,j} F_k^j / l(|X_k - X_j|)$.

Definition 17.3.1. Define the set of *SINR-neighbors* $V(X_i) = V(X_i, \tilde{\Phi})$ of $X_i \in \Phi$ as the union of $\{X_i\}$ and of the subset of potential receivers of Φ^0 which successfully capture the packet transmitted by X_i (if X_i transmits at the given time slot):

$$V(X_i) \quad = \quad \{X_i\} \cup \begin{cases} \{X_j : X_j \in \Phi^0 \text{ s.t. } \delta(X_i, X_j) = 1\} & \text{if } X_i \in \Phi^1 \\ \emptyset & \text{otherwise,} \end{cases} \tag{17.11}$$

with $\delta(X_i, X_j)$ the indicator of the SINR condition (17.10).

Remark 17.3.2. Nothing guarantees that the receivers of two different transmitters are different, so that unless a receiver can capture two different packets at the same time, a new type of collision should be taken into account. However, if $T \geq 1$, no two transmitters can ever be successful with the same receiver. Indeed, it follows from Lemma 17.3.4 that when $T \geq 1$ (which is often the case in practice), if X_1 and X_2 both belong to Φ_1, then $V(X_1) \cap V(X_2) = \emptyset$. Hence, even in the case where receivers cannot capture two different packets at the same time, this type of collision actually never happens for such T.

In what follows we focus on the properties of the set of SINR neighbors of the typical node. For this we define the directed graph $\mathcal{G}_{\text{SINR}}$ with set of nodes Φ and with directed edges connecting each X_i to each of its neighbors $V(X_i)$ (this graph was already considered in Chapter 8 in Volume I).

The number $\mathcal{H}_i^{out} = \text{card}(V(X_i))$ of SINR neighbors of node X_i in $\mathcal{G}_{\text{SINR}}$ is called the *out-degree* of this node. If X_i transmits, the out-degree of X_i is the number of nodes which receive the packet transmitted by node X_i plus 1 (due to the convention that $X_i \in V(X_i)$). If X_i does not transmit, then its out-degree is 1. Similarly, the *in-degree* $\mathcal{H}_i^{in}$ of $X_j \in \Phi$ is 1 if this node is a transmitter; if it is not a transmitter $\mathcal{H}_i^{in}$ is the number of transmitters captured by X_i at the given time slot, plus 1.

Note that $\mathcal{H}_i^{out}$ and $\mathcal{H}_i^{in}$ may be considered as new marks of the nodes of Φ and that the process $\widetilde{\Phi}$ enriched by these mark is still stationary (cf. Definition 2.1.4 in Volume I).

Denote by h^{out} and h^{in} the expected out- and in-degree, respectively, of the typical node of $\tilde{\Phi}$:

$$h^{out} = \mathbf{E}^0[\mathcal{H}_0^{out}], \quad h^{in} = \mathbf{E}^0[\mathcal{H}_0^{in}].$$

Notice that h^{out} (resp. h^{in}) is also the *spatial average* of the node out-degrees (resp. in-degree) due to the fact that our i.m. Poisson p.p. $\tilde{\Phi}$ is ergodic.

The first key result regarding the mean degrees of $\mathcal{G}_{\text{SINR}}$ follows from the *mass transport principle*:

Proposition 17.3.3. The mean in-degree of the typical node of $\mathcal{G}_{\text{SINR}}$ and its mean out-degree are equal; i.e. $h^{in} = h^{out} = h$.

Proof. This result should not be surprising. Each directed edge has two ends; call them edge-source and edge-destination, respectively. Heuristically (and this argument can be made precise using ergodic theory), h^{in} corresponds to the average number of edge-destinations per node, while h^{out} the average number of edge-sources per node. Since one edge-source corresponds exactly to one edge-destination both averages should coincide.

We prove this result formally using the stationarity of the marked p.p. $\{X_i, e_i, \mathcal{H}_i^{out}, \mathcal{H}_i^{in}\}$ and an argument similar to that used in Section 4.3 in Volume I in the proof of the Neveu exchange formula. Denote by $\mathbb{Z}^2$ the integer lattice. By Campbell's formula (2.9 in Volume I) we have

$$\begin{aligned}
\lambda h^{out} &= \lambda \int_{[0,1)^2} \mathbf{E}^0[\mathcal{H}_0^{out}]\,\mathrm{d}x \\
&= \mathbf{E}\Big[\sum_{X_i\in[0,1)^2} \mathcal{H}_i^{out}\Big] \\
&= \sum_{v\in\mathbb{Z}} \mathbf{E}\Big[\sum_{X_i\in[0,1)^2}\ \sum_{X_j\in[0,1)^2+v} (1+e_i(1-e_j)\delta(X_i,X_j))\Big]\,,
\end{aligned}$$

where the summations bear on the points X_i of Φ. By the stationarity of the underlying marked p.p., for each $v \in \mathbb{Z}^2$ we have

$$\mathbf{E}\Big[\sum_{X_i\in[0,1)^2}\ \sum_{X_j\in[0,1)^2+v} (1+e_i(1-e_j)\delta(X_i,X_j))\Big] = \mathbf{E}\Big[\sum_{X_i\in[0,1)^2-v}\ \sum_{X_j\in[0,1)^2} (1+e_i(1-e_j)\delta(X_i,X_j))\Big]\,,$$

and consequently

$$\begin{aligned}
\lambda h^{out} &= \sum_{v\in\mathbb{Z}} \mathbf{E}\Big[\sum_{X_i\in[0,1)^2-v}\ \sum_{X_j\in[0,1)^2} (1+e_i(1-e_j)\delta(X_i,X_j))\Big] \\
&= \mathbf{E}\Big[\sum_{X_j\in[0,1)^2} \mathcal{H}_i^{in}\Big] = \lambda h^{in}\,,
\end{aligned}$$

which concludes the proof, since $0 < \lambda < \infty$. □

Remark: The last lemma does not use the Poisson assumption. The result is applicable to all stationary i.m.p.p.s with a finite intensity.

Before evaluating the mean (in- equal to out-) degree h of $\mathcal{G}_{\text{SINR}}$, let us show that it is finite. This is a consequence of the following lemma which shows that $\mathcal{H}_i^{in}$ is bounded from above by a constant.

Lemma 17.3.4. For any of the OPL models OPL 1–OPL 3, the in-degree of any node of $\mathcal{G}_{\text{SINR}}$ is bounded from above by $\xi = \lceil 1/T \rceil + 1$.

Proof. Assume there is an edge to node X_j from nodes $(X_{i_1}, \ldots, X_{i_k})$, for some $k > 1$. Then for all $p = 1, \ldots, k$,

$$\frac{F_{i_p}^j}{l(|X_{i_p} - X_j|)} > \frac{T}{1+T}\left(\sum_{q=1}^{k} \frac{F_{i_q}^j}{l(|X_{i_q} - X_j|)}\right)\,.$$

The strict inequality stems from the fact that the interference created by nodes other than $(X_{i_1}, \ldots, X_{i_k})$ is a.s. positive for any attenuation function with infinite support. When summing up all these inequalities, one gets that $Tk < 1 + T$, that is $k \leq \lceil 1/T \rceil$. Since, by convention, the in-degree of an isolated node is equal to 1 (there is an edge from X to X for all X) the in-degree of any node is bounded from above by $\xi = \lceil 1/T \rceil + 1$. □

Notice that the proof is based on arguments similar to those leading to the so-called *pole capacity* of a cellular network (cf. Example 6.2.3 in Volume I). Again, the Poisson assumption is not used.

Remark: The fact that the mean in and out-degree of the typical node are equal does not imply that the distributions of $\mathcal{H}_0^{out}$ and $\mathcal{H}_0^{in}$ are equal under $\mathbf{P}^0$. The in-degree of a node is a.s. bounded by some constant. This differs significantly from what happens for its out-degree, which is a.s. finite (since its mean is finite) but has a distribution with an infinite support on $\mathbb{N}$. To understand why the last statement holds true, observe that, under $\mathbf{P}^0$, with a positive probability, $\tilde{\Phi}$ may have an arbitrary large cluster of receivers X_j (nodes marked $e_j = 0$) close to the transmitter $X_0 = 0$ (marked $e_0 = 1$) with the SN at all these receivers small enough to make $\text{SINR}_{0j} \geq T$.

Let us now evaluate h.

Proposition 17.3.5. The mean degree in $\mathcal{G}_{\text{SINR}}$ is equal to

$$h = \mathbf{E}^0[\text{card}(V(0))] = 1 + 2\pi\lambda p(1-p) \int_0^\infty r p_c(r, \lambda_1, T)\, \mathrm{d}r\,,$$

where $p_c(r, \lambda_1, T)$ is the probability of coverage at distance r for the Poisson bipolar model.

Proof. Consider the typical node $X_0 = 0$ under $\mathbf{P}^0$. We have

$$\begin{aligned}
\mathbf{E}^0[\text{card}(V(0))] &= 1 + \mathbf{E}^0\Big[e_0 \sum_{\Phi \ni X_j \neq 0} (1-e_j)\delta(0, X_j)\Big] \\
&= 1 + \mathbf{E}^0\Big[e_0 \sum_{\Phi \ni X_j \neq 0} (1-e_j)\mathbb{1}(F_0^j \geq Tl(|X_j|)(W + I_{0j}^1)\Big] \qquad (17.12)
\end{aligned}$$

Now, we would like to use Campbell's formula to replace the summation over points of Φ by an integral with respect to the Lebesgue measure. However, under $\mathbf{P}^0$, our i.m. p.p. $\tilde{\Phi}$ is not stationary and thus we cannot directly use formula (2.9 in Volume I). Recall from the discussion in Section 16.2.2 that, under $\mathbf{P}^0$, the nodes of the Poisson MANET and their marks follow the distribution of $\widetilde{\Phi} \cup \{(X_0 = 0, e_0, \mathbf{F}_0)\}$, where $\widetilde{\Phi}$ is a copy of the original Poisson p.p. representing the stationary MANET and $(e_0, \mathbf{F}_0)$ is a new copy of the mark independent of everything else and distributed like all other marks $(e_i, \mathbf{F}_i)$ of $\widetilde{\Phi}$ under $\mathbf{P}$. In view of the definition of I_{ij}^1 (see Equation (17.10)), I_{0j}^1 in (17.12) and the mark of the point $X_0 = 0$ are independent. We can consider I_{0j}^1 as a mark $I_j^{'1}$ of X_j. Also, considering $F_0^j = F^{'j}$ as a new mark of $X_j \in \tilde{\Phi}$ (note that the sequence $\{F_0^j : j\}$ is i.i.d.) and exploiting independence, we can rewrite (17.12) as follows using Campbell's formula (2.9 in Volume I):

$$\begin{aligned}
\mathbf{E}^0[\text{card}(V(0))] &= 1 + \mathbf{E}^0\Big[e_0 \sum_{\Phi \ni X_j \neq 0} (1-e_j)\mathbb{1}(F_0^j \geq Tl(|X_j|)(W + I_{0j}^1)\Big] \\
&= 1 + p\mathbf{E}[\sum_{\Phi \ni X_j} (1-e_j)\mathbb{1}(F^{'j} \geq Tl(|X_j|)(W + I_j^{'1})\Big] \\
&= 1 + \lambda p(1-p) \int_{\mathbb{R}^2} \mathbf{P}^0\{\, F^{'0} \geq Tl(|x|)(W + I^{'1})\,\}\, \mathrm{d}x \\
&= 1 + 2\pi\lambda p(1-p) \int_0^\infty r p_c(r, \lambda_1, T)\, \mathrm{d}r\,,
\end{aligned}$$

where the last equality follows from the fact that F'^0, I'^1 have the same distributions as the generic variables F, I^1 considered in Section 16.2.2. □

In the case of Rayleigh fading, by Proposition 16.2.2, we obtain the following more explicit result:

Corollary 17.3.6. For Rayleigh fading, the mean degree of the typical node of the graph $\mathcal{G}_{\text{SINR}}$ is equal to

$$h = \mathbf{E}^0[\text{card}(V(0))] = 1 + \lambda p(1-p)2\pi \int_0^\infty \mathcal{L}_W(\mu T l(r)) \exp\Big\{-2\pi\lambda p \int_0^\infty \frac{v}{1 + l(v)/(Tl(r))}\,\mathrm{d}v\Big\} r\mathrm{d}r\,.$$

In particular, for $W \equiv 0$ and OPL 3,

$$h = 1 + \frac{(1-p)\pi}{T^{2/\beta}K(\beta)}\,, \tag{17.13}$$

where $K(\beta)$ is defined in (16.9).

We consider now the case where F has a general distribution.

Recall from Section 16.2.4 that $\bar{p}_c(r) = p_c(r, 1, 1)$ denotes the value of the probability of coverage calculated in the Poisson bipolar MANET model with $T \equiv 1, \lambda_1 = 1, W \equiv 0$ and normalized virtual powers distributed as $\bar{F} = \mu F$.

Using Proposition 17.3.5 and the scaling properties of the coverage probability expressed in Proposition 16.2.9, we get:

Corollary 17.3.7. Assume $W \equiv 0$, OPL 3 and a general distribution of F. The mean degree of the typical node of the graph $\mathcal{G}_{\text{SINR}}$ is equal to

$$h = 1 + \frac{(1-p)2\pi}{T^{2/\beta}} \int_0^\infty s\bar{p}_c(s)\,\mathrm{d}s\,, \tag{17.14}$$

where the constant $\int_0^\infty s\bar{p}_c(s)\,\mathrm{d}s$ does not depend on any parameter of the model other than the distribution of the normalized virtual power $\bar{F}$.

This gives the dependence of the mean degree h in function of the basic model parameters. In particular, we have the same invariance w.r.t. the node density λ as in the coverage probability.

17.3.2 Shannon Multicast Throughput

Consider a multicast scenario with an adaptive coding scheme leading to the Shannon throughput introduced in Section 16.2.3. More precisely, we suppose that each transmitter $X_i, e_i = 1$ broadcasts some information using a multi-layer coding scheme that allows each receiver $X_j, e_j = 0$ to receive this information with the throughput $\mathcal{T}_{ij} = \log(1 + \text{SINR}_{ij})$ (for instance in video broadcast, if the throughput is high, several layers are sent and the video signal is received with high resolution; if it is low, fewer layers are sent and the quality is lower). Denote by $\mathcal{T}_i^{out} = e_i \sum_{X_j \in \Phi^0} \mathcal{T}_{ij}$ the total rate with which node X_i floods the network when it is transmitting. Similarly, denote by $\mathcal{T}_i^{in} = (1 - e_i) \sum_{X_\in \Phi^1} \mathcal{T}_{ji}$ the total rate with which receiver X_i can receive information from all MANET nodes. Let $\tau^{in} = \mathbf{E}^0[\mathcal{T}_0^{in}]$ and $\tau^{out} = \mathbf{E}^0[\mathcal{T}_0^{out}]$.

The following result is another example of the *mass transport principle* and can be proved along the same lines as Proposition 17.3.3.

Proposition 17.3.8. For the above multicast MANET model, $\tau^{in} = \tau^{out} = \tau^{mcast}$.

The mean total multicast rate τ^{mcast} can be evaluated in terms of the mean Shannon throughput in the corresponding bipolar model. The following result can be proved along the same lines as Proposition 17.3.5.

Proposition 17.3.9. The mean total throughput of a typical node in the multicast MANET model is equal to

$$\tau^{mcast} = 2\pi\lambda p(1-p) \int_0^\infty r\tau(r, \lambda_1)\, \mathrm{d}r\,,$$

where $\tau(r, \lambda_1)$ is the Shannon throughput evaluated for the Poisson bipolar model.

Using formula (16.13) and Proposition 17.3.5, τ^{mcast} can be further related to the coverage probability $p_c(r, \lambda_1, \cdot)$ and (interchanging the order of integration) to the mean degree of the multicast graph $\mathcal{G}_{\mathrm{SINR}}$. In particular, the following result follows from Proposition 17.3.9, formula (16.13) and the scaling properties of the coverage probability expressed in Proposition 16.2.9.

Corollary 17.3.10. Assume $W \equiv 0$, OPL 3 and a general distribution of F. The mean total throughput of typical node in the multicast MANET model described above is equal to

$$\tau^{mcast} = (1-p)\beta K(\beta) \int_0^\infty s\bar{p}_c(s)\, \mathrm{d}s\,, \tag{17.15}$$

where $K(\beta)$ is defined in (16.9) and the constants $\int_0^\infty s\bar{p}_c(s)\, \mathrm{d}s$ do not depend on any parameter of the model other than the distribution of the normalized virtual power $\bar{F}$. In particular, for Rayleigh fading (exponential F)

$$\tau^{mcast} = \frac{(1-p)\beta}{2}\,. \tag{17.16}$$

17.4 Opportunistic Receivers – MAC and Routing Cross-Layer Optimization

In this section we focus on:

- The outage scenario, where a transmission requires a SINR larger than some threshold T;
- The MANET receiver scenario, where the nodes $\Phi_0 = \Phi^0 = \Phi \setminus \Phi^1$ which are not allowed to access the shared medium form the set of potential receivers;
- The opportunistic routing scenario, where the receiver of a given transmitter is not prescribed in advance but rather selected so as to maximize the packet progress in a given direction.

17.4.1 Receivers Maximizing Instantaneous Directional Progress

To consider directional progress we need to extend the i.m. p.p. $\tilde{\Phi}$ by introducing marks d_i; the latter are i.i.d. unit vectors in $\mathbb{R}^2$ representing directions in which the nodes aim to send their packets. The MANET

model considered in this section assumes an i.m. p.p. $\tilde{\Phi} = \{X_i, e_i, \mathrm{d}_i, \mathbf{F}_i\}$ with Poisson nodes $\Phi = \{X_i\}$ and their MAC indicators $\{e_i\}$ as in Section 16.2.1, with the random cross-fading model with virtual powers $\mathbf{F}_i$ (see (4') of Section 17.3). In the opportunistic receiver selection:

(3") The receiver y_i of the transmitter $X_i \in \Phi$ is its SINR neighbor (cf. Definition 17.3.1) which maximizes the effective progress of the transmitted packet in the direction d_i

$$y_i = \underset{X_j \in V(X_i)}{\arg\max} \{\langle X_j - X_i, \mathrm{d}_i \rangle\} . \tag{17.17}$$

Note that $V(X_j)$ is non-empty ($X_i \in V(X_i)$) and almost surely finite (cf. Lemma 17.3.4). Then the "arg max" in the definition of y_i is almost surely well defined for all i (cf. also Lemma 4.2.2 in Volume I).

A major difference between this opportunistic mechanism and all previously considered cases is that it has much more chance to lead to a successful transmission: for instance, assume that the direction d_0 of node $X_0 = 0$ (under $\mathbf{P}^0$) is that of the x axis; then as soon as X_0 has SINR neighbors with a positive abscissa, the transmission is successful. Note that since $X_i \in V(X_i)$ the maximal value of $\langle X_j - X_i, \mathrm{d}_i \rangle$ in (17.17) is at least 0 and the case when the arg max is attained on X_i is considered as an unsuccessful transmission.

Denote by D_i the *effective directional progress* of the packet transmitted in the given time slot by transmitter X_i:

$$D_i = \langle y_i - X_i, \mathrm{d}_i \rangle = \max_{X_j \in \Phi^0} \{\langle X_j - X_i, \mathrm{d}_i \rangle^+ \delta(X_i, X_j)\} , \tag{17.18}$$

where $a^+ = a\mathbb{1}(a > 0)$.

In what follows we focus on the *mean effective directional progress* of the packet transmitted by the typical node of the MANET given it is transmitting in the tagged time slot:

$$\overline{prog}(\lambda, p) = \mathbf{E}^0[D_0 \,|\, e_0 = 1]$$

and on the spatial density of this progress:

$$d_{\overline{prog}}(\lambda, p) = \lambda p \, \overline{prog}(\lambda, p) = \lambda \mathbf{E}^0[D_0] ,$$

where the notation is meant to stress the difference with the effective progress (16.19) and its density (16.22) as considered in the bipolar network model.

17.4.2 Optimization of the Spatial Density of Directional Progress

One of the main objects of this subsection is

$$p^* = \underset{0<p\leq 1}{\arg\max} \{d_{\overline{prog}}(\lambda, p)\} , \tag{17.19}$$

whenever the argmax is well defined.

In § 16.3.1.4 we saw that in the Poisson bipolar MANET model, the joint optimization of the density of progress $d_{prog}(r, \lambda_1, T)$ in p and in the transmission distance r led to degenerate answers due to the fact that in this model r is not related to the node density.

In contrast, the next lemma shows that the optimization of $d_{\overline{prog}}(\lambda, p)$ w.r.t. p is not degenerate (i.e. $p = 0$ is not the optimal solution). For simplicity we limit ourselves to the OPL 3 model and to Rayleigh fading. This result can be extended to more general situations under some conditions on the moments of F and/or W.

Lemma 17.4.1. Assume the OPL 3 model and Rayleigh fading. Then $\lim_{p\to 0} d_{\overline{prog}}(\lambda, p) = 0$ and $d_{\overline{prog}}(\lambda, 1) = 0$.

Proof. Note that D_0 increases when the thermal noise decreases. Thus it is enough to prove the result for $W = 0$, which we assume in what follows. We have

$$\begin{aligned}
\mathbf{E}^0[D_0 \,|\, e_0 = 1] &= \int_0^\infty \mathbf{P}^0\{\, D_0 > s \,|\, e_0 = 1 \,\}\, \mathrm{d}s \\
&= \int_0^\infty \mathbf{P}^0\{\, V(0) \cap B_0^c(s) \neq \emptyset \,|\, e_0 = 1 \,\}\, \mathrm{d}s \\
&\leq \int_0^\infty \min\Big\{1, \mathbf{E}^0[\mathrm{card}(V(0) \cap B_0^c(s)) \,|\, e_0 = 1]\Big\}\, \mathrm{d}s\,. \qquad (17.20)
\end{aligned}$$

Following the same arguments as those used to express $\mathbf{E}^0[\mathrm{card}(V(0))]$ in the proof of Proposition 17.3.5 and (16.8), we have

$$\begin{aligned}
\mathbf{E}^0[\mathrm{card}(V(0) \cap B_0^c(s)) \,|\, e_0 = 1] &= 2\pi\lambda(1-p) \int_s^\infty r p_c(r, \lambda_1, T)\, \mathrm{d}r \\
&= 2\pi\lambda(1-p) \int_s^\infty r \exp(-\lambda p r^2 T^{2/\beta} K(\beta))\, \mathrm{d}r \\
&= \frac{\pi(1-p)}{pT^{2/\beta}K(\beta)} \exp(-\lambda p s^2 T^{2/\beta} K(\beta))\,.
\end{aligned}$$

The last expression is smaller than 1 for

$$s \geq s_0(p) = \sqrt{\frac{1}{\lambda p T^{2/\beta} K(\beta)} \left(\log\Big(\frac{\pi(1-p)}{pT^{2/\beta}K(\beta)}\Big)\right)^+}\,.$$

Using (17.20), we obtain

$$\begin{aligned}
\lambda p \mathbf{E}^0[D_0 \,|\, e_0 = 1] &\leq \lambda p s_0(p) + \frac{\pi\lambda(1-p)}{T^{2/\beta}K(\beta)} \int_{s_0(p)}^\infty \exp(-\lambda p s^2 T^{2/\beta} K(\beta))\, \mathrm{d}s \\
&= \lambda p s_0(p) + \frac{\pi\sqrt{\lambda}(1-p)}{\sqrt{p} T^{3/\beta} K(\beta)^{3/2}} \int_{s_0(p)\sqrt{\lambda p T^{2/\beta} K(\beta)}}^\infty e^{-s^2}\, \mathrm{d}s\,. \qquad (17.21)
\end{aligned}$$

Note that $s_0(1) = 0$ and $\int_0^\infty e^{-s^2}\, \mathrm{d}s < \infty$; thus expression (17.21) is equal to 0 for $p = 1$. In order to evaluate the limit of this expression when $p \to 0$, we use the inequality $\int_x^\infty e^{-s^2}\, \mathrm{d}s \leq e^{-x^2}$, which holds true for all $x \geq 1/2$ (to prove this, one can use the fact that $e^{-s^2} \leq e^{-x^2+x-s}$ for $s \geq x \geq 1/2$). Note that

$\sqrt{p}s_0(p) \sim \sqrt{\log(1/p)} \to \infty$ when $p \to 0$. Thus using (17.21) for sufficiently small p, we have

$$\begin{aligned} \lambda p \mathbf{E}^0[D_0 \,|\, e_0 = 1] &\leq \lambda p s_0(p) + \frac{\pi\sqrt{\lambda}(1-p)}{\sqrt{p}T^{3/\beta}K(\beta)^{3/2}} \exp\Big(-s_0^2(p)\lambda p T^{2/\beta}K(\beta)\Big) \\ &= \lambda p s_0(p) + \frac{\sqrt{\lambda p}}{T^{1/\beta}K(\beta)^{1/2}} \end{aligned}$$

which tends to 0 when $p \to 0$ since $ps_0(p) \sim \sqrt{p\log(1/p)} \to 0$. This completes the proof. □

The following invariance of p^* with respect to λ can be proved using some refinements of the arguments used in the proof of Proposition 16.2.9.

Proposition 17.4.2. Assume $W = 0$, OPL 3 and a general distribution for F. Then the maximal density of directional progress $d_{\overline{prog}}(\lambda, p)$ is attained for the MAP $p^* = p^*(T)$ satisfying

$$\sqrt{p^*}H(p^*, T) = \sup_{0 \leq p \leq 1} \sqrt{p}H(p, T),$$

for some function $H(p, T)$ that does not depend on λ.

Remark: This proposition has an important practical implication: it implies that the parameter p can be optimally tuned regardless of the spatial density of network nodes.

Proof. (of Proposition 17.4.2) The nodes of the Poisson p.p. $\tilde{\Phi} = \{X_i\}$ with intensity λ can be represented as $\{X_i = X_i'/\sqrt{\lambda}\}$, where $\Phi' = \{X_i'\}$ is a Poisson with intensity 1 (cf. Example 1.3.12 in Volume I). Let $\tilde{\Phi}'$ and $\tilde{\Phi}$ be the respective marked versions of these p.p.s with (path-wise) the same marks (i.e. the mark of each X_i' is equal to that of X_i). Note that under our OPL 3 and $W = 0$ assumptions, the SINR (in fact the SIR) is invariant with respect to dilations of the points of the p.p. Indeed,

$$l(|X_i'/\sqrt{\lambda} - X_j'/\sqrt{\lambda}|) = \lambda^{\beta/2} l(|X_i' - X_j'|)$$

and the factor $\lambda^{\beta/2}$ cancels out in the numerator and the denominator of the SINR expression in case $W = 0$. This means that

$$V(X_i, \tilde{\Phi}) = 1/\sqrt{\lambda} V(X_i', \tilde{\Phi}').$$

Moreover, the dilation (our scaling) is a conformal mapping (preserves angles). Consequently, the receiver y_i chosen in $V(X_i)$ according to the maximal directional progress principle (17.17) is equal to $y_i'/\sqrt{\lambda}$, where y_i' is chosen in $V(X_i', \tilde{\Phi}')$ according to the same principle. This concludes the proof. □

The functions $d_{\overline{prog}}(\lambda, p)$ and $H(p, T)$ are not known in closed form. In the next section we derive some bounds for them.

17.4.3 *Modified Progress — Bounds on Mean Progress

Consider the following function of $\tilde{\Phi}$ under $\mathbf{P}^0$, that we call *modified progress*.

$$\widetilde{D}_0 = \max_{X_j \in \Phi^0} \{\langle X_j, \mathrm{d}_0 \rangle^+ p_c(|X_j|, \lambda p, T)\}. \tag{17.22}$$

The only difference between progress D_0 and modified progress $\widetilde{D}_0$ is that one replaces the (random) indicator $\delta(0, X_j)$ by the expectation of this indicator given X_j, namely $p_c(|X_j|, \lambda_1, T)$ in the max. This modification will allow us to evaluate the mean values of $\widetilde{prog}(\lambda, p) = \mathbf{E}^0[\tilde{D}_0 \,|\, e_0 = 1]$ and $d_{\widetilde{prog}}(\lambda, p) = \lambda p \; \widetilde{prog}(\lambda, p)$. It is also of practical interest as the latter gives a lower bound to the former:

Proposition 17.4.3. For all λ, p we have $\overline{\widetilde{prog}}(\lambda, p) \geq \widetilde{prog}(\lambda, p)$. In consequence $d_{\overline{\widetilde{prog}}}(\lambda, p) \geq d_{\widetilde{prog}}(\lambda, p)$.

Proof. Recall that by the property of the independent thinning of Poisson p.p. (cf. Proposition 1.3.5 in Volume I), $\tilde{\Phi}^1$ and $\tilde{\Phi}^0$ form two independent Poisson p.p's. Since under $\mathbf{P}^0$, given X_j, the indicator $\delta(0, X_j)$ is a functional of $\tilde{\Phi}^1$ we have

$$\begin{aligned}
\mathbf{E}[\tilde{D} \,|\, e_0 = 1] &= \mathbf{E}^0\Big[\max_{X_j \in \Phi^0}\Big\{\langle X_j, \mathrm{d}_i\rangle^+ p_c(|X_j|, \lambda p, T)\Big\} \,\Big|\, e_0 = 1\Big] \\
&= \mathbf{E}^0\Big[\max_{X_j \in \Phi^0}\Big\{\langle X_j, \mathrm{d}_i\rangle^+ \mathbf{E}^0[\delta(0, X_j) \,|\, \Phi^0]\Big\} \,\Big|\, e_0 = 1\Big] \\
&= \mathbf{E}^0\Big[\max_{X_j \in \Phi^0}\Big\{\mathbf{E}^0[\langle X_j, \mathrm{d}_i\rangle^+ \delta(0, X_j) \,|\, \Phi^0]\Big\} \,\Big|\, e_0 = 1\Big] \\
&\leq \mathbf{E}^0\Big[\mathbf{E}^0\Big[\max_{X_j \in \Phi^0}\Big\{\langle X_j, \mathrm{d}_i\rangle^+ \delta(0, X_j)\Big\} \,\Big|\, \Phi^0\Big] \,\Big|\, e_0 = 1\Big] \\
&= \mathbf{E}^0[D_0 \,|\, e_0 = 1]\,,
\end{aligned}$$

where the last but one step follows from the following simple fact: for any r.vs $Z_1, Z_2, \ldots$ we have $\max_i\{\mathbf{E}[Z_i]\} \leq \max_i\{\mathbf{E}[\max_i\{Z_i\}]\}$. □

We now focus on the evaluation of $\widetilde{prog}(\lambda, p)$. For this, we use the notation introduced in Section 16.3.1.3, and in particular: $r_{\max} = r_{\max}(\lambda p) = \arg\max_{r \geq 0}\{prog(r, \lambda p, T)\}$ and $\rho = \rho(\lambda p) = prog(r_{\max}(\lambda, p), \lambda p, T)\}$.

For $z \in [0, 1]$, let

$$G(z) = \frac{2}{r_{\max}^2} \int\limits_{\{r \geq 0 : \rho z/(r p_c(r)) < 1\}} r \arccos\Big(\frac{\rho z}{r p_c(r)}\Big)\, \mathrm{d}r\,, \tag{17.23}$$

where the arguments $p\lambda$ and T are omitted.

Remark 17.4.4. For the $\frac{\text{GI}}{0+\text{M/GI}}$ model with OPL 3, Proposition 16.3.7 shows that $G(z)$ does not depend on the model parameters λ, p, T, μ. Indeed, in this case

$$G(z) = \frac{2}{\mathrm{const}_3} \int\limits_{\{r \geq 0 : \mathrm{const}_4 z/(r \bar{p}_c(r)) < 1\}} r \arccos\left(\frac{\mathrm{const}_4 z}{r \bar{p}_c(r)}\right)\, \mathrm{d}r\,,$$

with $\bar{p}_c(\cdot)$ the function defined in Lemma 16.2.9. In particular, for Rayleigh fading, we have

$$G(z) = 2 \int\limits_{\{t : e^t/\sqrt{2et} \leq 1/z\}} \arccos\Big(\frac{z e^t}{\sqrt{2et}}\Big)\, \mathrm{d}t\,. \tag{17.24}$$

The main result concerning $\tilde{D}$ is:

Proposition 17.4.5. We have

$$F_{\tilde{D}}(z) = \mathbf{P}^0\{\,\tilde{D} \le z \,|\, e_0 = 1\,\} = e^{-\lambda(1-p)(r_{\max}(\lambda p))^2 G(z/\rho(\lambda p))} \tag{17.25}$$

and

$$\widetilde{prog}(\lambda, p) = \mathbf{E}^0[\tilde{D} \,|\, e_0 = 1] = \rho(\lambda p) \int\limits_0^1 1 - e^{-\lambda(1-p)(r_{\max}(\lambda p))^2 G(z)}\, \mathrm{d}z\,. \tag{17.26}$$

Proof. Note in (17.22) that under $\mathbf{P}^0$ given $e_0 = 1$ and d_0 the variable $\tilde{D}$ has the form of an extremal SN $\max_{X_i \in \Phi^0} g(X_i)$ with the response function $g(x) = p_c(|x|)\langle x, \mathrm{d}_0\rangle^+$.

Using Proposition 2.4.2 in Volume I, we get:

$$\mathbf{P}(\tilde{D} \le z) = \exp\Bigl[-\lambda(1-p) \int\limits_{\mathbb{R}^2} \mathbb{1}(g(x) > z)\, \mathrm{d}x\Bigr]\,.$$

Passing to polar coordinates, we get

$$\int\limits_{\mathbb{R}^2} \mathbb{1}(g(x) > z)\, \mathrm{d}x \quad = \quad r_{\max}^2 G(z/\rho)\,,$$

which completes the proof. □

Corollary 17.4.6. For the $\frac{\text{GI}}{0+\text{M/GI}}$ model with OPL 3,

$$\widetilde{prog}(\lambda, p) \quad = \quad \frac{\text{const}_4}{T^{1/\beta}\sqrt{\lambda p}} \tilde{H}(p, T) \tag{17.27}$$

$$d_{\widetilde{prog}}(\lambda, p) \quad = \quad \frac{\text{const}_4 \sqrt{\lambda p}}{T^{1/\beta}} \tilde{H}(p, T)\,, \tag{17.28}$$

where

$$\tilde{H}(p, T) = \int\limits_0^1 1 - \exp\Bigl[\Bigl(1 - \frac{1}{p}\Bigr) \frac{G(z)}{\text{const}_3 T^{2/\beta}}\Bigr]\, \mathrm{d}z\,. \tag{17.29}$$

Note that we have the same scaling of $d_{\widetilde{prog}}(\lambda, p)$ in the main parameters of the model as that of $d_{\overline{prog}}(\lambda, p)$ given in Proposition 17.4.2.

Corollary 17.4.7. Under the assumptions of Corollary 17.4.6, the maximal density of modified progress $d_{\widetilde{prog}}(\lambda, p)$ is attained for the MAP $\tilde{p}^* = \tilde{p}^*(T)$ satisfying

$$\sqrt{\tilde{p}^*} H(p^*, T) = \sup_{0 \le p \le 1} \sqrt{p} \tilde{H}(p, T).$$

If such $\tilde{p}^*$ exists, it does not depend on λ. For Rayleigh fading, this is equivalent to

$$\int\limits_0^1 \Bigl(1 + \frac{G(z)}{\tilde{p}^* T^{2/\beta} C}\Bigr) \exp\Bigl[\Bigl(1 - \frac{1}{\tilde{p}^*}\Bigr) \frac{G(z)}{2T^{2/\beta} C}\Bigr]\, \mathrm{d}z = 1\,. \tag{17.30}$$

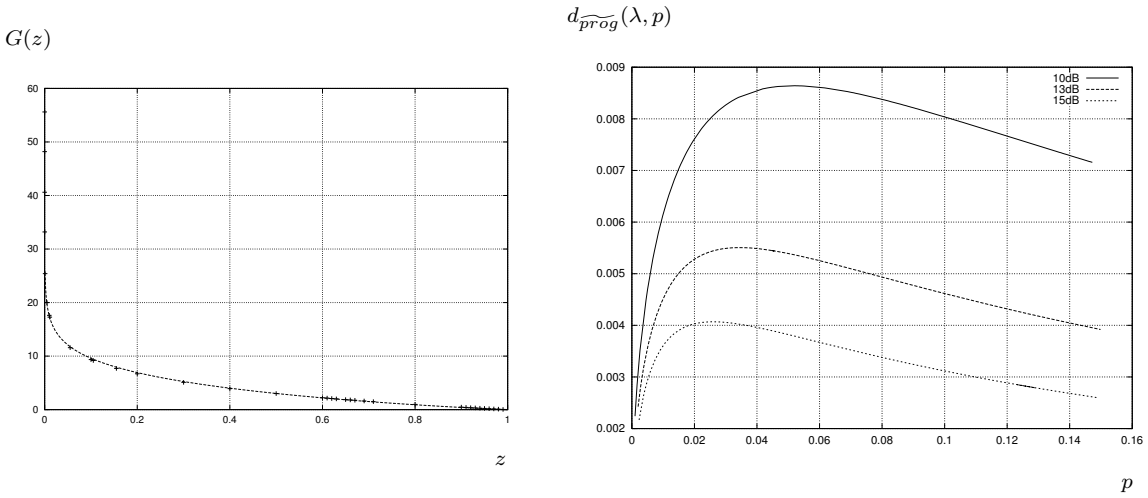

Fig. 17.1 **Left:** Plot of the function $G_\sim$ with points representing values of G. The total relative error $\frac{1}{36}\sqrt{\sum \frac{(G(z)-G_\sim(z))^2}{G^2(z)}}$, where the summation is taken over 36 points marked on the plot, is less then 1.27%. **Right:** Density of modified progress $d_{\widetilde{prog}}(\lambda, p)$ for the $\frac{\mathrm{M}}{0+\mathrm{M}/\mathrm{M}}$ model with OPL 3. Here $\beta = 3$, $\lambda = 1$ and with $T = \{10, 13, 15\}$dB (curves from top to bottom). The optimal values $(\arg\max, \max)$ are $\{(0.052, 0.0086), (0.035, 0.0055), (0.026, 0.0040)\}$ respectively.

Example 17.4.8. The aim of the present example is to numerically evaluate the G function defined in (17.23) and efficiently trace the function $d_{\widetilde{prog}}(\lambda, p)$ in the $\frac{\mathrm{M}}{0+\mathrm{M}/\mathrm{M}}$ model with OPL 3. For this, we use the so-called *Lambert W* functions LW^0 and LW^1. These functions can be seen as inverse of the function $t \to te^t$ in the domains $(-1, \infty)$ and $(-\infty, -1)$ respectively; more precisely, for $s \geq -1/e$, $\mathrm{LW}^0(s)$ is the unique solution of $\mathrm{LW}^0(s)e^{\mathrm{LW}^0(s)} = s$ satisfying $\mathrm{LW}^0(s) \geq -1$, whereas for $0 > s \geq -1/e$, $\mathrm{LW}^1(s)$ is the unique solution of $\mathrm{LW}^1(s)e^{\mathrm{LW}^1(s)} = s$ satisfying $\mathrm{LW}^1(s) \leq -1$. Let $L^0(s) = -\frac{1}{2}\mathrm{LW}^0(-s^{-2}e^{-1})$ and $L^1(s) = -\frac{1}{2}\mathrm{LW}^1(-s^{-2}e^{-1})$. The following representation of G is equivalent to that in (17.24):

$$\begin{aligned} G(z) &= 2\int_{L^0(1/z)}^{L^1(1/z)} \Big(L^1(s) - L^0(s)\Big)\,\mathrm{d}s\,, \\ &= 2\int_{\arcsin(z)}^{\pi/2} \left(L^1\left(\frac{\sin s}{z}\right) - L^0\left(\frac{\sin s}{z}\right)\right)\mathrm{d}s\,. \end{aligned}$$

Moreover, the following function

$$G_\sim(z) = \pi(1-z) - 2\ln(z)\arccos(z)$$

approximates G very well over the whole interval $0 < z < 1$; cf. Figure 17.1 (Left). We use this approximation to calculate numerically the value of $d_{\widetilde{prog}}(\lambda, p)$. Figure 17.1 (Right) shows the results for $\beta = 3$, $\lambda = 1$ and three values of the SINR threshold $T = \{10, 13, 15\}$dB. On the plot, we can identify the MAP $\tilde{p}^*$ that maximizes the density of progress for a given T.

17.4.4 *Location of the Optimal Receiver

17.4.4.1 Comparison to the Case with a Restricted Range for Receivers

In what follows we show that each transmitter can restrict its search for an optimal receiver to its vicinity. For this we show first that the optimal density of progress can be approximated by that in a model where the domain of reception is restricted to a certain neighborhood of the transmitter. By this we mean that we exclude in the definition of D or $\widetilde{D}$ the receivers lying outside some disk with a given radius R.

We have the following straightforward generalization of our previous results:

Proposition 17.4.9. Propositions 17.4.3 and 17.4.5 remain true if we take $\max_{X_i\in\Phi^0,|X_j|\le R}(\dots)$ (with $\max\emptyset = 0$) in (17.18) and (17.22). In this case the function G has to be modified by taking the integral in (17.23) over the region $\{0 \le r \le R : \rho z/(rp_c(r)) < 1\}$.

The case considered above will be referred to as the *restricted range model* in what follows.

We look for a reception radius R such that for a given p, the density of progress in the restricted range model is close enough to that of the unrestricted range model. It is convenient to relate the reception radius R to the intensity λ of transmitters. As we shall see later on, it is convenient to take $R = Kr_{\max}$ for some constant $K \ge 0$ (recall, that $r_{\max} = r_{\max}(\lambda p)$ is the distance at which the progress $prog(r, \lambda p, T) = rp_c(r, \lambda p, T)$ in the corresponding bipolar model is maximal). Denote by G_K the function defined by (17.23) with the integral taken over $\{0 \le r \le Kr_{\max} : \rho z/(rp_c(r)) < 1\}$ and by $\widetilde{prog}_K = \widetilde{prog}_K(\lambda, p)$ the associated mean modified progress in the restricted range model.

We have the following continuity result regarding $\widetilde{prog}_K$ and $\widetilde{prog} = \widetilde{prog}(\lambda, p)$.

Proposition 17.4.10. For the $\frac{\text{GI}}{0+\text{M/GI}}$ model with OPL 3 and $\mathbf{P}\{\, F > 0\,\} > 0$.

$$0 \le \widetilde{prog} - \widetilde{prog}_K \le \rho z_K\,, \tag{17.31}$$

for some function $K \mapsto z_K$, such that $\lim_{K\to\infty} z_K = 0$. For Rayleigh fading, we can take $z_K = Ke^{1/2-K^2/2}$, for $K \ge 1$.

Proof. Let $\bar{p}_c(\cdot)$ be the function defined in Lemma 16.2.9. By Proposition 17.3.5 and Lemma 17.3.4 we know that $\int_0^\infty r\bar{p}_c(r)\,\mathrm{d}r < \infty$. Moreover, by Proposition 16.3.6 and Proposition 2.2.6 in Volume I we know that $\bar{p}_c(r)$ is continuous in r. Thus, $r\bar{p}_c(r) \to 0$ when $r \to \infty$ and for any $K \ge 0$, there exists z_K such that $G_K(z) = G(z)$ for $z \ge z_K$. Moreover $z_K \to 0$ when $K \to \infty$. Thus (17.31) follows from Propositions 17.4.5 and 17.4.9. □

Example 17.4.11. Take for example, $p = 0.035$, $T = 13$dB and Rayleigh fading. In this case, the mean modified progress in the unrestricted model is approximately $\widetilde{prog} = 0.0055/0.035 = 0.157$ (cf. Figure 17.1 Right), whereas the best mean range is attained for the range attempt $r_{\max} = 0.506$ and is equal to $\rho = 0.307$. In order to have a relative difference $\epsilon = 0.01$ we find the minimal $K \ge 1$ such that $Ke^{1/2-K^2/2} \le 0.01 \cdot 0.157/0.307 = 0.00513$, which is $K = 3.768$. This means that in the model with reception radius $R = Kr_{\max} = 3.768 \cdot 0.506 = 1.905$, the mean modified progress (and its spatial density) is within 1% of the optimal value of the mean modified progress obtained in the unrestricted model.

17.4.4.2 Comparison to Smallest Hop in a Cone

Now we compare $\widetilde{prog}$ to the situation when the receivers are taken as the *nearest non-emitting points in a cone* pointing to the right direction and of some given angle. More precisely, consider the following modification of the MNR model of Section 17.2.2. Let for a given width $0 < \alpha \leq \pi$ of the cone

($3'^{\alpha}$) The receiver y_i of the transmitter $X_i \in \Phi$ is the point

$$y_i = Y_i^* = \underset{X_j \in \Phi^0, \frac{\langle X_j - X_i, \mathrm{d}_i \rangle}{|X_j - X_i|} \leq \frac{\alpha}{2}}{\arg\min} \{|X_j - X_i|\}\,.$$

The mean effective progress $prog_\alpha(\lambda, p) = \mathbf{E}^0[\langle y_0, \mathrm{d}_0 \rangle \,|\, e_0 = 1]$ in this case can be evaluated using the same arguments as in the proof of Proposition 17.2.2 (cf. also (17.6).

Corollary 17.4.12. We have

$$prog_\alpha(\lambda, p) = 2\lambda \sin(\alpha/2) \int_0^\infty r^2 \exp(-\lambda(1-p)\alpha r^2/2) p_c(r, \lambda p, T)\, \mathrm{d}r\,.$$

For the $\frac{\mathrm{M}}{0+\mathrm{M/M}}$ model with OPL 3, we have

$$prog_\alpha(\lambda, p) = \frac{\Gamma(3/2)}{\sqrt{\lambda}} \frac{\sin(\alpha/2)(1-p)}{\Big((1-p)\alpha/2 + pT^{2/\beta} K(\beta)\Big)^{3/2}}\,,$$

where $K(\beta)$ is defined in (16.9).

Example 17.4.13. Figure 17.2 compares the density of modified progress $d_{\widetilde{prog}}(1, p)$ to the density of "smallest progress in the cone" of width α; $d_{prog_\alpha}(1, p) = p\ prog_\alpha(1, p)$ for various values of α when $T = 10$dB and fading is Rayleigh. The optimal choice of α for $d_{prog_\alpha}(1, p)$ (over all p) is approximately $\alpha = 0.72\pi$; for this angle, the optimal MAP approximately $p = 0.056$, which gives $d_{prog_\alpha}(1, p) \approx 0.0080$, to be compared to $d_{\widetilde{prog}}(1, \tilde{p}^*) = 0.0086$ for $\tilde{p}^* = 0.052$. So the gain is small. But remember, $\widetilde{prog}(\lambda, p)$ is only a lower bound to the true opportunistic progress.

17.4.5 Impact of the Thermal Noise

The results of Proposition 17.4.2 and Corollary 17.4.6 (and actually of most of the quantitative results of the recent sections) are obtained under the assumption $W = 0$. We now show that for a sufficiently small but positive $W > 0$, the spatial density of progress $d_{\overline{prog}}(\lambda, p)$ is also of the order at least $\sqrt{\lambda}$ as $\lambda \to \infty$. Hence, the conclusions of the last sections are not due to a singular behavior at $W = 0$.

Denote by $\overline{prog}(\lambda, p, w)$ the expected directional progress in the model with constant thermal noise $W = w$. The main result is:

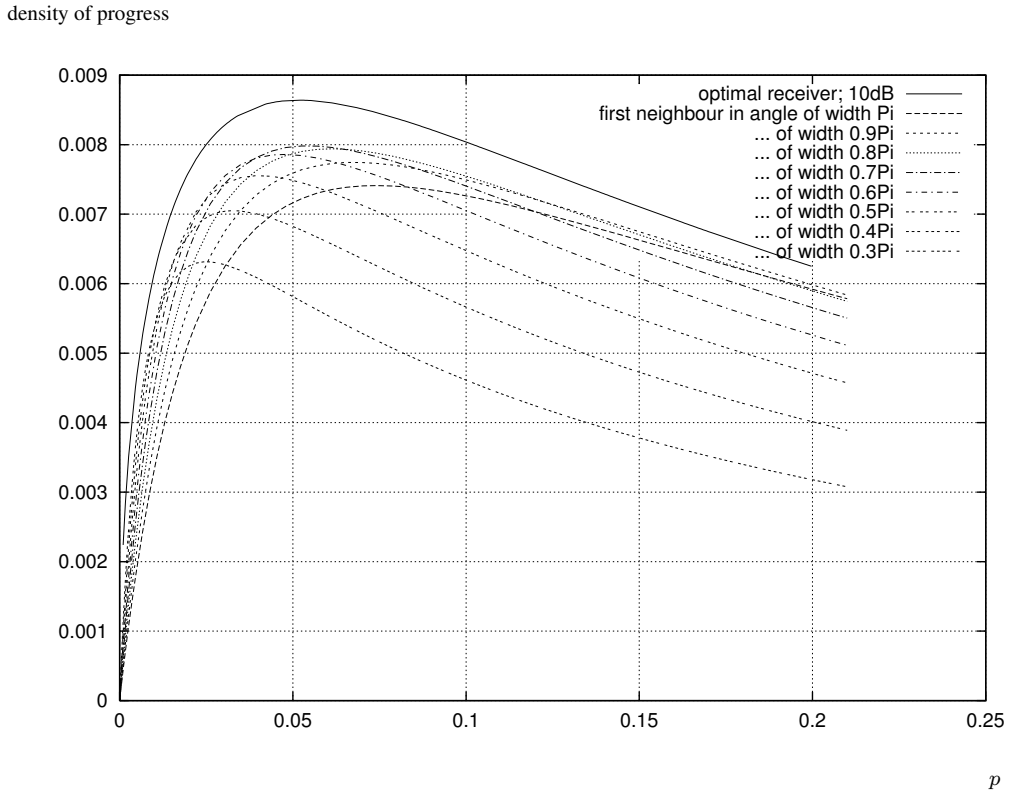

Fig. 17.2 Density of directional progress for the $\frac{\text{M}}{0+\text{M/M}}$ model with OPL 3 with $\beta = 3$, $\lambda = 1$, with $T = 10$dB. Comparison of the opportunistic and the "smallest hop in a cone" cases.

Proposition 17.4.14. For the $\frac{\text{GI}}{w+\text{M/GI}}$ model with OPL 3 and constant MAP p,

$$d_{\overline{prog}}(\lambda, p, w) = \lambda p\, \overline{prog}(\lambda, p, w) = \lambda p\, \overline{prog}(\lambda, p, 0) - \sqrt{\lambda}\, o(w\lambda^{-\alpha/2})\,,$$

when $w\lambda^{-\alpha/2} \to 0$, provided $\overline{prog}(\lambda, p, 0) < \infty$.

Proof. We use the same representation as in the proof of Proposition 17.4.2, in which the Poisson p.p. $\Phi = \{X_i\}$ of intensity λ is constructed from a given Poisson p.p. $\Phi' = \{X'_i\}$ of intensity 1 by taking $X_i = X'_i/\sqrt{\lambda}$ (cf. also Example 1.3.12 in Volume I). In this representation of the model, parameterized by λ and w, we denote by $D_0(w, \lambda)$ the progress (17.18) of the packet sent by node $X_0 = 0$ under $\mathbf{P}^0$. Note that $D_0(w, \lambda) \le D_0(0, \lambda)$ and

$$\begin{aligned} \lambda p\, \overline{prog}(\lambda, p, 0) - \lambda p\, \overline{prog}(\lambda, p, w) &\le \lambda \mathbf{E}^0\Big[D_0(0,\lambda)\mathbb{1}(D_0(0,\lambda) \neq D_0(w,\lambda))\Big] \\ &= \sqrt{\lambda}\mathbf{E}^0\Big[D_0(0,1)\mathbb{1}(D_0(0,1) \neq D_0(w\lambda^{-\beta/2},1))\Big]\,. \end{aligned}$$

Our assumptions imply that $\mathbf{E}^0[D_0(0,1)] < \infty$. The dominated convergence theorem shows that the expectation in the above expression tends to 0 provided $w\lambda^{-\beta/2} \to 0$ (the a.s. continuity of $D_0(w,1)$ in w follows from the fact that under our assumptions, the SINR level-sets are almost surely closed sets, cf. Corollary 5.2.1 in Volume I). This concludes the proof. □

17.5 Local Delays

This section focuses on the packet model. Its main aim is to discuss the mean time to transmit a packet under Aloha, which will be referred to as the *local delay* in what follows. This requires the discussion of the underlying time–space structure. It turns out that this mean time very much depends on the receiver model which is chosen and on the variability of the fading and noise over time.

17.5.1 Space-Time Scenarios

In what follows we add a time-dimension to the basic Poisson bipolar model of Section 16.2.1 and to its extensions considered in the present chapter, such as the independent Poisson receiver (INR) model, the MANET nearest receiver (MNR) and the nearest neighbor (MNN) model, as well as the multicast model. The idea, already described in Section 2.3.4 in Volume I, consists in assuming that the *nodes of the MANET* $\Phi = \{X_i\}$ *remain unchanged over time* and that the marks of these nodes representing their MAC status and other characteristics vary over time. More precisely, consider a common sequence of *time slots* $n = 0, 1, \ldots$ (w.r.t. which all the nodes are perfectly synchronized) and consider the following extensions of the marks introduced in Section 16.2:

- ($2^{s\times t}$) $e_i(n)$ is the MAC decision of point X_i of Φ at time n; we always assume that the random variables $e_i(n)$ are i.i.d. in i and n; i.e. in space and time, with $\mathbf{P}\{\, e_i(n) = 1 \,\} = 1 - \mathbf{P}\{\, e_i(n) = 0 \,\} = p$.
- ($3^{s\times t}$) $y_i(n)$ is the intended receiver of the node i at time n; this receiver may vary over time or not depending on the receiver model. For example it is fixed ($y_i(n) \equiv y_i$) in the basic Poisson bipolar model as well as in the MNN model (cf. (3') with $\Phi_0 = \Phi$). On the other hand, it varies in all the models where the choice of the receiver depends on the current MAC status, like for instance in the MNR and multicast models. For the Poisson INR model one may consider both a fixed Poisson receiver p.p. $\Phi_0(n) = \Phi_0$ or a sequence of Poisson p.p.s $\Phi_0(n)$ which is i.i.d. in n (this might be seen as what happens in the case of receiver Poisson p.p. with high mobility – see 1.3.10 in Volume I).
- ($4^{s\times t}$) $F_i^j(n)$ is the virtual power (comprising fading effects) emitted by node i to the receiver of node j (or to node j in the MANET receiver model) at time n. We adopt the following terminology with respect to the variability of the virtual powers in time.
  - By the *fast fading* case we understand the scenario when $F_i^j(n)$ are i.i.d. in n (recall, that the default option is that they are also i.i.d. in i, j).
  - The *slow fading* case is that where $F_i^j(n) \equiv F_i^j$, for all n.

Remark: [Terminology] Let us stress that the terminology used here about fading is proper to this monograph, where the meaning is that fading remains constant over a slot duration and can be seen as i.i.d. over different time slots. This does not correspond to what is used in many papers of literature. In these papers, fast fading is something not considered here where the channel conditions fluctuate much over a given time slot. What we call slow fading here would be called shadowing in this literature and what we call fast fading here would be be referred to as slow fading.

Regarding the noise variable W, one can consider both i.i.d. $W(n)$ (*fast noise*) and constant $W(n) \equiv W$ (*slow noise*) scenarios.

Note that the p.p. of transmitters $\Phi^1(n) = \sum_i \delta_{X_i} \mathbb{1}(e_i(n) = 1)$ varies over time due to the MAC decisions. So does the SN

$$I_i^1(n) = \sum_{X_j \in \widetilde{\Phi}^1(n),\, j \neq i} F_j^i(n)/l(|X_j - y_i(n)|)$$

of $\widetilde{\Phi}^1(n) \setminus \{X_i\}$ representing the interference at the receiver of the node X_i.

Denote by $\delta_i(n)$ the indicator that (16.2) holds at time n (with F, I and W considered at time n); namely, that location $y_i(n)$ (prescribed by the appropriate receiver model) is covered by transmitter X_i with the required quality at time n.

17.5.2 Local Delay

We now give a general definition of the local delay of the typical node, valid in all our receiver models except the multicast model of Section 17.3.

Definition 17.5.1. In all single-receiver models, the *local delay of the typical node* is the number of time slots needed for node $X_0 = 0$ (considered under the Palm probability $\mathbf{P}^0$ with respect to Φ) to successfully transmit:

$$\mathbf{L} = \mathbf{L}_0 = \inf\{n \geq 1 : \delta_0(n) = 1\}\,.$$

This random variable depends on the origin of time (here 1) but we focus on its law below, which does not depend on the chosen time origin.

The main objective of the remaining part of this section is to study the *mean local delay* $\mathbf{E}^0[\mathbf{L}]$. In particular, we show that it can be finite or infinite depending on the receiver model and fast or slow fading and noise model. For some models, it can exhibit the following phase transition: $\mathbf{E}^0[\mathbf{L}] < \infty$ or $\mathbf{E}^0[\mathbf{L}] = \infty$ depending on the model parameters (as p, distance r to the receiver, or the mean fading $1/\mu$). This will be referred to as the *wireless contention phase transition* in what follows.

Let $\mathcal{S}$ denote all the *static elements of the network model*: i.e. the elements which are random but which do not vary with time n. In all models, we have $\Phi \in \mathcal{S}$. Moreover, in the slow fading model, we have $\{\mathbf{F}_i\} \in \mathcal{S}$ and similarly in the slow noise model, $W \in \mathcal{S}$. For the fixed Poisson INR and MNN models, we also have $\Phi_0 \in \mathcal{S}$.

Given a realization of all the elements of $\mathcal{S}$, denote by

$$\pi_c(\mathcal{S}) = \mathbf{E}^0[e_0(1)\delta_0(1) \,|\, \mathcal{S}] \tag{17.32}$$

the conditional probability, given $\mathcal{S}$, that X_0 is authorized to transmit by the MAC and that this transmission is successful at time $n = 1$. Note that due to our time-homogeneity, this conditional probability does not depend on n. The following result allows us to express $\mathbf{E}^0[\mathbf{L}]$.

Lemma 17.5.2. In all the receiver models considered above, assuming that the elements which are not static (i.e. which are not in $\mathcal{S}$) are i.i.d., we have

$$\mathbf{E}^0[\mathbf{L} \,|\, \mathcal{S}] = \frac{1}{\pi_c(\mathcal{S})} \quad \text{and} \quad \mathbf{E}^0[\mathbf{L}] = \mathbf{E}^0\Big[\frac{1}{\pi_c(\mathcal{S})}\Big]\,. \tag{17.33}$$

Remark: One can interpret $\pi_c(\mathcal{S})$ as the *conditional throughput* of node X_0, given all the static elements of the network. Its inverse $1/\pi_c(\mathcal{S})$ is the conditional local delay of node X_0 in this environment. In many cases, this conditional throughput is a.s. positive (so that delays are a.s. finite) for all static environments. If this last condition holds true, by Campbell's formula, almost surely, all the nodes have a positive conditional throughput and finite conditional delay. However, the spatial irregularities of the network imply that this conditional throughput varies from node to node; in a Poisson configuration, one can find nodes which have an arbitrarily small conditional throughput (and consequently an arbitrarily large conditional delay). The mean local delay $\mathbf{E}^0[\mathbf{L}]$ is the spatial average of these conditional local delays. A finite mean indicates that the fraction of nodes in bad shape (for throughput or delay) is in some sense not significant. In contrast, $\mathbf{E}^0[\mathbf{L}] = \infty$ indicates that an important fraction of the nodes are in a bad shape. This is why the finiteness of the mean local delay is an important performance indicator of the network.

Proof. (of Lemma 17.5.2) Since the elements which are not in $\mathcal{S}$ do not change over time, given a realization of the elements of $\mathcal{S}$, the successive attempts of node X_0 to access to the channel and successfully transmit at time $n \geq 1$ are independent (Bernoulli) trials with probability of success $\pi_c(\mathcal{S})$. The conditional local delay $\mathbf{L} = \mathbf{L}_0$ is then a geometric random variable (the number of trials until the first success in the sequence of Bernoulli trials) with parameter $\pi_c(\mathcal{S})$. Its (conditional) expectation (given $\mathcal{S}$) is known to be

$$\mathbf{E}^0[\mathbf{L} \,|\, \mathcal{S}] \;\; = \;\; \sum_{n \geq 1} \mathbf{P}^0\{\, \mathbf{L} \geq n \,|\, \mathcal{S}\,\} = \sum_{n \geq 1} (1 - \pi_c(\mathcal{S}))^{n-1} = \frac{1}{\pi_c(\mathcal{S})}\,.$$

The result follows by integration with respect to the distribution of $\mathcal{S}$. □

Example 17.5.3. In order to understand the reasons for which $\mathbf{E}^0[\mathbf{L}]$ may or may not be finite, consider first the following two extremal situations. Suppose first that the whole network is independently re-sampled at each time slot (including node locations Φ, which is *not* our default option). Then $\mathcal{S}$ is empty (the σ-algebra generated by it is trivial) and the conditional throughput coincides with the the spatial average of the probability of success, namely $\pi_c(\mathcal{S}) = \mathbf{E}^0[e_0(1)\delta_0(1)] = p\,p_c$, where p_c is the coverage probability considered for the static model. Consequently, in this case of extreme variability (w.r.t. time), we have $\mathbf{E}^0[\mathbf{L}] = 1/(p\,p_c) < \infty$ provided $p_c > 0$, which holds true under very mild assumptions.

On the other hand, if nothing varies over time (including MAC status, which again is ruled out in our general assumptions), we have $\pi_c(\mathcal{S}) = e_0(1)\delta_0(1)$ (because the conditioning on $\mathcal{S}$ determines $e_0(1)\delta_0(1)$ in this case). In this case, under very mild assumptions (e.g. if $p < 1$), the conditional throughput $e_0(1)\delta_0(1)$ is zero with positive probability, making $\mathbf{E}^0[\mathbf{L}] = \infty$. Note that in this last case, some nodes in the MANET succeed in transmitting packets every time slot, whereas others never succeed. Having seen the above two extremal cases, it is not difficult to understand that the mean local delay strongly depends on how much the time-variability "averages out" the spatial irregularities seen by the MANET nodes.

Note that by Jensen's inequality,

$$\mathbf{E}^0[\mathbf{L}] \geq \frac{1}{\mathbf{E}^0[\pi_c(\mathcal{S})]} = \frac{1}{p\,p_c}\,.$$

The inequality is in general strict and we may have $\mathbf{E}^0[\mathbf{L}] = \infty$ while $p_c > 0$.

In the remaining part of this section we study several particular instances of space-time scenarios.

17.5.3 Local Delays in Poisson Bipolar Models

In the Poisson bipolar model, we assume a static location for the MANET nodes Φ and for their receivers $\{y_i\}$. The MAC variables $e_i(n)$ are i.i.d. in i and n. All other elements (fading and noise) follow different time scenarios.

17.5.3.1 Slow Fading and Noise Case

Let us consider first the situation where $\{\mathbf{F}_i\}$ and W are static.

Proposition 17.5.4. Assume the Poisson bipolar network model with slow fading and slow noise. If the distribution of F, W is such that $\mathbf{P}\{\, WTl(r) > F \,\} > 0$, then $\mathbf{E}^0[\mathbf{L}] = \infty$.

Proof. We have

$$\begin{aligned} \pi_c(\mathcal{S}) &= p\mathbf{E}^0[e_0(1)\delta_0(1) \,|\, \mathcal{S}] \\ &= p\mathbf{P}^0\{F_0^0 \geq Tl(r)(W + I_0^1(0)) \,|\, \mathcal{S}\} \\ &\leq p\mathbb{1}(F_0^0 \geq Tl(r)W)\,. \end{aligned}$$

This last indicator is equal to 0 with non-null probability by assumption. Using (17.33), we conclude that $\mathbf{E}^0[\mathbf{L}] = \infty$. □

17.5.3.2 Fast Fading Case

The following auxiliary result will be useful when studying fast Rayleigh fading.

Lemma 17.5.5. Consider the Poisson SN $I = \sum_{X_i \in \Phi} G_i / l(|X_i|)$, where Φ is some homogeneous Poisson p.p. with intensity α on $\mathbb{R}^2$, G_i are i.i.d. random variables with Laplace transform $\mathcal{L}_G(\xi)$ and $l(r)$ is any response function (in our case it will always be one of the OPL functions). Denote by $\mathcal{L}_I(\xi \,|\, \Phi) = \mathbf{E}[e^{-\xi I} \,|\, \Phi]$ the conditional Laplace transform of I given Φ. Then

$$\mathbf{E}\Big[\frac{1}{\mathcal{L}_I(\xi \,|\, \Phi)}\Big] = \exp\Big\{-2\pi\alpha \int_0^\infty v\Big(1 - \frac{1}{\mathcal{L}_G(\xi/l(v))}\Big)\,\mathrm{d}v\Big\}\,.$$

Proof. By the independence of G_i given Φ, we have

$$\begin{aligned} \mathbf{E}[e^{-\xi I} \,|\, \Phi] &= \prod_{X_i \in \Phi} \mathbf{E}[e^{-\xi \mathcal{L}_G(\xi/l(|X_i|))}] \\ &= \prod_{X_i \in \Phi} \mathcal{L}_G(\xi/l(|X_i|)) \\ &= \exp\Big\{\sum_{X_i \in \Phi} \log(\mathcal{L}_G(\xi/l(|X_i|)))\Big\}\,. \end{aligned}$$

Taking the inverse of the last expression and using the known formula for the Laplace transform of the Poisson p.p. (cf. Proposition 1.2.2 in Volume I), we obtain

$$\mathbf{E}\Big[\frac{1}{\mathcal{L}_I(\xi \,|\, \Phi)}\Big] = \exp\Big\{-\alpha \int_{\mathbb{R}^2} \Big(1 - e^{-\log(\mathcal{L}_G(\xi/l(|x|)))}\Big)\,\mathrm{d}x\Big\}\,. \tag{17.34}$$

Passing to polar coordinates completes the proof. □

Remark: The extension of the above result to a non-homogeneous Poisson p.p. Φ is straightforward and consists in replacing the integral $\alpha \int_{\mathbb{R}^2}(\ldots)\,\mathrm{d}x$ with respect to the Lebesgue measure $\alpha\,\mathrm{d}x$ on $\mathbb{R}^2$ in (17.34), by the integral of the same function with respect to the intensity measure of the considered non-homogeneous Poisson p.p. This extension is useful when we consider the local delay in the MNN model in Section 17.5.4, where the conditioning on the distance to the receiver modifies the intensity of the process of interferers (cf. Proposition 17.2.3) or in the MNN model with closest receiver in a cone (see Remark 17.5.14 below).

Coming back to local delays, let us now consider the situation where the random variables $\{\mathbf{F}_i(n)\}$ are i.i.d. in n. We consider only the Rayleigh fading case.

Proposition 17.5.6. Assume the Poisson bipolar network model with fast Rayleigh fading. We have

$$\mathbf{E}^0[\mathbf{L}] = \frac{1}{p}\mathcal{D}_W(Tl(r))\exp\left\{2\pi p\lambda \int_0^\infty \frac{vTl(r)}{l(v)+(1-p)Tl(r)}\,\mathrm{d}v\right\},$$

where

- $\mathcal{D}_W(s) = \mathcal{D}_W^{slow}(s) = \mathcal{L}_W(-s)$ for the slow noise case,
- $\mathcal{D}_W(s) = \mathcal{D}_W^{fast}(s) = 1/\mathcal{L}_W(s)$ for the fast noise case.

Proof. In the fast Rayleigh fading case, we have $\pi_c(\mathcal{S}) = \mathbf{P}\{F \geq Tl(r)(W + I^1)\,|\,\Phi\}$ for the fast noise case and $\pi_c(\mathcal{S}) = \mathbf{P}\{F \geq Tl(r)(W + I^1)\,|\,\Phi, W\}$ for the slow noise model. Using the assumption on F, we obtain

$$\pi_c(\mathcal{S}) = \mathcal{L}_W(\mu Tl(r))\mathbf{E}[e^{-\mu Tl(r)I^1}\,|\,\Phi]$$

in the fast noise case, and

$$\pi_c(\mathcal{S}) = e^{-\mu WTl(r)}\mathbf{E}[e^{-\mu Tl(r)I^1}\,|\,\Phi]$$

for the slow noise case. The result then follows from (17.33) and Lemma 17.5.5 with $G = eF$. Note that in this case, $\mathcal{L}_G(\xi) = 1 - p + p\mathcal{L}_F(\xi)$, which gives $\mathcal{L}_{eF}(\xi) = 1 - p + p\mu/(\mu + \xi)$. □

Remark 17.5.7 (Wireless contention phase transition for the mean local delay). Proposition 17.5.6 shows that in the fast fading and noise case, $\mathbf{E}^0[\mathbf{L}] < \infty$; indeed, $\int_0^\infty v/l(v)\,\mathrm{d}v < \infty$. However for the fast fading and slow noise case, the finiteness of the local delay depends on whether W has finite *exponential moments* of order $Tl(r)\mu$. This is a rather strong assumption concerning the tail distribution function of W. Often this moment is finite only for some sufficiently small value of $Tl(r)\mu$. For example, let us assume exponential noise with mean $1/\nu$. Then $\mathcal{L}_W(-\xi) = \nu/(\nu - \xi) < \infty$ provided $Tl(r)\mu < \nu$ and infinite for $Tl(r)\mu > \nu$. This means that in the corresponding Poisson bipolar MANET with a Rayleigh fading, exponential noise, we have the following *phase transition*: the mean local delay is finite whenever $Tl(r) < \nu/\mu$ and infinite otherwise. Here are a few incarnations of this phase transition:

- For fixed mean transmission power μ^{-1} (we recall that a typical situation is that where fading has mean 1 and where μ^{-1} is actually the effective transmission power) and mean thermal noise ν^{-1}, there is a threshold on the distance r between transmitter and receiver below which the mean local delays are finite and above which they are infinite;

- For fixed mean thermal noise ν^{-1} and fixed distance r, there is a threshold on mean transmission power μ^{-1} *above* which the mean local delays are finite and *below* which they are infinite;
- For fixed mean transmission power μ^{-1} and fixed distance r, there is a threshold on mean thermal noise power ν^{-1} *below* which the mean local delays are finite and *above* which they are infinite.

The fact that all transmissions contend for the shared wireless channel may lead to infinite mean local delays if the system is stressed by either of the phenomena listed above: too distant links, too high a thermal noise or too low a transmission power.

Remark 17.5.8 (Restart). There is a direct interpretation of the local delay in terms of the so-called *Restart algorithm*: assume a file of random size B is to be transmitted over an error prone channel. Let $\{A_n\}_{n\geq 1}$ be the sequence of channel inter-failure times. If $A_1 > B$ (resp. $A_1 \leq B$), the transmission succeeds (resp. fails) at the first attempt. If the transmission fails at the first attempt, one has to restart the whole file transmission in the second attempt and so on. Let

$$N = \inf\{n \geq 1 \; s.t. \; A_n > B\}$$

be the first attempt where the file is successfully transmitted. In the classical Restart scheme, the sequence $\{A_n\}_{n>0}$ is assumed to be i.i.d. and independent of B. It can then be proved (see (Asmussen, Fiorini, Lipsky, Rolski, and Sheahan 2008)) that when B has infinite support and A_n is light tailed (say exponential), then N is heavy tailed. This observation comes as a surprise because one can get heavy tails (including infinite first moments) in situations where B and A_n are both light tailed.

Consider the fast fading, slow noise case (and ignore the interference for simplicity). Then the local delay $\mathbf{L}_0$ of node X_0 under $\mathbf{P}^0$ can be seen as an instance of this algorithm with the following identification: $A_n = F_0^0(n)e_0(n)$ and $B = TWl(r)$. Later, in some nearest-receiver models we shall see other incarnations of the above Restart algorithm with deterministic W and where the role of the unboundedness of B is played by the distance to the receiver; cf. Remark 17.5.15.

We conclude this remark with a generic interpretation of the fact that the local delay of the typical node is heavy tailed. Let $\mathbf{L}_i$ be the time which elapses between time 0 and the time when the first packet is transmitted with success by node i. The ergodic interpretation of the Palm probability (see (10.9 in Volume I)) implies that, for all m,

$$P^0(\mathbf{L}_0 > m) = \lim_{R\to\infty} \frac{1}{\lambda|B_0(R)|} \sum_i 1_{X_i\in B_0(R), L_i > m},$$

where the last limit is in the almost sure sense. The fact that the distribution of $\mathbf{L}_0$ is heavy tailed under P^0 means that the discrete law $P^0(\mathbf{L}_0 > m)$ has no exponential moments. In view of the last equation, this is equivalent to saying that the limit of the empirical frequency of the nodes of a large ball which experience a (first) local delay of more than m time slots decreases slowly with m (more slowly than any exponential function).

17.5.4 Local Delay in the Nearest Receiver Model

In this section we study the Poisson INR and the MANET MNN models. We work out formulas for the mean local delay under the following conditions:

- fast Rayleigh fading,
- fast or slow noise,
- a fixed (i.e. not varying with time) pattern of potential receivers, which might be an independent Poisson process (as in the Poisson INR model) or the MANET pattern itself (as in the MNN model)).

Proposition 17.5.9. Assume fast Rayleigh fading and a fixed pattern of potential receivers.

- In the Poisson INR model, we have

$$\mathbf{E}^0[\mathbf{L}] = \frac{2\pi\lambda_0}{p} \int_0^\infty r e^{-\pi\lambda_0 r^2} \mathcal{D}_W(\mu T l(r))\, \mathcal{D}_I^{\mathrm{INR}}(\mu T l(r))\ \mathrm{d}r\,, \tag{17.35}$$

  where

$$\mathcal{D}_I^{\mathrm{INR}}(s) = \exp\left\{ 2\pi\lambda \int_0^\infty \frac{ps}{l(v)+(1-p)s} v\,\mathrm{d}v \right\} \tag{17.36}$$

  and $\mathcal{D}_W(s)$ is as in Proposition 17.5.6.
- In the MNN model, we have

$$\mathbf{E}^0[\mathbf{L}] = \frac{2\pi\lambda}{p(1-p)} \int_0^\infty r e^{-\pi\lambda r^2} \mathcal{D}_W(\mu T l(r))\, \mathcal{D}_I^{\mathrm{MNN}}(r, \mu T l(r))\ \mathrm{d}r\,, \tag{17.37}$$

  where

$$\mathcal{D}_I^{\mathrm{MNN}}(r,s) = \exp\left\{ \lambda\pi \int_0^\infty \frac{ps}{l(v)+(1-p)s} v\,\mathrm{d}v + \lambda \int_{\theta=-\frac{\pi}{2}}^{\frac{\pi}{2}} \int_{v>2r\cos\theta} \frac{ps}{l(v)+(1-p)s} v\,\mathrm{d}v\mathrm{d}\theta \right\} \tag{17.38}$$

  and $\mathcal{D}_W(s)$ is as in Proposition 17.5.6.

Proof. The proof follows the same lines as that of Proposition 17.5.6; the only modification bears on the conditioning on the distance r to the receiver; i.e. we have to use

$$E^0[\mathbf{L}] = \mathbf{E}^0[\mathbf{E}^0[\mathbf{L} \,|\, \mathcal{S}, r]] = \mathbf{E}^0\Big[\frac{1}{\pi_c(\mathcal{S}, r)}\Big]\,.$$

Recall also from Proposition 17.2.3, that in the MNN model, we also have to take into account how the conditioning on r modifies the density of the underlying Poisson p.p. of interferers. See the Remark after Proposition 17.5.5 on how to proceed in this situation. □

Notice that the integrals in (17.36) and (17.38) are finite for any of the OPL 1-3 models. However, the outer integrals (in r) in (17.35) and (17.37) may be infinite. In order to study this problem note first that we have the following bounds in the MNN model:

Remark 17.5.10. In the MANET receiver case, we have the bounds

$$\left(\mathcal{D}_I^{\mathrm{INR}}(s)\right)^{1/2} \leq \mathcal{D}_I^{\mathrm{MNN}}(r,s) \leq \mathcal{D}_I^{\mathrm{INR}}(s)\,. \tag{17.39}$$

The two next subsections study the finiteness of the mean local delays in particular cases.

17.5.4.1 Noise Limited Networks

Consider some fixed Poisson receiver model where interference is perfectly cancelled (and only noise has to be taken into account). In what follows we consider the fast noise scenario.

Independent Poisson Receiver Model (Poisson INR). Consider first the Poisson INR model. For the fast noise case, the next result follows from (17.35) with $\mathcal{D}_I(s) = 1$ and with $\mathcal{D}_W$ given in Proposition 17.5.6:

Corollary 17.5.11. In the Poisson INR model with fast Rayleigh fading and fast noise, if interference is perfectly canceled, then

$$\mathbf{E}^0[\mathbf{L}] = 2\pi\lambda_0 \int_0^\infty \frac{r\exp(-\pi\lambda_0 r^2)}{p\mathcal{L}_W(\mu l(r)T)}\mathrm{d}r.$$

Hence, $\mathbf{E}^0[\mathbf{L}] < \infty$ whenever

$$\mathcal{L}_W(\xi) \geq \eta\exp\left\{-\pi\lambda_0\left(\frac{\xi}{\mu T A^\beta}\right)^{2/\beta}\right\}\left(\xi^{2(1+\epsilon)/\beta}\right), \quad \xi\to\infty, \tag{17.40}$$

for some positive constants ϵ and η, and whenever some natural local integrability conditions also hold. This condition requires that there be a sufficient probability mass of W in the neighborhood of 0. For instance, under any of the OPL models, this holds true for a thermal noise with a rational Laplace transform (e.g. Rayleigh) but not for a constant and positive one.

The condition is sharp in the sense that when

$$\mathcal{L}_W(\xi) \leq \eta\exp\left\{-\pi\lambda_0\left(\frac{\xi}{\mu T A^\beta}\right)^{2/\beta}\right\}\left(\xi^{2(1-\epsilon)/\beta}\right), \quad \xi\to\infty, \tag{17.41}$$

for some positive constants ϵ and η, then $\mathbf{E}^0[\mathbf{L}] = \infty$.

MANET Nearest Neighbor (MNN) Model. In the MNN model (with $0 < p < 1$), similar arguments show that the same threshold as above holds with

$$\mathcal{L}_W(\xi) \geq \eta\exp\left\{-\pi\lambda\left(\frac{\xi}{\mu T A^\beta}\right)^{2/\beta}\right\}\left(\xi^{2(1+\epsilon)/\beta}\right), \quad \xi\to\infty, \tag{17.42}$$

implying that $\mathbf{E}^0[\mathbf{L}] < \infty$ and a similar converse statement.

17.5.4.2 Interference Limited Networks

In this section, we assume OPL 3 and $W \equiv 0$. We analyze the Poisson INR and the MNN models separately.

Independent Poisson Receiver Model. In the Poisson INR case, using the fact that

$$2\pi \int_0^\infty \frac{pTl(r)}{l(v)+(1-p)Tl(r)} v \, \mathrm{d}v = p(1-p)^{\frac{2}{\beta}-1} T^{\frac{2}{\beta}} K(\beta) r^2,$$

with $K(\beta)$ defined in (16.9), we get the following result from (17.35) and (17.36):

Corollary 17.5.12. In the Poisson INR model with $W = 0$, fast Rayleigh fading and OPL 3, we have

$$\mathbf{E}^0[\mathbf{L}] = 2\pi\lambda_0 \frac{1}{p} \int_0^\infty r \exp\left(-\pi\lambda_0 r^2 + \lambda\theta(p,T,\beta) r^2\right) \mathrm{d}r \,,$$

with

$$\theta(p,T,\beta) = \frac{p}{(1-p)^{1-\frac{2}{\beta}}} T^{\frac{2}{\beta}} K(\beta) \,. \tag{17.43}$$

Notice that $\theta(p,T,\beta)$ is increasing in p and in T. We hence get the following incarnation of the wireless contention phase transition:

- If $p \neq 0$ and $\lambda_0\pi > \lambda\theta(p,T,\beta)$, then

$$\begin{aligned} \mathbf{E}^0[\mathbf{L}] &= \frac{1}{p} \frac{\pi\lambda_0}{\pi\lambda_0 - \lambda\theta(p,T,\beta)} \\ &= \frac{1}{p} \frac{\lambda_0}{\lambda_0 - \lambda \frac{2}{\beta}\Gamma(\frac{2}{\beta})\Gamma(1-\frac{2}{\beta}) p (1-p)^{2/\beta-1} T^{2/\beta}} < \infty \,. \end{aligned} \tag{17.44}$$

- If either $\lambda_0\pi < \lambda\theta(p,T,\beta)$ or $p = 0$, then $\mathbf{E}^0[\mathbf{L}] = \infty$.

Remark 17.5.13 (Wireless contention phase transition). Here are a few comments on this phase transition.

- The fact that $p = 0$ ought to be avoided for having $\mathbf{E}^0[\mathbf{L}] < \infty$ is clear;
- The fact that λ_0 cannot be arbitrarily small when the other parameters are fixed is clear too as this implies that:
  - at any given time slot, the transmitters compete for too small a set of receivers;
  - each targeted receiver is too far away from its transmitter.
- For T and β fixed, stability requires that receivers outnumber potential transmitters by a factor which grows like $p(1-p)^{2/\beta-1}$ when p varies; if this condition is not satisfied, this drives the system to instability because some receivers have too persistent interferers nearby (for instance, if $p = 1$, a receiver may be very close from a persistent transmitter which most often succeeds, forbidding (or making less likely) the success of any other transmitter which has the very same receiver).

MANET Nearest Neighbor Model. Fix $a, r \geq 0$. We have

$$\int_{ar}^{\infty} \frac{pTl(r)}{l(v)+(1-p)Tl(r)} v \, \mathrm{d}v = \frac{1}{2} r^2 p (1-p)^{\frac{2}{\beta}-1} T^{\frac{2}{\beta}} H(a, T(1-p), \beta/2) \, ,$$

with

$$H(a,w,b) = \int_{a^2 w^{-1/b}}^{\infty} \frac{1}{1+u^b} \, \mathrm{d}u. \tag{17.45}$$

Let

$$J(w,b) = \int_{-\pi/2}^{\pi/2} H(2\cos(\theta), w, b) \, \mathrm{d}\theta \, . \tag{17.46}$$

From (17.37) and (17.38), we then get the same type of phase transitions as for the Poisson INR model above:

- If $p \neq 0$

$$\frac{p}{(1-p)^{1-\frac{2}{\beta}}} T^{\frac{2}{\beta}} \left(\frac{K(\beta)}{2} + J(T(1-p), \frac{\beta}{2}) \right) < \pi, \tag{17.47}$$

  then $\mathbf{E}^0[\mathbf{L}] < \infty$;
- If

$$\frac{p}{(1-p)^{1-\frac{2}{\beta}}} T^{\frac{2}{\beta}} \left(\frac{K(\beta)}{2} + J(T(1-p), \frac{\beta}{2}) \right) > \pi, \tag{17.48}$$

  then $\mathbf{E}^0[\mathbf{L}] = \infty$.

We can use the bounds of Remark 17.5.10 to get the following and simpler conditions:

- If $p \neq 0$ and $\theta(p, T, \beta) < \pi$ then $\mathbf{E}^0[\mathbf{L}] < \infty$.
- If $\theta(p, T, \beta) > 2\pi$ then $\mathbf{E}^0[\mathbf{L}] = \infty$.

Pole of the Attenuation Function. We show below that this phase transition is not linked to the pole of the OPL 3 model at the origin.

For this, consider the OPL 1 case with $\beta = 4$. Using (2.27 in Volume I) with $t = \mu(1-p)Tl(r)$, we get that in the fixed Poisson receiver model,

$$\begin{aligned} \int_0^{\infty} \frac{pTl(r)}{l(v)+(1-p)Tl(r)} v \, \mathrm{d}v \quad &= \quad \frac{p}{1-p} \left[-\frac{1}{2A^2} \sqrt{(1-p)Tl(r)} \arctan\left((Ar_0)^2 \sqrt{\frac{1}{(1-p)Tl(r)}} \right) \right. \\ &\left. + \frac{\pi}{4A^2} \sqrt{(1-p)Tl(r)} + \frac{r_0^2}{2} \frac{(1-p)Tl(r)}{(1-p)Tl(r) + (Ar_0)^4} \right] . \end{aligned}$$

Hence, since $l(r) = (Ar)^4$ for $r \geq r_0$, the dominant term in the last function is

$$\exp\left[\frac{\pi}{4} \frac{p}{\sqrt{1-p}} \sqrt{T} r^2 \right] ,$$

when r tends to ∞. Let us take the instance of the Poisson receiver model: we get from (17.35) and (17.36) that the mean delay is finite if $p \neq 0$ and

$$\lambda_0 > \lambda\hat{\theta} = \lambda\frac{\pi}{2}\frac{p}{\sqrt{1-p}}\sqrt{T}$$

and infinite if either $p = 0$ or $\lambda_0 < \lambda\hat{\theta}$.

Remark 17.5.14. It is easy to extend the results of Proposition 17.5.9 to the case where one selects the closest receiver in a cone rather than the closest receiver in the whole space. For instance, consider the MNN model and assume the angle of the cone is π, then

$$\mathbf{E}^0[\mathbf{L}] = \frac{2\pi\lambda_0}{p}\int_0^\infty re^{-\pi\lambda_0 r^2}\mathcal{L}_W(\mu Tl(r))\,\mathcal{D}_I(r, Tl(r))\;\mathrm{d}r\,, \tag{17.49}$$

where $\mathcal{D}_W(s)$ is as in Proposition 17.5.6 and

$$\begin{aligned}\mathcal{D}_I(r,s) \;=\; & \exp\left\{\pi\lambda\int_0^\infty \frac{ps}{l(v)+(1-p)s}v\,\mathrm{d}v\right\}\\ & \times\exp\left\{2\lambda\int_{\theta=0}^{\pi/4}\int_0^\infty \frac{r}{\cos(\theta)}\frac{ps}{l(v)+(1-p)s}v\,\mathrm{d}v\,\mathrm{d}\theta\right\}\\ & \times\exp\left\{2\lambda\int_{\theta=\pi/4}^{\pi/2}\int_{r\cos(\theta)}^\infty \frac{ps}{l(v)+(1-p)s}v\,\mathrm{d}v\,\mathrm{d}\theta\right\}.\end{aligned}$$

We get the same phase transition phenomena as above, though with different multiplicative constants. This is easily extended to the MANET receiver model.

Remark 17.5.15 (Restart, cont.). We continue the analogy with the Restart algorithm described in Remark 17.5.8. Consider the fast Rayleigh fading, with slow, constant noise $W = Const$ in the contex of one of the nearest receiver models. Then the local time of a packet can be seen as an instance of this algorithm with the following identification: $A_n = F_0^0(n)e_0(n)$ and $B = TWl(\mathcal{D})$, where $\mathcal{D}$ is the (random) distance between the node where the packet is located and the target receiver. The support of $l(\mathcal{D})$ is unbounded (for instance, in the Poisson receiver model, for all the OPL models, the density of $\mathcal{D}$ at $r > 0$ is $2\lambda_0\pi\exp(-\lambda_0\pi r^2)r$ for r large).

The interference limited case can be seen as an extension of the Restart algorithm where the file size varies over time. More precisely, the model corresponding to the MANET receiver case is that where at attempt n, the file size is $B_n = f(\Phi, C_n)$, where Φ is the Poisson p.p. and $\{C_n\}_{n>0}$ is an independent i.i.d. sequence (here C_n is the set of fading variables and MAC decisions at time n).

17.5.5 Finite Mean Delays and Diversity

We describe below a few ways of getting finite mean local delay in fast fading scenarios. All the proposed methods rely on an increase of *diversity*: more variability in fading, more receivers and more mobility.

17.5.5.1 Heavy Tailed Fading

Weibull Fading. Assume OPL 3 and deterministic $W > 0$. Recall from (17.40) that in this case, the mean local delay is infinite (due to the noise constraint) for (fast) Rayleigh fading. However if we assume that F is Weibull of shape parameter k i.e.

$$\mathbf{P}[F > x] = \exp(-(x/c)^k),$$

for some c, with c and k positive constants, then the condition $k < 2/\beta$ is sufficient to ensure $\mathbf{E}^0[\mathbf{L}] < \infty$ in the noise limited scenario. Indeed then

$$\mathbf{P}(F > l(r)WT) = \exp\left\{-(l(r)TW/c)^k\right\} \geq \exp\left\{-(TW/c)^k (Ar)^{2-\epsilon}\right\},$$

for $r \geq 1/A$, and some $\epsilon > 0$. Therefore the finiteness of $\mathbf{E}^0[\mathbf{L}]$ (with cancelled interference) follows from the fact that the integral

$$\int_{1/A}^{\infty} r \exp\left\{-\pi\lambda_0 r^2 + (TW/c)^k (Ar)^{2-\epsilon}\right\} \mathrm{d}r$$

is finite.

Lognormal Fading. Assume now F is lognormal with parameters (μ, σ), that is $\log(F)$ is $\mathcal{N}(\mu, \sigma^2)$ (Gaussian of mean μ and variance σ^2) and that W is constant. Then

$$\begin{aligned}
\mathbf{P}(F > x) &= \mathbf{P}\left(\frac{\log(F) - \mu}{\sigma} > \frac{\log(x) - \mu}{\sigma}\right) \\
&= \frac{1}{\sqrt{2\pi}} \int_{\frac{\log(x)-\mu}{\sigma}}^{\infty} \exp(-u^2/2)\mathrm{d}u \\
&\sim \frac{1}{(\log(x) - \mu)/\sigma} \exp\left(-(\log(x) - \mu)^2/2\sigma^2\right),
\end{aligned}$$

when $x \to \infty$. We also have

$$\mathbf{P}(F > x) \geq \frac{(\log(x) - \mu)/\sigma}{1 + (\log(x) - \mu)^2/\sigma^2} \exp\left(-(\log(x) - \mu)^2/2\sigma^2\right),$$

for all $x > 0$. Thus we get

$$\begin{aligned}
\mathbf{E}^0[\mathbf{L}] &\leq B + \frac{2\pi\lambda_0}{p} \int_{r, l(r)WT) > \mu + C} r \exp\left(-\pi\lambda_0 r^2\right) \exp\left(\frac{(\log(l(r)WT) - \mu)^2}{2\sigma^2}\right) \frac{1 + \frac{(\log(x)-\mu)^2}{\sigma^2}}{\frac{\log(x)-\mu}{\sigma}} \mathrm{d}r \\
&< \infty,
\end{aligned}$$

where B, C are finite positive constants.

Let us conclude that a fading with heavier tails may be useful *in the noise limited scenario* in that the mean delay may be infinite for the Rayleigh case and finite for this heavier tailed case.

17.5.5.2 Networks with an Additional Periodic Infrastructure

The second line of thought is based on the idea that extra receivers should be added to fill in big voids. We assume again fast Rayleigh fading in conjunction with the "Poisson + periodic" independent receiver model (cf. Section 17.2.1). In this receiver model, we assume that the pattern of potential receivers consists of a Poisson p.p. and an additional periodic infrastructure. Since there is a receiver at distance at most, say κ, from every point, the closest receiver from the origin is at a distance at most κ and

$$\mathbf{E}^0[\mathbf{L}] = \int_0^\kappa \mathcal{D}_W(\mu T l(r))\, \mathcal{D}_I^{\mathrm{INR}}(T l(r))\, D(\mathrm{d}r)\,,$$

where $\mathcal{D}_W$, $\mathcal{D}_I^{\mathrm{INR}}$ are as in Proposition 17.5.9 and $D(\cdot)$ is the distribution function of the distance from the origin to the nearest receiver in this model. This last integral is obviously finite.

Notice that periodicity is not required here. The only important property is that each location of the plane has a node at a distance which is upper bounded by a constant.

17.5.5.3 High Mobility Networks

It was already mentioned in Section 17.5.2 (see in particular Remark 17.5.15) that if one can assume that the whole network is independently re-sampled at each time slot (including node locations Φ, which is *not* our default option) — an assumption which can be justified when there is a high mobility of nodes (see Section 1.3.3 in Volume I) — then $\mathbf{E}^0[\mathbf{L}] = 1/(pp_c) < \infty$ provided $p_c > 0$. This observation can be refined in at least two ways:

- Assume the Poisson INR model, with fixed potential receives, and high mobility of MANETS nodes, i.e., with $\Phi = \Phi(n)$ i.i.d. re-sampled at each $n \geq 1$. Assume also fast noise and fading. Then one can easily argue that

  $$\mathbf{E}^0[\mathbf{L}] = 2\pi\lambda_0 \int_{r>0} r \exp(-\pi\lambda_0 r^2) \frac{1}{p\mathcal{L}_W(\mu l(r)T)\mathcal{L}_{I^1}(\mu l(r)T)} \mathrm{d}r.$$

  The finiteness of the last integral can be assessed using arguments similar to those given above.
- Assume now the Poisson INR model, with i.i.d. potential receives $\Phi_0(n)$ and static MANET Φ. Assume also fast noise and fast fading. Then one can easily argue that

  $$\mathbf{E}^0[\mathbf{L}] = \mathbf{E}^0\left[\frac{1}{p2\pi\lambda_0 \int_0^\infty r \exp(-\pi\lambda_0 r^2)\mathcal{L}_W(\mu l(r)T) \prod_{i\neq 0}\left(1 - p + p\frac{1}{1+Tl(r)/l(|X_i|)}\right)\, \mathrm{d}r}\right].$$

  We found no closed form expression for the last expression. However, a convexity argument shows that the R.H.S. is bounded from above by

  $$2\pi\lambda_0 \int_0^\infty \frac{r\exp(-\pi\lambda_0 r^2)}{p\mathcal{L}_W(\mu l(r)T)} \mathbf{E}^0\left[\frac{1}{\prod_{i\neq 0}\left(1 - p + p\frac{1}{1+Tl(r)/l(|X_i|)}\right)}\right]\, \mathrm{d}r\,.$$

  This last expression is precisely equal to (17.35), i.e., to the mean local delay in the (static) Poisson INR model.

Remark: An important remark is in order. In the examples considered in this section, we perform (at least some part of) the space average of the probability of success and then a time average to get the mean local delay. This operation, which makes sense in the case of high mobility (of potential receivers, MANET nodes) always leads to a finite mean local delay. In contrast, in the previous sections (case of static Φ and Φ_0), we perform the time average first and then the space average, and we get a different result, which can for instance be infinite. We shall return to the analysis of local delays in Part V.

17.5.5.4 Shannon Local Delay

One may argue that if the mean delays are infinite in § 17.5, it is primarily because of the *coverage logic*, where one transmits full packets at time slots when the receiver is covered at the required SINR and where one wastes all the other time slots. This results in a Restart mechanism (cf. Remark 17.5.8 and 17.5.8), which in turn explains why we have heavy tails and infinite means. Adaptive coding offers the possibility of breaking the coverage/Restart logic: it gives up with minimal requirements on SINR and it hence provides some non-null conditional throughput at each time slot, where this throughput depends on the current value of the SINR (e.g. via Shannon's formula as described on Section 16.2.3).

There is no difficulty in extending the scenario of Section 16.2.3 to the time dimension exactly as in Section 17.5.1). Let $\mathcal{T}_0$ be the bit rate (measured in bits per second) obtained by node X_0 at time slot 0 within this framework (see (16.12)). It is natural to define the *Shannon conditional local delay* of node X_0 as

$$\mathbf{L}^{Sh} = \mathbf{L}_0^{Sh} = \frac{1}{p\mathbf{E}^0[\mathcal{T}_0 \,|\, \mathcal{S}]} ,$$

namely as the inverse of the time average of $\mathcal{T}_0$ given all the static elements (cf. Section 17.5.2). This definition is the direct analogue of that of the conditional local delay in the packet model. Here, it gives the mean delay to transmit a bit, given all static elements (in particular the locations of the nodes). Using the same arguments as in the analysis of expression (16.13), we obtain

$$\mathbf{E}^0[\mathbf{L}^{Sh}] = \mathbf{E}^0\left[\frac{1}{\int_0^\infty \pi_c(v \,|\, \mathcal{S})/(v+1)\,\mathrm{d}v}\right] , \tag{17.50}$$

where $\pi_c(v\,|\Phi) = \pi_c(\Phi)$ is defined in (17.32) and where we made the dependence on $T = v$ explicit.

We now show two examples where $\mathbf{E}^0[\mathbf{L}] = \infty$ but $\mathbf{E}^0[\mathbf{L}^{Sh}] < \infty$.

Poisson Bipolar Model. Consider the Poisson bipolar model in the slow noise, fast Rayleigh fading scenario. We saw in Remark 17.5.7 that in the noise limited case, a necessary condition for $\mathbf{E}^0[\mathbf{L}] < \infty$ is that the noise W has finite exponential moment of order $Tl(r)\mu$ (namely $\mathbf{E}[e^{\{WTl(r)\mu}] < \infty$). For the mean Shannon local delay, we have

$$\mathbf{E}^0[\mathbf{L}^{Sh}] \;=\; \mathbf{E}\left[\frac{1}{\int_0^\infty e^{-Wvl(r)\mu}/(v+1)\,\mathrm{d}v}\right] = \mathbf{E}\left[\frac{W}{\int_0^\infty e^{-vl(r)\mu}/(v/W+1)\,\mathrm{d}v}\right] ,$$

in the noise limited case. It is easy to see that the last expression is finite provided $\mathbf{E}[W] < \infty$ (which is much less constraining than the finiteness of the exponential moment).

Poisson Nearest Neighbor Model Consider now the Poisson INR model, with fast Rayleigh fading and OPL 3. Throughout this paragraph, we assume that the network is interference limited.

For the packet model, it follows from the discussion after Corollary 17.5.12 that if $\lambda_0 \pi < \lambda\theta(p,T,\beta)$, where $\theta(\cdot)$ is given by (17.43), then $\mathbf{E}^0[\mathbf{L}] = \infty$.

We show below that for this scenario, the mean value of the Shannon local delay is always finite. Using (17.50) and a conditioning w.r.t. the distance to the nearest neighbor, we obtain that

$$\begin{aligned}
\mathbf{E}^0[\mathbf{L}^{Sh}] &= 2\pi\lambda_0 \frac{1}{p} \int_0^\infty r e^{-\lambda_0 \pi r^2} \mathbf{E}^0\left[\left(\int_0^\infty \frac{1}{u+1} \exp\Big\{ \sum_{X_i \neq X_0} \log \mathcal{L}_{eF}\big(\mu u (r/|X_i|)^\beta\big)\Big\} \mathrm{d}u\right)^{-1}\right] \mathrm{d}r \\
&= 2\pi\lambda_0 \frac{1}{p} \int_0^\infty r e^{-\lambda_0 \pi r^2} \mathbf{E}^0\left[\left(\int_0^\infty \frac{1}{v+r^\beta} \exp\Big\{ \sum_{X_i \neq X_0} \log \mathcal{L}_{eF}\big(\mu v/|X_i|^\beta\big)\Big\} \mathrm{d}v\right)^{-1}\right] \mathrm{d}r\,.
\end{aligned}$$

In order to derive an upper bound on the last expression, we make use of the following set of inequalities:

$$\begin{aligned}
\int_0^\infty \frac{\exp\{\dots\}}{v+r^\beta}\,\mathrm{d}v &\geq \frac{1}{2r^\beta}\int_0^{r^\beta} \exp\{\dots\}\,\mathrm{d}v + \int_{r^\beta}^\infty \frac{\exp\{\dots\}}{2v}\,\mathrm{d}v \\
&\geq \min\Big(\frac{1}{2r^\beta},1\Big)\int_0^\infty \min\Big(\frac{1}{2v},1\Big)\exp\{\dots\}\,\mathrm{d}v \\
&\geq \min\Big(\frac{1}{2r^\beta},1\Big)\int_0^{1/2} \exp\{\dots\}\,\mathrm{d}v\,,
\end{aligned}$$

and

$$\begin{aligned}
\mathcal{L}_{eF} &\geq 1-p \\
\log \mathcal{L}_{eF}\big(\mu v/|X_i|^\beta\big) &\geq -\mathbf{E}[eF]\mu v/|X_i|^\beta = -pv/|X_i|^\beta\,,
\end{aligned}$$

for all i, where the last inequality is a consequence of Jensen's inequality. Let $\rho > 0$ be some fixed constant. We have hence

$$\mathbf{E}^0[\mathbf{L}^{Sh}] \leq 2\pi\lambda_0 \frac{B}{p} \mathbf{E}^0\left[\exp\Big\{-\log(1-p)\Phi(\{X_i : |X_i| \leq \rho\})\Big\}\left(\int_0^{1/2} \exp\Big\{-pv \sum_{|X_i|>\rho} |X_i|^{-\beta}\Big\}\,\mathrm{d}v\right)^{-1}\right],$$

where

$$B = \int_0^\infty 2r/(\min(r^{-\beta},2)) e^{-\lambda_0\pi r^2}\,\mathrm{d}r < \infty.$$

We conclude that for proving $\mathbf{E}^0[\mathbf{L}^{Sh}] < \infty$, it is enough to prove that

$$\mathbf{E}^0\left[\exp\Big\{-\log(1-p)\Phi(B_0(\rho))\Big\}\left(\int_0^{1/2} \exp\Big\{-pv \sum_{|X_i|>\rho} |X_i|^{-\beta}\Big\}\,\mathrm{d}v\right)^{-1}\right] < \infty\,.$$

Using the independence of the Poisson p.p. in $B_0(\rho)$ and in $B_0^c(\rho)$ together with the fact that the Poisson variable $\Phi(\{X_i : |X_i| \leq \rho\})$ has finite exponential moments, we see that $\mathbf{E}^0[\mathbf{L}^{Sh}] < \infty$ if

$$\mathbf{E}^0\left[\left(\int_0^{1/2} \exp\Big\{-pv \sum_{|X_i|>\rho} |X_i|^{-\beta}\Big\}\,\mathrm{d}v\right)^{-1}\right] < \infty.$$

Let $J = \sum_{|X_i|>\rho} |X_i|^{-\beta}$. We have

$$\mathbf{E}^0\Big[\Big(\int_0^{1/2} \exp\Big\{-pv \sum_{|X_i|>\rho} |X_i|^{-\beta}\Big\}\,\mathrm{d}v\Big)^{-1}\Big] = \mathbf{E}^0\Big[\frac{pJ}{1-e^{-pJ/2}}\Big] < \infty\,.$$

Note that for J small, $pJ/(1-e^{-pJ/2})$ is close to 2, whereas for J bounded away from 0, we have

$$\mathbf{E}^0\Big[\frac{pJ}{1-e^{-pJ/2}}\mathbb{1}(J>\epsilon)\Big] \le (1-e^{-p\epsilon/2})p\mathbf{E}^0[J] = (1-e^{-p\epsilon/2})2p\pi\lambda\int_\rho^\infty t^{1-\beta}\,\mathrm{d}t < \infty$$

since $\beta > 2$. This concludes the proof of $\mathbf{E}^0[\mathbf{L}^{Sh}] < \infty$.

17.5.6 The Multicast Mode

In the multicast mode, we denote by $\mathbf{L}^m$ the time for a packet of the typical node to be captured by at least one among the potential receivers. This *multicast local delay* will be used in Part V and in particular in opportunistic routing, where it will be important to check whether (and when) at least one receiver was successful in capturing the transmitted packet.

The setting of the present section is the multicast mode of of Section 17.3, which is extended to the space-time scenario described in Section 17.5.1. We only consider the fast fading case and we adopt the following slight modification regarding the thermal noise, which varies from receiver to receiver. More precisely we consider the following *receiver dependent, fast noise assumption*:

($5^{s\times t}$) $\{W_i(n) : n \ge 1\}$ is an i.i.d. sequence, with generic random variable denoted by W, and where $W_i(n)$ represents the thermal noise at node X_i at time n.

Denote by $\delta(X_i, X_j, n)$ the indicator that (17.10) holds with F, I considered at time n and $W = W_j(n)$; namely, the indicator that node X_j is covered by transmitter X_i with the required quality at time n.

Definition 17.5.16. The local multicast delay of the typical node is the number of time slots needed for node $X_0 = 0$ (considered under the Palm probability $\mathbf{P}^0$ with respect to Φ) to successfully transmit to *some* node in Φ:

$$\mathbf{L}^m = \mathbf{L}_0^m = \inf\{n \ge 1 : \delta(X_0, X_j, n) = 1 \text{ for some } X_j \ne X_0 \in \Phi\}\,.$$

The local multicast number of trials is the number of time slots at which $X_0 = 0$ is authorized to transmit by the MAC which are needed for a successful transmission to some node in Φ:

$$\widetilde{\mathbf{L}}^m = \tilde{\mathbf{L}}_0^m = \#\{1 \le n \le \mathbf{L}_0^m : e_0(n) = 1\}\,.$$

Since the number of time slots between two tries is geometric of parameter p, the mean multicast local delay $\mathbf{E}^0[\mathbf{L}^m]$ is obtained from $\mathbf{E}^0[\widetilde{\mathbf{L}}^m]$ by the formula

$$\mathbf{E}^0[\mathbf{L}^m] = \frac{\mathbf{E}^0[\widetilde{\mathbf{L}}^m]}{p}\,.$$

In particular, both are finite or infinite at the same time, provided $p > 0$. As we shall see, the local multicast number of trials is often more handy to analyze in the present context.

In what follows we restrict our attention to the noise limited case, namely we assume that interference is perfectly cancelled and we give an explicit formula for the distribution function of the number of trials.

Proposition 17.5.17. Consider the multicast model with fast Rayleigh fading and receiver-dependent fast noise as described above. In the noise limited case, for all $q \geq 0$

$$\mathbf{P}^0[\widetilde{\mathbf{L}}^m > q] = \exp\left\{-2\pi\lambda \int_0^\infty r\Big(1 - \Big(1 - (1-p)\mathcal{L}_W(\mu T l(r))\Big)^q\Big)\,\mathrm{d}r\right\}. \tag{17.51}$$

Proof. As in the point-to point receiver models, conditioned on Φ, the number of trials until the first successful transmission is a geometric random variable. Denote by $\pi_c^m(\Phi)$ the parameter of this variable (i.e. the probability of success given Φ). Then

$$\mathbf{P}\{\,\widetilde{L}^m \geq q\,\} = \mathbf{E}^0[(1 - \pi_c^m(\Phi))^q]\,. \tag{17.52}$$

Let us calculate $1 - \pi_c^m(\Phi)$. Note that the latter is the probability that X_0 is *not* able to cover any node at time 0 given that it is authorized to transmit and given the location of all the nodes of Φ. In the noise limited scenario, we can exploit the independence structure of the marks to evaluate this probability as follows:

$$\begin{aligned}
1 - \pi_c^m(\Phi) &= \mathbf{E}^0\Big[\prod_{\Phi^0 \ni X_j \neq X_0} \Big(1 - \delta(X_0, X_j)\Big)\,\Big|\,\Phi\Big] \\
&= \prod_{X_j \neq X_0} \Big(1 - (1-p)\mathbf{P}\Big\{\,F_0^j > W_j T l(|X_j|)\,\Big|\,\Phi\,\Big\}\Big) \\
&= \exp\Big\{\sum_{X_j \neq X_0} \log\Big(1 - (1-p)\mathcal{L}_W(T l(|X_j|))\Big)\Big\},
\end{aligned}$$

where, for simplicity, we omitted the time parameter. Using (17.52) and the form of the Laplace transform of the SN (see Propositions 1.2.2 in Volume I and 2.2.4 in Volume I), we get (17.51) after passing to polar coordinates. □

Corollary 17.5.18. Under the assumptions of Proposition 17.5.17, we have

$$E^0[\mathbf{L}] = \frac{1}{p}\sum_{q=1}^\infty \exp\left\{-2\pi\lambda \int_0^\infty r\Big(1 - \Big(1 - (1-p)\mathcal{L}_W(\mu T l(r))\Big)^q\Big)\,\mathrm{d}r\right\}.$$

If we assume OPL 3,

$$E^0[\mathbf{L}] = \frac{1}{p}\sum_{q=1}^\infty \exp\left\{-\pi\lambda \int_0^\infty \Big(1 - \Big(1 - (1-p)\mathcal{L}_W(\mu T A^\beta v^{\beta/2}\beta)\Big)^q\Big)\,\mathrm{d}v\right\}.$$

Note that $\mathbf{E}^0[\mathbf{L}]$ is finite or infinite depending on whether the series on the R.H.S. in the above formulas converges or diverges. In what follows we work out a sufficient condition for convergence in the OPL 3 case.

Define the function

$$f(v) = (1-p)\mathcal{L}_W(\mu T A^\beta v^{\beta/2})\,. \tag{17.53}$$

Let $v_m(a)$ be the unique solution of $f(v) = \frac{a}{m}$ for any fixed a; (the existence and uniqueness follow from the monotonicity and continuity properties of the Laplace transform). If one denotes by $\mathcal{L}_W^{-1}$ the inverse of $\mathcal{L}_W$, then

$$v_m(a) = \left(\frac{\mathcal{L}_W^{-1}\left(\frac{a}{(1-p)m}\right)}{\mu T A^\beta} \right)^{2/\beta}\,.$$

Proposition 17.5.19. A sufficient condition for $\mathbf{E}^0[\mathbf{L}] < \infty$ is that the series

$$\sum_m \exp\Big\{ -\pi\lambda(1-e^{-a}) v_m(a) \Big\} \tag{17.54}$$

converges for some $a > 0$. For $a = 1$, a sufficient condition for this is that

$$\left(\frac{\mathcal{L}_W^{-1}(u)}{\mu T A^\beta} \right)^{2/\beta} \geq -\frac{1}{\pi\lambda} \log\left(\eta(u(1-p))^{1+\epsilon} \right), \quad u \to 0$$

for some positive constants η and ϵ, which holds true if

$$\mathcal{L}_W(x) \geq \frac{\kappa}{1-p} \exp\left(-\frac{\pi\lambda}{1+\epsilon} \left(\frac{x}{\mu T A^\beta} \right)^{2/\beta} \right), \quad x \to \infty\,, \tag{17.55}$$

for some positive constants κ and ϵ.

Proof. For m large enough, for v such that $f(v) \ll 1/m$, the function

$$v \to 1 - \Big(1 - (1-p)\mathcal{L}_W(\mu T A^\beta v^{\beta/2}) \Big)^m = 1 - (1-f(v))^m$$

is close to 0, whereas for $f(v) \gg 1/m$, it is close to 1. We have

$$\begin{aligned}
\int_{v>0} (1-(1-f(v)))^m)\ \mathrm{d}v &\geq \int_{v=0}^{v_m(a)} (1-(1-f(v)))^m)\ \mathrm{d}v \\
&\geq \int_{v=0}^{v_m(a)} (1-(1-f(v_m(a))))^m)\ \mathrm{d}v \\
&= \ v_m(a) \left(1 - \left(1 - \frac{a}{m} \right)^m \right) \geq v_m(a) \left(1 - e^{-a} \right),
\end{aligned}$$

where we used the monotonicity of $\mathcal{L}_W(\cdot)$ to obtain the second inequality and the bound $(1-a/m)^m \leq e^{-a}$ to get the last one. This proves the first statement of the result. The other statements follow from it. □

Here are two simple illustrations pertaining to these conditions.

Example 17.5.20 (Exponential Thermal Noise). If W is exponential with mean w, then

$$v_m(1) = \frac{1}{A^2\,(\mu T w)^{2/\beta}}(m(1-p)-1)^{2/\beta}$$

and the last series converges (as a corollary of the fact that (17.55) holds). This can be extended to the case when W has a rational Laplace transform.

Example 17.5.21 (Deterministic Thermal Noise). If W is deterministic with mean w, then

$$f(v) = (1-p)\exp(-w\mu T A^\beta v^{\beta/2})\,,$$

so that

$$v_m(1) = \frac{1}{A^2\,(\mu T w)^{2/\beta}}(\log(m(1-p)))^{2/\beta}$$

and the series (17.54) diverges.

Let us show that this implies that $\mathbf{E}^0[\mathbf{L}] = \infty$. By direct monotonicity arguments,

$$\int\limits_{v>0} (1-(1-f(v))^m)\,\mathrm{d}v \;\leq\; v_m(1) + \int\limits_{v_m(1)}^{\infty} (1-(1-f(v))^m)\,\mathrm{d}v.$$

But for all $\alpha > 1$, there exists an M such that for all $m \geq M$ and for all $v \geq v_m(1)$,

$$(1-f(v))^m \geq \exp(-\alpha m f(v)).$$

Hence, for all $m \geq M$,

$$\begin{aligned}
\int\limits_{v>0} (1-(1-f(v))^m)\,\mathrm{d}v &\leq v_m(1) + \int\limits_{v=v_m(1)}^{\infty} (1-\exp(-\alpha m f(v)))\;\mathrm{d}v \\
&\leq v_m(1) + \int\limits_{v=v_m(1)}^{\infty} \alpha m f(v)\,\mathrm{d}v \\
&= v_m(1) + \int\limits_{u=0}^{\infty} \alpha m f(u+v_m(1))\,\mathrm{d}u.
\end{aligned}$$

The second inequality follows from the fact that $1-\exp(-x) \leq x$. Using now the fact that $(u+v_m(1))^{\beta/2} \geq u + v_m(1)^{\beta/2}$ (which follows from a convexity argument and from the fact that $v_m(1) > 1$ for m large enough) and denoting by K the constant $w\mu T A^\beta$, we get that

$$\begin{aligned}
\int\limits_{u=0}^{\infty} m f(u+v_m(1))\,\mathrm{d}u &= \int\limits_{u=0}^{\infty} m(1-p)\exp(-K(u+v_m(1))^{\beta/2}))\,\mathrm{d}u \\
&\leq \int\limits_{u=0}^{\infty} m(1-p)\exp(-Ku - Kv_m(1)^{\beta/2})\,\mathrm{d}u = \frac{1}{K}\,,
\end{aligned}$$

since $(1-p)\exp(-Kv_m(1)^{\beta/2}) = 1/m$. Hence

$$\int_{v>0} (1-(1-f(v))^m)\, \mathrm{d}v \leq v_m(1) + \frac{1}{K}$$

and this implies that $E^0[\mathbf{L}] = \infty$.

Remark 17.5.22 (Time–Space Boolean isolation). In line with the general idea that a noise limited network can be seen as a Boolean model (see § 5.3 in Volume I), we can interpret the last results in terms of the following time–space extension of Boolean isolation: we declare a node $X \in \Phi$ isolated if the local delay of this node is infinite with positive probability, i.e. for all times n where X is a transmitter, for all nodes $X_j \in \Phi^0(n)$

$$|X - X_j| > l^{-1}\left(\frac{F_j(n)}{W_j(n)}\right).$$

A sufficient condition for a network to have no isolated node is that the (multicast) local delay of a typical node has a finite mean.

17.6 Conclusion

The receivers considered in the MANET receiver model introduced in § 17.2.2 need not be the final packet destinations. What was done in the present chapter is essentially one-hop analysis.

This one-hop analysis can however be used to assess the performance of multihop routing in a network with high node mobility; in this case, the configurations of nodes in two different time slots might be taken as independent and Poisson (see § 1.3.3 in Volume I and § 17.5.5.3); one can then use independence to analyze the fate of a packet along its route in terms of spatial averages for the one-hop case.

If this high mobility assumption cannot be made, multi-hop analysis is considerably more complex as we shall see in Part V and particularly in Chapter 22.

18

Carrier Sense Multiple Access

18.1 Introduction

As explained in §25.1.3, the general idea of Carrier Sense Multiple Access (CSMA) is to schedule transmissions in such a way that nodes which are close by never transmit simultaneously. This is of course expected to improve on Aloha where the rarity of the random channel access is the only mechanism for preventing the simultaneous transmission of such nodes.

The physical description of the mechanisms allowing the nodes of a network to realize this exclusion rule is as follows: one says that node y is in the *contention domain* of node x if the power received by x from y is above some detection threshold. The *neighbors* of a node are the nodes in its contention domain. Each node listens to the channel and senses an *idle medium* if there is no active transmitter in its contention domain. CSMA stipulates that each node can transmit only if it senses an idle medium. However, a strategy where a node transmits as soon as it senses an idle channel is not good since it may lead to a situation where several nodes simultaneously start transmitting when their common neighbor terminates its transmission. To prevent this, the following backoff mechanism is implemented. Each node senses the medium continuously and it maintains a timer; if its medium is sensed busy, a node freezes its timer until the medium becomes idle; when its medium is sensed idle, a node decreases its timer by one unit per time slot and it is only when its timer expires that a node starts transmitting. After the transmission is completed, the timer is randomly reinitialized. If the chance that timers of close by nodes expire at the same time is small enough and if we neglect propagation delays, this mechanism leads to what is expected, namely a distributed mechanism where when a node transmits, there is never an active transmitter in its contention domain. Note however that due to non-negligible propagation delays and other phenomena, collisions can nevertheless occur. Of course the protocol is designed to cope with such collisions but we do consider this question here.

The first challenge of the present chapter is that of the representation of a snapshot of the the set of nodes which simultaneously access the channel at some tagged time slot. It is clear that even if the initial set of MANET nodes is some realization of a Poisson p.p. Φ, then the set of nodes which transmit at the tagged time slot cannot be obtained by an independent thinning of Φ. Indeed, the latter is again a Poisson p.p. and such a p.p. does in no way exclude the presence of nearby nodes as we know (see Chapter 1 in Volume I).

In § 18.2, we propose to represent this exclusion rule by a Matérn hard-core model (see Section 2.1.3 in Volume I).

The analytical framework proposed in § 18.2 allows us to derive closed form expressions for the density of nodes accessing the shared medium at the tagged time slot in § 18.3 and for the probability that two nodes of Φ at some given distance access the channel at the tagged time slot in § 18.4. We then show how the expressions obtained for the last two quantities can be used for evaluating quantities similar to those obtained in the Aloha case. In § 18.5, we focus on the bipolar network model and we derive the probability that a transmitting node is successful in 'covering' its receiver. This then allows us to optimize the density of successful transmissions w.r.t. the main protocol parameter, namely the detection threshold. We exemplify the potential of this analytical framework by comparing the performance of Aloha and CSMA when each protocol is optimized (Aloha w.r.t. the MAP and CSMA w.r.t. the detection threshold).

18.2 Matérn-like Point Process for Networks using Carrier Sense Multiple Access

Let $\widetilde{\Phi} = \{(X_i, m_i, \mathbf{F}_i)\}$ be an i.m. Poisson p.p., with intensity λ on $\mathbb{R}^2$ that integrates a discrete cross-fading model (cf. Example 2.3.9 in Volume I), where

(1) $\Phi = \{X_i\}$ denotes the locations of potential transmitters;
(2) $\{m_i\}$ are i.i.d. marks, uniformly distributed on $[0, 1]$
(3) $\{\mathbf{F}_i = (F_i^j : j)\}_i$ where F_i^j denotes the *virtual power* emitted by node i (provided it is authorized by the MAC mechanism) towards node X_j (this is similar to (4) of Aloha in Section 16.2). We assume that the random variables F_i^j i, j are i.i.d., with mean $1/\mu$. We denote by $G(t) = \mathbf{P}\{ F \leq t\}$ the d.f. of a generic fading variable F.

We specify later the locations of receivers to which the nodes $\{X_i\}$ wish to transmit their packets.

For $X_i \in \Phi$, let

$$\mathcal{N}(X_i) = \{(X_j, m_i, \mathbf{F}_j) \in \widetilde{\Phi} : F_j^i / l(|X_i - X_j|) \geq P_o, j \neq i\}\,, \tag{18.1}$$

be the set of neighbors of node X_i. In this definition, $P_o > 0$ is the detection threshold alluded to above and $l(\cdot)$ is some OPL model (for example one of OPL1–OPL3).

The medium access indicators $\{e_i\}_i$ are additional *dependent* marks of the points of Φ defined as follows:

$$e_i = \mathbb{1}\left(\forall_{X_j \in \mathcal{N}(X_i)}\, m_i < m_j\right) \tag{18.2}$$

(note that $\mathbf{P}\{m_i = m_j\} = 0$ for $i \neq j$). The point process

$$\Phi_{\mathrm{M}} := \{X_i \in \Phi : e_i = 1\}\,, \tag{18.3}$$

will be referred to as the *Matérn CSMA* point process. It defines the set of transmitters retained by CSMA as a *non-independent* thinning of the Poisson p.p. Φ.

Remark 18.2.1. A few important observations are in order:

- This model captures the key requirement that a retained node never has another retained node in its contention domain.

- The rationale for the above definition is that CSMA grants a transmission to a given node if this node has the minimal back-off timer among all nodes in its contention domain. The assumption that back-off timers are i.i.d. makes sense if the timers are initialized according to a memoryless law (in place of uniform, one can take any other distribution with a density to get an equivalent model).
- This construction leads to the following scenario: node x_1 is *not* retained because of it detects its neighbor x_2; moreover node x_2 in turn is *not* retained because it detects its neighbor x_3 (i.e, $m_1 > m_2 > m_3$, where m_i is the mark of x_i). Consequently, in the above Matérn CSMA model neither x_1 nor x_2 is retained. But if x_3 is *not* the neighbor of x_1, and if x_3 does not detect any of its neighbors then a more reasonable MAC would allow x_1 and x_3 to transmit simultaneously. Such scenario shows that the Matérn CSMA model is conservative.

Unlike in Aloha, in this Matérn CSMA model, the probability of medium access of a typical node $p = \mathbf{E}^0[e_i]$ is not given a priori and it has to be determined.

18.3 Probability of Medium Access

Denote by $\bar{\mathcal{N}} = \bar{\mathcal{N}}(\lambda)$ the expected number of neighbors of the typical node; $\bar{\mathcal{N}} = \mathbf{E}^0[\#\mathcal{N}(0)]$. By (18.1), Slivnyak's theorem and Campbell's formula we have

$$\bar{\mathcal{N}} = \mathbf{E}^0\Big[\sum_{(X_j,m_i,\mathbf{F}_j^0)\in\widetilde{\Phi}} \mathbb{1}(F_j^0/l(|X_i-X_j|) \geq P_o)\Big] = \lambda \int_{\mathbb{R}^2} \mathbf{P}\{\, F \geq P_o l(|x|)\,\}\,\mathrm{d}x = 2\pi\lambda \int_0^\infty \big(1-G(P_o l(r))\big)\, r\,\mathrm{d}r\,. \tag{18.4}$$

Example 18.3.1. Here are a few particular cases:

- for Rayleigh fading (exponential F with mean $1/\mu$)

$$\bar{\mathcal{N}} = 2\pi\lambda \int_0^\infty e^{-P_o\mu l(r)} r\mathrm{d}r\,.$$

- it is also easy to check that under OPL3, the last expression gives

$$\bar{\mathcal{N}} = \frac{2\pi\lambda\Gamma(2/\beta)}{\beta(P_o\mu)^{2/\beta}A^2}\,.$$

Proposition 18.3.2. Under the assumptions of the last section,

$$p = \mathbf{E}^0[e_0] = (1 - e^{-\bar{\mathcal{N}}})/\bar{\mathcal{N}}. \tag{18.5}$$

Proof. Under $\mathbf{E}^0$ let us condition on the event $m_0 = t$. Given this condition, we express e_0 as the value of some extremal shot-noise (cf. Section 2.4 in Volume I). For fixed t define

$$L(y, x, (m, f)) = \mathbb{1}\Big(f \geq P_o l(|x - y|) \text{ and } m < t\Big)\,, \tag{18.6}$$

where $x, y \in \mathbb{R}^2$, $0 \leq m \leq 1$, $f \geq 0$. Note that $L(0, X_i, (m_i, F_i^0)) = 1$ iff the node at the origin (assuming $m_0 = t$) detects its neighbor $(X_i, m_i, \mathbf{F}_i)$) and this neighbor has a timer smaller than t. By (18.2)

$$e_0 = \mathbb{1}\Big(\forall\, (X_j, m_j, \mathbf{F}_j) \in \widetilde{\Phi},\ L(0, X_j, (m_j, F_j^0)) = 0\Big) = \mathbb{1}(Z_{\widetilde{\Phi}} = 0)\,,$$

where $Z_{\widetilde{\Phi}}(0)$ is the following extremal shot-noise variable

$$Z_{\widetilde{\Phi}}(0) = \max_{(X_j, m_j, \mathbf{F}_j) \in \widetilde{\Phi}} L(0, X_j, (m_j, F_j^0))\,.$$

Note that $Z_{\widetilde{\Phi}}(0)$ takes only two values 0 or 1 and consequently

$$\mathbf{E}^0[e_0 | m_0 = t] = \mathbf{P}^0\{\, Z_{\widetilde{\Phi}} = 0 | m_0 = t\,\} = \mathbf{P}^0\{\, Z_{\widetilde{\Phi}} \leq 0 | m_0 = t\,\}\,.$$

By Slivnyak's Theorem and Proposition 2.4.2 in Volume I we have

$$\begin{aligned}
\mathbf{E}^0[e_0 | m_0 = t] &= \exp\Big\{-\lambda \int_{\mathbb{R}^2} \int_0^\infty \int_0^1 \mathbb{1}(L(0, x, (m, f)) = 1)\, \mathrm{d}m G(\mathrm{d}f)\}\mathrm{d}x\Big\} \\
&= \exp\Big\{-\lambda t \int_{\mathbb{R}^2} (1 - G(P_o l(|x|))\,\}\mathrm{d}x\Big\} = \exp\{-t\bar{\mathcal{N}}\}\,.
\end{aligned}$$

The result follows from (18.4) and deconditioning with respect to t. □

Remark: Note by the ergodicity of the model that p represents some spatial average, namely an average over all nodes of the Poisson configuration. More precisely λp is the density of the Matérn CSMA point process of nodes authorized to transmit at a given time slot. However, it does not mean that *any* given node is selected by the MAC with the time frequency p, even if in different time slots the marks $\{m_i\}$ are re-sampled in an i.i.d. manner.

Corollary 18.3.3. The probability $p = p(\lambda)$ is asymptotically equivalent to $1/\bar{\mathcal{N}}$ when λ tends to ∞.

The last results can be extended in various ways. Consider for instance the conditional probability, under $\mathbf{E}^0$, that node $X_0 = 0$ is retained given that there is a another node of Φ at distance r from the origin. Assuming Rayleigh fading, calculations similar to those made above show that this conditional probability is equal to

$$p_r = \int_0^1 e^{-t\bar{\mathcal{N}}} \Big(t\Big(1 - e^{-P_o \mu l(r)}\Big) + (1 - t)\Big)\,\mathrm{d}t = p - e^{-P_o \mu l(r)} \left(\frac{1 - e^{-\bar{\mathcal{N}}}}{(\bar{\mathcal{N}})^2} - \frac{e^{-\bar{\mathcal{N}}}}{\bar{\mathcal{N}}}\right). \tag{18.7}$$

18.4 Probability of Joint Medium Access

Unfortunately, neither the distribution function nor the Laplace Transform of the Matérn CSMA p.p. are known in closed form. This means that we cannot proceed to evaluate the probability of events of the form (16.2) pertaining to coverage. Instead, we study below the probability of joint medium access for several nodes. If such a probability is known for an arbitrary number of points with arbitrary locations, then the Laplace transform of Φ_{M} and thus the distribution of the selected points is determined.

18.4.1 k fold Palm Distribution of the Poisson Point Process

The distribution of the i.m. Poisson p.p. $\widetilde{\Phi}$ given its has k points located at y_i $(i = 1, \ldots, k)$ is the so-called k fold Palm distribution of $\widetilde{\Phi}$. For describing it, we need the following independent random objects:

- an i.m. Poisson point process $\widetilde{\Phi}$ defined as in Section 18.2;
- the random variables $\{\widehat{m}_i : i = 1, \ldots, k\}$, which represent the timers of the k additional points and which are assumed to be i.i.d. and uniformly distributed on $[0, 1]$;
- the random vectors
  - $\widehat{\mathbf{F}}_j = (\widehat{F}_j^i : i = 1, \ldots k)$, $j \geq 1$,
  - $\widehat{\mathbf{H}}_i = (\widehat{H}_i^j : j \geq 1)$, $i = 1, \ldots k$,
  - $\mathbf{H}_i = (H_i^j : j = 1, \ldots k, j \neq i)$, $i = 1, \ldots k$,

  all with i.i.d. components with distribution G. $\widehat{\mathbf{F}}_j$, $\widehat{\mathbf{H}}_i$ and $\mathbf{H}_i$ respectively represent the vectors of virtual powers emitted by the points of $\widetilde{\Phi}$ to the points $\{y_i\}$, by the points of $\{y_i\}$ to $\widetilde{\Phi}$ and from the points of $\{y_i\}$ to themselves.

Consider the following i.m.p.p.

$$\widehat{\Phi} = \left\{ \left(X_j, \left(m_j, \mathbf{F}_j, \widehat{\mathbf{F}}_j \right) \right) : (X_j, m_j, \mathbf{F}_j) \in \widetilde{\Phi} \right\} \cup \left\{ \left(y_i, \left(\widehat{m}_i, \mathbf{H}_i, \widehat{\mathbf{H}}_i \right) \right) : i = 1, \ldots, k \right\}. \tag{18.8}$$

The k fold Palm distribution of the i.m. Poisson p.p. $\widetilde{\Phi}$ at $y_1, \ldots, y_j$ is precisely the law of $\widehat{\Phi}$.

Define the neighbors of y_i in $\widehat{\Phi}$ by

$$\mathcal{N}(y_i) = \mathcal{N}_{\Phi}(y_i) \cup \mathcal{N}_{\mathbf{y}}(y_i)\,,$$

where

$$\begin{aligned} \mathcal{N}_{\Phi}(y_i) &= \{X_j \in \Phi : \widehat{F}_j^i / l(|X_j - y_i|) \geq P_o\}\,, \\ \mathcal{N}_{\mathbf{y}}(y_i) &= \{y_j : H_j^i / l(|y_j - y_i|) \geq P_o, j = 1, \ldots, k, j \neq i\} \end{aligned}$$

and its CSMA status $\widehat{e}_i$ by

$$\widehat{e}_i = \mathbb{1}\left(\forall\, X_j \in \mathcal{N}_{\Phi}(y_i),\ \widehat{m}_i < m_j \right) \mathbb{1}\left(\forall\, y_j \in \mathcal{N}_{\mathbf{y}}(y_i),\ \widehat{m}_i < \widehat{m}_j \right), \tag{18.9}$$

with the convention $\widehat{e}_i = 1$ if $\mathcal{N}(y_i) = \emptyset$.

We can now prove the following result.

Proposition 18.4.1. Let $\widehat{\Phi}$ be the above i.m. point process. Assume $t_1 < \cdots < t_k$. We have

$$\mathbf{P}\big\{\,\forall\, i=1,\ldots,k,\ \widehat{e}_i = 1 \,|\, \widehat{m}_i = t_1, \ldots, \widehat{m}_k = t_k\,\big\} \tag{18.10}$$

$$= \exp\Big\{-\lambda \sum_{J\subset\{1,\ldots,k\}} (-1)^{\#J+1} t_{\min_{i\in J}} \int_{\mathbb{R}^2} \prod_{i\in J}\Big(1 - G\big(P_o l(|x-y_i|)\big)\Big)\,\mathrm{d}x\Big\} \prod_{j=1}^{k}\prod_{i<j} G\big(P_o l(|y_i-y_j|)\big)\,.$$

Proof. We express $\cap_{i=1}^k \mathbb{1}(\widehat{e}_i = 1)$ using some extremal shot-noise as in the proof of Proposition 18.3.2 and use the first statement of Proposition 2.4.2 in Volume I. □

Corollary 18.4.2. The probability that the k points $y_1, \ldots, y_k$ jointly access the medium in the Matérn CSMA model given that the underlying Poisson p.p. has points at $y_1, \ldots, y_k$ is equal to

$$p(y_1,\ldots,y_k) = k! \int_{[0,1]^k} \mathbb{1}(0 \le t_1 < \ldots < t_k \le 1)\mathbf{P}\big\{\,\forall\, i=1,\ldots,k,\ \widehat{e}_i = 1 \,|\, \widehat{m}_i = t_1, \ldots \widehat{m}_k = t_k\,\big\}\, \mathrm{d}t_1 \ldots \mathrm{d}t_k\,.$$

We need the following corollary of the last results:

Corollary 18.4.3. Assume Rayleigh fading. Conditionally on the facts that $\widetilde{\Phi}$ has two points at y_1 and y_2 with $|y_1 - y_2| = r$ and that y_2 is retained in the CSMA Matérn point process, the probability of also retaining node y_1 is:

$$h(r) = \frac{\frac{2}{b(r)-\bar{\mathcal{N}}}\left(\frac{1-e^{-\bar{\mathcal{N}}}}{\bar{\mathcal{N}}} - \frac{1-e^{-b(r)}}{b(r)}\right)\left(1-e^{-P_o\mu l(r)}\right)}{\frac{1-e^{-\bar{\mathcal{N}}}}{\bar{\mathcal{N}}} - e^{-P_o\mu l(r)}\left(\frac{1-e^{-\bar{\mathcal{N}}}}{(\bar{\mathcal{N}})^2} - \frac{e^{-\bar{\mathcal{N}}}}{\bar{\mathcal{N}}}\right)}\,, \tag{18.11}$$

where $\bar{\mathcal{N}}$ is defined in (18.4) and

$$b(r) = 2\bar{\mathcal{N}} - \lambda \int_{\mathbb{R}^+}\int_0^{2\pi} e^{-P_o\mu\left(l(\tau))+l(\sqrt{\tau^2+r^2-2r\tau\cos(\theta)})\right)}\tau\,\mathrm{d}\theta\mathrm{d}\tau. \tag{18.12}$$

Proof. Consider the point process $\widehat{\Phi}$ with $k=2$ and with y_1 and y_2 as above. Given that the marks of y_1 and y_2 are t_1 and t_2 respectively, with $t_2 > t_1$, Proposition 18.4.1 gives

$$\mathbf{P}\big\{\,\widehat{e}_1 = 1, \widehat{e}_2 = 1 \,|\, \widehat{m}_i = t_1, \widehat{m}_2 = t_2\,\big\} = e^{\Psi}\left(1 - e^{-P_o\mu l(r)}\right)\,,$$

with

$$\begin{aligned}
\Psi &= \lambda t_1 \int_{\mathbb{R}^2} e^{-P_o\mu l(|x-y_1|)} e^{-P_o\mu l(|x-y_2|)}\mathrm{d}x - \lambda t_1 \int_{\mathbb{R}^2} e^{-P_o\mu l(|x-y_1|)}\mathrm{d}x - \lambda t_2 \int_{\mathbb{R}^2} e^{-P_o\mu l(|x-y_2|)}\mathrm{d}x \\
&= -\lambda t_1 \int_{\mathbb{R}^2} \left(1 - \left(1 - e^{-P_o\mu l(|x-y_1|)}\right)\left(1 - e^{-P_o\mu l|x-y_2|}\right)\right)\mathrm{d}x - (t_2 - t_1)\bar{\mathcal{N}} \\
&= -\lambda t_1 b(r) - (t_2 - t_1)\bar{\mathcal{N}}\,.
\end{aligned}$$

By deconditioning as indicated in Corollary 18.4.2, we get

$$\mathbf{P}\{\,\widehat{e}_1 = 1, \widehat{e}_2 = 1\,\} = \frac{2}{b(r) - \bar{\mathcal{N}}} \left(\frac{1 - e^{-\bar{\mathcal{N}}}}{\bar{\mathcal{N}}} - \frac{1 - e^{-b(r)}}{b(r)} \right) \left(1 - e^{-P_o \mu l(r)} \right).$$

The result then follows from (18.7). □

Notice that $\lim_{r\to\infty} b(r) = 2\bar{\mathcal{N}}$, so that (18.11) gives the following very much expected result: $\lim_{r\to\infty} h(r) = p = (1 - e^{-\bar{\mathcal{N}}})/\bar{\mathcal{N}}$. The $h(\cdot)$ function is plotted in Figure 18.1.

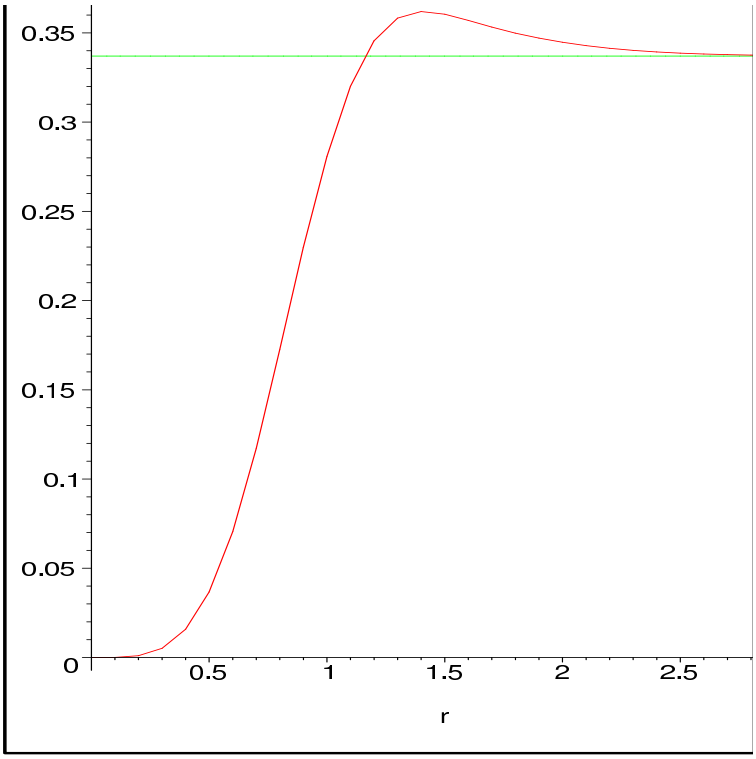

Fig. 18.1 The h function of Corollary 18.4.3. Here $P_o = 0.1$, $p \approx 0.337$, $\lambda = 1$, $\beta = 4$, $A = 1$, $T = 1$, $\mu = 10$.

18.5 Coverage

The aim of this section is twofold: 1) we exemplify the use of the Matérn p.p. framework for evaluating the probability of coverage of a receiver by its transmitter and the density of successful transmissions; 2) we show how to optimize the latter in a way similar to that of the Aloha case.

18.5.1 Definition

The probabilistic setting of this section is that of §18.2 with Rayleigh fading (F is exponential with parameter μ). Let x be a node of $\Phi_{\rm M}$. With definitions similar to those in Section 16.2, a receiver located at z is covered by x with level T if:

$$\text{SINR}(z) = \frac{F/l(|x - z|)}{W(z) + \sum_{x_i \in \Phi_{\rm M} \setminus x} F_i/l(|x_i - z|)} > T\,, \tag{18.13}$$

with F, F_i, $i \geq 1$, i.i.d. exponential random variables with parameter μ representing the virtual powers to point z.

Example 18.5.1. For commercial WiFi devices, the transmitted power $P = 1/\mu$ is around 100mW. For 802.11b, a SINR level of $T_1 = 4$dB is the minimum required for the receiver to be covered; it then gets an instantaneous bit-rate of (at least) ρ_1 =1 Mb/s. Similarly $T_2 = 7$dB, $T_3 = 11$dB and $\beta_4 = 16$dB are required for the higher bit-rates of ρ_2 =2 Mb/s, ρ_3 =5.5 Mb/s and ρ_4 =11 Mb/s, respectively. If the SINR at y is less than $T_1 = 4$dB, the user is not covered.

By analogy with what was done in the bipolar model for the Aloha case (see § 16.2), we assume that each transmitter has a single receiver at distance r and we look for the probability $p_c(r, P_o)$ that a transmitter covers his receiver with level T, where T is a constant. By this, we mean the probability that (18.13) be satisfied given that x is granted the right to transmit by the MAC.

18.5.2 Poisson Approximation

Assume without loss of generality that $x = 0$, so that $|z| = r$. By the same arguments as in the Aloha case,

$$\begin{aligned} p_c(r, P_o) &= \mathbf{P}^0(F/l(r)) \geq WT + \sum_{x_i \in \Phi_{\mathrm{M}} \backslash 0} F_i T/l(|x_i - z|) \mid 0 \in \Phi_{\mathrm{M}}) \\ &= \mathcal{L}_W(\mu T l(r)) \mathbf{E}^0 \left(\exp\left(-\mu T l(r) I_{\Phi_{\mathrm{M}} \backslash 0}(z) \right) \mid 0 \in \Phi_{\mathrm{M}} \right) , \end{aligned}$$

where P^0 denotes the Palm probability of the marked Poisson p.p. $\widetilde{\Phi}$. Since the (conditional) Laplace transform of

$$I_{\Phi_{\mathrm{M}} \backslash 0}(z) = \sum_{x_i \in \Phi_{\mathrm{M}} \backslash 0} F_i / l(|x_i - z|)$$

is not known in closed form, we resort to an approximation based on Corollary 18.4.3 and which consists in approximating the law of $\Phi_{\mathrm{M}} \backslash 0$ conditional on the event $\{0 \in \Phi_{\mathrm{M}}\}$ by that of a non-homogeneous Poisson point process of intensity λh with h the function defined in (18.11), that is

$$\mathbf{E}^0 \left(\exp\left(-s I_{\Phi_{\mathrm{M}} \backslash 0}(z) \right) \mid 0 \in \Phi_{\mathrm{M}} \right) \approx \exp\left(-\lambda \int_{\mathbb{R}^+} \int_0^{2\pi} \frac{\tau h(\tau)}{1 + \mu l\left(\sqrt{\tau^2 + r^2 - 2r\tau \cos(\theta)} \right)/s} \mathrm{d}\tau \mathrm{d}\theta \right) .$$

For instance, if $W = 0$ and OPL3 is used,

$$p_c(r, P_o) \approx \exp\left(-\lambda \int_{\mathbb{R}^+} \int_0^{2\pi} \frac{\tau h(\tau)}{1 + \frac{(\tau^2 + r^2 - 2r\tau \cos(\theta))^{\beta/2}}{T r^{\beta}}} \mathrm{d}\tau \mathrm{d}\theta \right) . \tag{18.14}$$

18.5.3 Optimization

We proceed as in the Aloha case. For some given transmission distance r, we look for the value of the detection threshold P_o which maximizes the density of successful transmissions which, in this setting, is equal to:

$$d_{suc}(r, P_o) = \lambda p p_c(r, P_o) \tag{18.15}$$

with p the probability for a node to be granted access to the channel given in (18.5).

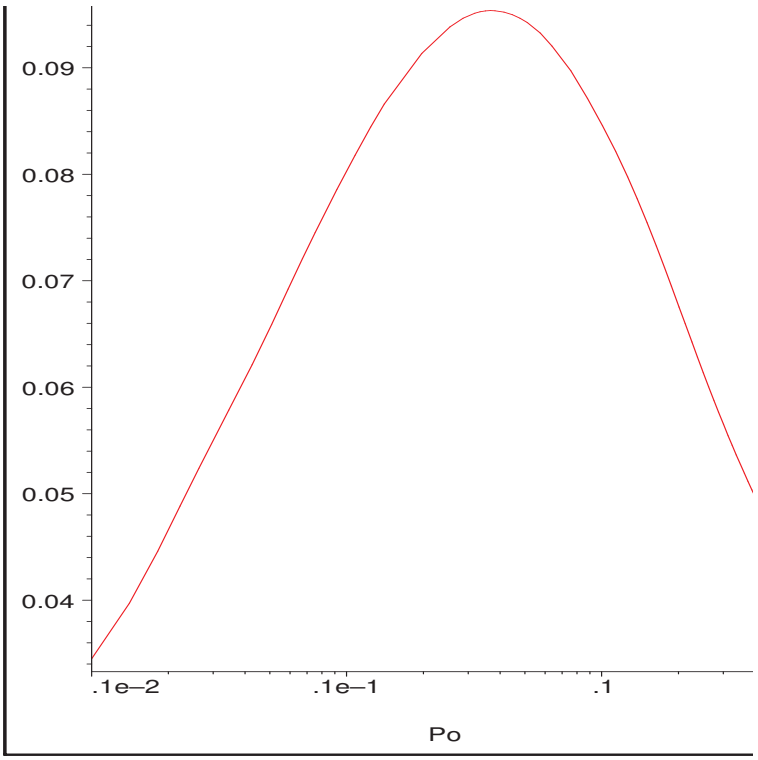

Fig. 18.2 The density of successful transmissions as defined in (18.15) for $r = 1$ as a function of P_o. Here $\lambda = 1, \beta = 4, A = 1, T = 1, \mu = 10$.

Example 18.5.2 (Numerical Example). Figure 18.2 plots the numerical values of $d_{suc}(1, P_o)$ in function of P_o. The underlying model is OPL3 with $W \equiv 0$ and the parameters are $\lambda = 1$, $\mu = 10$, $A = 1$ and $\beta = 4$.

The optimal value P_o^* of P_o is appr. 4.10^{-2}, which leads to a value for the probability of transmission p of appr. 0.22 and an optimal density of successful transmissions $d_{suc}(1, P_o^*)$ of appr. 0.095. Using the formulas of Proposition 16.3.2, we get that the corresponding values for Aloha with the same parameters are $p \approx 0.20$ and $d_{suc}(1, \lambda_{\max}) \approx 0.075$. So the adaptive nature of CSMA leads to a gain of appr. 25% in terms of density of successful transmissions compared to Aloha.

18.6 Conclusion

We conclude with a few words on what more could be done with the tools developed in this chapter and what should be done to refine the model.

We have shown that Matérn-like point processes offer a conservative computational framework for the evaluation of the channel acces probability and of the density of successful transmissions in large CSMA networks with randomly located nodes. This framework could also be used for evaluating other per-node or social MANET performance metrics (e.g. pertaining to throughput or transport). For the slotted CSMA case (which is used for instance in 802.15.4), the time-space analysis of § 17.5 could also in principle be extended.

A first model refinement would focus on the Request To Send – Clear to Send (RTS-CTS) mechanism. This mechanism, which is used in the 802.11 (WiFi) protocols, consists in checking the presence of contenders at the receiver and at the transmitter. The geometry of this mechanism should be amenable to an

analysis similar to the one performed here. It is only when the typical distance between transmitter and receiver is small compared to the mean distance between two nodes of Φ, that the model without RTS-CTS (considered above) can be considered as a reasonable approximation of the situation with RTS-CTS.

A second and more challenging refinement would consist in the design of more accurate (i.e. less conservative) hard core models (see Remark 18.2.1). Models based on e.g. Gibbs fields can be contemplated (see the bibliographical notes) but they do not lead to closed form expressions, at least in the random location networks considered here.

Non-slotted CSMA is more appropriate for the modeling of 802.11. For a Gibbsian analysis of this class of MAC on the grid, see (Durvy, Dousse, and Thiran 2009) and the references therein.

19

Code Division Multiple Access in Cellular Networks

19.1 Introduction

This chapter is devoted to the modeling of the Code Division Multiple Access (CDMA). In contrast with Aloha or CSMA where some transmitters are prevented from accessing the channel, in CDMA, all simultaneously access the shared medium and use a direct-sequence spread-spectrum mechanism (see Chapter 25 and Section 24.3.3) to cope with interference.

The two main novelties of this chapter are

(1) the fact that we take power control (see § 25.2 in Chapter 25), into account, which means that each transmission power is adjusted so as to satisfy the required SINR at the corresponding receiver and no more. We already saw that it was not always possible to solve this power control problem;
(2) the fact that we consider a cellular network (see § 25.3.2 in Chapter 25) rather than a MANET (as in the last three chapters). Such a network features base stations (BS) and mobiles connected to these base stations. Both on the uplink (UL) and the downlink (DL), we assume that each mobile is served by exactly one BS.

Section 19.2 is focused on the algebraic framework for stating the power control problem. It gives both a necessary and sufficient and a sufficient condition for the feasibility of power control within this cellular network setting. The sufficient condition is shown to lead to distributed power control mechanisms.

The stochastic setting, which is described in § 19.3, is based on a bi-variate p.p. model with a first p.p. representing the set of BSs and a second one representing the set of mobile users. We use the Voronoi tessellation w.r.t. the former to define the cells. The main general results are i) a 0-1 law stating that for a given infinite plane cellular network model, power control is feasible with probability either 0 or 1; ii) a proof of the fact that for all models based on a Poisson user p.p. the feasibility probability is 0.

When power control is not feasible, some admission (or rate) control protocol has to be used to reduce the configuration of mobiles (or to decrease their SINR target) so as to reach a new configuration (or new SINR targets) which is (are) feasible. This is the main objective of § 19.4 where we consider the case of large homogeneous networks represented by such bi-variate point processes and where we investigate:

- the relations between the density of BSs and the density of mobiles which can be served at a given bit-rate;
- the optimal way to share bandwidth between users when the latter have no minimal bit-rate requirements.

We show in § 19.5 that the spatial analysis conducted in the first sections of the present chapter can be used to answer questions which arise in time–space scenarios. We exemplify this on the case where users join and leave the network according to some random processes. We show how the spatial analysis allows one to evaluate the so-called *blocking probability*, which is the probability that an arriving user is denied access to the network because of the unfeasibility of power control.

19.2 Power Control Algebra in Cellular Networks

We first revisit the power control problem introduced in § 25.2 of Chapter 25 in the particular setting of cellular networks.

19.2.1 Notation

We use the following notation concerning BS locations and path loss:

- $\{X_u\}_u$ denotes the locations of BSs;
- $\{Y_m^u\} = S_u$ denotes the locations of the mobiles served by BS u;
- ${l_{\downarrow}}_m^u$ is the path-loss (possibly including some fading model) of the signal on the downlink $X_u \to Y_m^u$;
- ${l_{\uparrow}}_m^u$ is the path-loss (possibly including some fading model) of the signal on the uplink $Y_m^u \to X_u$.

We assume a direct-sequence spread-spectrum coding (see Section 24.3.3) with some interference cancellation (see Section 24.3.4). Although this is not critical for our analysis, we assume that this interference cancellation factor is equal to 1 on the UL as well as on the DL between two different BSs. We denote by

- α_u the DL-interference cancellation factor between mobiles of the same BS u. We also use the notation
$$\alpha_{uv} = \begin{cases} \alpha_u & \text{if } u = v \\ 1 & \text{if } u \neq v; \end{cases}$$
- ξ_m^u the SINR target for mobile Y_m^u. We use the notation ${\xi_{\downarrow}}_m^u$, ${\xi_{\uparrow}}_m^u$ if it is necessary to distinguish between the DL and the UL. Moreover, for each SINR ξ, we define a *modified SINR* ξ' by
$$ {\xi'_{\downarrow}}_m^u = \frac{{\xi_{\downarrow}}_m^u}{1 + \alpha_u {\xi_{\downarrow}}_m^u}, \qquad {\xi'_{\uparrow}}_m^u = \frac{{\xi_{\uparrow}}_m^u}{1 + {\xi_{\uparrow}}_m^u}, \tag{19.1}$$
- ${P_{\downarrow}}_m^u$ the power of the dedicated BS u for the channel $u \to m$;
- ${P_{\uparrow}}_m^u$ the power transmitted by mobile m to BS u;
- $\widetilde{P}^u$ the maximal total power allowed for BS u;
- Q^u the total power of the common channels (used for signaling);
- $P^u = Q^u + \sum_m {P_{\downarrow}}_m^u$ denotes total power transmitted by BS u;
- $\widetilde{P}_m^u$ the maximal power allowed for mobile $m \in S_u$;
- W^u, W_m^u, the power of the thermal noise at BS u and at mobile $m \in S_u$, respectively.

19.2.2 Feasibility of Power Control with Power Constraints

We now describe the power control problems with power constraints (the so-called *feasibility problems*).

Downlink. We say that the *(downlink) power control with power limitations is feasible* if there exist non-negative, finite powers $P_{\downarrow m}^{u}$ for all base stations u and mobiles m, which satisfy the following two conditions:

(1) SINR condition:

$$\frac{P_{\downarrow m}^{u}/l_{\downarrow m}^{u}}{W_m^u + \sum_v \alpha_{uv}(Q^v + \sum_{n\in S_v} P_{\downarrow n}^{v})/l_{\downarrow m}^{v}} \geq \xi'^{u}_{\downarrow m}, \quad \forall u, m \in S_u\,. \tag{19.2}$$

(2) Total power limitation condition:

$$\sum_{m\in S_u} P_{\downarrow m}^{u} + Q^u \leq \widetilde{P}^u, \quad \forall u.$$

We say that the downlink power control problem (without power limitations) is feasible if there exist non-negative powers $P_{\downarrow m}^{u}$ such that condition (1) above is satisfied.

Consider the square matrix $\mathbb{A} = (a_{uv})$, $a_{uv} = \alpha_{uv}\sum_{m\in S_u} \xi'^{u}_{\downarrow m} l_{\downarrow m}^{u}/l_{\downarrow m}^{v}$, the vector $\mathbf{b} = (b_u)$, $b_u = Q^u + \sum_{m\in S_u} \xi'^{u}_{\downarrow m} W_m^u l_{\downarrow m}^{u}$ and the identity matrix $\mathbb{I}$, all with the same dimension equal to the number of BSs (which is possibly infinite).

Lemma 19.2.1. The feasibility of the DL power control problem without power constraint is equivalent to the existence of finite, non-negative solutions $\mathbf{P} = (P_u)$ of the following linear inequality

$$(\mathbb{I} - \mathbb{A})\mathbf{P} \geq \mathbf{b}\,. \tag{19.3}$$

Proof. Assume that there exists a finite solution $P_{\downarrow m}^{u}$ to (19.2). Then

$$P_{\downarrow m}^{u} \geq l_{\downarrow m}^{u}\xi'^{u}_{\downarrow m}(W_m^u + \sum_v \alpha_{uv}Q^v) + \sum_{n\in S_v} P_{\downarrow n}^{v} l_{\downarrow m}^{u}/l_{\downarrow m}^{v}\xi'^{u}_{\downarrow m} \quad \forall u, m \in S_u\,.$$

By summing this set of inequalities over the mobiles $m \in S_u$, we get that $P_u = \sum_{n\in S_u} P_{\downarrow n}^{u}$ is a finite solution of (19.3).

Conversely, assume that (19.3) admits a finite solution $\mathbf{P} = (P_u)$. Then

$$P_{\downarrow m}^{u} = l_{\downarrow m}^{u}\xi'^{u}_{\downarrow m}(W_m^u + \sum_v \alpha_{uv}Q^v) + P_v l_{\downarrow m}^{u}/l_{\downarrow m}^{v}\xi'^{u}_{\downarrow m} \quad \forall u, m \in S_u$$

is a finite solution of (19.2) since for all v, $\sum_{n\in S_v} P_{\downarrow n}^{v} = P_v$. □

The existence of finite positive solutions of (19.3) depends on the spectral radius of the non-negative matrix $\mathbb{A}$. Since we want to treat the case when there is a countably infinite number of BSs, we define the spectral radius of $\mathbb{A}$ in the case where this matrix is of infinite dimension (see (Kitchens 1998) for details).

Let us denote by $\mathbb{A}^n = (a_{uv}^n)$ the nth power of $\mathbb{A}$, with $\mathbb{A}^0 = \mathbb{I}$ the identity matrix. Moreover, let

$$\mathbb{A}^* = (a_{uv}^*) = \sum_{n=0}^{\infty} \mathbb{A}^n.$$

Note that $\mathbb{A}^n$ (for all $n \geq 0$) and $\mathbb{A}^*$ are well defined, but that they may have some or all their entries infinite. If ${\xi'}_{\downarrow m}^{u} > 0$ and $\#S_u > 0$ for all u, m, then $a_{uv}^n > 0$ for all $n > 1$. Thus excluding the case of BSs serving no mobiles (and mobiles requiring ${\xi'}_{\downarrow m}^{u} = 0$), we get a positive and therefore irreducible matrix $\mathbb{A}$ for which all the power series

$$A_{uv}(z) = \sum_{n=0}^{\infty} a_{uv}^n z^n,$$

for $u, v = 1, 2, \ldots$, have a common convergence radius $0 \leq \mathcal{R} < \infty$ called the convergence radius of $\mathbb{A}$. The reciprocal $1/\mathcal{R}$ is called the Perron value of $\mathbb{A}$ or the spectral radius $\rho(\mathbb{A})$ of $\mathbb{A}$ (if $\mathbb{A}$ is finite, it is the Perron-Frobenius eigenvalue of $\mathbb{A}$). Moreover $A_{uv}(\mathcal{R}) < \infty$ for all $u \neq v$, and $A_{uu}(\mathcal{R})$ is either finite for all u (in which case $\mathbb{A}$ is said to be *transient*) or infinite for all u (in which case $\mathbb{A}$ is said to be *recurrent*).

Lemma 19.2.2. The condition $\rho(\mathbb{A}) \leq 1$ is necessary for the downlink power allocation problem without power constraint to be feasible. In case of equality, $\mathbb{A}$ has to be transient and $\mathbf{b} = \mathbf{0}$. Then, any solution of (19.3) is of the form $\mathbb{A}^*(\mathbf{b} + \boldsymbol{\xi}) + \mathbf{z}$, where $\boldsymbol{\xi} \geq 0$ and $\mathbf{z} \geq 0$ s.t. $\mathbf{z} = \mathbb{A}\mathbf{z}$, with the last term existing only in the infinite-dimensional case.

Remark: It may happen that $\mathbb{A}^*$ has all its entries finite and that the minimal solution $\mathbb{A}^* \mathbf{b}$ has all its entries infinite. With this precaution, and excluding $\mathbf{b} = \mathbf{0}$, we say for short that (19.3) has solutions iff the spectral radius of $\mathbb{A}$ is strictly less than one.

Note that any solution $\mathbf{P} = (P_u)$ of (19.3) has the following *coordinate-wise solidarity property*: if for any u, $P_u = \infty$, then $P_u = \infty$ for all u.

The successive iterations Ψ^n of the linear operator Ψ defined by $\Psi(\mathbf{s}) = \mathbb{A}\mathbf{s} + \mathbf{b}$ tend coordinate-wise with $n \to \infty$ to a solution $\mathbb{A}^*\mathbf{b} + \mathbf{z}$ and $\Psi^n(\mathbf{0})$ increases to the minimal solution.

The condition $\rho(\mathbb{A})$ is difficult to verify, in particular when the number of BSs is large. This explains the use of the following two sufficient conditions.

Lemma 19.2.3. (1) If for each BS u

$$\sum_{m \in S_u} \sum_{v} \frac{\alpha_{uv} {\xi'}_{\downarrow m}^{u} l_{\downarrow m}^{u}}{l_{\downarrow m}^{v}} < 1, \tag{19.4}$$

then the DL power control problem without power limitation is feasible.

(2) If for each BS u

$$\sum_{m \in S_u} \left(W_m^u + \sum_{v} \frac{\alpha_{uv} \widetilde{P}^v}{l_{\downarrow m}^{v}} \right) \frac{l_{\downarrow m}^{u} {\xi'}_{\downarrow m}^{u}}{\widetilde{P}^u} \leq 1 - \frac{Q^u}{\widetilde{P}^u}, \tag{19.5}$$

then the DL power control with power limitation is feasible.

Proof. A sufficient condition for the spectral radius of $\mathbb{A}$ to be less than 1, is the substochasticity of $\mathbb{A}$ (i.e. all its line-sums are less than 1). This last condition is equivalent to (19.4). Condition (19.5) is equivalent to saying that $(\mathbb{I} - \mathbb{A})\widetilde{\mathbf{P}} \geq \mathbf{b}$ where $\widetilde{\mathbf{P}} = (\widetilde{P}^u)$. This is obviously sufficient for the existence of solutions of (19.3) which satisfy the total power condition. □

It can also be shown that if $\widetilde{\mathbf{P}} = (\widetilde{P}^u)$ satisfies (19.3) then $P_{\downarrow m}^{u} = \widetilde{P}^u f_{\downarrow m}^{u}$ with

$$f_{\downarrow m}^{u} = \left(W_m^u + \sum_{v} \alpha_{uv} \widetilde{P}^v / l_{\downarrow m}^{v} \right) l_{\downarrow m}^{u} {\xi'}_{\downarrow m}^{u}, \quad m \in S_u$$

is the minimal solution of the DL power control problem with power limitation.

Uplink. We say that the UL power control with power constraint is feasible if there exist nonnegative, finite powers $P_{\uparrow m}^{u}$ such that the following two conditions are satisfied:

(1) SINR condition:

$$\frac{P_{\uparrow m}^{u}/l_{\uparrow m}^{u}}{W^{u}+\sum_{v}\sum_{n\in S_v}P_{\uparrow n}^{v}/l_{\uparrow n}^{u}}\geq \xi_{\uparrow m}^{\prime\, u},\quad \forall u, m\in S_u. \tag{19.6}$$

(2) power limitation condition:

$$P_{\uparrow m}^{u}\leq \widetilde{P}_{m}^{u},\quad \forall u \text{ and } m\in S_u.$$

We say that the UL power control without power constraint is feasible if there exist nonnegative finite powers $P_{\uparrow m}^{u}$ such that condition (1) above is satisfied.

Let $\mathbf{J}=(J_u)$ be the vector with entries $J_u=W^u+\sum_v\sum_{n\in S_v}P_{\uparrow n}^{v}/l_{\uparrow n}^{u}$, $\mathbf{W}$ the vector (W^u) and let $\mathbb{B}=(b_{uv})$ be the square matrix with entries $b_{uv}=\sum_{n\in S_v}\xi_{\uparrow n}^{\prime\, v}l_{\uparrow n}^{v}/l_{\uparrow n}^{u}$, all with dimension equal to the number of BSs.

Simple algebraic manipulations similar to those in the proof of Lemma 19.2.1 show that the feasibility of the UL power control problem without power constraint is equivalent to the existence of a non-negative finite solution $\mathbf{J}=(J_u)$ to the inequality

$$(\mathbb{I}-\mathbb{B})\mathbf{J}\geq \mathbf{W}. \tag{19.7}$$

Thus, we have the following result (cf. Lemma 19.2.2 for a more precise statement).

Lemma 19.2.4. The uplink power allocation problem without power constraint is feasible if and only if the spectral radius of $\mathbb{B}$ is less than 1.

Again, the substochasticity of $\mathbb{B}$ is a sufficient condition for the feasibility of the UL power allocation problem without power constraint.

Lemma 19.2.5. If for each BS u

$$\sum_{m\in S_u}\sum_{v}\frac{\xi_{\uparrow m}^{\prime\, u}l_{\uparrow m}^{u}}{l_{\uparrow m}^{v}}<1 \tag{19.8}$$

then the uplink power control without power limitation is feasible.

Taking the maximal power constraint of mobiles into account is more tricky than in the DL case and we do not present this here (some conditions can be found in (Baccelli, Błaszczyszyn, and Karray 2004)).

Decentralization of Power Control. We say that a power control condition COND is *decentralized* if it is of the form

$$\mathrm{COND}\equiv \forall_u\, \mathrm{COND}(u)\,,$$

where $\mathrm{COND}(u)$ is a condition that depends on the locations and parameters of the mobiles $\{m\in S_u\}$ and possibly on the locations and parameters of all other BSs, but *not* on the number, the location and the parameters of $\{n\in S_v\}$ for $v\neq u$. The conditions based on the spectral radius of the matrix $\mathbb{A}$ or $\mathbb{B}$ are not

decentralized. The conditions (19.4), (19.5) and (19.8) are decentralized and in each case, $\mathrm{COND}(u)$ has the following linear form

$$\mathrm{COND}(u) \equiv \sum_{m \in S_u} f_m \leq C_u \,, \tag{19.9}$$

where $f_m = f_m^u$ is some *virtual load* associated to mobile m of BS u (which depends on the considered condition) and C_u is the *maximal virtual load* of the BS allowed by this condition:

- For condition (19.5), the DL load brought by mobile $m \in S_u$ is:

$$f_{\downarrow m}^{\ u} = \left(W_m^u + \sum_v \frac{\alpha_{uv} \widetilde{P}^v}{l_{\downarrow m}^{\ v}} \right) \frac{l_{\downarrow m}^{\ u} \xi'^{\,u}_{\downarrow m}}{\widetilde{P}^u} \tag{19.10}$$

  and the maximal total load authorized by (19.5) is equal to $C_u = 1 - Q^u/\widetilde{P}^u$. Taking $\widetilde{P}^v = \widetilde{P}^u = \infty$ in the above formulas gives the load and the maximal load related to condition (19.4).
- For condition (19.8) The UL load brought by mobile m served by BS u is equal to

$$f_{\uparrow m}^{\ u} = \left(\sum_v \frac{1}{l_{\uparrow m}^{\ v}} \right) \xi'^{\,u}_{\uparrow m} l_{\uparrow m}^{\ u} \tag{19.11}$$

  and C_u is equal to 1.

Remark: Note that the load $f_{\downarrow m}^{\ u}$ (resp. $f_{\uparrow m}^{\ u}$) brought by mobile m is the product of the modified SINR target $\xi'^{\,u}_{\uparrow m}$ (resp. $\xi'^{\,u}_{\uparrow m}$), which determines its bit-rate (see Section 24.3.3) and some quantity which depends on the path-loss conditions of this users, which is primarily related to the network geometry and the fading (as well as the noise, the maximal BS powers and the interference cancellation factor in the case of (19.5)).

19.3 Spatial Stochastic Models

This section describes natural stochastic frameworks for analyzing the power control problem. We model the locations of BSs and mobiles maximal powers, noise, target SINRs etc. by marked point processes. As usual in our approach, we are primarily interested in models on the whole plane that allow one to evaluate spatial averages.

19.3.1 General Stationary Ergodic Model

Let the locations and characteristics of BSs (with their mobiles) be modeled by the following m.p.p.

$$\widetilde{\Phi} = \left\{ \left(X_u, W^u, Q^u, \alpha_u, \left\{ \left(Y_m^u, \xi'^{\,u}_{\downarrow m}, \xi'^{\,u}_{\uparrow m}, W_m^u \right) : m \in S_u \right\} \right) \right\}_u . \tag{19.12}$$

Assume the following path-loss model with cross-fading (cf. Example 2.3.9 in Volume I).

$$\frac{1}{l_{\downarrow m}^{\ u}} = \frac{F_{\downarrow m}^{\ u}}{l(|X_u - Y_m^u)}, \quad \frac{1}{l_{\uparrow m}^{\ u}} = \frac{F_{\uparrow m}^{\ u}}{l(|X_u - Y_m^u)}, \quad \text{for all } u, m \,, \tag{19.13}$$

where $l(\cdot)$ is some mean path-loss function (e.g. one of OPL1–OPL3). We have the following general result.

Proposition 19.3.1. Assume that the point process $\widetilde{\Phi}$ with the cross-fading model $\{F_{\downarrow m}^{\ u}, F_{\uparrow m}^{\ u}\}_{u,m}$ is stationary and ergodic. Then the (downlink or uplink) power control problem without power constraint is feasible with probability either 0 or 1.

Proof. We consider here only the downlink case (the proof for the case of uplink is similar). Note that the events $\{\mathbb{A}^*\mathbf{b} < \infty\}$, $\{$ convergence radius $\mathcal{R} \leq 1\}$, $\{$ convergence radius $\mathcal{R} > 1\}$, $\{$ matrix $\mathbb{A}$ is transient $\}$, $\{$ matrix $\mathbb{A}$ is recurrent $\}$ are invariant with respect to the discrete shift in $\mathbb{R}^2$. Thus, by ergodicity each of them has probability 0 or 1. If view of Lemma 19.2.2 the feasibility of the power allocation problem without power constraints can be expressed by means of standard Boolean operations on the above events. □

Note that the spectral radius of the random matrix $\mathbb{A}$ in the general ergodic model is deterministic too.

19.3.2 Poisson and Honeycomb Voronoi Access Network Model

We use the cellular network model introduced in Section 4.5 in Volume I to describe the locations of BSs and mobiles.

Suppose that $\widetilde{\Phi}_{\rm BS} = \{(X_u, W^u, Q^u, \alpha_u,)\}_u$ is some stationary, independently marked point process with intensity $0 < \lambda_{\rm BS} < \infty$ describing the locations and characteristics of BSs.

Consider a second independently marked Poisson point process $\widetilde{\Phi}_{\rm Mo} = \left\{\left(Y_m, \xi'_{\downarrow m}, \xi'_{\uparrow m}, W_m\right)\right\}_m$ with intensity $\lambda_{\rm Mo}$ describing the mobiles and their characteristics. We assume that $\widetilde{\Phi}_{\rm Mo}$ is independent of $\widetilde{\Phi}_{\rm BS}$.

Let the pattern S_u of mobiles served by the BS located at X_u be the set of points of $\Phi_{\rm Mo}$ located in the Voronoi cell of point X_u w.r.t. the point process $\Phi_{\rm BS}$; i.e., $S_u = \Phi_{\rm Mo} \cap \mathcal{C}_u(\Phi_{\rm BS})$, for all u. In other words

$$S_u = \left\{Y_m \in \Phi_{\rm Mo} : |Y_m - X_u| \leq |Y_m - X_v| \text{ for all } X_v \neq X_u \in \Phi_{\rm BS}\right\}.$$

In accordance with our general notation, we write $Y_m = Y_m^u$ for $Y_m \in S_u$. We call $\mathcal{C}_u = \mathcal{C}_u(\Phi_{\rm BS})$ the cell of the BS X_u. Note that with probability one no point of $\Phi_{\rm Mo}$ belongs to two or more cells. Assume moreover the path-loss model (19.13) with $F_{\downarrow m}^{\ u}, F_{\uparrow m}^{\ u}$ i.i.d. w.r.t. u and m.

Recall from Section 4.5 in Volume I that the mean number of mobiles per BS is $\bar{M} = \frac{\lambda_{\rm Mo}}{\lambda_{\rm BS}}$. It is convenient to relate $\lambda_{\rm BS}$ to the radius R of the (virtual) disc whose area is equal to that of the mean volume of the typical cell $\mathbf{E}^0[\mathcal{C}_0] = 1/\lambda_{\rm BS}$:

$$\frac{1}{\lambda_{\rm BS}} = \pi R^2 \,. \tag{19.14}$$

Bearing this definition in mind, we call R the radius of the (typical) cell.

We consider the following two models for BSs.

Poisson Model. In this case $\Phi_{\rm BS}$ is a Poisson p.p. on the plane, with intensity $\lambda_{\rm BS}$. This scenario will be referred to as the Poisson-Voronoi (PV) model.

Honeycomb Model. In the honeycomb model, BSs are placed on a regular hexagonal grid. The radius R of the point process is determined by the distance Δ between two adjacent BSs by the formula $\Delta^2 = 2\pi R^2/\sqrt{3}$. More precisely under the Palm distribution $\mathbf{P}^0$, the BSs are located on the grid denoted by

$$\Phi_{\rm BS} = \{X_u : X_u = \Delta(u_1 + u_2 e^{i\pi/3}),\ u = (u_1, u_2) \in \{0, \pm 1, \ldots\}^2\}$$

on the complex plane. In order to obtain a stationary distribution for $\Phi_{\rm BS}$, one randomly shifts the pattern of BSs by a vector uniformly distributed in the cell $\mathcal{C}_0$ (cf. Example 4.2.5 in Volume I). Note that the density of the BSs is related to Δ by the formula $\lambda_{\rm BS} = 1/(\pi R^2) = 2\pi\sqrt{3}/\Delta^2$. This model will be referred to as the Hex model.

The above models can be seen as two extreme and complementary cases: the Honeycomb model represents large perfectly structured networks and the Poisson-Voronoi model takes into account the irregularities observed in large real networks.

We have the following important negative result.

Proposition 19.3.2. Consider the Poisson-Voronoi model. For any $\lambda_{\rm BS} > 0$, $\lambda_{\rm Mo} > 0$ the (uplink or downlink) power control without power limitations is feasible with probability 0.

Proof. We consider here only the downlink. The uplink case is similar. With probability 1, the Poisson point process $\Phi_{\rm BS}$ has a cluster of BSs that leads to a super-stochastic (sum of elements in lines > 1) block in matrix $\mathbb{A}$. Thus the spectral radius of $\mathbb{A}$ is larger than 1. In fact, for all arbitrarily large $a > 0$, we can find a block with line-sums larger than a and this shows that $\rho(\mathbb{A}) = \infty$. □

This surprising property reveals some feature of the Poisson-Voronoi model in an infinite plane: the possible clustering of the BSs allowed by the Poisson model renders the power allocation problem unfeasible whatever the parameters of the model. However, even if the geometry of BS is perfectly regular, similar negative results hold:

Proposition 19.3.3. Consider the Honeycomb model. For any $\lambda_{\rm BS} > 0$, $\lambda_{\rm Mo} > 0$ the (uplink or downlink) power control without power limitations is feasible with probability 0.

Proof. This time, we use the clustering property of the Poisson p.p. $\Phi_{\rm Mo}$ and find with probability 1 a cluster of cells (hexagons) with some large enough number of mobiles in each one; this makes the associated block of matrix $\mathbb{A}$ super-stochastic. Thus the spectral radius of $\mathbb{A}$ is larger than any given arbitrarily large real number a. Consequently, the spectral radius of $\mathbb{A}$ is again infinite. □

So even for a very low density of mobiles or a very high density of BS, both the Poisson-Voronoi and the Honeycomb network architectures require some reduction of mobiles or of their target SINR's in order to make the power allocation problem feasible.

19.4 Maximal Load Estimation

Tha aim of this section is to show how the decentralized conditions of Section 19.2.2 can be used to enforce the feasibility of power control.

Two types of mechanisms are considered: admission and rate control.

Population Admission Control. Assume the bit-rates of all mobiles (or equivalently all ${\xi'}^u_{\downarrow m}, {\xi'}^u_{\uparrow m}$ parameters) are fixed. This is the situation for voice calls or certain types of streaming. Admission control then consists in reducing the population of mobiles so as to satisfy the sufficient condition ensuring the feasibility of power control.

Bit-rate Control. For so-called elastic traffic (data), one does not need any guarantee on the bit rates (or equivalently the ${\xi'}^u_{\downarrow m}, {\xi'}^u_{\uparrow m}$ parameters may be adapted). In this case the feasibility of power control can be attained via a reduction of the bit rates (i.e. a decrease of the SINR targets) of all users in some fair manner.

The decentralized admission/rate control policies defined and analyzed below provide conservative bounds for the maximal load of the network since these conditions are sufficient for the feasibility of power control but not necessary. In what follows we consider a snapshot of such a network and ask the following questions:

- For the fixed bit-rate traffic case, given $\lambda_{\rm BS}$, what is the maximal density of mobiles $\lambda_{\rm Mo}$ such that the decentralized conditions of Section 19.2.2 hold with sufficiently high probability?
- For the elastic traffic case, given $\lambda_{\rm BS}$, and $\lambda_{\rm Mo}$ what are the maximal fair bit-rates such that the decentralized conditions of Section 19.2.2 hold?

19.4.1 Mean Value Approach

We first analyze the conditions of Section 19.2.2 "in mean". Assume the stochastic Poisson-Voronoi or Honeycomb access network model of Section 19.3.2 with fixed maximal BS powers $\widetilde{P}^u \equiv \widetilde{P}$. Denote by $\alpha = \mathbf{E}[\alpha_u]$, $\overline{W} = \mathbf{E}[W]$, $\bar{\xi}'_\downarrow = \mathbf{E}[\xi'_\downarrow]$ and $\bar{\xi}'_\uparrow = \mathbf{E}[\xi'_\uparrow]$ the mean values of the interference cancellation factor, the thermal noise and the modified SINRs, respectively.

Let $\bar{\pi} = \mathbf{E}[Q]/\widetilde{P}$ be the mean fraction of the maximal power devoted to the common channels. Recall that $\bar{M} = \lambda_{\rm Mo}/\lambda_{\rm BS}$ is the mean number of mobiles per BS. We have the following "mean result" for the downlink, where $\mathbf{P}^0$ denotes the Palm distribution w.r.t. $\widetilde{\Phi}_{\rm BS}$.

Proposition 19.4.1. Assume the OPL3 model with constant fading $F^v_{\downarrow m} = F^v_{\uparrow m} = 1$ and constant maximal powers $\widetilde{P}^u \equiv \widetilde{P}$. Suppose that the pairs W^u_m, ${\xi'}^u_{\downarrow m}$ and α_u, ${\xi'}^u_{\downarrow m}$ are independent random variables for each u, m. Then

$$\begin{aligned}
\mathbf{E}^0\Big[\sum_{m\in S_0} f^0_{\downarrow m}\Big] &= \bar{M}\bar{\xi}'_\downarrow\Big(\alpha + \bar{f} + l(R)\bar{W}\bar{g}/\bar{P}_\downarrow\Big)\\
\mathbf{E}^0\Big[\sum_{m\in S_0} f^0_{\uparrow m}\Big] &= \bar{M}\bar{\xi}'_\uparrow(1+\bar{f})\,,
\end{aligned}$$

where R is the radius of the Voronoi cell (see (19.14)) and where $\bar{f}, \bar{g}$ are given by

$$\bar{f} = \begin{cases} \bar{f}_{\rm PV} = 2/(\beta-2) & \text{for the PV model}\\ \bar{f}_{\rm Hex} \approx 0.9365/(\beta-2) & \text{for the Hex model}\end{cases} \tag{19.15}$$

and

$$\bar{g} = \begin{cases} \bar{g}_{\rm PV} = \Gamma(1+\beta/2) & \text{for the PV model}\\ \bar{g}_{\rm Hex} \approx (1+\beta/2)^{-1} & \text{for the Hex model.}\end{cases} \tag{19.16}$$

($\bar{f}_{\rm Hex}, \bar{g}_{\rm Hex}$ are some constants depending only on β, which are not explicitly known; the above approximation are reasonable for $\beta \in [2.2, 5]$).

Proof. Note by (19.10) with $\widetilde{P}^u \equiv \widetilde{P}$

$$f^0_{\downarrow m} = \frac{W^0_m {\xi'}^0_{\downarrow m} l^0_{\downarrow m}}{\widetilde{P}} + \alpha_0 {\xi'}^0_{\downarrow m} + \sum_{v\neq 0} \frac{l^u_{\downarrow m}{\xi'}^u_{\downarrow m}}{l^v_{\downarrow m}}\,.$$

By the Neveu exchange formula (see Theorem 4.3.1 in Volume I)

$$\begin{aligned}
\mathbf{E}^0\Big[\alpha_0 \sum_{m\in S_0} \xi'^{\,0}_{\downarrow m}\Big] &= \frac{\lambda_{\rm Mo}}{\lambda_{\rm BS}}\mathbf{E}[\alpha_0 \xi'^{\,0}_{\downarrow}] = \bar{M}\alpha\bar{\xi}'_{\downarrow}\,,\\
\mathbf{E}^0\Big[\sum_{m\in S_0} W^0_m \xi'^{\,0}_{\downarrow m} l^{\,0}_{\downarrow m}\Big] &= \bar{M}\overline{W}\bar{\xi}'_{\downarrow} l(R)\bar{g}\,,\\
\mathbf{E}^0\Big[\sum_{m\in S_0}\sum_{v\neq 0} \frac{l^{\,u}_{\downarrow m}\xi'^{\,u}_{\downarrow m}}{l^{\,v}_{\downarrow m}}\Big] &= \bar{M}\bar{\xi}'_{\downarrow}\bar{f}\,,
\end{aligned}$$

where $\bar{f}$ and $\bar{g}$ depend only on the path-loss exponent β of the OPL 3 model. For the PV model, $\bar{f} = \overline{(RPL)}/\bar{M} = 2/(\beta-2)$, $\bar{g} = \overline{(PL)}/(\bar{M}l(R)) = \Gamma(1+\beta/2)$, are evaluated in Example 4.5.1 in Volume I. For the Hex model, these values have to be evaluated numerically. The proof for the up-link is similar. □

Corollary 19.4.2. Under the assumptions of Proposition 19.4.1, in order to satisfy condition (19.5) in mean (i.e. taking expectation w.r.t. $\mathbf{E}^0$ on both sides of (19.5) with $u = 0$), we need

$$\bar{M} \le \frac{1-\bar{\pi}}{\bar{\xi}'_{\downarrow}(\alpha + \bar{f} + l(R)\bar{\mathcal{N}}\bar{g}/\bar{P}_{\downarrow})}\,, \tag{19.17}$$

where $\bar{M} = \frac{\lambda_{\rm Mo}}{\lambda_{\rm BS}}$ is the mean number of mobiles per BS. We get the mean version of condition (19.4) by letting $\bar{P}_{\downarrow} \to \infty$ and $\bar{\pi} \to 0$ in (19.17).

Similarly, in order to satisfy condition (19.8) in mean, we need

$$\bar{M} \le \frac{1/\bar{\xi}'_{\uparrow}}{1+\bar{f}}, \tag{19.18}$$

where $\bar{f}$ is given by (19.15).

Figure 19.1 displays some numerical examples illustrating the above result.

19.4.2 Feasibility Probability

Another and more accurate load estimation is based on the feasibility probability. Let COND by a decentralized condition (see Section 19.2.2).

Definition 19.4.3. We define the power control feasibility probability with respect to the decentralized condition COND (*feasibility probability* for short) by $\mathbf{P}^0\{\,\mathrm{COND}(0)\,\}$; this is also the probability that this condition holds for the typical BS, or equivalently the fraction of BSs satisfying this condition.

Here is a refined load estimation based on the feasibility probability:

Definition 19.4.4. For a given density of BS $\lambda_{\rm BS} > 0$ (equivalently, typical cell radius $R < \infty$) and a cell rejection probability (CRP) $\epsilon > 0$, let $\lambda^{\epsilon}_{\rm Mo} = \lambda^{\epsilon}_{\rm Mo}(\lambda_{\rm BS})$ be the maximal density of mobiles (equivalently, the mean number $\bar{M} = \bar{M}^{\epsilon}(R)$ of users per cell) such that

$$\mathbf{P}^0\{\,\mathrm{COND}(0)\,\} \ge 1-\epsilon\,. \tag{19.19}$$

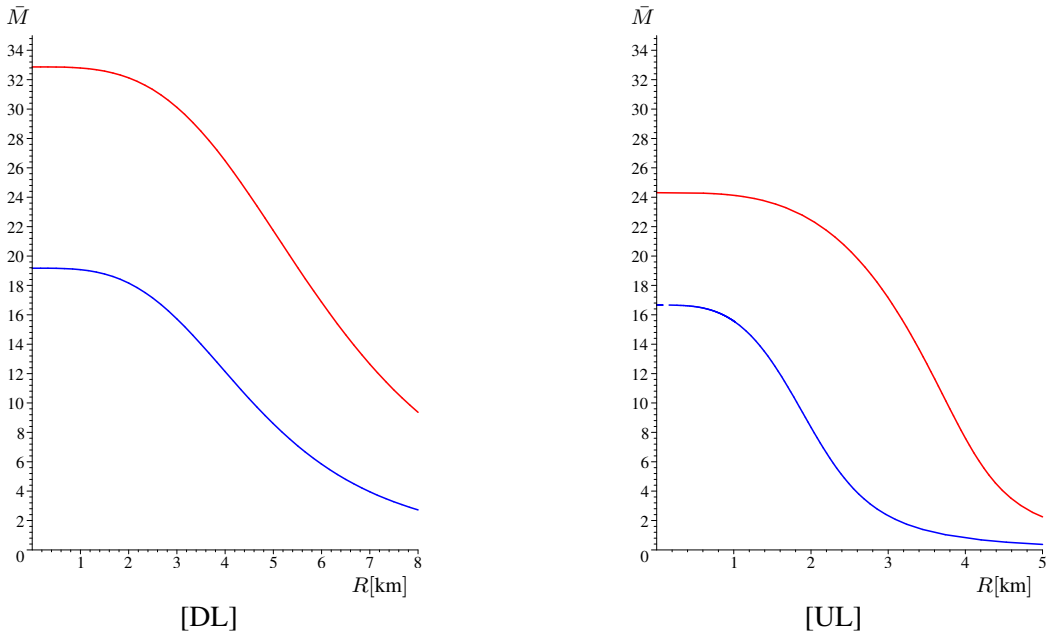

Fig. 19.1 Mean-load estimations for the downlink (DL) and uplink (UL), for the Hex model (upper curves) and PV model (lower curves). The numerical assumptions are: $\alpha = 0.4$, $\xi_\downarrow = \xi_\uparrow = -16$dB, $W^u = -105$dBm, $W_m = -103$dBm, $\widetilde{P}^u = 52$dBm, $Q = 42.73$dBm (these values correspond to the UMTS system); the parameters of the OPL 3 model are $\beta = 3.38$ and $A = 8667$, which gives $\bar{g}_{\rm PV} = 1.5325$, $\bar{g}_{\rm Hex} = 0.3717$, $\bar{g}_{{\rm Hex}|2\beta} = 0.2283$, $\bar{f}_{\rm PV} = 1.4493$, $\bar{f}_{\rm Hex} = 0.6564$, $\overline{f^2}_{\rm Hex} = 0.8703$, $\overline{1\!f}_{\rm Hex} = 0.4394$

The evaluation of the maximal density of mobiles $\lambda^{\epsilon}_{\rm Mo}$ with respect to a decentralized condition COND of the form (19.9) requires estimates for the distribution functions of the sum $\sum_{m\in S_0} f_m$ (and not only its means), or equivalently estimates of the probability of events of the form:

$$\mathcal{E}(z) = \Big\{ \sum_{m\in S_0} f_m \geq z \Big\}, \tag{19.20}$$

where f_m is the load associated to the mobile m under this condition. We briefly review the main ideas for estimating these distributions.

Chebychev's inequality This requires some ways of estimating (upper-bounding) $\mathrm{Var}[\sum_{m\in S_0} f_m]$. When this is available, then

$$\mathbf{P}^0(\mathcal{E}(z)) \leq \frac{\mathrm{Var}[\sum_{m\in S_0} f_m]}{\big(z - \mathbf{E}^0[\sum_{m\in S_0} f_m]\big)^2}.$$

Gaussian Approximation. If an estimator (an upper bound is enough) of $\mathrm{Var}[\sum_{m\in S_0} f_m]$ is available, then

$$\mathbf{P}^0(\mathcal{E}(z)) \approx Q\Big(\frac{z - \mathbf{E}^0[\sum_{m\in S_0} f_m]}{\sqrt{\mathrm{Var}[\sum_{m\in S_0} f_m]}}\Big),$$

where $Q(z) = 1/\sqrt{2\pi}\int_z^\infty e^{-t^2/2}\,\mathrm{d}t$ is the Gaussian tail distribution function.

The following result gives the variances for the Honeycomb model.

Proposition 19.4.5. Under the assumptions of Proposition 19.4.1 we have the following results for the Honeycomb model:

$$\begin{aligned}\mathrm{Var}\Big[\sum_{m\in S_0} f_{\downarrow m}^{0}\Big] &= \bar{M}\bar{\xi}_{\downarrow}'^{2}\Big(\bar{W}^2 l^2(R)\bar{g}_{|@2\beta}/\bar{P}_{\downarrow}^{2} + \alpha^2 + \overline{f^2} + 2\Big(\alpha\bar{f} + \bar{W}l(R)(\alpha\bar{g} + \overline{lf})/\bar{P}_{\downarrow}\Big)\Big)\\ \mathrm{Var}\Big[\sum_{m\in S_0} f_{\uparrow m}^{0}\Big] &= \bar{M}\bar{\xi}_{\uparrow}'^{2}(\overline{f^2} + 1 + 2\bar{f})\end{aligned}$$

where $\bar{f}, \bar{g}$ are given by (19.15), (19.16), $\bar{g}_{|@2\beta}$ denotes $\bar{g}$ calculated at doubled path-loss exponent and

$$\overline{f^2} = \overline{f^2}_{\text{Hex}} \approx \frac{0.2343}{(\beta-2)} + \frac{1.2907}{(\beta-2)^2} \tag{19.21}$$

and

$$\overline{lf} = \overline{lf}_{\text{Hex}} \approx \frac{0.6362}{\beta-2}; \tag{19.22}$$

these approximations are appropriate least square fits for $\beta \in [2.5, 5]$.

Proof. Note that for the Honeycomb model, the sum $\sum_{m\in S_0} f_m$ is a compound Poisson random variable and we have $\mathrm{Var}\Big[\sum_{m\in S_0} f_m\Big] = \bar{M}\mathbf{E}^0[f_m^2]$. The moments of the random variable f_m are calculated numerically. □

Remark: The corresponding (exact) values for the PV model are $\overline{f^2}_{\text{PV}} = 8/(\beta-2)^2 + 1/(\beta-1)$ and $\overline{lf}_{\text{PV}} = \Gamma(2+\beta/2)/2$, but the formula for the variance requires some positive correcting term due to the randomness of the cell size.

We can now give explicit results for the maximal mobile density given some CPR.

Corollary 19.4.6. Under the assumptions of Proposition 19.4.1, using the Gaussian approximation for the Honeycomb model, we get the following maximal mean number of mobiles per cell allowed in the downlink by condition (19.5) at a given CPR ϵ:

$$\bar{M} \le \bar{M}_{\downarrow} - \frac{(Q^{-1}(\epsilon))^2\overline{X_{\downarrow}^2}}{2\bar{X}_{\downarrow}^2}\left(\sqrt{\frac{4(1-\bar{\pi})\bar{X}_{\downarrow}}{\bar{\xi}_{\downarrow}'\overline{X_{\downarrow}^2}} + 1} - 1\right), \tag{19.23}$$

where $\bar{M}_{\downarrow}$ is the upper bound for $\bar{M}$ given by the mean model (i.e., the right-hand-side of (19.17)) and

$$\begin{aligned}\bar{X}_{\downarrow} &= \alpha + \bar{f}_{\text{Hex}} + l(R)\bar{W}\bar{g}_{\text{Hex}}/\bar{P}_{\downarrow}\\ \overline{X_{\downarrow}^2} &= \bar{W}^2 l^2(R)\bar{g}_{\text{Hex}|@2\beta}/\bar{P}_{\downarrow}^{2} + \alpha^2 + \overline{f^2}_{\text{Hex}} + 2\Big(\alpha\bar{f}_{\text{Hex}} + Wl(R)(\alpha\bar{g}_{\text{Hex}} + \overline{lf}_{\text{Hex}})/\bar{P}_{\downarrow}\Big),\end{aligned}$$

Similarly for the uplink (condition (19.8))

$$\bar{M} \le \bar{M}_{\uparrow} - \frac{(Q^{-1}(\epsilon))^2\overline{X_{\uparrow}^2}}{2\bar{X}_{\uparrow}^2}\left(\sqrt{\frac{4\bar{X}_{\uparrow}}{\bar{\xi}_{\uparrow}'\overline{X_{\uparrow}^2}} + 1} - 1\right), \tag{19.24}$$

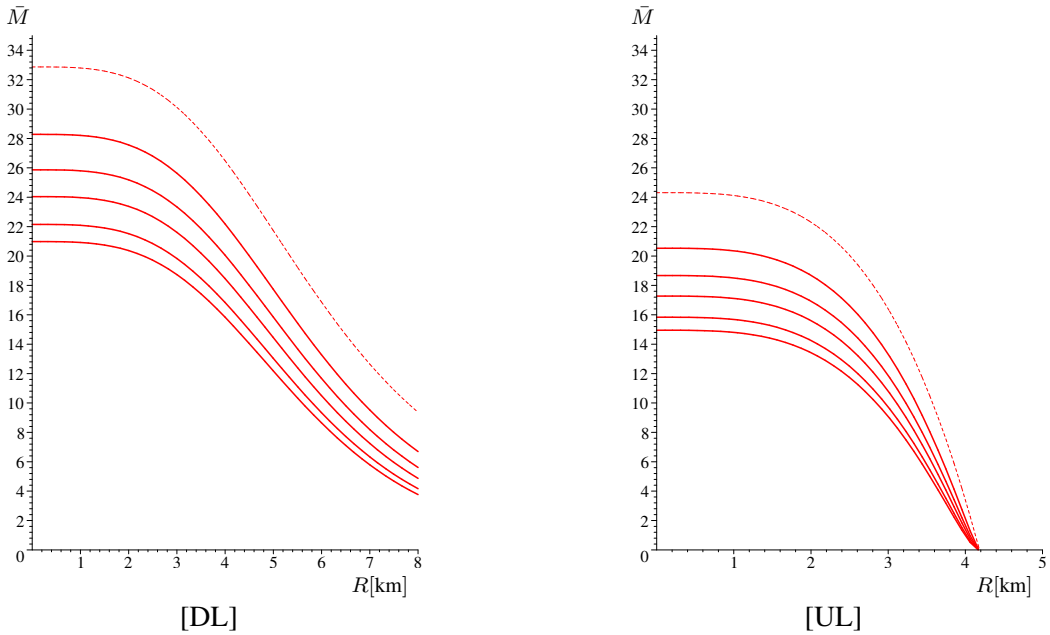

Fig. 19.2 Maximal load estimations in Honeycomb model at a given CPR $\epsilon = 0.2, 0.1, 0.05, 0.02, 0.01$ (solid lines) for the downlink (DL) and uplink (UL). The dashed curves represent the values for the mean model. The numerical assumptions are as on Figure 19.1.
User maximal power constraints are taken into account on UL as proposed in (Baccelli, Błaszczyszyn, and Karray 2004).

where $\bar{M}_{\uparrow}$ is the upper bound for $\bar{M}$ given by the mean model (i.e., the right-hand-side of (19.18)) and

$$\begin{aligned} \bar{X}_{\uparrow} &= 1 + \bar{f}_{\text{Hex}} \\ \overline{X^2_{\uparrow}} &= 1 + \overline{f^2}_{\text{Hex}} + 2\bar{f}_{\text{Hex}} \,. \end{aligned}$$

Figure 19.2 illustrates the above result.

19.4.3 Rate Control

We now show how our decentralized conditions can be used to control the bit-rates of mobiles. We use the notions of an *optimal*, *max-min*, α*-fair*, and *proportional fair* policy, which are recalled in Chapter 11 in Volume I.

Consider a decentralized condition of the form (19.9) for the feasibility of power control. In what follows, we concentrate on the typical BS and we omit the superscript $u = 0$. We suppose that all the mobiles of this BS are served and we look for fair bit-rates which can be sustained when taking condition (19.9) for defining the set of all feasible rates. Note that this condition is linear in the modified SINR $\boldsymbol{\xi}'$. However, we want to study rate (and not SINR) allocation policies and thus we have to relate $\boldsymbol{\xi}'$ to the corresponding bit-rates $\mathbf{R} = \{R_i\}$.

In order to simplify the analysis, we work under the following *linearization assumption*:

(L) the bit-rate $R = R(\xi)$ is some linear function of the SINR ξ with $R(0) = 0$ ([1]).

[1] This assumption is justified for small SINR. Indeed Shannon's relation gives $\log_2(1+\xi) \approx \xi / \log 2$ for small SINR.

Note that by (19.1) $\xi'_n \le \xi_n$ and thus under assumption (L), the following condition

$$\sum_{n\in S} R_n\gamma_n \le 1, \tag{19.25}$$

where $\gamma_n = f_n/(\xi'_n C)$ is also a sufficient condition for the feasibility of power control. So $R_n\gamma_n$ can be seen as a new load brought by mobile n.

Denote by $\mathcal{R}$ the set of all non-negative rate vectors $\mathbf{R} = \{R_n\}$ satisfying condition (19.25). We can now identify fair policies under this linear assumption.

Proposition 19.4.7. For $\alpha > 0$ consider the rate allocation problem under the constraint (19.25). The policy $R_m = \gamma_m^{-1/\alpha}/\big(\sum_{k\in S}\gamma_k^{1-1/\alpha}\big)$ is α-fair optimal. Consequently,

$$R_n = \frac{1}{\sum_{k\in S}\gamma_k} \text{ is the max-min fair allocation,} \tag{19.26}$$

$$R_n = \frac{1}{(\#S)\gamma_n} \text{ is the proportional fair allocation,} \tag{19.27}$$

$$R_n = \frac{\mathbb{1}\{n\in J\}}{\sum_{j\in J}\gamma_j} \text{ is an optimal allocation,} \tag{19.28}$$

where J is any non-empty subset of the set $\{j \in S : \gamma_j = \min_i \gamma_i\}$.

Proof. Let

$$h(\mathbf{R}) = \sum_{i=1}^{\#S} \frac{R_i^{1-\alpha}}{1-\alpha}, \quad \varphi(\mathbf{R}) = \sum_{i=1}^{\#S} \gamma_i R_i - 1\,.$$

For $\alpha > 0$, the function $h(\mathbf{R})$ is strictly concave (for $\alpha = 1$ we interpret $r^{1-\alpha}/(1-\alpha)$ as $\log r$). Moreover, the set $\{\mathbf{R} \ge 0 : \varphi(\mathbf{R}) = 0\}$ is non-empty, compact and convex. Thus h attains a unique maximum on this set. Denote it by $\mathbf{R}^*$. Then, by the Lagrange multiplier theorem, there exists λ such that

$$\frac{\partial h}{\partial R_m} = \lambda \frac{\partial \varphi}{\partial R_m}\,.$$

Hence $R_m^{-\alpha} = \lambda\gamma_m$ which combined with the constraint $\varphi(\mathbf{R}) = 0$ gives the form of the α-fair policy. By Proposition 11.0.5 in Volume I we obtain the form of the max-min, proportional fair and optimal allocation letting $\alpha \to \infty$, 1 and 0, respectively. □

We can also consider a weighted modification of the optimal allocation (19.28)

$$R_n = \frac{\mathbb{1}\{m\in J_w\}}{\sum_{j\in J_w}\gamma_j}\,, \tag{19.29}$$

where J_w is any non-empty subset of $\{j \in S : w_j\gamma_j = \min_i w_i\gamma_i\}$ and $w = (w_k : k \in S)$ are given weights. Let us call (19.29) a *weight-based optimal allocation*. Note that it maximizes $\sum_{m\in S} w_m R_m$ under the constraint (19.25).

Remark: The mean bit-rate offered to the typical user by the proportional fair policy (19.27) in a Poisson-Voronoi network can be evaluated in an explicit way and approximated in Honeycomb one. Note also by the Neveu exchange formula, that this it is equal to $\mathbf{E}^0[1/(\#S_0)\sum_{m\in S_0} f_m/(\xi'_m C_0)]$.

19.5 A Time–Space Loss Model

The decentralized admission control conditions established in Section 19.2 can be used to prevent the occurrence of certain 'infeasible' configurations of users in a cell. For defining these configurations, two types of metrics can be considered within this setting:

- A *BS-centric* one, which consists in analyzing the frequency of the cells where an unconstrained (say Poisson) configuration of users is forbidden, namely cannot be entirely accepted by the corresponding BS. This leads to the evaluation of the *(in)feasibility probability*. This approach was studied in Section 19.4.2 based on the snapshot analysis of the spatial stochastic scenario of Section 19.3.
- A *user-centric* one; for defining the latter, we have to consider a dynamical system, where users join and leave, and where a new user may be lost; this happens when the power control of the configuration obtained by the new user, together with the set of users already present at his arrival, is not feasible. The user-centric metric in question is then the probability that such a new user is lost. This probability, which is the main object of the present section, will be called the *blocking probability*. It is defined as the time–ergodic frequency of users which are lost in this dynamical system.

In the remaining part of this section, we show that the two last approaches are in fact equivalent, provided an appropriate time–space scenario is considered for the dynamical system alluded to above. This equivalence is established through a *spatial Erlang loss formula*.

19.5.1 The Classical Erlang Formula

Let us first recall the classical *Erlang loss queueing system*, which is the simplest instance where a feasibility probability and a blocking probability can be defined and compared.

Customers arrive to some infinite server queue (for more on relevant queueing theory, see e.g. (Kleinrock 1975)) according to a time Poisson p.p. with intensity λ and each customer has an exponential service time with mean τ. The number of customers in service in the steady state regime of such an unconstrained model is a Poisson random variable N with mean $\lambda\tau$ (as easily shown by checking that the latter solves the global or local balance equations of the Markov chain on $\mathbb{N}$ describing the evolution of the number of customers in the system). Consider now some positive integer C. We define the *feasibility (resp. infeasibility) probability* for C as $\mathbf{P}(N \leq C)$ (resp. $\mathbf{P}(N > C)$).

In the constrained queueing system, one has the same arrival and service laws, but one drops the customers which arrive when there are C customers already in service and serves normally those which arrive when there are less than C customers. The number of customers present in the system is again a Markov chain, this time on $\{0, 1, \ldots, C\}$. We define the *blocking probability* as the ergodic frequency with which customers are dropped in this Markov chain. Erlang's formula (see e.g. (Kelly 1991)) states that the blocking probability b is

$$b = \frac{\mathbf{P}(N = C)}{\mathbf{P}(N \leq C)} = \frac{(\lambda\tau)^C}{C!} \left(\sum_{n=0}^{C} \frac{(\lambda\tau)^n}{n!} \right)^{-1}, \tag{19.30}$$

where N is the Poisson random variable describing the steady state of the non-constrained system. This immediately follows from the fact that the steady state of the constrained process is the truncation [2] of the

[2] By truncation of the probability distribution F, defined on E, to some subset A of E, we mean the probability distribution $F(.)/F(E)$ on A.

Poisson distribution of N to the state space $\{0, 1, \ldots, C\}$. The last property is a direct consequence of the reversibility of the unconstrained Markov chain.

19.5.2 A Spatial Erlang Formula

The objective of this section is to establish a similar connection between the notion of the feasibility probability of Definition 19.4.3 and the blocking probability of an appropriate dynamical system.

19.5.2.1 The Unconstrained Process

Fix one cell of the honeycomb model described in Section 19.3.2, say that corresponding to BS 0; for simplicity we omit the superscript 0 in what follows. Denote this cell by $\mathbb{D} \subset \mathbb{R}^2$. We model the unconstrained process of arrivals to (and departures from) $\mathbb{D}$ as a *spatial birth-and-death* (SBD) process.

- *Arrival times and locations:* We assume that for all given subsets $A \subset \mathbb{D}$, the inter-arrival times to A are i.i.d. exponential random variables with mean $1/\Lambda(A)$, where $\Lambda(\cdot)$ is some spatial intensity measure (see § 1.1 in Volume I). The homogeneous traffic condition is that where $\Lambda(\mathrm{d}x) = \lambda \mathrm{d}x$. Here λ is the mean number of arrivals per unit of area and per unit of time. In particular, users arrive to $\mathbb{D}$ according to the stationary time Poisson p.p. with intensity $\lambda(\mathbb{D})$ and "choose" their location in $\mathbb{D}$ independently, according to the distribution $\Lambda(\cdot)/\Lambda(\mathbb{D})$.
- *User holding times:* We assume that each user arriving in $\mathbb{D}$ requires a service from BS X_0 for some random, exponential duration with mean τ. The service times of different users are independent.

Denote by $\Phi(t) = \Phi_{\mathrm{Mo}}^{\mathbb{D}}(t)$ the configuration of users present in $\mathbb{D}$ at time $t \in \mathbb{R}$. We consider $\Phi(t)$ as a point measure (cf. Chapter 1 in Volume I) on $\mathbb{D}$; i.e. $\Phi(t) \in \mathbb{M}$, where

$$\mathbb{M} = \{\nu = \{Y_m\}_{m=1,\ldots,n} \text{ with } Y_m \in \mathbb{D}, m = 1, \ldots, n, \text{for some } n \geq 0\}$$

denotes the set of all possible configurations $\nu = \{Y_m\}$ of users in cell $\mathbb{D}$.

Proposition 19.5.1. The stationary distribution of the unconstrained SBD process $\Phi(t)$ is that of a Poisson p.p. on $\mathbb{D}$ with intensity measure $\tau\Lambda(\cdot)$.

Proof. The distribution of the Poisson p.p. satisfies the global balance equation of the Markov chain $\{\Phi(t)\}$ (see (Baccelli, Błaszczyszyn, and Karray 2005; Baccelli, Błaszczyszyn, and Karray 2007) for details on $\mathbb{M}$-valued Markov chains). □

We also consider the independently marked version

$$\widetilde{\Phi}(t) = \widetilde{\Phi}_{\mathrm{Mo}}^{\mathbb{D}}(t) = \left\{\left(Y_m \in \Phi(t), \xi'_{\downarrow m}, \xi'_{\uparrow m}, W_m\right)\right\}_m$$

of $\Phi(t)$, where the marks are as in Section 19.3.2.

Denote by $\tilde{\mathbb{M}}$ set of possible values of $\tilde{\Phi}$. By Proposition 19.5.1, which can easily be extended to i.m. Poisson p.p.s, the stationary distribution of $\widetilde{\Phi}(t)$ is that of an i.m. Poisson p.p. $\tilde{\Phi}$ with intensity $\tau\Lambda(\cdot)$. We denote by $\mathbf{P}$ the probability under which $\Phi(t)$ has its stationary distribution.

Remark: In the spatially homogeneous case $\Lambda(\mathrm{d}x) = \lambda \mathrm{d}x$, the stationary distribution of $\widetilde{\Phi}(0)$ is that of the i.m. Poisson p.p. $\widetilde{\Phi}_{\mathrm{Mo}}$ considered in Section 19.4 and restricted to $\mathbb{D}$; we have $\lambda_{\mathrm{Mo}} = \tau\lambda$.

19.5.2.2 The Constrained Process

Consider now the situation where the arrival process described in Section 19.5.2.1 is modified in that it is subject to some admission control scheme based on a set of condition of the form (19.9) with $u = 0$. More precisely, assume the user configuration $S_0 = S$, which satisfies (19.9) with $C_0 = C$, is that at the arrival epoch of a new user; the latter is accepted if the configuration obtained by adding the new customer to S still satisfies the set of conditions (19.9) with $C_0 = C$; it is rejected otherwise. Accepted users are served for an exponential service time. Rejected users are lost.

A few observations are in order:

- The set of conditions of the form (19.9) could be a singleton i.e. be a single condition like (19.4) or (19.5) or (19.8); it could also be the conjunction of some of these conditions.
- Consider for instance the case of Condition (19.4). We proved that if it is satisfied in each cell u, then the global (i.e. whole plane) DL power control problem is feasible. It is why in spite of the fact we concentrate on a single cell here, the results still bear on the global inter-cell power control problem. This of course extends to the other conditions.
- Since the same admission control is enforced in each cell, what happens in one of them is typical of what happens in all of them and this explains why we concentrate on the cell of X_0.

Denote by $\tilde{\Phi}^f(t)$ the (marked) configuration of users served by the BS X_0 at time t under this admission control. By definition, the process $\tilde{\Phi}^f(t)$, lives in the space of *feasible configurations*,

$$\tilde{\mathbb{M}}^f = \left\{ (Y_m, \xi'_{\downarrow m}, \xi'_{\uparrow m}, W_m) \in \tilde{\mathbb{M}} : \text{condition (19.9) holds} \right\}.$$

The following result gives the stationary distribution of $\tilde{\Phi}^f(t)$:

Proposition 19.5.2. The stationary distribution of the constrained process $\{\tilde{\Phi}^f(t);\, t \geq 0\}$ is the truncation of the distribution of the stationary free process $\tilde{\Phi}(0)$ to $\tilde{\mathbb{M}}^f$, i.e.

$$\mathbf{P}\{\, \tilde{\Phi}^f(0) \in \Gamma \,\} = \frac{\mathbf{P}\{\, \tilde{\Phi}(0) \in \Gamma \,\}}{\mathbf{P}\{\, \tilde{\Phi}(0) \in \tilde{\mathbb{M}}^f \,\}},$$

for all $\Gamma \subset \tilde{\mathbb{M}}^f$.

Proof. This truncation property follows from the reversibility of $\tilde{\Phi}(t)$ (cf. Proposition 3.14 in (Serfozo 1999)). □

19.5.2.3 Blocking Rates

Define the *blocking rate* b_x at $x \in \mathbb{D}$ as the ergodic frequency with which users are rejected in the stationary regime of the constrained dynamics in some infinitesimal neighborhood of location x (see (Baccelli, Błaszczyszyn, and Karray 2005) for a precise definition).

Our main result is:

Proposition 19.5.3 (Spatial Erlang loss formula). The blocking rate of the constrained process described in Section 19.5.2.2 is equal to

$$b_x = \frac{\mathbf{P}\Big\{ C - f_x \leq \sum_{m\in\tilde{\Phi}(0)} f_m < C \Big\}}{\mathbf{P}\{\, \tilde{\Phi}(0) \in \tilde{\mathbb{M}}^f \,\}}\,, \tag{19.31}$$

where f_x is the virtual load of a user located at x and independently marked with a mark having the same law as those of the other points of $\tilde{\Phi}$.

Proof. The proof follows from the truncation property established in Proposition 19.5.2. Details can be found in (Baccelli, Błaszczyszyn, and Karray 2005). □

Note that (19.31) has the same form as the Erlang loss formula (19.30). In particular, the feasibility probability $\mathbf{P}\{\, \tilde{\Phi}(0) \in \tilde{\mathbb{M}}^f \,\}$ (cf. Definition 19.4.3) is the normalizing constant.

19.5.2.4 Approximations of the Blocking Rates

In order to calculate the blocking rates via formula (19.31), one needs the distribution function of

$$I = \sum_{m\in\tilde{\Phi}(0)} f_m$$

under $\mathbf{P}$ (recall that $\mathbf{P}\{\, \tilde{\Phi}(0) \in \tilde{\mathbb{M}}^f \,\} = \mathbf{P}\{\, I \leq C\}$). For this, we can use e.g. the Gaussian approximations developed in Section 19.4.2; i.e. we approximate I by the Gaussian random variable with mean μ and variance σ^2 equal to those of I under $\mathbf{P}$. These statistics are calculated in Section 19.4 (cf. Propositions 19.4.1 and 19.4.5).

Corollary 19.5.4. Under assumptions of Proposition 19.4.1, the Gaussian approximation of the blocking rate is given by:

$$b_x \approx \frac{\mathbf{E}[Q\big((C - f_x - \mu)/\sigma\big)] - Q\big((C-\mu)/\sigma\big)}{1 - Q\big((C-\mu)/\sigma\big)}\,, \tag{19.32}$$

where $Q(z)$ is the Gaussian tail distribution function and the expectation $\mathbf{E}$ is with respect to the virtual load f_x of the user located at x (which might be random due to the marks). Moreover, for constant and small values of f_x/σ, the following approximation can by justified

$$b_x \approx \frac{f_x e^{-(C-\mu)^2/(2\sigma^2)}}{\sqrt{2\pi}\sigma^2\Big(1 - Q\big((C-\mu)/\sigma\big)\Big)}\,. \tag{19.33}$$

Note that in each of the conditions (19.4), (19.5) and (19.8), the function f_x is some linear mapping of the function

$$f(x) = \sum_{v\neq 0} \frac{l(|x|)}{l(|X_v - x|)}\,,$$

where the summation is over all base stations of the Honeycomb model other than that located at 0. This function depends only on the geometry of the BS network and on the path-loss model. In (Karray 2007), the following approximation of $f(x)$ is derived assuming the OPL 3 path loss model:

$$f(x) \approx \zeta(\eta-1)L(|x|)\left(\frac{1}{L(\Delta-|x|)}+\frac{1}{L(\Delta+|x|)}+\frac{4}{L\left(\sqrt{\Delta^2+|x|^2}\right)}\right), \quad \text{for } |x| \le R\,,$$

where $\zeta(s)=\sum_{n=1}^{\infty} 1/n^s$ is the Riemann zeta function (recall that Δ is the distance between two adjacent BSs in the hexagonal network and R is the radius of the disc with area equal to that of the cell).

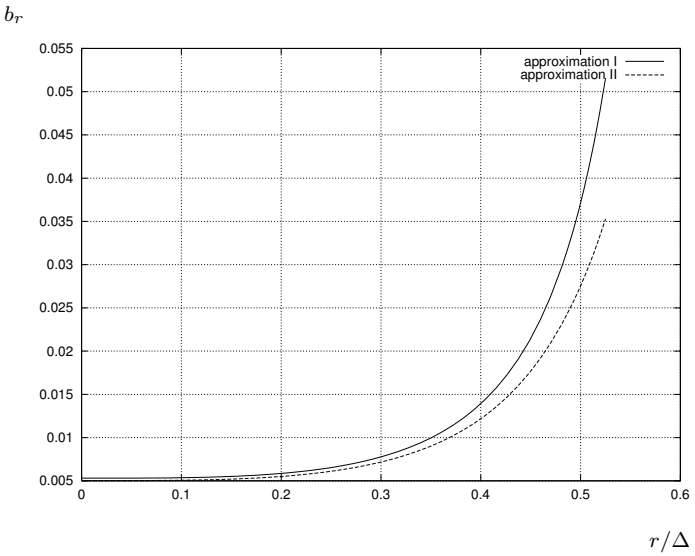

Fig. 19.3 Downlink blocking rates b_x in the Honeycomb model with a distance Δ between adjacent BSs, calculated via approximations (19.32) — I and (19.33) — II as functions of the normalized distance $r/\Delta = |x|/\Delta$ for $\bar{M} = 27$.

Figure 19.3 plots the blocking rates $b_r(\bar{M})$ calculated by the two approximations (19.32) and (19.33), for fixed $\bar{M} = 27$, as functions of the normalized distance r/Δ. Note that both approximations give similar numerical values; however, their values differ more at the cell edge, where the difference is appr. 30%. The blocking rate b_r increases with the distance r of the user to its base station; at the cell edge ($r/\Delta \approx 0.525$), it is appr. 10 times bigger than at the cell center. Figure 19.4 shows the average blocking rate, the blocking rate at cell edge b_R, both calculated using (19.32), and the infeasibility probability, as functions of the mean number $\bar{M}$ of users per cell. The numerical assumptions are as in Figure 19.1.

19.6 Conclusion

The Voronoi representation of cellular networks considered in the present chapter can be extended to other MAC protocols. A typical example is that of WiFi networks. The model features a collection of access points and a set of users where each user is served by the closest access point. For instance, the downlink involves 1) contention between the access points; 2) some form of time sharing between the users in the Voronoi cell of each access point (see (Kauffmann, Baccelli, Chaintreau, Mhatre, Papagiannaki, and Diot 2007) for an exploitation of this model in the context of load balancing algorithms in WiFi networks).

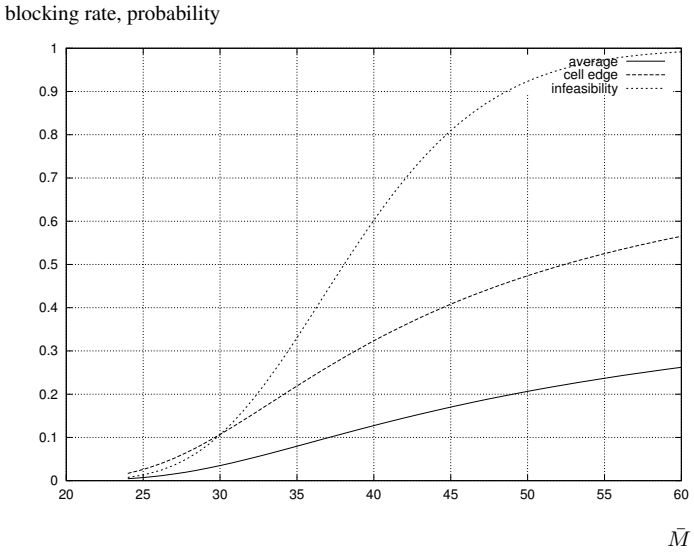

Fig. 19.4 Downlink average blocking rate: the blocking rate at the cell edge and the infeasibility probability as functions of the mean number of users $\bar{M}$ per cell.

The main conclusion of the present chapter is that at least in the CDMA framework, power control can be integrated into the spatial modeling tools advocated in this monograph. Power control can also be considered within this frameworks for e.g. CSMA. However, there are very few mathematical results on power control in infinite networks. For instance, consider the SINR graph of Definition 8.2.1 in Volume I. We recall that in the basic SINR graph model, the transmission powers are constant. Consider a model where the SINR graph does not percolate for these constant transmission powers. Assume now that one can control the power of each transmitter so as to open certain links or so as to diminish the interference created by useless links. We do not know whether such a power control can let the SINR graph percolate when leaving all other network parameters unchanged.

We showed in § 19.5 that the proposed approach extends to time–space scenarios and leads to spatial extensions of the classical loss model. This was exemplified through the Spatial Erlang formula established in Proposition 19.5.3. This was done for the constant bit rate (or SINR) scenario. The case of elastic traffic (where no minimal bit rate is required) can also be studied along the same lines. In this case, each arrival is associated with some volume of data. The users of a BS are then all accepted and are served in a weighted processor sharing way; the weights determine bit-rates and are chosen in such a way that 1) the feasibility condition is satisfied; 2) some global utility function is maximized (see Chapter 11 in Volume I); the users leave the system after having transmitted their data. For this case, explicit formulas for the mean throughput and the mean delay can be found in (Błaszczyszyn and Karray 2007).

Bibliographical Notes on Part IV

Chapter 16 follows (Baccelli, Blaszczyszyn, and Mühlethaler 2003) and (Baccelli, Blaszczyszyn, and Mühlethaler 2009a), where two-dimensional (2D) scenario is considered. The specificity of 1D scenario (in the context of Linear Vehicular Ad-hoc NETworks (VANETs)) is explored in (Błaszczyszyn, Mühlethaler, and Toor 2009). Extensions of the analysis to the plain (non-slotted) Aloha and comparisons of to the slotted Aloha in 2D scenario can be found in a forthcoming paper (Błaszczyszyn and Mühlethaler 2010).

Among other papers which have proposed methods allowing one to analyze coverage under general fading conditions, let us quote (Hunter, Andrews, and Weber 2008), where one can find an analysis of the impact of certain fading scenarios such as e.g. Nakagami. The formalism based on the Fourier L_2 isometry which is developed in Chapter 16 and which allows one to cope with arbitrary fading (like e.g. Rician) was proposed in (Baccelli, Blaszczyszyn, and Mühlethaler 2009a). Example 16.2.3 is borrowed from (Hunter, Andrews, and Weber 2008). Several papers have considered the evaluation of the mean throughput in the context of a Poisson MANET (e.g. (Ehsan and Cruz 2006) and (Haenggi 2009)). In (Ehsan and Cruz 2006), the authors evaluate the optimal SINR target T that a Poisson MANET using Spatial Aloha ought to use in order to maximize the mean throughput per unit area. The throughput is evaluated as the product of the probability of coverage and the logarithm of $1+T$ (Shannon's capacity). This definition underestimates the real throughput obtained by transmitters: given that transmission is successful, namely given that the actual SINR θ at the receiver is larger than T, the throughput is the logarithm of $1+\theta$, which is larger than the logarithm of $1+T$. The approach developed in § 16.2.3 tells us how much larger, since we actually compute the distribution and the mean of the logarithm of $1+\theta$. In (Haenggi 2009), closed form expressions are derived for specific fading scenarios.

Opportunistic Aloha was also considered in (Venkataraman and Haenggi 2004), where it was analyzed using a Gaussian approximation for the interference, and in (Weber, Andrews, and Jindal 2007), where it was called "threshold scheduling". The exact analysis of opportunistic Aloha presented in § 16.4 is based on (Baccelli, Blaszczyszyn, and Mühlethaler 2009a).

Chapter 17 is primarily based on (Baccelli and Blaszczyszyn 2010). Formula (17.16) on the multicast case is due to (Jacquet 2008). In relation with smallest hop in a cone, let us quote (Haenggi 2005), where a "n th-nearest-neighbor-in-a-cone" model is used to compare the efficiency of different routing schemes in a

Poisson MANET using ALOHA. The space-time scenario described in Section 17.5.1 will be used in Chapter 22 and allows one to address many important questions. In particular, it was introduced independently in (Ganti and M. 2009) to analyze the spatio-temporal correlation coefficient of slotted ALOHA.

When applied to Aloha, stochastic geometry can be used to analyze many other interesting problems which are not considered in Chapters 16 and 17, such as the optimal division of the available bandwidth into different sub-bands (Jindal, Weber, and Andrews 2008) or power control to compensate for random fading (Jindal, Andrews, and Weber 2008).

The problem of infinite mean local delays observed in Section 17.5 is related to (Jelenković and Tan 2007a; Jelenković and Tan 2007b), where it was shown that a finite population ALOHA model with variable and unbounded size packets has power law transmission delays (although the physical phenomena at hand are quite different there and in our spatial MANET model with fixed-packet-sizes).

Chapter 18 follows (Nguyen, Baccelli, and Kofman 2007).

The first part of Chapter 19 is based on (Baccelli, Błaszczyszyn, and Tournois 2003; Baccelli, Błaszczyszyn, and Karray 2004). The feasibility probability was considered in different frameworks in in (Audrey M. Viterbi and Viterbi 1993), where it is called blocking probability and in (Liu and El Zarki 1994) and (Evans and Everitt 1999), where it is called the outage probability. Section 19.5 follows (Baccelli, Błaszczyszyn, and Karray 2005). The authors of (Liu and El Zarki 1994) consider the blocking probability (as defined in this section) in a time–space framework and give simulation results which show that the feasibility and blocking probabilities are different in general. The time–space scenario considered in Section 19.5 has several other incarnations: the case with elastic traffic is considered in (Błaszczyszyn and Karray 2007); the case with user mobility, which causes call cuts due to displacements, is analyzed in (Błaszczyszyn and Karray 2008a). In (Sidi and Starobinski 1997), explicit expressions of blocking probabilities are given for two limiting regimes: no mobility and infinite mobility. Further extensions can be found in (Błaszczyszyn and Karray 2008b; Błaszczyszyn and Karray 2009). The whole approach is well summarized in (Karray 2007).

Part V

Multihop Routing in Mobile ad Hoc Networks

In this part, we study the performance of multihop routing in large MANETs. Readers not familiar with routing can find some brief introduction to this topic in Part VI. The context is again that of a MANET of the Euclidean plane with randomly located nodes represented by a point process. The route followed by a packet is then is a random geometric object on this p.p., which depends on the routing algorithm which is used. In this part, two main mathematical objects are introduced to describe and analyze these random geometric objects: the notion of *point map* on the p.p. of nodes, which can be seen as a way of describing the routing algorithm, and the notion of *route average*, which allows one to define the statistics seen by a packet following the route.

Point Maps

Consider a locally finite set of points $\phi = \{x_i\}$ of $\mathbb{R}^2$, for instance some realization of a Poisson p.p. A key feature of any routing scheme is that the *next hop* decision for a packet located at node X, and bound to the end destination D, should depend on D and X and not on where the packet comes from. Hence a routing mechanism to D can be defined through a point map on ϕ, namely a mapping $\mathcal{A} = \mathcal{A}_D : \phi \mapsto \phi$, where $\mathcal{A}(X)$ is the next hop from node X. Let $\mathcal{A}^k$ denote the k-th iterate of $\mathcal{A}$.

Definition. A point map $\mathcal{A} = \mathcal{A}_D$ on the pattern of points ϕ is a *routing to destination* $D \in \phi$ if $\mathcal{A}(D) = D$ and, for all $x \in \phi$, $\mathcal{A}^h(x) = D$, for some finite $h = h(x) \geq 1$.

Here are a few definitions related to such a routing.

- The smallest integer $h = h(x)$ such that $\mathcal{A}^h(x) = D$ is the *number of hops* of the *route* from x to D; the latter is defined as the sequence of points $p(x, D) = \big(x, \mathcal{A}(x), \mathcal{A}^2(x), \ldots, \mathcal{A}^h(x) = D\big)$.
- The vector $J(x) = \mathcal{A}(x) - x \in \mathbb{R}^2$ is the *jump vector* from point x.
- The real number $P(x) = |x - D| - |\mathcal{A}(x) - D| \in \mathbb{R}$ is the *progress* to destination from point x.

Point Maps Associated with Graphs

Often, in addition to the node p.p., we have some underlying graph, where the vertices of the graph are the nodes and the edges represent the links which serve as a support to (or constraints for) the routing protocol. Let $\mathcal{G} = (\phi, \mathcal{E})$ be such a graph, with $\mathcal{E} \subset \phi \times \phi$ the set of (non-directed) edges. The elements of the set $\mathcal{N}(x) = \{y \in \phi : (x, y) \in \mathcal{E}\}$ will then be referred to as the neighbors of $x \in \phi$.

Definition. A graph point map associated with the graph $\mathcal{G} = (\phi, \mathcal{E})$ is a point map $\mathcal{A}$ on ϕ such that $(x, \mathcal{A}(x)) \in \mathcal{E}$ for each $x \in \phi$. In other words $\mathcal{A}(x) \in \mathcal{N}(x)$, for all $x \in \phi$.

Examples of graphs

Let ϕ be some realization of a homogeneous Poisson p.p. Φ; the following examples of graphs, with set of nodes Φ, are pertinent for modeling multihop wireless communications and are used throughout this part:

- **Poisson–Delaunay graph**: in connection with Example 4.4.2 in Volume I, we call Poisson–Delaunay graph the graph $\mathcal{G}_{Delaunay} = (\Phi, \mathcal{E}_{Delaunay})$ the edges of which are the sides of the Delaunay triangles generated by the Poisson p.p. Φ (cf. Definition 4.4.1 in Volume I). Recall that

the edges $\mathcal{E}_{Delaunay} = \{(x, y) : x \in \Phi, y \in \mathcal{N}_x(\Phi)\}$ of this graph connect each point $x \in \Phi$ of the Poisson p.p. to all its Voronoi neighbors $\mathcal{N}_x(\Phi)$ (cf. Lemma 4.4.3 in Volume I). This graph is very convenient in that it is almost surely connected. Its main weakness within the present context is the lack of realism of Delaunay edges for representing wireless links.

- **Random geometric graph**: this is the Boolean connectivity graph, obtained when having an edge between two points of the Poisson p.p. iff the distance between them is less than some threshold R_{max}. In the wireless setting, this graph is often referred to as the *transmission range graph*. Here, the neighborhood depends not only on the geometry of the p.p. but also on the parameter R_{max}, which is often used to model the maximal transmission range of a wireless node (e.g. taking $R_{max} = \max\{r : P/l(r) \geq P_o\}$, where P is the power of the transmitter, $l(r)$ some OPL function and P_o is the minimal detection power). This model is equivalent to the connectivity graph of the Boolean Model (BM) with spherical grains of deterministic radius. The main problem with this model is that the graph on the whole plane is not connected (more precisely, it is disconnected with probability 1; cf. Proposition 3.2.4 in Volume I). This means that, on this graph, routing is only possible between points of Φ which belong to the same connected component. A natural idea is to assume that the BM percolates and to consider routing on the unique infinite connected component of the BM (cf. Section 3.2.2 in Volume I). This however considerably complicates the analysis.
- **Connected component of the SINR graph**: A more pertinent but more complicated model is the SINR connectivity graph $\mathcal{G}_{\text{SINR}}$ (see Definition 8.2.1 in Volume I). Recall that for the $\frac{\text{M/D}}{W+\text{M/D}}$ model, this graph percolates (cf. Section 8.3 in Volume I) and one can consider routing on its giant component. [3]

Spatial Averages and Route Averages — Routing Paradox

Our main objective within this framework is the analysis of various classes of routing algorithms, when operated on Poisson p.p. For all routing algorithms, we are particularly interested in *route averages* and *spatial averages*, defined below and on fluctuations around these averages. It is customary to fix the origin of the plane O at the destination node D and to consider routing $\mathcal{A} = \mathcal{A}_D = \mathcal{A}_O$ *to* the origin of the plane. Let g be some function from $\mathbb{R}^2$ to $\mathbb{R}$.

- The route average of g w.r.t. point map $\mathcal{A}$ is defined as
$$r = \lim_{|x|\to\infty} \frac{1}{h(x)} \sum_{k=0}^{h(x)-1} g(\mathcal{A}^{k+1}(x) - \mathcal{A}^k(x)) \,,$$
whenever the last a.s. limit exists and is independent of the direction with which x tends to ∞. This definition requires a subsequence of points of Φ which tends to infinity in some fixed direction; this will be made precise when needed (see e.g. Definition 20.3.1). In this definition, $h(x)$ is the number of hops of the $\mathcal{A}$-route from x to O. For instance, if $g(x) = |x|$, r is the route average of the jump size.
- The spatial average of g w.r.t. the point map $\mathcal{A}$ is defined as
$$s = \lim_{\rho\to\infty} \frac{1}{|\phi(B_O(\rho))|} \sum_{x\in\phi\cap B_O(\rho)} g(\mathcal{A}(x) - x)) \,,$$

[3] It is natural to conjecture that the infinite component of this graph is unique, provided it exists; we are not aware of any published proof of this fact.

whenever the last almost sure limit exists. In this definition, $B_O(\rho)$ is the ball of center O and radius ρ.

As we shall see, these two types of averages do not coincide in general. This observation belongs to the class of *Palm biases* and continues in a sense Feller's paradox. Feller's paradox is concerned with stationary p.p. on the real line (interpreted as time below). The paradox is that statistics made by an observer, which measures the length of the interval that separates time t to the first point of the p.p. after t, in general differ when t is an arbitrary instant of time (say 0) and when it is the typical point of the p.p.

In the same vein, one can obtain different statistics on e.g. the jump vector associated to a point map $\mathcal{A}$, when this jump is taken from a typical point of the point pattern and when it is taken from the typical point of some (long) route prescribed by the very same point map $\mathcal{A}$. By analogy, this will hence be called the *routing paradox*.

The Price of Anarchy in Routing

Another key concern is the *price of anarchy* within this setting. For most kinds of routing paradigms, one can define both *optimal* and *greedy* versions. The optimal schemes are all based on dynamic programming; they often come with heavy computational and state construction overheads which are problematic in this wireless and infrastructure-less MANET context. Suboptimal and in particular greedy versions, which are based on local optimizations and require less exchange of information are often preferred as they come with a much smaller computational cost. Locality can be either in time or space depending on the cases. The main question is then the quantification of the loss of performance between optimal and greedy solutions, which it is then natural to be baptized *price of anarchy* (in routing). This price is analyzed in terms of the space and route averages alluded to above.

Structure of Part V

Chapter 20 studies optimal (shortest path or minimal weight) routing. Chapter 21 is focused on *greedy* near-neighbor routing. These two first chapters focus on routes which are made of a collection of adjacent and feasible links seen in a snapshot of the network. In these two chapters, we consider conventional routing protocols (like e.g. shortest path routing); in these conventional schemes, when a route is determined between an origin and a destination, this route remains the same as long as the network nodes do not move and links remain stable; once the route is determined, the MAC is then used to let packets progress from origin to destination along this route. This allows one to separate the routing problem from the MAC protocol.

In Chapter 22, we study *time-space* routing where the next relay on the route to the destination changes from a packet to the next and where the next hop is selected among the nodes having successfully received the packet (if any), which again depends on the SINR at the receivers. Such a scheme allows one to take advantage of the local pattern of transmissions as determined by the MAC and by the fading variables, at each hop and at each time. Within this context, one can again define both optimal and greedy versions. One of the important objects within this framework is *Opportunistic routing*, a greedy algorithm where, at each time slot, each node selects the best relay to route the packet towards its end destination. By best, we mean e.g. the relay which maximizes the progress of the packet towards the destination. These SINR-based routing schemes are analyzed in terms of random and time-space point maps.

20

Optimal Routing

20.1 Introduction

This chapter is focused on optimal multihop routing on (weighted) graphs associated with stationary point processes of the Euclidean plane and in particular Poisson point processes. We focus on the existence and the evaluation of route averages. More precisely, we establish a generic scaling law which shows that for a large class of optimal routing schemes, which includes shortest path and minimal weight routing on such graphs, the length (or weight) of the optimal path is asymptocically linear in the distance between source and destination. The main tool used here is the sub-additive ergodic theorem. The main technicalities bear on proving that the constants in the sub-additive ergodic theorem are not degenerate.

20.2 Optimal Multihop Routing on a Graph

Weights. Consider a locally finite pattern of points $\phi = \sum_i \varepsilon_{x_i}$ on $\mathbb{R}^2$. Consider a graph $\mathcal{G} = (\phi, \mathcal{E})$ on this point pattern and assume some non-negative weights $w(x, y)$ to be associated with each edge $(x, y) \in \mathcal{E}$. The following examples of weights are of interest: for $y \in \mathcal{N}(x)$,

- *Graph distance*: $w(x, y) = w_{graph}(x, y) = 1$;
- *Euclidean distance*: $w(x, y) = w_{Euclid}(x, y) = |x - y|$ (more generally one can consider $w_\alpha(x, y) = |x - y|^\alpha$, for some $0 \leq \alpha < \infty$);
- *Random weights* e.g. $w(x, y) = w(y, x)$ are i.i.d. random variables.

When a marked pattern of points is considered, more elaborate weights can be contemplated. For instance, consider a standard stochastic scenario for a SN of the M/GI type. For all pairs of points $x, y \in \Phi$, let $I_{x,y}(.)$ denote the SN generated by $\Phi \setminus \{x, y\}$. Then, in the wireless context, it is natural to consider e.g. $w(x, y) = \max(I_{x,y}(x), I_{x,y}(y))$. Another natural example related to the digital communication model framework is that where the weight of a link is the *bidirectional delay* of this link, namely

$$w_{delay}(x, y) = \max\left(\left(\log\left(1 + \frac{F_x^y / l(|x - y|)}{W + I_{x,y}(y)}\right)\right)^{-1}, \left(\log\left(1 + \frac{F_y^x / l(|x - y|)}{W + I_{x,y}(x)}\right)\right)^{-1}\right), \quad (20.1)$$

where F_x^y is the fading from x to y.

It is often convenient to extend the definition of weights to all pairs of nodes $(x, y) \in \phi^2$ by taking $w(x, y) = \infty$ for $y \notin \mathcal{N}(x)$.

Optimal Paths. Consider the collection of all paths π of $\mathcal{G} = (\phi, \mathcal{E})$ between S and D. Each of them is a sequence of the form $x_1, \ldots, x_n$ with n integer, $x_1 = S$ and $x_n = D$. Pick some non-negative weight function w and define the weight of π as

$$|\pi| = \sum_{i=1}^{n-1} w(x_i, x_{i+1}) .$$

We define $p^*(S, D)$ to be the minimal weight path in this collection.

Note that it is not guaranteed that such an optimal path exists (at least on an infinite collection of nodes). However, if ϕ is locally finite (recall that the realizations of a point process are a.s. locally finite by definition), then a minimal weight path always exists for w_{graph} or w_{Euclid}. Even if we have existence, uniqueness is not guaranteed. When existence is granted, the collection of minimal weight paths satisfy the dynamic programming equation

$$|p^*(x, D)| = \min_{y \in \mathcal{N}(x)} \left(w(x, y) + |p^*(y, D)| \right) . \tag{20.2}$$

Dijkstra's algorithm (see § 25.3.1.2) uses this to recursively build the optimal paths. Whenever the argmin is almost surely uniquely defined for all x, so is the optimal path from S to D. This is the case for w_{Euclid} but not for w_{graph}.

Assume uniqueness is granted. Then it follows from the dynamic programming equation that if both $p^*(S, D)$ and $p^*(S', D)$ contain node x, then the subpaths of $p^*(S, D)$ and $p^*(S', D)$ from x to D coincide (and are equal to $p^*(x, D)$). Hence, under the above existence and uniqueness assumptions, there is a point map associated with minimal weight paths to D and this point map is a routing to D.

We have similar results in case we have no uniqueness (e.g. for w_{graph}). Let $P^*(S, D)$ denote the collection of optimal paths from S to D. Assume that x belongs to some paths of $P^*(S, D)$ and of $P^*(S', D)$. Then the collection of all subpaths of $P^*(S, D)$ from x to D coincides with that of all subpaths of $P^*(S', D)$ from x to D and with $P^*(x, D)$. In order to define a point map in this case, it is enough to select one of the paths of $P^*(S, D)$ in an appropriate way (e.g. the one with minimal Euclidean distance).

Definition 20.2.1. Let D be some destination in ϕ. We call *minimal weight routing (MWR)* and denote by $\mathcal{A}^* = \mathcal{A}^*_D$ the point map associated with the minimal weight path.

If the weights are w_{graph} or w_{Euclid}, MWR is often referred to as *shortest path routing*. Note that for all routings $\mathcal{A}$ to D on $(\phi, \mathcal{E})$, for all $x \in \phi$,

$$|p^*(S, D)| = \sum_{i=1}^{h^*(x)} w\Big(\mathcal{A}^{*i-1}(x), \mathcal{A}^{*i}(x)\Big) \leq \sum_{i=1}^{h(x)} w\Big(\mathcal{A}^{i-1}(x), \mathcal{A}^{i}(x)\Big) . \tag{20.3}$$

Here $h(x)$ (resp. $h^*(x)$) is the number of hops from x to D in $\mathcal{A}$ (resp. $\mathcal{A}^*$).

20.3 Asymptotic Properties of Minimal Weight Routing

In this section, we assume that the random graph $\mathcal{G} = (\Phi, \mathcal{E})$ is jointly stationary with its edge weights $w(x_i, y_i)$; i.e. the distribution of the triple $\tilde{\mathcal{G}} = (\Phi, \mathcal{E}, w(\cdot))$ is the same as that of $\tilde{\mathcal{G}} + a = (\Phi + a, \mathcal{E} + a, w(\cdot + a))$, for all $a \in \mathbb{R}^2$, where $(x, y) + a = (x + a, y + a)$ is the shifting of the edge $(x, y) \in \mathcal{E}$ by the vector a. This holds for all the instances of weights considered above. We also assume that Φ is a simple p.p. and a/the MWR $\mathcal{A}^*(w, D)$ almost surely exists, for all destinations $D \in \Phi$. If we have no uniqueness, we assume that $|p^*(x_i, x_j)|$ is uniquely defined, almost surely for all $x_i, x_j \in \Phi$.

By asymptotic property, we mean here the behavior of the total weight of the optimal route between typical points of Φ when the Euclidean distance between them tends to infinity.

The appropriate way of defining "typical" points $x_i, x_j \in \Phi$ that are more and more distant is based on an extension of the notion of routing to routing from s to t, where s, t are not necessarily points of Φ. By Lemma 4.2.2 in Volume I, for all $t \in \mathbb{R}^2$, the point of Φ which is the nearest to t, which is denoted by $x(t)$ below, is almost surely uniquely defined.

Definition 20.3.1. The MWR to $t \in \mathbb{R}^2$ w.r.t. $(\Phi, \mathcal{E}, w)$, where t is not necessarily a point of Φ, is defined as the MWR $\mathcal{A}^*_{x(t)}$, w.r.t. $(\Phi, \mathcal{E}, w)$, to the point $x(t) \in \Phi$. The MWR route $p^*(s, t)$ from $s \in \mathbb{R}^2$ to $t \in \mathbb{R}^2$ is defined as the optimal route $p^*(x(s), x(t))$ from $x(s) \in \Phi$ w.r.t. $\mathcal{A}^*_{x(t)}$.

In order to underline the fact that $p^*(s, t)$ depends on the realization of $\tilde{\mathcal{G}}$ not only through $x(s)$, $x(t)$ and all other points of Φ, but also through the realizations of the weights if the latter are random, we sometimes use the notation $p^*(s, t, \tilde{\mathcal{G}})$.

First principles show that the family of minimal weight routes $p^*(s, t)$, $s, t \in \mathbb{R}^2$, satisfies the following *subadditivity* property:

Lemma 20.3.2. Assume that MWR routes are almost surely well defined between all pairs of points $s, t \in \mathbb{R}^2$. Then for all $s, t, v \in \mathbb{R}^2$

$$|p^*(s, t, \tilde{\mathcal{G}})| \leq |p^*(s, v, \tilde{\mathcal{G}})| + |p^*(v, t, \tilde{\mathcal{G}})|\,.$$

We are now in a position to prove the following general result.

Theorem 20.3.3 (Kingman's subadditive theorem). Assume that $\tilde{\mathcal{G}} = (\Phi, \mathcal{E}, w)$ is stationary with non-negative edge weights $w(\cdot, \cdot)$ and suppose that $|p^*(x_i, x_j, \tilde{\mathcal{G}})|$ is almost surely well-defined for all $x_i, x_j \in \Phi$. For all vectors $\mathrm{d} \in \mathbb{R}^2$ with $|\mathrm{d}| = 1$ and such that

$$\mathbf{E}[|p^*(0, \mathrm{d}, \tilde{\mathcal{G}})|] < \infty, \tag{20.4}$$

the limit

$$\lim_{\gamma \to \infty} \gamma^{-1} \mathbf{E}[|p^*(0, \gamma\mathrm{d}, \tilde{\mathcal{G}})|] = \inf_{\gamma > 0} \gamma^{-1} \mathbf{E}[|p^*(0, \gamma\mathrm{d}, \tilde{\mathcal{G}})|] = \kappa_{\mathrm{d}} \tag{20.5}$$

exists with $\kappa_{\mathrm{d}} < \infty$. If moreover

$$\mathbf{E}\Big[\sup_{\gamma_1 < \gamma_2, \gamma_1, \gamma_2 \in I} |p^*(\gamma_1\mathrm{d}, \gamma_2\mathrm{d}, \tilde{\mathcal{G}})|\Big] < \infty\,, \tag{20.6}$$

for some non-degenerate finite interval $I \subset \mathbb{R}$, then the following limit exists almost surely

$$K_{\mathrm{d}} = \lim_{\gamma \to \infty} \gamma^{-1} |p^*(0, \gamma \mathrm{d}, \tilde{\mathcal{G}})| \tag{20.7}$$

and $\mathbf{E}[K_{\mathrm{d}}] = \kappa_{\mathrm{d}}$.

Proof. The result follows from Lemma 20.3.2 and the continuous-parameter sub-additive ergodic theorem (see (Kingman 1973, Theorem 4)). □

Remark: If $\tilde{\mathcal{G}}$ is motion invariant (stationary and rotation invariant), then the distribution of K_{d} does not depend on the direction d.

If $\tilde{\mathcal{G}} = (\Phi, \mathcal{E}, w)$ is stationary and ergodic (cf. Definition 1.6.7 in Volume I and Proposition 1.6.10 in Volume I), then the random variable K_{d} is constant and equal to κ_{d} (i.e. it does not depend on the realization of $\tilde{\mathcal{G}}$).

If $\tilde{\mathcal{G}} = (\Phi, \mathcal{E}, w)$ is motion invariant and ergodic, then $\kappa_{\mathrm{d}} \equiv \kappa$.

20.3.1 MWR on the Poisson–Delaunay Graph

Consider the Poisson–Delaunay graph $\mathcal{G}_{Delaunay} = (\Phi, \mathcal{E}_{Delaunay})$ defined in Example 4.4.2 in Volume I. On $\mathcal{G}_{Delaunay}$, the shortest Euclidean distance paths are almost surely well defined. The same does *not* hold true for the minimal number of hop routing; however the minimal number of hops $|p^*(S, D)|$ required to go from S to D is uniquely defined (cf. Corollary 25.3.2).

Proposition 20.3.4. Consider the Delaunay graph $\mathcal{G}_{Delaunay} = (\Phi, \mathcal{E}_{Delaunay}, w)$, on some homogeneous Poisson p.p. Assume edges are independently marked by non-negative random weights $w(x, y) = w(y, x)$ with distribution function F. Then MWR routing on this graph satisfies (20.5) and (20.7) with $0 \leq K_d = \kappa_d = \kappa < \infty$ if and only if

$$\mathbf{E}[\min(w_1, w_2, w_3)] = \int_0^\infty (1 - F(u))^3 \, \mathrm{d}u < \infty \,, \tag{20.8}$$

where w_i are independent copies of the generic weight.

We sketch the main line of the proof (given in (Vahidi-Asl and Wierman 1990)), which is based on the following fact concerning the *site-percolation model* (cf. (Russo 1987)).

Lemma 20.3.5. Consider a super-critical site percolation model on the square lattice. Let B be a finite set of sites. Denote by C the smallest open circuit around B (which exists with probability one in the super-critical regime) and by N the number of sites surrounded by C. Then $\mathbf{E}[N^\alpha] < \infty$ for all $\alpha > 0$.

Proof. [of Proposition 20.3.4] Fix two points, say $0, t \in \mathbb{R}^2$. We first show that for all t, $\mathbf{E}[|p^*(0, t)|] < \infty$. For this, consider a square-lattice of side length A and associate a site with each square. It is not difficult to show that if each site of some given circuit of sites is "densely populated" by points of the Poisson p.p. Φ, then one can find two disjoint circuits in the Poisson–Delaunay graph of Φ which are covered by this circuit of sites (cf. Figure 20.1 and see (Vahidi-Asl and Wierman 1990) for details).

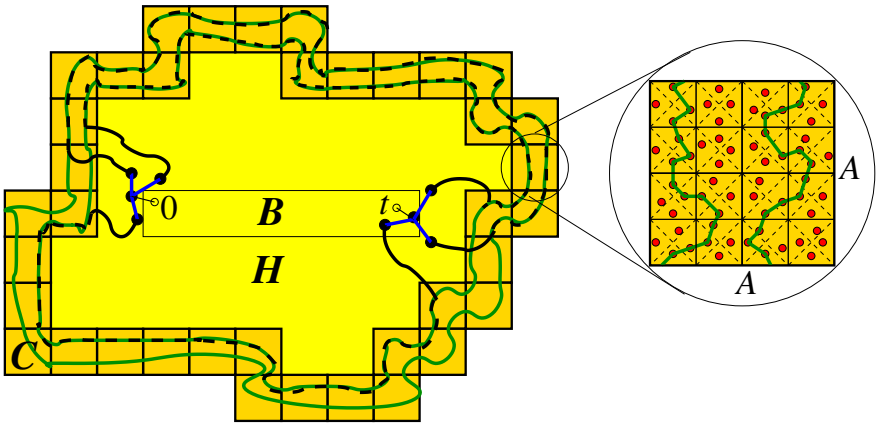

Fig. 20.1 Three disjoint paths of the Delaunay graph connecting 0 to t.

The probability that a given site is "densely populated" tends to 1 when A tends to ∞. Thus, for A large enough, this probability is larger than the critical site-percolation probability. From now on, fix A large enough for this to hold.

Let B be the smallest rectangular set of sites covering the interval $[0,t]$. Denote by C the smallest circuit of "densely populated" sites around B and by H the set of sites surrounded by C. Since both points $x(0) \in \Phi$ and $x(t) \in \Phi$ have (at least) three neighbors in the Delaunay graph, it is possible to find (at least) three disjoint paths on this graph connecting $x(0)$ to $x(t)$, which lay in $C \cup H$ (cf. Figure 20.1). Call these paths p_i, $i = 1,2,3$. We have

$$\mathbf{E}[|p^*(0,t)|] \le \mathbf{E}[\min_{i=1,2,3} |p_i|] = \sum_{k=0}^{\infty} \mathbf{P}\{ \min_{i=1,2,3} |p_i| > k \} = \sum_{k=0}^{\infty} \Big(\mathbf{P}\{ |p_1| > k \} \Big)^3 .$$

Denote by L the number of hops and by $w_1, \ldots, w_L$ the weights of the edges of p_1. We have $|p_1| = \sum_{i=1}^{L} w_i$ and

$$\mathbf{P}\{ |p_1| > k \,|\, L = l \} \le \sum_{i=1}^{l} \mathbf{P}\{ w_i > k/l \} \le l(1 - F(k/l)) .$$

Thus

$$\mathbf{E}[|p^*(0,t)|] \le \mathbf{E}\Big[L^3 \sum_{k=0}^{\infty} (1 - F(k/L))^3 \Big] \le \mathbf{E}[L^3] + \mathbf{E}[L^4] \int_0^{\infty} (1 - F(u))^3 \, \mathrm{d}u ,$$

and in order to conclude the proof, it remains to prove that $\mathbf{E}[L^4] < \infty$.

Since $p_1 \subset C \cup H$, and the path p_1 can be taken without loops, we have $L \le \Phi(C \cup H) = \sum_{n=1}^{N} \Phi(\Delta_n)$, where Δ_n are the sites of $C \cup H$ and N is the number of sites in $C \cup H$. Note that the random variables $\Phi(\Delta_n)$ are neither i.i.d. nor Poisson distributed because they are defined from the circuit of "densely populated" sites C. However, when considering all possible values for the set $C \cup H$, we get

$$\begin{aligned} \mathbf{E}[L^4] &= \sum_{n=1}^{\infty} \sum_{K = D_1 \cup \ldots \cup D_n} \mathbf{E}[L^4 \, \mathbb{1}(C \cup H = K)] \\ &\le \sum_{n=1}^{\infty} \sum_{K = D_1 \cup \ldots \cup D_n} \mathbf{E}\Big[\Big(\sum_{i=1}^{n} \Phi(D_i) \Big)^4 \mathbb{1}(C \cup H = K) \Big] , \end{aligned}$$

where the summation is over all possible finite configurations K of n sites D_i, $i = 1, \ldots, n$. Note that $C \cup H = (C \cup H)(\Phi)$ is a stopping set with respect to Φ (see Definition 1.5.1 in Volume I). More precisely, for any bounded set $K = \sum_{i=1}^{n} D_i$, where D_i are fixed sites, one can check whether the event $\{ C \cup H(\Phi) = \sum_{i=1}^{n} D_i \}$ holds or not knowing only which sites D_i, $i = 1, \ldots, n$, are "densely populated". Moreover, for any given site D,

$$\begin{aligned} \mathbf{E}[(\Phi(D))^4 \mid D \text{ is not "densely populated"}] &\leq \mathbf{E}[(\Phi(D))^4] \\ &\leq \mathbf{E}[(\Phi(D))^4 \mid D \text{ is "densely populated"}] \equiv m_0 < \infty \,, \end{aligned}$$

for some constant m_0. Thus

$$\begin{aligned} \mathbf{E}[L^4] &\leq \sum_{n=1}^{\infty} \sum_{K=D_1 \cup \ldots \cup D_n} \mathbf{E}\Big[\Big(\sum_{i=1}^{n} \Phi(D_i) \Big)^4 \mathbb{1}(C \cup H = K) \Big] \\ &\leq \sum_{n=1}^{\infty} \sum_{K=D_1 \cup \ldots \cup D_n} n^4 m_0^4 \mathbf{E}\Big[\mathbb{1}(C \cup H = K) \Big] \\ &= m_0^4 \mathbf{E}[N^4] < \infty \,, \end{aligned}$$

where the last inequality follows from Lemma 20.3.5. This completes the proof that $\mathbf{E}[|p^*(0,t)|] < \infty$. Now, in order to obtain the result for the supremum $\mathbf{E}[\sup_{u,v \in [0,t]} |p^*(u,v)|] < \infty$ as required in (20.6), one can consider the *sum* of all the lengths of the minimal paths from any point u to any v, both in the interval $[0,t]$. Using similar arguments as above and noting that the number of couples $x(u)$ and $x(v)$ does not exceed N^2 one can conclude the result from the fact that $\mathbf{E}[N^6] < \infty$. □

Note that the constant κ in Proposition 20.3.4 can be null. Intuitively $\kappa > 0$ provided the weights w are not too small. For addressing this question, consider the independent bond percolation model on the Poisson–Delaunay graph $\mathcal{G}_{Delaunay}$, namely the model where each bond (edge of $\mathcal{G}_{Delaunay}$) is open or closed independently of everything else. Denote by A_n the event that there is an open horizontal crossing of the rectangle $[0, 3n] \times [0, n]$ in this model. Let $\eta^*(p) = \liminf_{n \to \infty} \mathbf{P}_p\{A_n\}$, where $\mathbf{P}_p$ denotes the law of the model where the probability that a bond is open is p. Finally, denote by $p_c^* = \inf\{p > 0 : \eta^*(p) = 1\}$.[1] The following result was proved in (Pimentel 2006).

Proposition 20.3.6. Under assumption (20.8), if $F(0) < 1 - p_c^*$, then the constant κ in Proposition 20.3.4 satisfies $0 < \kappa < \infty$.

Since the metric w_{graph} is equivalent to $w(x,y) \equiv 1$, for all $(x,y) \in \mathcal{E}_{Delaunay}$, and since it obviously satisfies condition (20.8) and $F(0) = 0$, we have:

Corollary 20.3.7. For the metric w_{graph}, $0 < \kappa_{graph} < \infty$.

We now focus on the Euclidean metric. Some realization of the Euclidean shortest path route is depicted in Figure 20.2.

[1] It is shown in (Pimentel 2006) that $p_c^* \geq 1 - p_c$, where p_c is the critical probability for the independent bond percolation on the Poisson–Delaunay graph $\mathcal{G}_{Delaunay}$. Moreover, it is conjectured that $p_c + p_c^* = 1$.

Proposition 20.3.8. Consider the homogeneous Poisson–Delaunay graph $\mathcal{G}_{Delaunay} = (\Phi, \mathcal{E}_{Delaunay}, w_{Euclid})$ with Euclidean weights. The shortest path on this graph satisfies (20.5) and (20.7) with $1 \leq K_d = \kappa_d = \kappa \leq \frac{2\pi}{3\cos(\pi/6)} < \infty$.

The above result can be proved using the following fact from (Keil and Gutwin 1992).

Lemma 20.3.9. Given any finite set ϕ of points on the plane. For any two points $x, y \in \phi$, the Euclidean shortest path $p^*(x, y)$ satisfies

$$\frac{|p^*(x,y)|}{|x-y|} \leq \frac{2\pi}{3\cos(\pi/6)} \approx 2.42\,.$$

Proof. [of Proposition 20.3.8]. Fix two points, say $0, t \in \mathbb{R}^2$. One can find a bounded set $G = G(\Phi)$, large enough so as to have $p^*(0, t, \Phi) = p^*(0, t, \Phi \cap G(\Phi))$. For example $G = C \cup H$ as defined in the proof of Proposition 20.3.4. By Lemma 20.3.9

$$|p^*(0,t)| = |p^*(0,t,\Phi \cap G(\Phi))| \leq \frac{2\pi}{3\cos(\pi/6)}|x(0) - x(t)|$$

and

$$\sup_{s\in[0,t]} |x(0) - x(s)| \leq t + 2|x(t/2) - t/2|\,.$$

Using the stationarity

$$\mathbf{E}[|x(t/2) - t/2|] = \mathbf{E}|x(0)|] < \infty\,.$$

To justify the upper bound on κ note that

$$\begin{aligned}
\kappa &\leq \lim_{|t|\to\infty} \frac{2\pi}{3\cos(\pi/6)} \frac{\mathbf{E}[|x(0) - x(t)|]}{|t|} \\
&\leq \frac{2\pi}{3\cos(\pi/6)} \left(1 + \lim_{|t|\to\infty} \frac{\mathbf{E}[|x(0)|]}{|t|} + \lim_{|t|\to\infty} \frac{\mathbf{E}[|x(t) - t|]}{|t|}\right) \\
&= \frac{2\pi}{3\cos(\pi/6)} \left(1 + 2\lim_{|t|\to\infty} \frac{\mathbf{E}[|x(0)|]}{|t|}\right) \\
&= \frac{2\pi}{3\cos(\pi/6)}\,.
\end{aligned}$$

For the lower bound on κ, one can use the triangle inequality to obtain $|p^*(x(0), x(t)| \geq |x(0) - x(t)|$ and

$$\frac{|p^*(0,t)|}{|t|} = \frac{|p^*(x(0),x(t)|}{|t|} \geq \frac{|x(0) - x(t)|}{|t|} \geq 1 - \frac{|x(0)|}{|t|} - \frac{|x(t) - t|)}{|t|}\,.$$

Thus by (20.5)

$$\kappa \geq 1 - \lim_{|t|\to\infty} \left(\frac{\mathbf{E}[|x(0)|]}{|t|} - \frac{\mathbf{E}[|x(t) - t|])}{|t|}\right) = 1 - 2\lim_{|t|\to\infty} \frac{\mathbf{E}[|x(0)|]}{|t|} = 1\,.$$

□

Remark: The conditions ensuring the non-degeneracy of the constant κ_{delay} associated with minimal delay routing are not known as to the writing of this monograph.

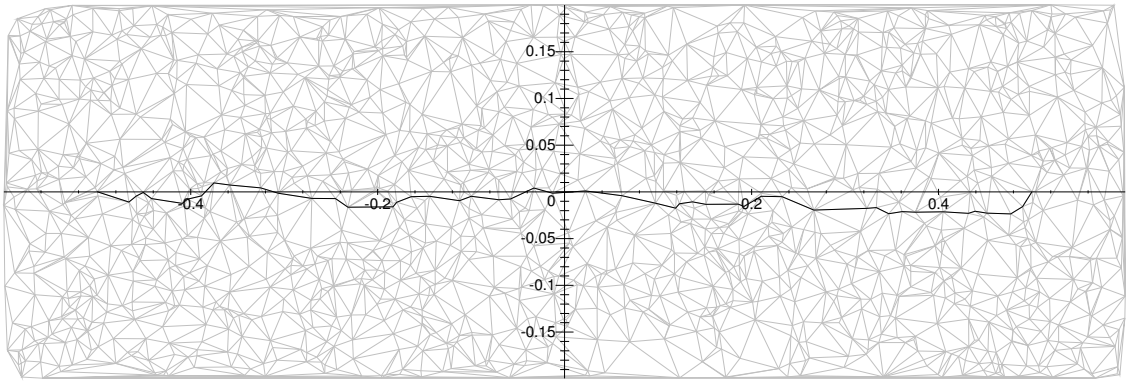

Fig. 20.2 Euclidean shortest path routing on the Poisson–Delaunay graph.

20.3.2 Scale Invariance of the Poisson–Delaunay Subadditive Constants

We now study the scale invariance properties of the Poisson–Delaunay subadditive constants $\kappa_{graph}, \kappa_{Euclid}$ with respect to the intensity λ of the underlying Poisson p.p. Recall that if $\Phi = \{x_i\}$ is a realization of the Poisson p.p. of intensity $\lambda = 1$, then $\Phi(\lambda) = \{x_i/\sqrt{\lambda}\}$ is a realization of the Poisson p.p. of intensity λ (cf. Example 1.3.12 in Volume I). Moreover, if $p^*(s,t,\Phi) = (x_1, \ldots, x_k)$ is a shortest path from s to t on $\mathcal{G}_{Delaunay}(\Phi, \mathcal{E}_{Delaunay})$, then $p^*(s,t,\Phi)/\sqrt{\lambda} = (x_1/\sqrt{\lambda}, \ldots, x_k/\sqrt{\lambda})$ is a shortest path from $s/\sqrt{\lambda}$ to $t/\sqrt{\lambda}$ on the Delaunay graph generated by $\Phi(\lambda)$. Thus, for w_{Euclid}, we have

$$|p^*_{Euclid}(s/\sqrt{\lambda}, t/\sqrt{\lambda}, \Phi(\lambda))| = |p^*_{Euclid}(s,t,\Phi)|/\sqrt{\lambda}$$

and for w_{graph}, we have

$$|p^*_{graph}(s/\sqrt{\lambda}, t/\sqrt{\lambda}, \Phi(\lambda))| = |p^*_{graph}(s,t,\Phi)|.$$

Consequently for the Euclidean shortest path routing, the ergodic constant does not depend on λ since

$$\begin{aligned} \kappa_{Euclid}(\lambda) &= \lim_{|t|\to\infty} 1/|t||p^*_{Euclid}(0,t,\Phi(\lambda)| \\ &= \lim_{|t|\to\infty} \sqrt{\lambda}/|t||p^*_{Euclid}(0,t,\Phi)|/\sqrt{\lambda} \\ &= \kappa_{Euclid}(1) = \kappa_{Euclid}\,, \end{aligned} \tag{20.9}$$

whereas for the graph distance shortest path routing,

$$\begin{aligned} \kappa_{graph}(\lambda) &= \lim_{|t|\to\infty} 1/|t||p^*_{graph}(0,t,\Phi(\lambda)| \\ &= \lim_{|t|\to\infty} \sqrt{\lambda}/|t||p^*_{graph}(0,t,\Phi)| \\ &= \sqrt{\lambda}\kappa_{graph}(1)\,. \end{aligned} \tag{20.10}$$

We say that that the Euclidean shortest path routing on the Poisson–Delaunay graph *approximates the Euclidean distance with a constant stretch of* κ_{Euclid}. Simulations show that κ_{Euclid} is approximately equal to 1.05.

20.3.3 MWR on the Random Geometric Graph

As already mentioned, the random geometric graph has a positive fraction of isolated nodes for all transmission ranges r. Nevertheless, the MWR path between two nodes is well defined when adopting the convention

that the weight between two nodes which are not connected by an edge have a fictitious edge with an infinite weight. When the connectivity range is such that the associated random geometric graph percolates, then one can consider the MWR between nodes of the infinite connected component of this graph. Letting $X(t)$ denote the node of this infinite component which is the closest to t, where $t \in \mathbb{R}^2$ and $p^*(s,t)$ the MWR path from $X(s)$ to $X(t)$, then for all s, t and $v \in \mathbb{R}^2$,

$$|p^*(s,t)| \leq |p^*(s,v)| + |p^*(v,t)| \,.$$

Hence, the linear scaling of (20.7) holds in this case too provided the integrability condition (20.4) holds.

20.3.4 MWR on the SINR Graph

By the same argument as above, when the bidirectional SINR graph $\mathcal{G}_{\text{SINR}}$ of Definition 8.2.1 in Volume I percolates, then the same subadditive inequality holds and this implies a linear scaling of the optimal paths under a condition of the type (20.4).

20.4 Largest Bottleneck Routing

One may think of a routing which realizes the optimality principle expressed in Definition 20.2.1 but with the sum of the weights $\sum_{i=1}^{k} w(\ldots)$ replaced by the maximum weight, namely for all routings $\mathcal{A}$ to D on $(\phi, \mathcal{E})$, for all $x \in \phi$,

$$\max_{i=1}^{h^*(x)} w\Big(\mathcal{A}^{*i-1}(x), \mathcal{A}^{*i}(x)\Big) \leq \max_{i=1}^{h(x)} w\Big(\mathcal{A}^{i-1}(x), \mathcal{A}^{i}(x)\Big) \,. \tag{20.11}$$

For example, if the weight $w_{delay}(x,y)$ is the inverse of the throughput of the link as defined in (20.1)), such a routing would select paths with the largest possible (throughput) bottleneck.

Remark: Note that the question whether there exists a path between two given points with all its weights smaller than a given threshold is in fact a percolation question. If the weights are the inverse of throughput as defined in (20.1), then this boils down to the SINR percolation model studied in Chapter 8 in Volume I.

20.5 Optimal Multicast Routing on a Graph

Consider a finite point pattern ϕ with an underlying weighed graph $(\phi, \mathcal{E}, w)$ The optimal multicast tree of this point pattern is the minimal weight spanning tree on this graph (see Chapter 13 in Volume I). If the graph is the complete one and the weight is w_{Euclid}, this is the MST (see § 3.2 in Volume I).

20.6 Conclusion

We shall revisit optimal paths in Chapter 22 in the context of time–space routing. However, in the wireless context, a major drawback of all these classes of optimal routing schemes is the large overhead associated with the evaluation of the routing table: in order to determine $\mathcal{A}^*_D(x)$, the neighbor of node x to which a packet with destination D should be sent, Dijkstra's algorithm requires that node x discover node D (cf. the last remark in § 25.3.1.2). Of course this search can be organized in a distributed way by exchanging information between neighbors as indicated in § 25.3.1.2, but it terminates only after all the paths originating from x and of weight smaller than $|p^*(x,D)|$ have been discovered (cf. the last statement of Proposition 25.3.1). Moreover, when the topology changes somewhere in the network, the algorithm has to be restarted, which is

quite problematic in a mobile network. This explains the interest of the networking community in suboptimal but locally defined paths such as those considered in the next chapter and at the end of Chapter 22. The loss in performance due to suboptimality being often more than compensated by the reduction in routing table overhead.

21

Greedy Routing

21.1 Introduction

The present chapter is focused on greedy geographic routing. By greedy, we mean that we replace global optimality as considered in the last chapter by local (and hence sub-optimal or greedy decisions). The local decisions of a given node are based on the exchange of location information with its neighbors only (here again, we assume the existence of some underlying graph allowing one to define neighborhoods). Hence the term 'geographic'.

Among the drawbacks of this class of algorithms, let us first quote the fact that they are only applicable to networks of nodes located in the Euclidean plane (or space); in addition, these algorithms require that nodes have some knowledge of their position, and also that the position of the destination be known. Finally, they are sub-optimal. But all this is compensated by the fact that the overhead associated with the construction of the routing table vanishes.

In the present chapter, we first list a few basic geographic routing algorithms and their associated point maps (§ 21.2). We study a couple of them. The first one, next-in-strip routing, is a toy example which consists in using the nodes located in a strip containing the source and the destination as relays. In the second one, smallest hop routing, the next relay is the node which is the closest among those which are closer to the destination. The rationale, which was already mentioned in Chapter 16, is that it is in a sense best to favor hops to the nearest neighbors.

The main results of the analysis consist of spatial averages which are obtained using new types of stochastic geometry arguments (§ 21.4), and route averages, which are based on Markovian analysis (§ 21.7).

A key observation is that these two types of averages do not coincide in general. In the smallest hop case, the latter has better performance than the former.

In addition to point-to-point routes, we also consider the multicast (either one-to-many or many-to-one) case. For this, we use the spanning trees that are obtained by taking the union of greedy routes to some common destination and which we call *radial spanning trees* (RST). These spanning trees can be used either on a large population of nodes as considered in § 21.5 (e.g. for diffusion in a MANET), or in a mesh or a sensor network context, where the main problem consists in building a collection of 'small spanning

trees' allowing each node to reach certain special nodes (gateways in the mesh network case, cluster heads in the sensor network case) in a multi-hop fashion. These collections of small RSTs are considered in § 21.8.

21.2 Examples of Geographic Routing Algorithms

Consider a locally finite point pattern ϕ of the Euclidean plane and some graph $\mathcal{G} = (\phi, \mathcal{E})$ on ϕ (e.g. the Delaunay graph of the point pattern, its geometric graph or the complete graph). We denote by $\mathcal{N}(x)$ the set of neighbors of $x \in \phi$ in this graph.

21.2.1 Best Hop, Smallest Hop, Next-in-Strip

Here are a few simple instances of geographic routing to some destination D:

- **Best hop to destination**: the next relay from node x is the neighbor of x which is the closest to the destination, namely $\mathcal{A}(D) = D$ and for all $x \neq D$, $\mathcal{A}(x) = y$ iff $y \in \mathcal{N}(x)$ and

$$|y - D| = \min_{z \in \mathcal{N}(x)} |z - D| \,.$$

  This is used for instance in GPSR (Greedy Perimeter Stateless Routing for Wireless Networks, (Karp and Kung 2000)). Note also that the minimization of the remaining distance to D is equivalent to the maximization of the progress to the destination

$$|y - D| = \max_{z \in \mathcal{N}(x)} |z - D| - |x - D| \,.$$

- **Smallest hop closer to destination**: the next relay node from x is the closest amongst the neighbors of x which are closer from the destination than x, namely $\mathcal{A}(D) = D$ and for all $x \neq D$, $\mathcal{A}(x) = y$ iff $y \in \mathcal{N}(x)$,

$$|y - D| < |x - D| \quad \text{and} \quad \phi(B_D^\circ(|x - D|) \cap B_x^\circ(|y - x|)) = 0 \,,$$

  where $B_x^\circ(r)$ denotes the open ball of radius r and center x. At first glance, it may look strange to consider such a smallest hop strategy. In the wireless setting this however often makes sense (see § 16.3.1.4).
- **Next-in-strip to destination**: For a given direction $\mathrm{d} \in [0, 2\pi)$ of the Euclidean plane, consider lines parallel to the direction d and regularly spaced at distance a from one another (here a is a fixed positive parameter). If the first of these lines crosses the perpendicular to d at $y = A$, where A is uniform on $[0, a]$, then these lines form a *stationary process of parallel lines*.
  Assume $\vec{SD} = u \cdot \mathrm{d}$ with $u > 0$ the distance between S and D. Consider the strip $\mathcal{S}$ formed by the stationary process of parallel lines, which contains S and D (we assume that neither S nor D belong to two strips). By projecting the points of $\Phi \cap \mathcal{S}$ on the d direction, one gets a total order which allows one to number the points of $\Phi \cap \mathcal{S}$ (according to their order in this projection). Then, for all x in this strip, $\mathcal{A}(x) = y$ iff $y \in \mathcal{N}(x)$ and y is the successor of x in this total order (or equivalently if the successor of x in this total order belongs to $\mathcal{N}(x)$). This is clearly a rather inefficient algorithm but it allows us to introduce and exemplify important ideas in a simple way.

A first question is whether these point maps are well defined; if so, another natural question is whether these point maps are indeed routings converging to D (see the definition in the preliminary to Part V).

21.2.2 Geographic Routing on a Poisson Point Process

In this section, we address the last questions when ϕ is some realization of a homogeneous Poisson p.p. Φ, under its Palm distribution, namely with an additional point at D.

Random Geometric Graph. On the random geometric graph, with a positive probability, the set $\mathcal{N}(x)$ is $\emptyset$ (or $\{x\}$ depending on the convention), Hence, on this graph, none of these point maps are routings in that there exists a positive fraction of the nodes for which these point maps do not converge to the destination.

One natural solution is to assume that the random geometric graph percolates (see § 3.2 in Volume I) and to limit the ambitions of routing to (source and destination) nodes which belong to the infinite component. However, this does not work either due the following *dead end* problem: consider any of the routing mechanisms described above (best hop, smallest hop or next-in-strip to destination D). Even if we assume that there is a path of the random geometric graph between S and D, the geographic routing algorithm may reach a dead end node, namely a node X such that all neighbors of X in the random geometric graph are more distant from D than X. Let us look at what then happens:

- If we take the convention that $x \notin \mathcal{N}(x)$ for all x, then smallest hop routing and next-in-strip routing are undefined at X. For best hop, assume for instance that X was first reached from node Y and that $\mathcal{A}(X) = Y$; then best hop reaches a limit cycle $Y, X, Y, X, \ldots$.
- If we take the convention that $x \in \mathcal{N}(x)$ for all x, then smallest hop and next-in-strip are again ill defined at X whereas best hop stop at X and remains there.

Hence, because of the dead end problem, these algorithms may not converge to the destination when used on the random geometric graph.

Poisson Delaunay Graph.

Lemma 21.2.1. For all D and x, the set $\mathcal{N}(x) \cap B_D^\circ(|x - D|))$ is almost surely non-empty.

Proof. If D belongs to $\mathcal{N}(x)$, then $D \in \mathcal{N}(x) \cap B_D^\circ(|x-D|))$. If $D \notin \mathcal{N}(x)$, then x lies oustide the Voronoi flower of point x w.r.t ϕ. Consider the Voronoi tessellation of the finite point pattern $\{x\} \cup \mathcal{N}(x)$. In this tessellation, x has the same Voronoi flower as in that w.r.t. ϕ. Since the Voronoi flower contains the Voronoi cell, D belongs to at least one of the infinite Voronoi cells of the points of the set $\mathcal{N}(x)$. That is, there is (at least) a point of $\mathcal{N}(x)$ closer to D than x. □

Using this and the fact that the probability that there are two points at the same distance from x is zero, we get that the point map is almost surely well and uniquely defined for both best and smallest hop routing. In addition

---

Proposition 21.2.2. On the Poisson-Delaunay graph, both best and smallest hop point maps are well defined routings.

Proof. From the last lemma, either the next hop is D or the distance to D decreases. Since Poisson point patterns are almost surely locally finite, each point map leads to D in a finite number of steps. □

Complete Graph. Best hop is clearly well and uniquely defined on the complete graph and (it reaches D in one hop from all points x!).

Smallest hop, which is illustrated in Figure 21.1 is well defined too: (1) since the set of points closer

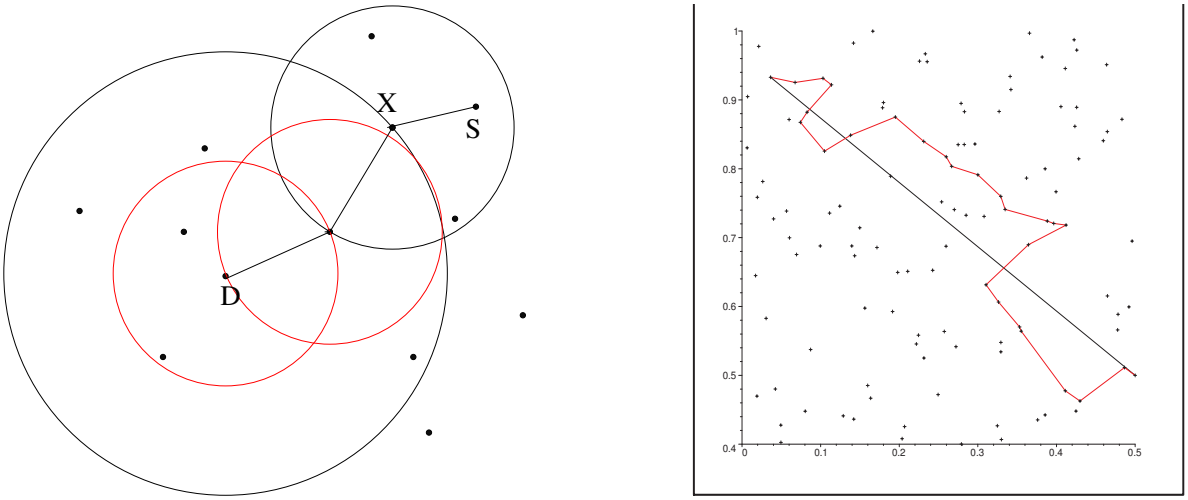

Fig. 21.1 Left: the next hop from point X on the route from S to D. Right: in red, the near-neighbor greedy route on a Poisson point process; in black, the straight line between the source and the destination, located in (.5,.5).

from D always contains point D, the set of neighbors which are closer to the destination is non-empty and almost surely finite; (2) almost surely, the nearest point is unique; (3) this defines a routing by the same decreasing distance argument as above.

There is (a.s.) no problem with next-in-strip routing either. Hence

---

Proposition 21.2.3. On the complete graph of a Poisson p.p., the point maps associated with best hop, smallest hop and next-in-strip are a.s. well defined and are routings to destination D.

General Observations. Here are a few observations on these greedy geographic routing schemes:

- Assuming one knows the location of the destination D, the route can be built at each step based on the exchange of mere geographic position information with one's near-neighbors. For instance, if the Delaunay graph is used, this exchange of information involves the Voronoi neighbors, the mean number of which is 6 (see (Møller 1994)). If smallest hop is used on the complete graph, it is easy to check that $\mathcal{A}(x)$ is one of the Voronoi neighbors of x w.r.t. the restriction of the point process Φ to $B_D(|x - D|)$. As already mentioned, in contrast, MWR requires solving dynamic programming equations which by essence are non-local.
- In MWR, the nodes used in the optimal path from S to D are the same as those in the optimal path from D to S. This symmetry property is lost in general in some of the geographic routing schemes considered here (like for instance smallest hop on the complete graph).
- It should be noticed that only one among the graphs which were considered above takes the inherent distance limitations of wireless communications into account: this is the random geometric graph, which assumes a maximal communication range. It is puzzling that geographic routing does not work properly on this graph. We shall discuss this question again in Chapter 22.

21.2.3 Radial and Directional Geographic Routing

Because of their radial symmetry w.r.t. D, the geographic routings $\mathcal{A}_D$ defined above will be referred to as *radial point maps* in what follows. Although this symmetry is in law only, it is quite visible on the paths as illustrated by Figure 21.2, where we plot the union of all routes from x to D when varying x over the collection of all nodes of the Poisson p.p. ϕ. The routing scheme used is smallest hop on the complete graph. This defines a tree which can be used either for the (multipoint to point) transport of data to D or for the point to multipoint broadcast of information from D to all the points of ϕ. The former is more natural in view of the fact that the building of the tree should be initiated by the sources. This tree is called the *radial spanning tree* (RST) associated with the routing.

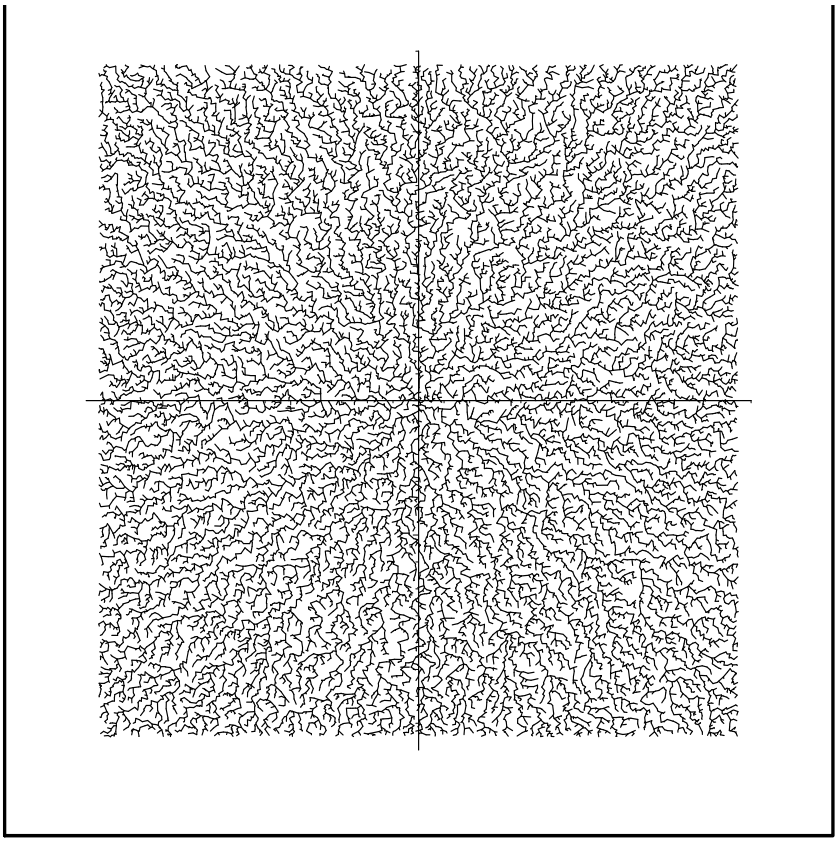

Fig. 21.2 Radial spanning tree of a Poisson p.p. in the unit square. The routing is 'smallest hop' and the graph is the complete one.

As we shall see, it is quite useful to consider the *case where D is at infinity*, say on the abscissa axis. The basic geographic routings considered above can then be rephrased as:

- *Best hop*: the next relay from node x is the neighbor of x with the largest abscissa;
- *Smallest hop*: the next relay node from x is the closest amongst the neighbors of x with an abscissa larger than that of x.
- *Next-in-Strip*: the next relay node from x is the next in the total order induced by the horizontal strip which contains node x.

These point maps will be referred to as *directional point maps* and is denoted by $\mathcal{A}_{\rm d}$ when the direction is d. The point is that the directional routes in general well approximate the radial ones on large S-D distances, except at the neighborhood of D.

The collection of all directional paths will be referred to as the directional spanning forest (DSF) associated with the routing scheme.

Remark: The question whether the DSF of a Poisson p.p. on the whole plane is an infinite tree is open for all the cases mentioned above.

This chapter primarily focuses on two instances of routing on an homogeneous Poisson point process: next-in-strip and smallest hop. We consider both point to point and multicast schemes and both the radial and the directional cases.

21.3 Next-in-Strip Routing

We consider here next-in-strip routing on the complete graph. We focus on the directional case assuming that the destination node is located at + infinity along the x direction.

Spatial Averages. From each relay node X, the progress $P(X)$ is an exponential random variable with parameter λa, where λ is the intensity of the Poisson p.p. and a is the width of the strip. Using the fact that the absolute value of the difference between two independent uniform random variables on $[-a/2, a/2]$ has a density at u equal to $\frac{2u}{a^2}$ for $0 \leq u \leq a$ and equal to 0 elsewhere, we get that the length $L(X)$ of the edge to the next hop has for Laplace transform

$$\mathcal{L}_L(s) = \int_{r>0} \int_{0\leq u\leq a} \exp(-s\sqrt{r^2+u^2}) \frac{2u}{a^2} \lambda a \exp(-\lambda a r) \mathrm{d}u\mathrm{d}r$$

and for mean value

$$\mathbf{E}^0(L) = \int_{r>0} \int_{0\leq u\leq a} \sqrt{r^2+u^2} \frac{2u}{a^2} \lambda a \exp(-\lambda a r) \mathrm{d}u\mathrm{d}r\,,$$

with $L = L(0)$.

Route Averages. The progress sequence is i.i.d. so that the route average progress coincides with the spatial average progress and is equal to $1/(\lambda a)$.

Let $X_i = (x_i, y_i)$. The sequence $\{y_i\}$ is i.i.d. and each y_i is uniform on $(-a/2, a/2]$. The sequence $\{y_{i+1} - y_i, x_{i+1} - x_i\}$ is stationary and ergodic. Let

$$l_i = \sqrt{(y_{i+1} - y_i)^2 + (x_{i+1} - x_i)^2}\,.$$

Due to the pointwise ergodic theorem, the route average of the hop lengths $\frac{1}{n}\sum_{i=0}^{n} l_i$ converges a.s. to the spatial mean $\mathbf{E}^0(L)$ (evaluated above) when n tends to infinity. One can also evaluate the geometric inefficiency of the algorithm defined as

$$\lim_{n\to\infty} \frac{1}{n} \sum_{i=0}^{n} |y_{i+1} - y_i|$$

by the same argument.

We now give a result generalizing the above observations.

Lemma 21.3.1. The projection of the points of the strip on the x axis forms a Poisson p.p. $\Psi = \{T_i\}$ on the line with intensity λa. Let $\widetilde{\Phi}_i = S_{T_i}\Phi$ (resp. $\Phi_i = S_{X_i}\Phi$), $i \in \mathbb{Z}$, be the node point process Φ translated in such a way that point T_i (resp. X_i) stands at the origin — see Chapter 10 in Volume I for these definitions. For all functions $g : \mathbb{M} \to \mathbb{R}^+$,

$$\lim_{n\to\infty} \frac{1}{n} \sum_{i=1}^{n} g(\widetilde{\Phi}_i) = \mathbf{E}[g(\Phi + \delta_V)] \tag{21.1}$$

$\mathbf{P}$ a.s. where $V = (0, U)$ with U uniform on $[-a/2, a/2]$ and independent of Φ. In addition

$$\lim_{n\to\infty} \frac{1}{n} \sum_{i=1}^{n} g(\Phi_i) = \mathbf{E}^0_\Phi[g(\Phi)] \tag{21.2}$$

$\mathbf{P}$ a.s.

Proof. Since $\{\widetilde{\Phi}_i\}$ (resp. $\{\Phi_i\}$) is a sequence of marks of Ψ, it follows that $\widetilde{\Psi} = \{T_i, \widetilde{\Phi}_i\}$ (resp. $\widetilde{\Psi} = \{T_i, \Phi_i\}$) is a stationary and ergodic marked point process. The stationarity and the ergodicity are inherited from the fact that the translation operator in the x direction is $\mathbf{P}$-invariant and ergodic. Hence, by the ergodic theorem, for all functions $g : \mathbb{M} \to \mathbb{R}^+$,

$$\lim_{n\to\infty} \frac{1}{n} \sum_{i=1}^{n} g(\widetilde{\Phi}_i) = \mathbf{E}^0_\Psi[g(\widetilde{\Phi}_0)], \quad (\text{resp. } \lim_{n\to\infty} \frac{1}{n} \sum_{i=1}^{n} g(\Phi_i) = \mathbf{E}^0_\Psi[g(\Phi_0)])$$

$\mathbf{P}$ a.s. where $\mathbf{P}^0_\Psi$ is the Palm distribution w.r.t. Ψ. This shows the convergence of route averages. But by Slivnyak's theorem,

$$\mathbf{E}^0_\Psi[g(\widetilde{\Phi}_0)] = \mathbf{E}[g(\Phi + \delta_V)]$$

and

$$\mathbf{E}^0_\Psi[g(\Phi_0)] = \mathbf{E}[g(\Phi + \delta_0)] = \mathbf{E}^0_\Phi[g(\Phi)].$$

□

21.4 Smallest Hop Routing — Spatial Averages

This section focuses on smallest hop routing on the complete graph of a Poisson p.p.

21.4.1 Edge Length and Progress in Radial Routes

Throughout this section, X is a point of $\mathbb{R}^2$ and $\mathbf{P}^{O,X}$ is the Palm probability of the Poisson p.p. Φ at (O, X), namely the law of a stationary Poisson p.p. with two additional points, one at the origin O and one at X. Without loss of generality, we assume that the destination is $D = O$.

Scale Invariance. Since the route is scale-invariant, without loss of generality, we can set $\lambda = 1$; for a general λ, all results follow by multiplying distances by $\sqrt{\lambda}$.

Edge Length. Let $X \in \mathbb{R}^2$ and $L(X) = |X - \mathcal{A}(X)|$. For all $r \geq 0$,

$$\mathbf{P}^{O,X}(L(X) \geq r) = \mathbb{1}(r \leq |X|)\mathbf{P}(\Phi(B_X^\circ(r) \cap B_O^\circ(|X|)) = 0) = \mathbb{1}(r \leq |X|)e^{-M(|X|,r)}, \tag{21.3}$$

where $M(x, r)$ is the surface of the lens of the right part of Figure 21.3. Using the formula for the surface depicted by the left part of Figure 21.3, we get that :

$$M(x, r) = x^2 \left(\phi - \frac{\sin(2\phi)}{2}\right) + r^2 \left(\frac{\pi}{2} - \frac{\phi}{2} - \frac{\sin(\phi)}{2}\right), \tag{21.4}$$

with $\phi = 2 \arcsin \frac{r}{2x}$. Notice that the distribution function of $L(X)$, which only depends on $|X|$, is not

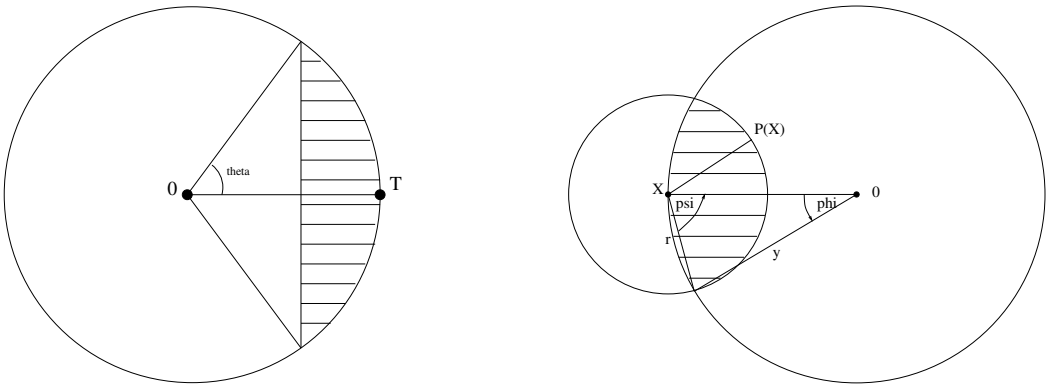

Fig. 21.3 Left: the surface of this auxiliary dashed lens is equal to $\frac{|T|^2}{2}|2\theta - \sin 2\theta|$. Right: the dashed lens with surface $M(x, r)$.

stochastically monotone in $|X|$. Its mean, which is plotted in Figure 21.4, is not monotone in $|X|$ either.

Given $L(X) = r < |X|$, consider the angle $\theta(X)$ of the edge from X to $\mathcal{A}(X)$. Using the property of the right part of Figure 21.3 that $\psi = \pi/2 - \phi/2$, we get that $\theta(X)$ is uniformly distributed on the interval $(\pi + \arg(X) - \psi, \pi + \arg(X) + \psi)$, with $\cos\psi = \sin(\phi/2) = r/(2|X|)$, that is $\psi = \arccos \frac{r}{2|X|}$. Given $L(X) = |X|$, the angle $\theta(X)$ is $\pi + \arg(X)$.

The joint distribution function of $(L(X), \theta(X))$ is equal to

$$\mathbb{1}(r \in (0, |X|))\frac{d}{dr}M(|X|, r)e^{-M(|X|,r)}\mathrm{d}r \times \mathbb{1}(\theta \in (\pi + \arg(X) - \psi, \pi + \arg(X) + \psi))\frac{\mathrm{d}\theta}{2\psi}$$
$$+\delta_{|X|}(\mathrm{d}r)\delta_{\pi+\arg(X)}(\mathrm{d}\theta)e^{-M(|X|,|X|)}. \tag{21.5}$$

Progress. The progress from point $X \in \Phi$ is defined as $P(X) = |X| - |\mathcal{A}(X)|$. It is equal to the length of the projection of the edge $(X, \mathcal{A}(X))$ on the $\overline{0X}$ line. The mean progress is plotted in function of $|X| = x$ in Figure 21.4.

21.4.2 Asymptotic Analysis

We now look at what happens when $|X|$ tends to infinity. A direct computation gives:

$$\lim_{|X|\to+\infty} \mathbf{P}^{O,X}(L(X) \geq r) = \exp(-\frac{\pi r^2}{2}). \tag{21.6}$$

In particular,

$$\lim_{|X|\to+\infty} \mathbf{E}^{O,X}[L(X)] = \int_0^\infty e^{-\frac{\pi r^2}{2}} \mathrm{d}r = \frac{1}{\sqrt{2}}. \tag{21.7}$$

By similar arguments, the asymptotic progress has for Laplace transform

$$\begin{aligned}\lim_{|X|\to+\infty} \mathbf{E}^{O,X}(e^{-sP(X)}) &= \frac{1}{\pi} \int_{r=0}^{\infty} \int_{\theta=-\pi/2}^{\pi/2} e^{-sr\cos\theta} \exp(-\frac{\pi r^2}{2}) \pi r \mathrm{d}r\mathrm{d}\theta \\ &= \int_{r=0}^{\infty} \int_{\theta=-\pi/2}^{\pi/2} e^{-sr\cos\theta} \exp(-\frac{\pi r^2}{2}) r \mathrm{d}r\mathrm{d}\theta. \end{aligned} \tag{21.8}$$

In particular, the mean asymptotic progress is

$$\lim_{|X|\to+\infty} \mathbf{E}^{O,X}(P(X)) = \frac{1}{\pi} \int_{r=0}^{\infty} \int_{\theta=-\pi/2}^{\pi/2} \exp(-\frac{\pi r^2}{2}) \cos\theta \mathrm{d}r\mathrm{d}\theta = \frac{\sqrt{2}}{\pi}. \tag{21.9}$$

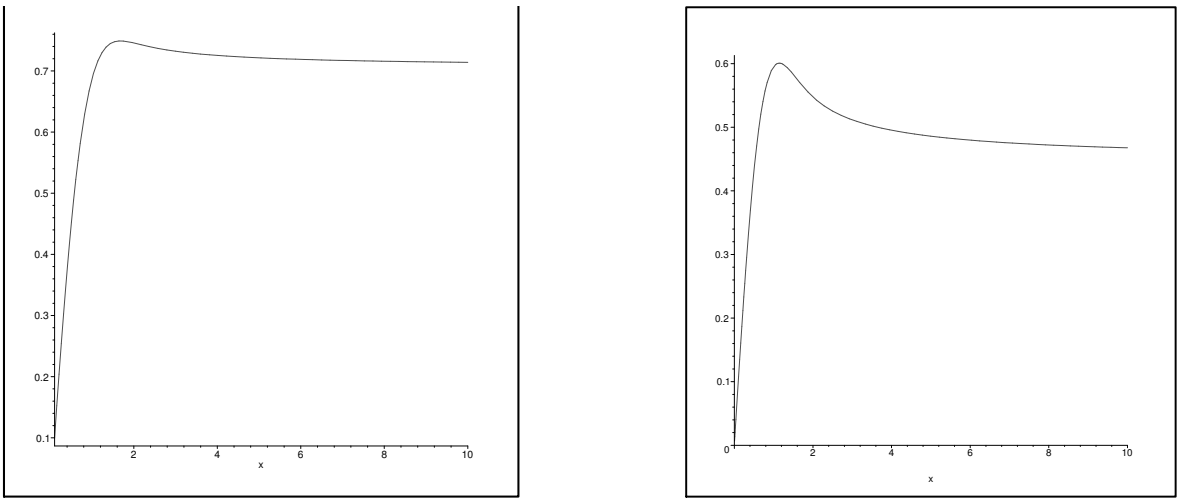

Fig. 21.4 Left: Mean of $L(X)$ in function of x. Right: Mean of $P(X)$ in function of $x = |X|$.

21.5 Smallest Hop Multicast Routing — Spatial Averages

This section is focused on the RST associated with smallest hop routing. In what follows, we study the degree of nodes in the RST $\mathcal{T}$ associated with a Poisson p.p. Φ of intensity 1 which is considered under its Palm version at O (the root is the origin of the plane).

- when the tree is used for multicasting, the degree determines the number of times a given symbol received by the node should be forwarded to the offspring nodes;
- when the tree is used for the gathering of information at the root (see Remark 25.3.3), the degree determines the number of links converging to the node.

21.5.1 Degree of Nodes

The degree of the source node O is

$$D(O) = \sum_{x_i \in \Phi \setminus O} \mathbb{1}(\Phi(B^\circ_{x_i}(|x_i|) \cap B^\circ_O(|x_i|)) = 0).$$

Hence, using Campbell's formula, we get

$$\mathbf{E}^O D(O) = 2\pi \int_0^\infty e^{-r^2(2\pi/3 - \sin(2\pi/3)} r \mathrm{d}r = \frac{\pi}{2\pi/3 - \sqrt{3}/2} \sim 2.56. \tag{21.10}$$

Lemma 21.5.1. The degree of node O is bounded from above by 5 a.s.

Proof. Order the points directly attached to the origin by increasing polar angle. Let X and Y denote two neighboring points in this sequence. Assume $|\vec{OX}| < |\vec{OY}|$. Denote by ϕ the angle between these two vectors. We have

$$|\vec{XY}|^2 = |\vec{OX}|^2 + |\vec{OY}|^2 - 2|\vec{OX}||\vec{OY}| \cos\phi.$$

Since Y is attached to the origin, necessarily $|\vec{XY}|^2 > |\vec{OY}|^2$, which implies that

$$2|\vec{OX}||\vec{OY}| \cos\phi < |\vec{OX}|^2.$$

Using now the assumption that $|\vec{OX}| < |\vec{OY}|$, we get $\cos\phi < 1/2$. Hence $|\phi| > \pi/3$. □

The degree of node $X \neq O$ is given by :

$$D(X) = 1 + \sum_{x_i \in \Phi} \mathbb{1}(|x_i| \geq |X|)\mathbb{1}(\Phi(B^\circ_{x_i}(|X - x_i|) \cap B^\circ_O(|x_i|)) = 0)\mathbb{1}(O \notin B^\circ_{x_i}(|X - x_i|)). \tag{21.11}$$

Indeed, a point x of norm larger than $|X|$ shares an edge with X if and only if there is no point of smaller norm closer from x than X.

Let $X \neq 0$ and $|X| = r$. Obviously, $\mathbf{E}^{0,X} D(X)$ depends on r only and with an abuse of notation, we often write $\mathbf{E}D(r)$ in place of $\mathbf{E}^{0,X} D(X)$. Taking the expectation of Equation (21.11) w.r.t $\mathbf{P}^{O,X}$, using the fact that the p.p. outside the ball of radius r is Poisson and making use of Campbell's formula, we get

$$\begin{aligned} \mathbf{E}D(r) &= 1 + \mathbf{E} \sum_{x_i \in \Phi} \mathbb{1}(\Phi(B^\circ_{x_i}(|X - x_i|) \cap B^\circ_O(|x_i|)) = 0)\mathbb{1}(r \leq |x_i|)\mathbb{1}(|x_i| > |X - x_i|) \\ &= 1 + \int_{\rho > r} \int_{-\arccos(\frac{r}{2\rho})}^{\arccos(\frac{r}{2\rho})} e^{-Q(r,\rho,\theta)} \rho \mathrm{d}\rho \mathrm{d}\theta, \end{aligned}$$

where $Q(r, \rho, \theta)$ is the dashed surface in Figure 21.5 for $X = (r, 0)$ and $x = (\rho, \theta)$. The condition that $|x| > |X - x|$ (or equivalently that θ belongs to the interval $(-\arccos(\frac{r}{2\rho}), \arccos(\frac{r}{2\rho}))$ translates the fact that the origin should not be contained in this lens. Hence

$$\mathbf{E}D(r) = 1 + \int_{\rho > r} \int_{-\arccos(\frac{r}{2\rho})}^{\arccos(\frac{r}{2\rho})} e^{-\frac{\rho^2}{2}|2\alpha - \sin 2\alpha|} e^{-\frac{\rho^2 + r^2 - 2\rho x \cos\theta}{2}|2\beta - \sin 2\beta|} \rho \mathrm{d}\rho \mathrm{d}\theta,$$

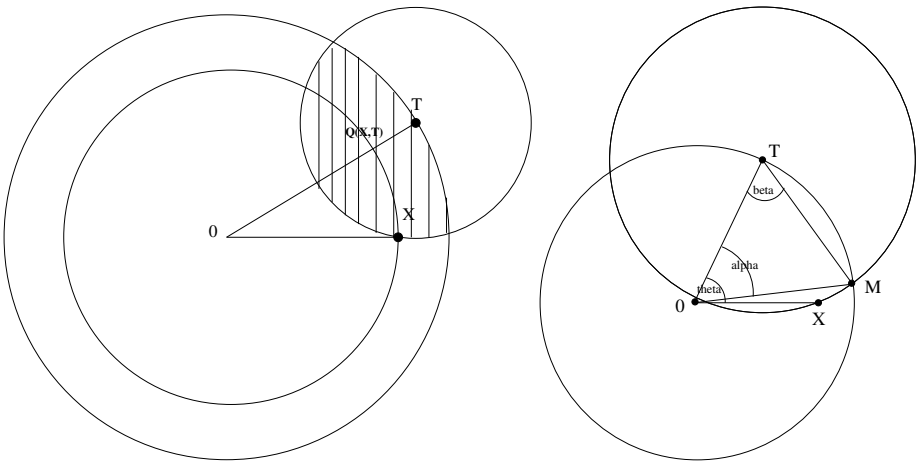

Fig. 21.5 Left : $Q(r,\rho,\theta)$. Right : The α and β angles.

where α and β are the angles depicted in Figure 21.5.

If $u=\frac{\rho}{r}$, we have $\cos\alpha=(1-u^{-2})/2+u^{-1}\cos\theta$ and $\beta=(\pi-\alpha)/2$. Finally,

$$\mathbf{E}D(r) \;=\; 1+2r^2\int\limits_{u>1}\int\limits_{0}^{\arccos(\frac{1}{2u})} e^{-\frac{u^2r^2}{2}(2\alpha-\sin 2\alpha)}e^{-\frac{r^2}{2}(1+u^2-2u\,cos\theta)(\pi-\alpha-\sin\alpha)}u\mathrm{d}u\mathrm{d}\theta. \quad (21.12)$$

We also have the following asymptotic result on the mean degree:

$$\lim_{r\to+\infty}\mathbf{E}D(r) \;=\; 1+\int\limits_{Half-Plane}\exp(-\frac{\pi|x|^2}{2})\mathrm{d}x = 1+\int\limits_{-\frac{\pi}{2}}^{\frac{\pi}{2}}\int\limits_{0}^{+\infty}\exp(-\frac{\pi\rho^2}{2})\rho\mathrm{d}\rho\mathrm{d}\theta = 2.$$

The mean degree is plotted in Figure 21.6.

21.6 Smallest Hop Directional Routing

21.6.1 Directional Point Map

Let $(0,b_1,b_2)$ be an orthonormal basis of $\mathbb{R}^2$. The directional point map with direction $-b_1$ is defined as follows: the successor of $X\in\Phi$ is the nearest point of Φ which has a strictly smaller b_1-coordinate. More generally, for all fixed directions d with $|\mathrm{d}|=1$, the directional point map $\mathcal{A}_d$ with direction d is defined by $\mathcal{A}_d(X)=Y$ iff

$$\langle Y,\mathrm{d}\rangle > \langle X,\mathrm{d}\rangle \text{ and } \Phi(H_X(\mathrm{d})\cap B_X^\circ(|Y-X|))=0,$$

where $\langle x,y\rangle$ denotes the scalar product in $\mathbb{R}^2$ and $H_X(\mathrm{d})$ the half-plane $\langle x,\mathrm{d}\rangle > \langle X,\mathrm{d}\rangle$. The associated directional route originating from O is defined by

$$\begin{cases} T_0=O, \\ T_{n+1}=\mathcal{A}_\mathrm{d}(T_n,\Phi) \quad \text{for } n\geq 0\,. \end{cases} \quad (21.13)$$

Directional routing can be seen as the "limit" of radial routing far away from the destination in the d direction. We already know some of the local properties of directional routing through the asymptotic results of §21.4.2 and 21.5.1.

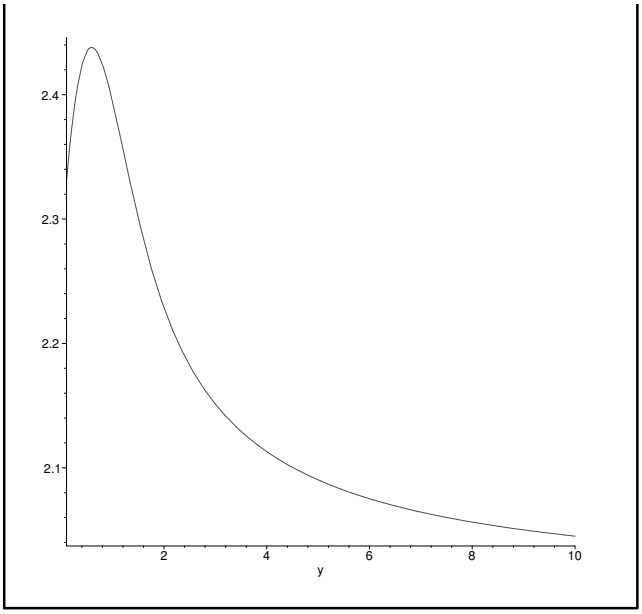

Fig. 21.6 $\mathbf{E}D(r)$ as function of $r > 0$.

21.6.2 Directed Spanning Forest

We define the *Directed Spanning Forest* (DSF) $\mathcal{T}_d$ as the union of all the directional routes stemming from all the points of Φ.

The following lemma, on the support of the degree of the DSF, is surprising in view of Lemma 21.5.1.

Lemma 21.6.1. The degree of a node of the DSF is not bounded and in the RST, a.s.

$$\sup_{x\in\Phi} D(x) = +\infty.$$

Proof. Without loss of generality we take $\mathrm{d} = -b_1$. The DSF built on the point set $\{X_n = (2^{-n}, 3^n), n \in \mathbb{N}\} \cup \{O\}$ gives: for all n, $\mathcal{A}_d(X_n) = 0$, in particular the degree of the origin is infinite.

We now prove prove the second statement of the lemma.

Let $M \in \mathbb{N}^*$; for $n \geq 0$, we define $\mathbb{U}_n = [2^{-n} - \epsilon, 2^{-n} + \epsilon] \times [3^n - \epsilon, 3^n + \epsilon]$, $\mathbb{U}_{-1} = [-\epsilon, \epsilon] \times [-\epsilon, \epsilon]$, $A_M = B_O(4^M) \backslash \big(\cup_{-1\leq n\leq M} \mathbb{U}_n \big)$ and

$$E_M(X) = \{\Phi(X + A_M) = 0, \Phi(X + \mathbb{U}_n) = 1, -1 \leq n \leq M\}.$$

We have $\mathbf{P}(E_M(X)) = \delta > 0$ and if $|X - Y| > 2.4^M$, $E_M(X)$ and $E_M(Y)$ are independent (for ϵ small enough).

For ϵ small enough, if $E_M(X)$ occurs, the point in $\mathbb{U}_{-1}(X)$ has degree at least M in $\mathcal{T}_d$. Similarly for the RST, if $|X|$ is large enough and if $E_M(X)$ occurs, the point in $\mathbb{U}_{-1}(X)$ has degree at least M in $\mathcal{T}$.

Using the independence of the events $E_M(2k4^M b_1)$, $k \in \mathbb{N}$, we deduce that these events appear infinitely often. □

21.7 Space and Route Averages of Smallest Hop Routing

21.7.1 Spatial Averages

The mean values computed in the previous sections are in fact spatial averages. We illustrate this statement on the edge length case.

Consider the RST with root 0 under $\mathbf{P}^O$. Let $\mathcal{L}_r$ be the sum of the edge length over all points included in the ball $B_0(r)$, namely:

$$\mathcal{L}_r = \sum_{X\in\Phi} \mathbb{1}(X \in B_0(r))|X - \mathcal{A}(X)| = \sum_{X\in\Phi\setminus\{O\}} \mathbb{1}(X \in B_0(r))|X - \mathcal{A}(X)|. \tag{21.14}$$

From Campbell's formula

$$\mathbf{E}^O\mathcal{L}_r = \int_{B_O(r)} \mathbf{E}^{O,x}(L(x))\mathrm{d}x = 2\pi \int_0^r \mathbf{E}^{(0,0),(0,t)}(L((0,t)))t\mathrm{d}t\,.$$

The change of variable $u = \frac{t}{r}$ gives

$$\mathbf{E}^O\frac{\mathcal{L}_r}{r^2} = 2\pi \int_0^1 u\mathbf{E}^{(0,0),(0,ru)}L((0,ru))\mathrm{d}u.$$

The dominated convergence theorem together with Equation (21.7) gives

$$\lim_{r\to\infty} \mathbf{E}^O\frac{\mathcal{L}_r}{r^2} = 2\pi \int_0^1 u\frac{1}{\sqrt{2}}\mathrm{d}u = \pi/\sqrt{2}. \tag{21.15}$$

The following stronger result is proved in (Baccelli and Bordenave 2007) using concentration inequalities:

Lemma 21.7.1. Almost surely and in L^1,

$$\lim_{r\to\infty} \frac{\mathcal{L}_r}{\pi r^2} = \lim_{|X|\to+\infty} \mathbf{E}^{O,X}[L(X)] = \frac{1}{\sqrt{2}}. \tag{21.16}$$

This extends to other quantities of the form $g(\mathcal{A}(X) - X)$, where g is some function from $\mathbb{R}^2$ to $\mathbb{R}$, which allows one to consider e.g. progress.

21.7.2 Route Averages

21.7.2.1 Existence

Two natural questions arise in connection with the definition of e.g. the directional greedy route in (21.13). For all g as above, let

$$S_n = \frac{1}{n}\sum_{k=1}^{n} g(T_{k-1} - T_k), \tag{21.17}$$

be the empirical route averages associated with g. Here are the two main questions related with this:

(1) Does S_n a.s. converge to some limit when n tends to infinity?
(2) If so, does this limit coincide with the corresponding spatial average?

The answer to the first question is positive:

Theorem 21.7.2. There exists a unique probability measure π on $\mathbb{R}^2$ such that for all measurable functions g such that $g(X) \leq \max(C, |X|^\alpha)$ for some $C > 0$ and $\alpha > 0$,

$$\lim_{n\to\infty} \frac{S_n}{n} = \int_{\mathbb{R}^2} g(x)\pi(\mathrm{d}x) = \pi(g). \tag{21.18}$$

This theorem, which is proved in (Baccelli and Bordenave 2007), leverages the fact that certain subsequences of the sequence of segments that constitute a directional route form a Markov chain with a non-discrete state space. This chain is a Harris chain. It admits a small set and it is geometrically ergodic (Meyn and Tweedie 1993). This result allows one to characterizes the asymptotic behavior of directional routes:

Corollary 21.7.3. There exists positive constants p and p_y such that

$$\lim_{n\to\infty} \frac{1}{n} \sum_{k=0}^{n-1} \langle T_k - T_{k+1}, b_1 \rangle \quad = \quad p_x \;=\; p, \tag{21.19}$$

$$\lim_{n\to\infty} \frac{1}{n} \sum_{k=0}^{n-1} |\langle T_k - T_{k+1}, b_2 \rangle| \quad = \quad p_y\,, \tag{21.20}$$

where p is the route average of the directional progress and p_y that of the typical inefficiency; for all $\alpha > 0$, there exists a constant l_α such that

$$\lim_{n\to\infty} \frac{1}{n} \sum_{k=0}^{n-1} |T_{k+1} - T_k|^\alpha \quad = \quad l_\alpha. \tag{21.21}$$

21.7.2.2 The Routing Paradox and the Price of Anarchy in Routing

The answer to the second question is negative (in contrast with what happens in the strip routing case): by simulation of 20000 transitions of the chain, one obtains that $p \approx .504$, $p_y \approx .46$ and $l_1 \approx .75$. The value of p is significantly larger than the spatial average of the mean asymptotic progress as evaluated in (21.9), which is approx. equal to 0.450. A similar observation holds for l_1 when compared to (21.6): as it is the case for progress, the mean magnitude of the hop from a point to its successor ($l_1 \approx .75$) is "boosted" by the fact that one is located on a long route, compared to the spatial average value (which is appr. equal to .71). The analysis of the Markov chain alluded to above allows one to understand why this happens.

It can in addition be proved that route averages over long radial paths coincide with route averages on long directional routes (see (Baccelli and Bordenave 2007) for a proof). Hence, one can rephrase the results of the last corollary as follows: consider the greedy route from a source to a destination at distance t from one another; then for a p.p. Φ with intensity λ,

- The mean number of hops on the greedy route scales like $1.98t/\sqrt{\lambda}$ (since this mean number of hops is approximately equal to $t/0.504$ for large t when $\lambda = 1$);
- The greedy route κ-approximates Euclidean distance with $\kappa \approx 1.48$ (since the mean length of the route is approximately equal to $t * 0.75/0.504$ for large t when $\lambda = 1$).

Comparing these results to the corresponding ones on optimal routes on the Poisson–Delaunay graph (see § 20.3.2), we can say that the price of anarchy which we define as the ratio of the greedy cost and of the optimal cost is $1.48/1.05 \approx 1.41$ in terms of Euclidean distance.

21.7.2.3 Maximal Deviation

We end this section with a result on the deviation of the path from its mean, also proved in (Baccelli and Bordenave 2007). Let $R(x)$ or $R(X)$ denote the path from $X = (x, 0)$ in the DSF with direction $-b_1$; $R(x)$ may be parameterized as a piecewise linear curve $(t, Y(t))_{t \le x}$ in $\mathbb{R}^2$. The maximal deviation of this curve between x' and x with $x' \le x$ is defined as

$$\Delta(x, x') = \sup_{t \in [x', x]} |Y(t)|. \tag{21.22}$$

Theorem 21.7.4. For all $x \ge x'$, for all $\epsilon > 0$ and all integers n,

$$\mathbf{P}(\Delta(x, x') \ge |x - x'|^{\frac{1}{2}+\epsilon}) = O(|x - x'|^{-n}).$$

21.8 Radial Spanning Tree in a Voronoi Cell

In this section, we extend the RST to situations where there is a collection of trees (a forest) rather than a single one. We use the context of sensor networks (see Remark 25.3.3) to describe the construction. Consider two independent Poisson p.p.: $\Phi_0 = \{x_n^0\}$, the p.p. of cluster heads, of intensity λ_0 and $\Phi_1 = \{x_n^1\}$, the p.p. of sensor nodes, with intensity λ_1. The first p.p. tessellates the plane in Voronoi cells. We denote by V_n the Voronoi cell of point x_n^0 w.r.t. the points of Φ_0. Two forests can then be defined in relation with this VT:

- The family of *internal* RSTs: the n-th tree of this forest, $\mathcal{T}_n$, is the RST built using the points of Φ_1 that are contained in V_n, with x_n^0 as a root.
- The family of *local* RSTs: if node X belongs to V_n, one defines its successor as the point of $(\Phi_1 \cup \{x_n^0\}) \cap B^\circ_{x_n^0}(|X - x_n^0|)$ that is the closest to X. Notice that this successor does not necessarily belong to V_n. Nevertheless, this rule defines a forest too (see Lemma 21.8.1). One then defines the n-th local RST tree $\mathcal{U}_n$ as the tree which is the union of all the routes from sensor nodes with ultimate successor x_n^0.

In what follows, we concentrate on the second case which can be analyzed using the same type of tools as in §21.5. Figure 21.7 depicts a sample of such a forest.

Lemma 21.8.1. Almost surely, there exists no node X of Φ_0 such that the sequence of successors of X based on the local RST rule contains node X.

Proof. Let $\{Y_i\}_{i \ge 0}$ be the sequence of successors of $X = Y_0$. If $Y_i = X$ for some $i > 0$, then necessarily the points of $\{Y_i\}$ belong to different Voronoi cells (if this were not the case, then the distance to the cluster head of the cell to which all points belong would be strictly decreasing, which forbids cycles). Then one can rewrite $\{Y_i\}_{i \ge 0}$ as

$$\{Y_i\}_{i \ge 0} = \{Z_0(1), \ldots, Z_0(n_0), Z_1(1), \ldots, Z_1(n_1), \ldots, Z_j(1), \ldots, Z_j(k), ...\}$$

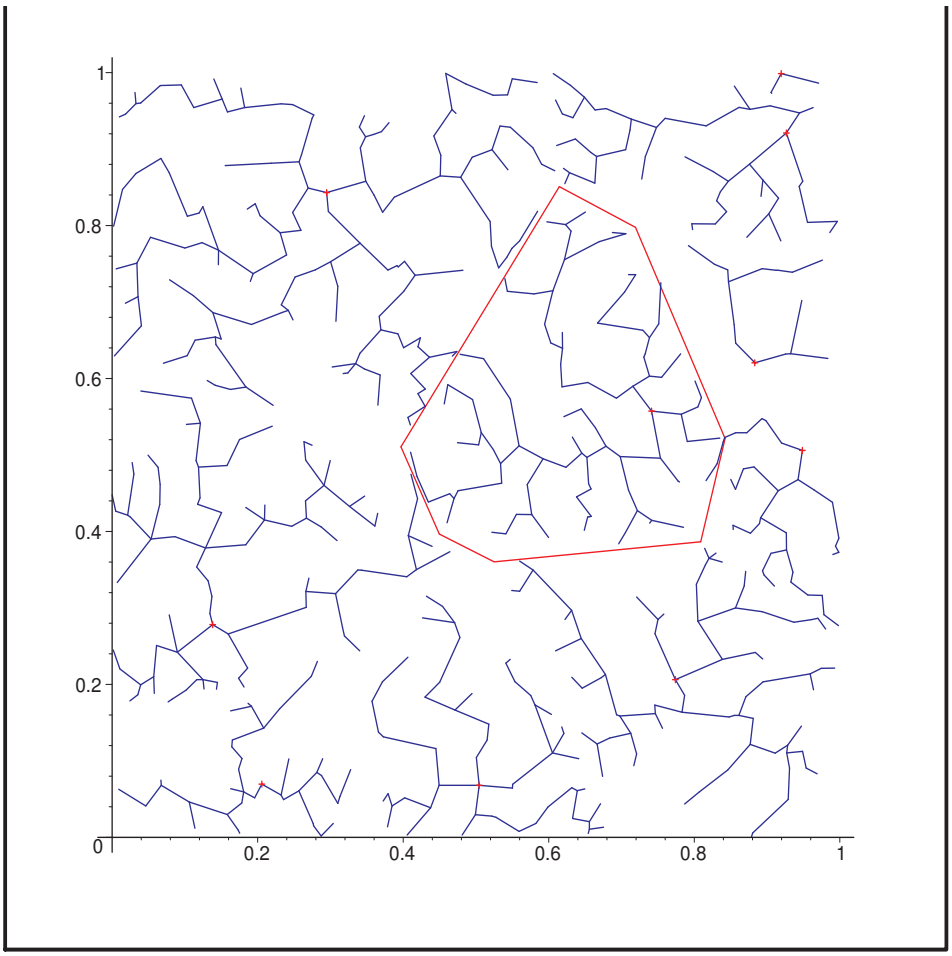

Fig. 21.7 Local Voronoi radial spanning trees (in blue) of 600 sensor nodes uniformly and independently distributed in the unit square, w.r.t 10 cluster heads (in red), also uniformly and independently distributed in the unit square. The Voronoi cell of one of the cluster heads is depicted in red.

with $Z_l(1), \ldots, Z_l(n_l) \in W_l$ for all $0 \leq l \leq j$, where $\{W_j\}_{j \geq 0}$ is a sequence of cells such that $W_l \neq W_{l+1}$ for all $l < j$, n_l is a sequence of integers and $Z_j(k) = X$. Let S_l denote the cluster head of W_l. Then the definition of the local RST implies that a.s.

$$|X - S_0| = |Z_0(1) - S_0| > |Z_0(2) - S_0| > \cdots > |Z_0(n_0) - S_0| > |Z_1(1) - S_0|.$$

Since $Z_1(1)$ belongs to W_1, we have a.s.

$$|Z_1(1) - S_0| > |Z_1(1) - S_1|.$$

For the same reasons, for all $l = 1, \ldots, j-1$

$$|Z_l(1) - S_l| > |Z_l(2) - S_l| > \cdots > |Z_l(n_l) - S_l| > |Z_{l+1}(1) - S_l|$$

and

$$|Z_{l+1}(1) - S_l| > |Z_{l+1}(1) - S_{l+1}|, \quad a.s.$$

In addition

$$|Z_j(1) - S_j| > |Z_l(2) - S_l| > \cdots > |Z_j(k) - S_j| = |X - S_0|.$$

Hence a contradiction. □

Let $\mathcal{L}_n$ denote the total length of all edges from nodes in V_n. Let $\mathbf{E}^0$ denote the Palm probability w.r.t. Φ_0. We have

$$\mathcal{L}_n = \sum_m \mathbb{1}(x_m^1 \in V_n) L_m,$$

where L_m is the length of the link that connects x_m^1 to its successor. Using the fact that $x_m^1 \in V_n$ iff $\Phi_0(B^\circ_{x_m^1}(|x_m^1 - x_n^0|)) = 0$ and the fact that $L_m > u$ with $u < |x_m^1 - x_n^0|$ iff $\Phi_1(B^\circ_{x_m^1}(u) \cap B^\circ_{x_n^0}(|x_m^1 - x_n^0|)) = 0$, we get from Campbell's formula that

$$\mathbf{E}^0\left(\sum_m \mathbb{1}(x_m^1 \in V_n) L_m\right) = 2\pi\lambda_1 \int_{r=0}^{\infty} e^{-\lambda_0 \pi r^2} \left(\int_{u=0}^{r} e^{-\lambda_1 M(r,u)} \mathrm{d}u\right) r \mathrm{d}r,$$

with $M(r,u)$ the surface of the lens defined in §21.4. Hence

$$\mathbf{E}^0(\mathcal{L}_0) = 2\pi\lambda_1 \int_{r=0}^{\infty} e^{-\lambda_0 \pi r^2} \left(\int_{u=0}^{r} e^{-\lambda_1 M(r,u)} \mathrm{d}u\right) r \mathrm{d}r. \tag{21.23}$$

21.9 Conclusion

There are several interesting problems in relation with the topics considered in the present chapter. The first line of thought concerns the extension of the analysis conducted for "smallest hop closer to destination" to other natural routing schemes.

A second and more general question concerns the classification of greedy routing schemes according to the following criteria:

- Price of anarchy: how much does the greedy path lose (e.g. in terms of Euclidean length or in terms of number of hops) compared to the optimal path(s)?
- Comparison of spatial and route averages: given that the latter are more difficult to evaluate than the former, it would be interesting to learn whether there are general comparison rules between the two. For instance, for strip routing the two types of averages coincide, whereas for "smallest hop closer to destination", they differ. Does there exist a general criterion for deciding whether a given routing scheme is of the first kind (with both averages coinciding) or of the second? In "smallest hop closer to destination", route averages are "better" than spatial averages (e.g. in terms of progress). Can one identify the class of greedy schemes for which this property holds true?

In Chapter 20 and in the present chapter, the physical constraints of wireless links were essentially ignored. Consider for instance "smallest hop closer to destination", which was argued to be the most sensible representation of routing in a wireless network within the context considered in the present chapter. The distance from a node to the next hop node may still be arbitrarily large as we saw; in addition the latter node may be surrounded by interferers which would result in a very small probability to have a good SINR on the considered link. This example shows that the routing principles considered so far should be revisited within the SINR geometry framework, which is the object of the next chapter.

22

Time-Space Routing

22.1 Introduction

In Chapters 20 and 21, MAC and detection were ignored as already mentioned. But in addition time was absent (we considered routes on a snapshot as already mentioned) and when throughput was considered, it was in terms of a Shannon like formula.

In contrast, the time–space multihop routing schemes considered in this chapter take MAC decisions and fading variables into account as well as their variability w.r.t. time. The setting is again a Poisson MANET with a MAC of the Aloha type. The packet communication model is used, with a definition for the capture of packets which is based on the SINR model of § 16.2.

Here is a first basic dichotomy for the routing schemes to be considered in this chapter. We distinguish between:

- *Layer-aware* routing schemes, where the route between S and D is defined once and for all (e.g. through a static point map as considered in the last two chapters) and where the MAC is then asked to realize this route coping with the time and space variations of fading;
- *Cross-layer* routing schemes, where there is no predefined route and where the routing scheme tries to take advantage of the variability of MAC and fading to decide on the next relay for each packet at each time slot.

Section 22.2 describes the stochastic setting allowing us to define time–space routing. Section 22.3 focuses on the key notions pertaining to this type of routing. In particular, we introduce a new random graph that we call the *time–space SINR graph* and the notion of *time–space point map*. We also define the notions of route averages associated with these maps.

The other sections of the chapter focus on instances of such time–space routing algorithms. Section 22.4.2 bears on the layer-aware case whereas all other sections bear on the cross-layer case. Section 22.5 is concerned with minimal weight time–space routes. These optimal routes have no practical meaning as their determination would require full knowledge of the future fading and MAC variables of all nodes. However, their mathematical properties shed light on many other algorithms and in particular on greedy

time–space routes. They also provide intrinsic performance limitations on this class of schemes. Greedy time–space routing (called *opportunistic routing* below) is studied in § 22.6. Let us stress that opportunistic routing is based on the inherent multicast nature of Spatial Aloha and not on Opportunistic Aloha as defined in Chapter 16.

In terms of performance evaluation, the chapter contains several open questions and a few negative results, like e.g. the fact that in several cases, either the mean end-to-end delay of a packet scales super-linearly with the distance between source and destination, or the asymptotic velocity of a typical packet is 0, even if this packet is considered as a priority packet and experiences no queuing in the nodes. Among the positive results, let us quote the optimal tuning of the MAC parameters and the proof of scaling laws. Another practical conclusion of this chapter is that for source-destination pairs at finite distance, opportunistic routing very significantly outperforms layer-aware routing schemes. This holds true even when the latter use optimal static routing algorithms as considered in § 20.2.

22.2 Stochastic Model

We adopt the MANET receiver model introduced in § 17.5, which is briefly recalled below.

22.2.1 MANET Model

In this model the nodes can be represented by an i.m. p.p.. with cross fading (cf. Section 2.3.3.2 in Volume I) and node dependent noise. More precisely we consider the space-time scenario of Section 17.5.1 (see also Section 17.5.6), described by $\widetilde{\Phi} = \{(X_i, \mathbf{e}_i(n), \mathbf{F}_i(n), \mathbf{W}_i(n))\}$, where:

(1^{rout}) $\Phi = \{X_i\}$ denotes the locations of the MANET nodes. Two options are considered in what follows:

- *Poisson MANET*, where Φ is a Poisson p.p. with intensity λ. This is our default option denoted by $\frac{\text{GI}}{W+\text{M}/\text{GI}}$.
- *Poisson MANET Model with an Additional Periodic Infrastructure:* we also consider networks with an additional periodic infrastructure, denoted by $\frac{\text{GI}}{W+(\text{M}+G_s)/\text{GI}}$ in which $\Phi = \Phi_M + \Phi_{G_s}$; here Φ_M is some homogeneous Poisson p.p. with intensity λ_M and Φ_{G_s} is a stationary p.p. of periodic nodes. The points of Φ_{G_s} are assumed to be located on a square grid G_s with edge length s. See Example 4.2.5 in Volume I on how to construct such a stationary periodic structure. We assume that Φ_M and Φ_{G_s} are independent. The intensity of Φ_{G_s} is $1/s^2$ and that of Φ is $\lambda = \lambda_M + 1/s^2$. The MAC and the multi-hop routing mechanisms take place on *all* the nodes of Φ.

(2^{rout}) $\mathbf{e}_i(n) = \{e_i(n) : n\}_i$ are the MAC indicators of the node i at time n; $e_i(n)$ are i.i.d. in i and n with with $\mathbf{P}\{\, e(n) = 1 \,\} = 1 - \mathbf{P}\{\, e(n) = 0 \,\} = p$.

(4^{rout}) $\mathbf{F}_i = \{F_i^j(n) : j, n\}_i$ are the virtual powers (comprising fading effects) emitted by node i to nodes j at time n. We consider the following scenarios for the time dependence between the fading variables:

- *No fading* case: $F_i^j(n) \equiv \mu^{-1}$ for all i, j, n;
- *Slow fading* case: $F_i^j(n) = F_i^j(0)$ for all i, j, n and F_i^j are i.i.d. as F with mean μ^{-1}. This means that the fading is sampled independently for each transmitter–receiver pair and stay constant for all time slots.

– *Fast fading* case: $F_i^j(n)$ are i.i.d. for all i, j, n, where F has mean μ^{-1}.

Cf. Remark 17.5.1 on the fast/slow fading terminology.

(5^{rout}) $\mathbf{W}_i = \{W_i(n) : n\}_i$ is a sequence of i.i.d. (in i and n) non-negative random variables representing the thermal noise at node i and at time n. This scenario, already considered in Section 17.5.6 was called there *receiver dependent, fast noise case*.

For all points $X, Y \in \mathbb{R}^2$, let $\Phi^{X,Y} = \Phi \cup \{X, Y\}$. Let $\mathbf{e}_X$ and $\mathbf{e}_Y$ be two independent MAC indicator sequences distributed like $\mathbf{e}$, that one attributes to nodes X and Y respectively, with similar definitions for $\mathbf{F}_X$ and $\mathbf{F}_Y$. By arguments similar to those of § 18.4.1, in the Poisson MANET case, the marked p.p. $\widetilde{\Phi}^{X,Y}$ is also the Palm version of $\widetilde{\Phi}$ w.r.t. the two points $\{X, Y\}$. We denote the corresponding Palm probability and expectation by $\mathbf{P}^{X,Y}, \mathbf{E}^{X,Y}$ respectively (i.e., $\widetilde{\Phi}$ under $\mathbf{P}^{X,Y}$ has the same distribution as $\Phi^{X,Y}$ under $\mathbf{P}$.)

22.2.2 SINR coverage

We assume that all the nodes are perfectly synchronized and at (discrete) time n the p.p. of transmitters is denoted by $\Phi^1(n) = \sum_i \delta_{X_i} \mathbb{1}(e_i(n) = 1)$. The interference at the node X_j with respect to the signal emitted by the node X_i at time n (i.e., the power of the sum of all signals received at X_j at time n except this emitted by X_i) denoted by $I_{ij}^1(n)$, can be represented as the shot-noise variable

$$I_{ij}^1(n) = I_{\Phi^1(n)\setminus\{X_i\}} = \sum_{X_k \in \Phi^1(n),\, k \neq i,j} F_k^j(n)/l(|X_j - X_k|).$$

Denote by $\delta(X_i, X_j, n)$ the indicator that the node X_i covers the node X_j at time n with the SINR at least T, provided X_i is emitter $X_i \in \Phi^1(n)$ and X_j is potential receiver $X_j \in \Phi^0(n) = \Phi \setminus \Phi^1(n)$ at time n. Formally $\delta(X_i, X_j, n)$ is the indicator that the condition (17.10) holds with F, I considered at time n and $W = W_j(n)$.

22.3 The Time–Space Signal-to-Interference Ratio Graph and its Paths

In this section we will introduce an SINR graph with *space-time* vertexes. In this framework, as in the SINR graph of Chapter 8 in Volume I, the random point process on the plane describes the locations of the users of an ad-hoc network, however we consider also the discrete time dimension, which corresponds to successive time slots in which these nodes exchange information (here packets). As we will see the study of this new model is motivated by multihop routing protocols. In this extended setting, a directed edge represents the feasibility of the wireless transmission between two given network nodes at a given time.

22.3.1 Definition

Consider a general stationary MANET model $\widetilde{\Phi}$ as above.

Define the set of *SINR-neighbors* of $X_i \in \Phi$ at time n as the set of receivers which successfully capture the packet transmitted by X_i at time n if X_i transmits at that time, and as $\{X_i\}$ otherwise:

$$V(X_i, n) = \begin{cases} \{X_i\} \cup \{X_j : X_j \in \Phi^0(n) \text{ s.t. } \delta(X_i, X_j, n) = 1\} & \text{if } X_i \in \Phi^1(n) \\ \{X_i\} & \text{otherwise.} \end{cases} \tag{22.1}$$

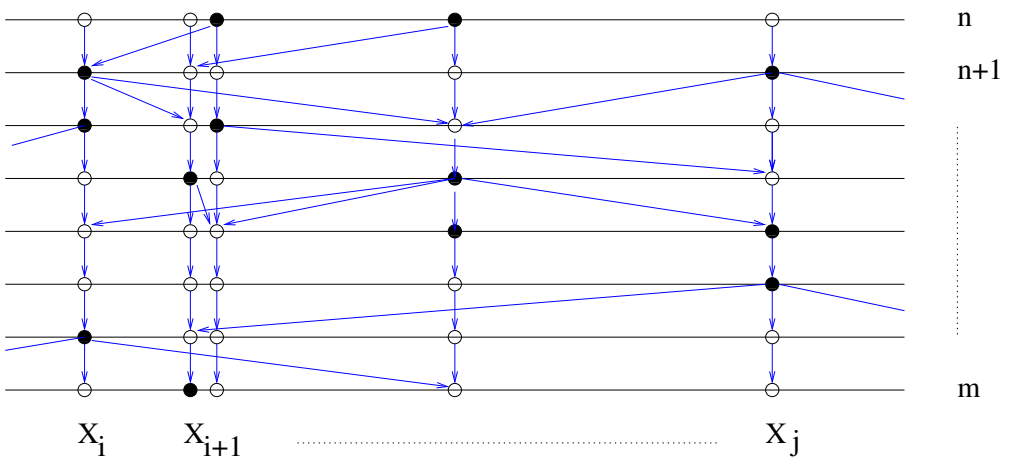

Fig. 22.1 The directed graph $\mathbb{G}_{\text{SINR}}$ on $\Phi \times \mathbb{Z}$, where Φ is a p.p. on the real line. The transmitters are depicted by black dots and the potential receivers by white ones.

The time–space SINR graph $\mathbb{G}_{\text{SINR}}$ is a directed graph on $\Phi \times \mathbb{Z}$ defined as follows: the nodes of $\mathbb{G}_{\text{SINR}}$ are all the pairs of the form (X_i, n) with $X_i \in \Phi$ and $n \in \mathbb{Z}$; all edges are of the form $((X_i, n), (X_j, n+1))$; there is an edge from (X_i, n) to $(X_j, n+1)$ if $X_j \in V(X_i, n)$ (see Figure 22.1 which gives an illustration of this graph in the case of a 1D MANET).

Let us stress an important convention in our terminology. By network node, or point, we understand a point of Φ. A (graph) vertex is an element of $\Phi \times \mathbb{Z}$; i.e. it represents some network node at some time. The existence of a graph edge is to be interpreted as the possibility of a successful communication between two network nodes (those involved in the edge) at time n. This can be rephrased as follows. Suppose that at time n the network node X_i has a packet (containing some information). Then the set of graph neighbors of the vertex (X_i, n) describes all the nodes that can decode this packet at time $n+1$. Thus any path on the graph $\mathbb{G}_{\text{SINR}}$ represents some possible route of the packet in space and time.

22.3.2 Time–Space Paths

Note first that $\mathbb{G}_{\text{SINR}}$ has no isolated nodes in the usual sense. Indeed, we have always (X_i, n) connected to $(X_i, n+1)$. We will consider directed paths on $\mathbb{G}_{\text{SINR}}$ and call them paths for short. Note that these paths are self-avoiding due to the fact that there are no loops in the time dimension.

In view of what was said, a path of $\mathbb{G}_{\text{SINR}}$ originating from node (S, k) and with q (time) steps is a collection of nodes

$$\{(Z_i, i)\}_{i=k,\dots,k+q}$$

such that $Z_i \in \Phi$ for all i, $Z_k = S$ and $Z_{i+1} \in V(Z_i, i)$ (or equivalently, there is an edge from (Z_i, i) to $(Z_{i+1}, i+1)$ in $\mathbb{G}_{\text{SINR}}$) for all $i = k, \dots, q-1$.

The following general terminology is used in the context of such a path:

- its *Euclidean length* is $\sum_{i=0}^{q-1} |Z_{i+1} - Z_i|$;
- its *time length* is its total number of time steps q;
- its *number of hops* H is the number of *different* points of Φ visited by the path;
- if $Z_{i-1} \neq X$ and $Z_i = X$, its local delays at (X, i), denoted by $\mathbf{L}(X, i)$ is the smallest integer $j > 0$ such that $Z_{i+j} \neq X$ (see § 17.5).

Denote by $\mathcal{H}_i^{out,k}(n)$ the number of paths of length k (i.e. with k edges) *originating* from (X_i, n). Similarly, denote by $\mathcal{H}_i^{in,k}(n)$ the number of such path *terminating* at (X_i, n). In particular $\mathcal{H}_i^{out}(n) = \mathcal{H}_i^{out,1}(n)$ and $\mathcal{H}_i^{in}(n) = \mathcal{H}_i^{in,1}(n)$ are respectively, the out- and in-degree of the node (X_i, n).

The following two results regarding the number of paths are obtained under a general p.p. and fading assumptions.

Lemma 22.3.1. For a general p.p. Φ and a general fading model, the in-degree $\mathcal{H}_i^{in}$ of any node of $\mathbb{G}_{\text{SINR}}$ is bounded from above by the constant $\xi = 1/T + 2$.

Proof. It follows immediately from the proof of Lemma 17.3.4. □

Note also that under some additional assumptions one can take $\xi = 1/T + 1$ (cf Lemma 17.3.4.)

Let

$$h^{out,k} = \mathbf{E}^0[\mathcal{H}_0^{out,k}(n)] = \mathbf{E}^0[\mathcal{H}_0^{out,k}(0)]$$

and

$$h^{in,k} = \mathbf{E}^0[\mathcal{H}_0^{in,k}(n)] = \mathbf{E}^0[\mathcal{H}_0^{in,k}(0)]$$

be the expected numbers of paths of length k originating or terminating at the typical node, respectively. In particular $h^{out} = h^{out,1}$ and $h^{in} = h^{in,1}$ are the mean out- and in-degree of the typical node, respectively.

Lemma 22.3.2. For a general p.p. Φ and a general fading model

$$h^{in,k} = h^{out,k}\,. \tag{22.2}$$

Proof. We use the mass transport principle to get that $\mathbf{E}^0[\mathcal{H}_0^{out,k}(0)] = \mathbf{E}^0[\mathcal{H}_0^{in,k}(0)]$, which implies the desired result. Indeed, Campbell's formula and stationarity give

$$\begin{aligned}
\lambda h^{out,k} &= \lambda \int_{[0,1)^2} \mathbf{E}^0[\mathcal{H}_0^{out,k}(0)]\mathrm{d}x \\
&= \mathbf{E}\Big[\sum_{X_i \in \Phi \cap [0,1)^2} \mathcal{H}_i^{out,k}(0)\Big] \\
&= \sum_{v \in \mathbb{Z}} \mathbf{E}\Big[\sum_{X_i \in [0,1)^2} \sum_{X_j \in [0,1)^2 + v} \#\text{ of paths from } (X_i, 0) \text{ to } (X_j, k)\Big] \\
&= \sum_{v \in \mathbb{Z}} \mathbf{E}\Big[\sum_{X_i \in [0,1)^2 - v} \sum_{X_j \in [0,1)^2} \#\text{ of paths from } (X_i, 0) \text{ to } (X_j, k)\Big] \\
&= \lambda \int_{[0,1)^2} \mathbf{E}^0[\mathcal{H}_0^{in,k}(k)]\mathrm{d}x = \lambda h^{in,k}\,,
\end{aligned}$$

where $\#$ denotes the cardinality. This completes the proof. □

Here are immediate consequences of the two above lemmas.

Corollary 22.3.3. Under the assumptions of Lemma 22.3.1:

- $\mathbb{G}_{\text{SINR}}$ is locally finite (both on in- and out-degrees of all nodes are $\mathbf{P}$-a.s. finite).
- $\mathcal{H}_i^{in,k}(n) \leq \xi^k$ $\mathbf{P}$-a.s for all i, n, k.
- $h^{in,k} = h^{out,k} \leq \xi^k$ for all k.

Here is a graph theoretic summary of further results that one can prove on $\mathbb{G}_{\text{SINR}}$ graph (see (Baccelli, Błaszczyszyn, and Mirsadeghi 2009) for the details). Some of these results will be revisited in the remaining part of this chapter.

- This graph is *a.s. connected* in the sense that for all S and D in Φ and all $k \in \mathbb{Z}$, there a.s. exists a path from (S, k) to the set $\{(D, k + l)\}_{l \in \mathbb{N}}$ (cf. Corollary 22.4.4).
- For the $\frac{\text{M}}{W+(\text{M}+G_{\text{S}})\,/\,\text{M}}$ fast fading case, if thermal noise is positive, then the first passage percolation *delay rate* is *finite* (Proposition 22.5.6) and has a *positive mean* (Proposition 22.5.5). By first passage percolation, we mean here the path from (S, k) to the set $\{(D, k + l)\}_{l \in \mathbb{N}}$ with the smallest number of time steps N. By delay rate, we mean the limit when it exists of the ratio $N/|S - D|$, when $|S - D|$ tends to infinity. In many first passage percolation models, the limit of this ratio is a constant and is then referred to as the *time constant*. As we shall see, this is not the case here and this explains our terminology.
- For the $\frac{\text{M}}{W+\text{M}\,/\,\text{M}}$ fast fading case, if thermal noise is positive, then the mean value of the first passage percolation delay rate is infinite (cf. Proposition 22.5.9 for the precise statement).

22.4 Routing and Time–Space Point Maps

We now use the time–space SINR graph $\mathbb{G}_{\text{SINR}}$ in the context of routing in ad-hoc networks. We have already seen in previous chapters that in many cases the route followed by a packet can be naturally described by means of the iterations of some point map. We now extend this concept to the time–space scenario of $\mathbb{G}_{\text{SINR}}$.

22.4.1 Time–Space Point Maps

A time–space path is often defined from a *time–space point map*, that is a collection of point maps $\{\mathcal{A}_n\}$, where $\mathcal{A}_n(X)$ is an algorithm which selects the next hop for a packet located at X at time n in the set $V(X, n)$. The path originating from node (S, k) is then defined by the recursion

$$Z_{i+1} = \mathcal{A}_i(Z_i), \quad i = k, \ldots, q - 1\,, \tag{22.3}$$

with initial condition $Z_k = S$. This gives the route followed by a priority packet[1] starting from node $S \in \Phi$ at time k.

The fact that this algorithm builds a path of $\mathbb{G}_{\text{SINR}}$ implies that two key phenomena are taken into account: collisions (lack of capture by any node) and contention for channel (only time slots where the relay tosses heads are used for transmission); in particular, if there is no channel access for X at time k, then $V(X, k) = \{X\}$.

[1] In the considered MANET, a node may have to relay packets of several flows, namely associated with several S-D pairs; packets located on a given node may hence have to queue for accessing the shared channel. By priority packet, we mean a packet which is assumed to be scheduled according to a preemptive priority rule on each node and which hence never experiences such queuing.

22.4.1.1 Radial Point Maps

The following definition is adopted by analogy with our definition of Chapter 21:

Definition 22.4.1. A time–space point map $\{\mathcal{A}_n\}$ is a *radial routing to* D if $\mathcal{A}_i(D) = D$, for all i, and if in addition, for all (S,k), $Z_i = D$, for all $i \geq k + \Delta$ and for some $\Delta = \Delta(S,k) \in \mathbb{N}$.

The following terminology is used in the context of such a radial routing:

- its progress at time i is $\mathcal{P}_i = |Z_i - D| - |Z_{i+1} - D|$, which may be 0 in case of collision or denial of channel access;
- its *end-to-end delay* $\Delta = \Delta(S,k)$ is the total number of time steps required for the priority packet to go from (S,k) to D;
- its number of hops $H = H(S,k)$ is the number of different nodes on the path;
- if X is a node of the path originating from (S,k) (which we assume to be self avoiding) the local delay $\mathbf{L}(X) = \mathbf{L}(X,S,k)$ at node X is the number of time steps spent by the path at node X.

The following relation holds between these quantities:

$$\Delta = \sum_{i=1}^{H-1} \mathbf{L}(X_i)\,,$$

when denoting by $S = X_1, \ldots, X_H = D$ the sequence of (different) nodes of the time–space path.

Notice that the path and the end-to-end delay from (S,k) to D and that from (S,k') to D differ in general as typical in time–space routing.

Definition 22.4.2. A radial time–space routing satisfies the *ball property* if the route from S to D is contained in the ball $B_D(|D-S|)$.

22.4.1.2 Directional Point Maps

We also consider the case where D is located at infinity in some direction d of the plane (cf. Section 21.2.3). A time–space point map which converges to D will then be called a d-directional routing. In line with our previous definitions, when D is located at infinity in direction d, for all functions $g : \mathbb{R}^2 \to \mathbb{R}$, the almost sure limit

$$\lim_{N\to\infty} \frac{1}{N} \sum_{n=0}^{N-1} g(Z_{n+k+1} - Z_{n+k}) \tag{22.4}$$

is called the (time–space) route average of g (provided the limit exists). There are other natural route averages taken hop by hop rather than w.r.t. time, like for instance the route average of the local delay

$$l = \lim_{M\to\infty} \frac{1}{M} \sum_{m=0}^{M-1} \mathbf{L}_m\,, \tag{22.5}$$

where $\mathbf{L}_m$ is the local delay at the m-th hop of the route. If the last almost sure limit exists, then one can interpret $v = l^{-1}$ as the *route average velocity* (measured in number of hops per time step):

$$v = \lim_{M\to\infty} \frac{M}{\sum_{m=0}^{M-1} \mathbf{L}_m}\,. \tag{22.6}$$

The remaining sections investigate the properties of a few basic classes of time–space routing algorithms.

22.4.2 Layer-aware Time–Space Point Maps

The simplest time–space routing algorithms are those where routing and MAC are fully separated. Namely, at any time step, the next relay node for a packet located at node X is $\mathcal{A}(X)$, where $\mathcal{A}$ is some static point map on $\Phi = \{X_i\}$. More precisely the time–space route is then defined by the following time–space point map:

$$\mathcal{B}_n(X) = \begin{cases} \mathcal{A}(X) \text{ if } \mathcal{A}(X) \in V(X,n), \\ X \text{ otherwise.} \end{cases} \tag{22.7}$$

Note that given Φ, $\mathcal{B}_n(X)$ is a random variable with two possible outcomes: X and $\mathcal{A}(X)$; as long as $\mathcal{A}(X)$ is not an SINR-neighbor of X, the packet stays at X. The first time it is an SINR-neighbor of X, the packet jumps there.

A key property, which contrasts with our findings on the existence of dead ends in geographic routing (see § 21.2.2), is that, for all X and all $\mathcal{A}$ such that $\mathcal{A}(X)$ is at finite distance from X, all packets located at X make it to $\mathcal{A}(X)$ in *finite time* under natural assumptions:

Lemma 22.4.3. Assume that $0 < p < 1$. Then, under either of the following assumptions:

(a) the law of F has an infinite support on $\mathbb{R}^+$ (i.e. $\mathbf{P}\{F > s\} > 0$ for all s) and we have fast fading,
(b) $W \equiv 0$,

the local time $\mathbf{L}(X,n)$ of a packet starting at time n in node X is a.s. finite for all $n \in \mathbb{Z}$.

Remark: Note that the infinite support assumption holds for all fading models considered so far: Rayleigh, Rician, Nakagami, Lognormal, etc.

Proof. We show that for all $X \in \Phi$ and all $n \in \mathbb{Z}$, the probability that $\mathcal{A}(X) \notin V(X, n+l)$ for all $l \geq 1$ is 0.

We consider first case (a). Denote by $\mathcal{G}$ the σ-algebra generated by Φ (without its marks). Using the fast fading assumption, we get that conditionally on $\mathcal{G}$,

$$\mathbf{P}\left[\, \mathbf{L}(X,0) \geq l \mid \mathcal{G} \,\right] = \prod_{i=0}^{l-1} \mathbf{P}\left[\, \mathcal{A}(X) \notin V(X,i) \,|\, \mathcal{G} \,\right] = \Big(\mathbf{P}\left[\, \mathcal{A}(X) \notin V(X,0) \,|\, \mathcal{G} \,\right] \Big)^l ,$$

so that it is enough to prove that $\mathbf{P}\left[\, \mathcal{A}(X) \notin V(X,0) \,|\, \mathcal{G} \,\right] < 1$ to conclude the proof. But we have

$$\mathbf{P}\left[\, \mathcal{A}(X) \in V(X,0) \mid \mathcal{G} \,\right] = p(1-p)\mathbf{P}\left[\frac{F/l(|X - \mathcal{A}(X)|)}{W + I_{\Phi^1 \setminus \{X, \mathcal{A}(X)\}}} \geq T \mid \mathcal{G}, e_X = 1, e_{\mathcal{A}(X)} = 0 \right] ,$$

where F is the fading from X to $\mathcal{A}(X)$ at time 0, e_X (resp. $e_{\mathcal{A}(X)}$) is the MAC decision of X (resp. $\mathcal{A}(X)$) at time 0 and $I_{\Phi^1 \setminus \{X, \mathcal{A}(X)\}}$ is the interference at $\mathcal{A}(X)$ at time 0. Since F and $I_{\Phi^1 \setminus \{X, \mathcal{A}(X)\}}$ are independent,

$$\begin{aligned} &\mathbf{P}\left[\frac{F/l(|X - \mathcal{A}(X)|)}{W + I_{\Phi^1 \setminus \{X, \mathcal{A}(X)\}}} \geq T \mid \mathcal{G}, e_X = 1, e_{\mathcal{A}(X)} = 0 \right] \\ &\quad = \int_{\mathbb{R}_+} \int_{\mathbb{R}_+} \overline{H}\left(T(w+z) l(|X - \mathcal{A}(X)|) \right) f_{\mathcal{A}(X)}(\mathrm{d}z) g(\mathrm{d}w) > 0 , \end{aligned}$$

where $\overline{H}$ is the tail of the c.d.f. of F, $f_{\mathcal{A}(X)}$ is the conditional law of $I_{\Phi^1\setminus\{X,\mathcal{A}(X)\}}$ given $\mathcal{G}, e_X = 1, e_{\mathcal{A}(X)} = 0$ and g the law of W. The last (strict) inequality follows from the fact that $I_{\Phi^1\setminus\{X,\mathcal{A}(X)\}}$ is a.s. finite (because the path-loss exponent β is larger than 2) and from the assumption made on the support of F (that it is infinite). This concludes the proof in this case.

Consider now case (b). Let $\mathcal{H}$ denote the σ-algebra generated by Φ and the fading variables (under the slow fading case, these variables do not vary over time). Using the fact that the MAC decisions are i.i.d., we get that

$$\mathbf{P}\left[\,\mathbf{L}(X,0) > l \,|\, \mathcal{H},\right] = \mathbf{P}\left[\,\mathcal{A}(X) \notin V(X,0) \,|\, \mathcal{H}\right]^l ,$$

so that it is enough to prove that $\mathbf{P}\left[\,\mathcal{A}(X) \notin V(X,0) \,|\, \mathcal{H}\right] < 1$. But

$$\begin{aligned}
&\mathbf{P}\left[\,\mathcal{A}(X) \in V(X,0) \,|\, \mathcal{H}\right] \\
&= \mathbf{P}\left[\frac{F/l(|X-\mathcal{A}(X)|)}{I_{\Phi^1\setminus\{X,\mathcal{A}(X)\}}} \geq T,\, e_X = 1, e_{\mathcal{A}(X)} = 0 \mid \mathcal{H}\right] \\
&= p(1-p)\mathbf{P}\left[I_{\Phi^1\setminus\{X,\mathcal{A}(X)\}} \leq \frac{F/l(|X-\mathcal{A}(X)|)}{T} \mid \mathcal{H},\, e_X = 1, e_{\mathcal{A}(X)} = 0\right] > 0\,,
\end{aligned}$$

where the last inequality follows from the fact that the $\mathcal{H}$-conditional law of the Poisson SN process $I_{\Phi^1\setminus\{X,\mathcal{A}(X)\}}$ puts a positive mass on the interval $[0,z]$ for all positive z. □

The following corollary shows that these layer-aware mechanisms are time–space routings to D provided the underlying static point map is a routing to D (see the introduction of Part V for the definition):

Corollary 22.4.4. Consider a static point map $\mathcal{A}$ which is a routing to D (resp. a d-directional routing). Let $\{\mathcal{B}_n\}$ be the associated layer-aware time–space point map (22.7). Under the assumptions of Lemma 22.4.3, $\{\mathcal{B}_n\}$ is a time–space routing to D (resp. a d-directional time–space routing).

Proof. Conditionally on Φ (or $\mathcal{H}$), each local delay is a.s. finite at each node of the route. Hence for all S, all $n \geq 1$ and all $k \in \mathbb{Z}$, the number of time steps required by this time–space path to reach node $\mathcal{A}^n(S)$ (the n-th node of the static route) is a.s. finite. In particular the end-to-end delay to reach D is a.s. finite. The proof of the d-directional case is similar. □

When taking 'smallest hop to destination' as static point map (see § 21.2.1) in the last corollary, we get that there exists a time–space point map which satisfies the ball property and which is a routing to D.

Here are a few comments on the differences between the static greedy geographic routing schemes considered in Chapter 21 and the layer-aware time–space greedy routings considered here. We found out in Chapter 21 that next-in-strip routing on the random geometric graph (which takes the range limitations of wireless communication into account) does not work properly because of the dead end problem. Corollary 22.4.4 shows that the time–space version considered here works better, in that a packet makes it to any finite destination (or any finite distance node of the route) in finite time under assumptions (a) or (b) and hence does not suffer of the dead end problem.

Remark 22.4.5. From the proof of the Lemma 22.4.3, we deduce that

- In case (a), conditionally on $\mathcal{G}$, for all X and n, $L(X,n)$ is a geometric random variable with a parameter that depends on X but not on n.

- In case (b), the same holds true conditionally on $\mathcal{H}$.

We conclude this section with the analysis of two special cases: directional strip routing and directional smallest hop routing. We show that in these two cases, under rather natural conditions, the route average of the velocity of a priority packet is 0 (in a sense to be described precisely below). One can rephrase this by saying that these schemes do not work properly over large scale routes in most practical cases.

22.4.2.1 Directional Strip Routing

Take directional strip routing (see § 21.3) as static point map and consider the associated time–space routing algorithm as defined by (22.7). We deduce from what precedes that under either (a) or (b), a packet initially located at S reaches the n-th hop of the (static) route in finite time for all n.

Consider now the route average local delay of a prioritypacket in this time–space routing framework. Rather than defining it through (22.5), we define this quantity as

$$\lim_{n\to\infty} \frac{1}{n} \sum_{i=0}^{n} \mathbf{E}[\mathbf{L}(X_i) \mid \mathcal{G}] \,,$$

where $\mathcal{G}$ denotes the σ-algebra of the Poisson p.p. Φ (without its marks). This allows us to use Lemma 21.3.1 by posing $g(\Phi_i) = \mathbf{E}[\mathbf{L}(X_i) \mid \mathcal{G}]$ (see the definition of Φ_i in this lemma) which implies that $\mathbf{P}$ a.s.,

$$\lim_{n\to\infty} \frac{1}{n} \sum_{i=0}^{n} \mathbf{E}[\mathbf{L}(X_i) \mid \mathcal{G}] = \mathbf{E}^0[\mathbf{L}(0)] \,.$$

The immediate conclusion is that when $\mathbf{E}^0[\mathbf{L}(0)] = \infty$, then the route average local delay is infinite, so that this routing mechanism does not work properly on a more global scale.

Example 22.4.6. Consider the example of fast Rayleigh fading (which falls in the considered framework under assumption (a) of Lemma 22.4.3). In most practical cases, we have $\mathbf{E}^0[\mathbf{L}(0)] = \infty$.

- In the noise limited case, if the thermal noise is bounded from below by a constant W, then, by the same arguments as in Proposition 17.5.9 (cf. also the discussion in Section 17.5.9), we get that
$$\mathbf{E}^0[\mathbf{L}(0)] \geq \frac{\lambda a}{p(1-p)} \int_{r\geq 0} \exp(-\lambda a r) \exp(\mu T W l(r)) \mathrm{d}r = \infty,$$
for all OPL attenuation models considered in this monograph.
- In the interference limited case, by the same arguments as in Section 17.5.4.2, when using the fact that the interference at the receiver is larger than that created by Φ^1 in the half plane on the right of the receiver, we get that in the OPL 3 case,
$$\mathbf{E}^0[\mathbf{L}(0)] \geq \frac{\lambda a}{p(1-p)} \int_{r\geq 0} \exp(-\lambda a r) \exp\left(\lambda \pi p (1-p)^{\frac{2}{\beta}-1} K(\beta) T^{\frac{2}{\beta}} r^2\right) \mathrm{d}r = \infty,$$
for all values of p and T.

22.4.2.2 Smallest Hop Directional Routing

Take now for static point map 'smallest hop' on the complete graph as defined in § 21.2. More precisely, consider the directional point map associated with some direction d. Under Assumption (a) of Lemma 22.4.3, conditionally on $\mathcal{G}$, the local delay at each node of the path is a geometric random variable with a non-degenerate parameter so that the routing mechanism works locally.

The conditions under which the route average local delay is finite are unknown as to the publication of this monograph. The fact that the spatial average of the local delay $\mathbf{E}^0[\mathbf{L}]$ in a cone of angle π is infinite (see Remark 17.5.14) does not immediately imply that l is infinite too. However, if $\mathbf{E}^0[\mathbf{L}] = \infty$ and the almost sure limit (22.5) holds for some finite l, then the last limit cannot hold in L_1.

22.5 Minimal End-to-End Delay Time–Space Paths

The aim of this section is to define optimal paths from S to D within this time–space setting. As already mentioned, these optimal paths, which can in principle be obtained by dynamic programming, are in fact impractical. In addition to requiring global knowledge, namely knowledge of what happens far away in space, they also require the knowledge of *future* fading variables and MAC indicators. This explains our focus on greedy routing schemes in the forthcoming sections. Nevertheless, the scaling law established below on minimal weight paths is useful for the analysis of these greedy schemes in that it provides the fundamental limitations of all possible time–space schemes.

We focus here on paths with the smallest number of time steps. This is tantamount to finding minimal weight paths on $\mathbb{G}_{\text{SINR}}$ when associating a weight $w = 1$ to each edge of this graph.

Consider the set $\mathcal{C}(k, i, j)$ of all self-avoiding paths of $\mathbb{G}_{\text{SINR}}$ which start at time k from node X_i, reach X_j at some time $l > k$ and satisfy the ball property. It follows from Corollary 22.4.4 (or from Lemma 22.6.1 below) that if either of the two conditions (a) and (b) of Lemma 22.4.3 holds, then for all i, j and k, this set is non-empty. Since in addition the number of hops in each path of this set is bounded from above by $\Phi(B_{X_j}(|X_i - X_j|))$ (thanks to the ball property and the self-avoidance assumption), we have the following existence result for optimal time–space routes:

Lemma 22.5.1. Under either of the two assumptions (a) or (b) of Lemma 22.4.3 above, for all i, j and k, there almost surely exists at least one path of $\mathcal{C}(k, i, j)$ with minimal number of time steps in $\mathbb{G}_{\text{SINR}}$.

Remark: These optimal paths can also be rephrased in terms of first passage percolation in $\mathbb{G}_{\text{SINR}}$: among all paths of $\mathbb{G}_{\text{SINR}}$ starting from node (X_i, k), the minimal weight path is the 'first' to reach node X_j.

We can use the same construction as in § 20.3: for $t \in \mathbb{R}^2$, let $X(t)$ be the point of Φ which is closest to t. For $s, d \in \mathbb{R}^2$, define $p^*(s, d, \widetilde{\Phi}, k)$ as a path of $\mathbb{G}_{\text{SINR}}$ from node $(X(s), k)$ to the set $\{(X(d), l), l > k\}$, with minimal number of time steps as defined above. Denote by $|\pi|$ the length of path π. For all triples of points s, v and d in $\mathbb{R}^2$, we have

$$|p^*(s, d, \widetilde{\Phi}, 0)| \leq |p^*(s, v, \widetilde{\Phi}, 0)| + |p^*(v, d, \widetilde{\Phi}, |p^*(s, v, \widetilde{\Phi}, 0)|)| \,. \tag{22.8}$$

Let

$$\overline{|p^*(s, d, \widetilde{\Phi})|} = \mathbf{E}\left(|p^*(s, d, \widetilde{\Phi}, 0)| \;\middle|\; \mathcal{G}\right) \tag{22.9}$$

be the conditional expectation of $|p^*(s, d, \widetilde{\Phi}, 0)|$ given the σ-algebra $\mathcal{G}$ generated by Φ (excluding the marks).

Using the strong Markov property (w.r.t. time), we get that, conditionally on Φ, the law of $|p^*(v,d,\widetilde{\Phi},|p^*(s,v,\widetilde{\Phi},0)|)|$ is the same as that of $|p^*(v,d,\widetilde{\Phi},0)|$. Assume now the three points to be collinear and such that $d \in [s,t]$. Then, the last relation and (22.8) give

$$\overline{|p^*(s,d,\widetilde{\Phi})|} \leq \overline{|p^*(s,v,\widetilde{\Phi})|} + \overline{|p^*(v,d,\widetilde{\Phi})|}\,. \tag{22.10}$$

We are now in a position to use the subadditive ergodic theorem (as in Chapter 20) to derive scaling laws. For this, we have to check the integrability conditions required by this theorem. We start with a positive result on the $\frac{\mathrm{M}}{W+(\mathrm{M}+G_s)\,/\,\mathrm{M}}$ model and then give a partially negative result on the $\frac{\mathrm{M}}{W+\mathrm{M}\,/\,\mathrm{M}}$ model.

22.5.1 Network with an Additional Periodic Infrastructure

In this section, we consider the $\frac{\mathrm{M}}{W+(\mathrm{M}+G_s)\,/\,\mathrm{M}}$ model introduced in § 22.2. We first present the main result. Proofs are given in Section 22.5.1.1 below.

Proposition 22.5.2. For the $\frac{\mathrm{M}}{\mathrm{W}+(\mathrm{M}+G_s)/\mathrm{M}}$ model with fast (Rayleigh) fading, for all unit vectors $\mathrm{d} \in \mathbb{R}^2$, the non-negative limit κ_{d}

$$\kappa_{\mathrm{d}} = \lim_{t\to\infty} \frac{\overline{|p^*(0,t\mathrm{d},\tilde{\Phi})|}}{t}\,,$$

exists and is $\mathbf{P}$-a.s. *finite*. The convergence also holds in L_1.

Proof. The result follows from the subadditivity (22.10) and Proposition 22.5.6 (stated and proved in Section 22.5.1.1 below) by Kingman's theorem; see Theorem 20.3.3. □

Remark 22.5.3. The limit κ_{d} is the *first passage percolation delay rate* namely minimal asymptotic delay per unit Euclidean distance on $\mathbb{G}_{\mathrm{SINR}}$. It depends on the direction $\mathrm{d} \in \mathbb{R}^2$. In general, for d fixed, κ_{d} is not a constant but a random variable. For example, for d parallel to the horizontal axis of the grid Φ_{Gs}, the limit κ_{d} depends on the distance from the line $\{t\mathrm{d} : t \in \mathbb{R}\}$ to the nearest parallel (horizontal) line of the grid Φ_{Gs}, i.e. on the shift U_G U_G which makes the grid stationary (see 4.2 in Volume I). For a more precise statement of this fact and its proof, see (Baccelli, Błaszczyszyn, and Mirsadeghi 2009).

Let us rephrase the above results in different terms.

Corollary 22.5.4. Consider the time–space path(s) starting at time 0 from the point of Φ which is the closest to the origin and reaching the point of Φ which is the closest to $t = x\cdot\mathrm{d} \in \mathbb{R}^2$ in the smallest possible number of time steps. Let $\Delta^*(t)$ denote the number of time slots of this (these) path(s). Under the foregoing assumptions (fast Rayleigh fading and an additional periodic infrastructure), on the optimal path(s), packets have a *positive* asymptotic velocity v_d in direction d in the sense that

$$\lim_{x\to\infty} \frac{x}{\Delta^*(x\cdot\mathrm{d})} = v_{\mathrm{d}}, \quad a.s. \tag{22.11}$$

with $v_{\mathrm{d}} = \kappa_{\mathrm{d}}^{-1}$ a *positive* (possibly infinite) random variable which only depends on d and on the shift U_G which makes the grid stationary.

Note that the same asymptotic velocity is obtained when shifting time (i.e. starting at time k rather than time 0).

The main remaining question is whether the κ_{d} is strictly positive, The following lemma gives a natural sufficient condition for $\mathbf{E}[\kappa_{\mathrm{d}}] > 0$.

Proposition 22.5.5. For the $\frac{\mathrm{M}}{W+(\mathrm{M}+G_s)/\mathrm{M}}$ model with OPL 3 and fast fading, if W is constant and strictly positive, then $\mathbf{E}[\kappa_{\mathrm{d}}]$ is strictly positive for all directions d.

The proof is given in Section 22.5.1.1.

Note that from the above result, we cannot conclude that the mean velocity $\mathbf{E}[v_{\mathrm{d}}]$, with $[v_{\mathrm{d}}$ defined in (22.11), is finite for all d.

Jensen's inequality gives the bound $\mathbf{E}[v_{\mathrm{d}}] \geq 1/\mathbf{E}[\kappa_{\mathrm{d}}]$.

22.5.1.1 Proofs*

The following technical result was used in the proof of Proposition 22.5.2.

Proposition 22.5.6. Consider the $\frac{\mathrm{M}}{W+(\mathrm{M}+G_s)\,/\,\mathrm{M}}$ MANET model introduced in Section 22.2. Assume fast Rayleigh fading, fast thermal noise and OPL 3. Then for all points u, v of $\mathbb{R}^2$,

$$\mathbf{E}\left[\sup_{u_1,v_1\in[u,v]} \overline{|p^*(u_1,v_1,\widetilde{\Phi})|}\right] < \infty\,,$$

where the supremum is taken over u_1, v_1 belonging to the interval $[u, v] \subset \mathbb{R}^2$.

In order to prove the last proposition, we first establish the following auxiliary result:

Lemma 22.5.7. Under the assumptions of Proposition 22.5.6, let $x, y \in \Phi \cap B_0(R)$ for some $R > 0$, where $\Phi = \Phi_M + \Phi_{G_s}$. Then the conditional expectation of the local delay $\mathbf{L}(x, y)$ for a direct transmission from x to y, given Φ is such that

$$\begin{aligned}
\mathbf{E}[\mathbf{L}(x,y)\,|\,\Phi] &= \frac{1}{p(1-p)\mathcal{L}_W(T\mu A^\beta|x-y|^\beta)}\exp\Big\{-\sum_{\Phi\ni X_i\neq x,y}\log\mathcal{L}_{eF'}\Big(\frac{T|x-y|^\beta}{|y-X_i|^\beta}\Big)\Big\} && (22.12)\\
&\leq \frac{1}{p(1-p)\mathcal{L}_W(T\mu(A2R)^\beta)}\\
&\quad\times e^{-49\log(1-p)+(2R)^\beta pTC(s,\beta)} && (a)\\
&\quad\times e^{-\Phi_M(B_0(2R))\log(1-p)} && (b)\\
&\quad\times\exp\Big\{-\sum_{X_i\in\Phi_M,|X_i|>2R}\log\Big(1-p+\frac{p(|X_i|-R)^\beta}{(|X_i|-R)^\beta+T(2R)^\beta}\Big)\Big\}\,, && (c)
\end{aligned}$$

where $C(s, \beta) < \infty$ is some constant (which depends on s and β but not on Φ), F' is an exponential random variable of mean 1 and $\mathcal{L}_{eF'}(\cdot)$ is the Laplace transform of eF'.

Proof. The equality in (22.12) follows from (17.33) and from the same type of arguments as in the proof of Proposition 17.5.6. The bound $|x-y| \le 2R$ used in the Laplace transform of W leads to the first factor of the upper bound. We now factorize the exponential function in (22.12) as the product of three exponential functions

$$\alpha := \exp\Big\{-\sum_{\Phi_{G_s} \ni X_i \neq x,y}\Big\}, \quad \beta := \exp\Big\{-\sum_{\Phi_M \ni X_i \neq x,y | X_i| \le 2R}\Big\}, \quad \gamma := \exp\Big\{-\sum_{\Phi_M \ni X_i, |X_i|>2R}\Big\}.$$

Next we prove that the last three exponentials are upper-bounded by (a), (b) and (c) in (22.12), respectively.

(a) We use $|x-y| \le 2R$ and Jensen's inequality to get

$$\log \mathcal{L}_{eF'}\Big(\frac{T|x-y|^\beta}{|y-X_i|^\beta}\Big) \ge \log \mathcal{L}_{eF'}\Big(\frac{T(2R)^\beta}{|y-X_i|^\beta}\Big) \ge \frac{-T(2R)^\beta \mathbf{E}[eF']}{|y-X_i|^\beta} = -pT(2R)^\beta |y-X_i|^{-\beta}.$$

We now prove that

$$\sum_{\Phi_{G_s} \ni X_i : |y-X_i|>3\sqrt{2}s} |y-X_i|^{-\beta} \le C(s,\beta),$$

for some constant $C(s,\beta)$. This follows from an upper-bounding of the value of $|y-X_i|^{-\beta}$ by the value of the integral $1/s^2 \int (|y-x| - \sqrt{2}s)^{-\beta}\, \mathrm{d}x$ over the square with corner points X_i, $X_i + (s,0)$, $X_i + (0,s)$ and $X_i + (s,s)$. In this way we obtain

$$\begin{aligned} \sum_{\Phi_{G_s} \ni X_i : |y-X_i|>3\sqrt{2}s} |y-X_i|^{-\beta} &\le \frac{1}{s^2} \int\limits_{|x-y|>2\sqrt{2}s}^{\infty} (|y-x| - \sqrt{2}s)^{-\beta}\, \mathrm{d}x \\ &= \frac{2\pi}{s^2} \int\limits_{\sqrt{2}s}^{\infty} \frac{t+\sqrt{2}s}{t^\beta}\, \mathrm{d}t =: C(s,\beta) < \infty\,. \end{aligned}$$

Combining this and what precedes, we get that

$$\exp\left\{-\sum_{X_i \in \Phi_{G_s}, |y-X_i|>2\sqrt{s}} \log \mathcal{L}_{eF'}\Big(\frac{T|x-y|^\beta}{|y-X_i|^\beta}\Big)\right\} \le \exp(T(2R)^\beta C(s,\beta)).$$

We also have

$$\log \mathcal{L}_{eF'}\Big(\frac{T(2R)^\beta}{|y-X_i|^\beta}\Big) \ge \log \mathcal{L}_{eF'}(\infty) = \log(1-p)\,,$$

for all $X_i \in \Phi_{G_s}$ and in particular for $|y-X_i| \le 3\sqrt{2}s$. Hence we obtain

$$\exp\{-\sum_{X_i \in \Phi_{G_s}} (\dots)\} \le e^{-49\log(1-p) + T(2R)^\beta C(s,\beta)}\,,$$

where 49 upper-bounds the number of points $X_i \in \Phi_{G_s}$ such that $|y-X_i| \le 3\sqrt{2}s$.

(b) Using the bound $|x-y| \le 2R$ and the inequality $\log \mathcal{L}_{eF'}(\xi) \ge \log \mathcal{L}_{eF'}(\infty) = \log(1-p)$, we obtain

$$\exp\{-\sum_{\Phi_M \ni X_i \neq x,y, |X_i| \le 2R} (\dots)\} \le e^{-\Phi_M(B_0(2R))\log(1-p)}\,.$$

(c) Using the bounds $|x-y| \le 2R$ and $|y-X_i| \ge |X_i| - R$ (the latter follows from the triangle inequality) and the expression $\mathcal{L}_{eF'}(\xi) = 1 - p + \frac{p}{1+\xi}$, we obtain

$$\exp\Big\{ - \sum_{\Phi_M \ni X_i, |X_i|>2R} (\dots) \Big\} \le \exp\Big\{ - \sum_{X_i \in \Phi_M, |X_i|>2R} \log\Big(1 - p + \frac{p(|X_i|-R)^\beta}{(|X_i|-R)^\beta + T(2R)^\beta}\Big)\Big\}.$$

This completes the proof.

□

Proof of Proposition 22.5.6. Without loss of generality, we assume that $(v+u)/2$ is the origin of the plane, O. Let $B = B_O(R)$ be the ball centered at O and of radius R such that no modification of the points in the complement of B modifies $X(z)$ for any $z \in [u,v]$ (recall that $X(z)$ is the point of Φ which is the closest from z). Since $\Phi = \Phi_M + \Phi_{G_s}$, with Φ_{G_S} the square lattice p.p. with intensity $1/s^2$, it suffices to take $R = |u-v|/2 + \sqrt{2}s$. Let $B' = B_0(2R)$. Given the location of the points of Φ, given two points $x, y \in \Phi \cap B$, $\overline{|p^*(x,y)|}$ is not larger than the mean delay $\mathbf{L}(x,y)$ of the direct transmission from x to y, given Φ. Note now that

$$\sup_{u_1,v_1 \in [u,v]} \overline{|p^*(u_1,v_1,\Phi)|} \le \sum_{x,y \in \Phi \cap B} \mathbf{E}[\mathbf{L}(x,y) \,|\, \Phi]$$

and using the result of Lemma 22.12 we obtain

$$\begin{aligned}\sup_{u_1,v_1 \in [u,v]} \overline{|p^*(u_1,v_1,\Phi)|} \;\le\; & \frac{e^{-49\log(1-p) + (2R)^\beta p T C(s,\beta)}}{p(1-p)\mathcal{L}_W(T\mu A(2R)^\beta)} \\ & \times \exp\Big\{ - \sum_{X_i \in \Phi_M, |X_i|>2R} \log\Big(1 - p + \frac{p(|X_i|-R)^\beta}{(|X_i|-R)^\beta + T(2R)^\beta}\Big)\Big\} \\ & \times \Big(\Phi_M(B) + \pi(R+\sqrt{2}s)^2/s^2\Big) e^{-\Phi_M(B')\log(1-p)},\end{aligned}$$

where $\pi(R+\sqrt{2}s)^2/s^2$ is an upper bound of the number of points of Φ_{G_s} in B. The first factor in the above upper bound is deterministic. The two other factors are random and independent due to the independence property of the Poisson p.p. The finiteness of the expectation of the last expression follows from the finiteness of the exponential moments (of any order) of the Poisson random variable $\Phi_M(B')$. For the expectation of the second (exponential) factor, we use the known form of the Laplace transform of the Poisson SN (see Proposition 1.2.2 in Volume I) to obtain the following expression

$$\mathbf{E}\Big[\exp\Big\{-\sum(\dots)\Big\}\Big] = \exp\Big\{2\pi p \lambda_M \int_R^\infty \frac{T(2R)^\beta}{v^\beta + (1-p)T(2R)^\beta}(v+R)\,\mathrm{d}v\Big\} < \infty$$

as in Proposition 17.5.6.

Proof of Proposition 22.5.5. For all $t \in \mathbb{R}^2$, the sequence $\{Z_i\}_{i \ge 0}$ of different points of the path from $(O,0)$ to $(t, k>0)$ with minimal end-to-end delay is such that

$$\sum_{i=1}^{\Delta^*(t)} |Z_{i-1} - Z_i| \ge |t| - \sqrt{2}s\,. \tag{22.13}$$

Since the set of SINR-neighbors of each node is finite at each time step, $\Delta^*(\mathrm{t}) \to \infty$ a.s. when $|t| \to \infty$.

Assume that $\mathbf{E}[\kappa_{\mathrm{d}}] = 0$. Then Proposition 22.5.4 shows that $\overline{\Delta^*(t)}/|t|$ tends to 0 as t tends to infinity in the d direction, which implies that for some subsequence $\{t_k\}$ tending to infinity in this direction, $\Delta^*(t_k)/|t_k|$ tends to 0 a.s. That is for all $\epsilon > 0$, there exists a random τ such that for all $|t_k| > \tau$, $\Delta^*(t_k) < \epsilon |t_k|$.

This and (22.13) imply that, almost surely, there exists an increasing sequence of integers n_k tending to ∞ with k and such that for all k, the event $\pi(n_k)$ holds, with:

Event $\pi(n)$: there exists a time–space path in $\mathbb{G}_{\mathrm{SINR}}$ which is self-avoiding, originates from $(O, 0)$, has n time steps and an Euclidean length larger than n/ϵ.

We conclude the proof by showing that the property $\pi(n)$ can only happen for a finite number of integers n when ϵ is small enough. This contradiction implies that $\kappa_{\mathrm{d}} > 0$.

Let $\mathcal{P}_W^n$ denote the set of paths σ of $\mathbb{G}_{\mathrm{SINR}}$ with n steps and originating from O at time 0, for the constant thermal noise W. Note that by monotonicity,

$$\mathcal{P}_W^n \subset \mathcal{P}_0^n. \tag{22.14}$$

Let $\mathbf{P}_{\mathcal{G}}$ denote the conditional expectation definition given the σ-algebra $\mathcal{G}$ generated by Φ (excluding the marks). By definition,

$$\mathbf{P}_{\mathcal{G}}(\pi(n)) = \mathbf{P}_{\mathcal{G}}(\bigcup_{\sigma \in \mathcal{P}_W^n} \{|\sigma| \geq n/\epsilon\}), \tag{22.15}$$

where $|\sigma|$ denotes the Euclidean length of the time–space path σ. So

$$\begin{aligned} \mathbf{P}_{\mathcal{G}}(\pi(n)) &\leq \sum_{\sigma} \mathbf{P}_{\mathcal{G}}(\sigma \in \mathcal{P}_W^n, |\sigma| \geq n/\epsilon) \\ &= \sum_{\sigma} \mathbf{P}_{\mathcal{G}}(\sigma \in \mathcal{P}_W^n, |\sigma| \geq n/\epsilon) \mid \sigma \in \mathcal{P}_0^n) \mathbf{P}_{\mathcal{G}}(\sigma \in \mathcal{P}_0^n), \end{aligned} \tag{22.16}$$

where the sum bears on all possible sequences σ of n-tuples $Z_1, \cdots, Z_n$ of points of Φ and where we used (22.14) to get the last relation. But

$$\begin{aligned} &\mathbf{P}_{\mathcal{G}}(\sigma \in \mathcal{P}_W^n, |\sigma| \geq n/\epsilon \mid \sigma \in \mathcal{P}_0^n) \\ \leq &\sup_{\substack{Z_1, \ldots, Z_n \in \Phi \\ \sum_{i=1}^n |Z_i - Z_{i-1}| \geq n/\epsilon}} \mathbf{E}_{\mathcal{G}} \left(\delta(O, Z_1, 0, W) \delta(Z_1, Z_2, 1, W) \cdots \delta(Z_{n-1}, Z_n, n-1, W) \mid \sigma \in \mathcal{P}_0^n \right), \end{aligned}$$

where $\delta(x, y, k, W)$ is the indicator of the feasibility of the link from x to y at step k (condition (17.10) at time k) for the thermal noise W. Using now the fast fading assumptions, we get

$$\begin{aligned} &\mathbf{E}_{\mathcal{G}}(\delta(O, Z_1, 0, W) \delta(Z_1, Z_2, 1, W) \cdots \delta(Z_{n-1}, Z_n, n-1, W) \mid \sigma \in \mathcal{P}_0^n) \\ &= \prod_{k=0}^{n-1} \mathbf{E}_{\mathcal{G}}(\delta(Z_{k-1}, Z_k, k-1, W) \mid \delta(Z_{k-1}, Z_k, k-1, 0) = 1). \end{aligned}$$

Using now the Rayleigh fading assumptions (and more precisely the memoryless property of the exponential random variable),

$$\begin{aligned} \mathbf{E}_{\mathcal{G}}(\delta(Z_{k-1}, Z_k, k-1, W) \mid \delta(Z_{k-1}, Z_k, k-1, 0) = 1) &= \exp\left(-\mu l(|Z_k - Z_{k-1}|) TW\right) \\ &= \exp\left(-\mu (A|Z_k - Z_{k-1}|)^{\beta} TW\right). \end{aligned}$$

Hence

$$\begin{aligned}
&\sup_{\substack{Z_1,\ldots,Z_n\in\Phi\\ \sum_{i=1}^n |Z_i-Z_{i-1}|\geq n/\epsilon}} \mathbf{E}_{\mathcal{G}}(\delta(0,Z_1,0)\delta(Z_1,Z_2,1)\cdots\delta(Z_{n-1},Z_n,n_1) \mid \sigma\in\mathcal{P}_0^n)\\
&\leq \sup_{\substack{Z_1,\ldots,Z_n\in\Phi\\ \sum_{i=1}^n |Z_i-Z_{i-1}|\geq n/\epsilon}} \prod_{k=0}^{n-1} \exp\left(-\mu(A|Z_k-Z_{k-1}|)^\beta TW\right)\\
&\leq \exp\left(-\mu A^\beta TWn\epsilon^{-\beta}\right),
\end{aligned}$$

where the last inequality follows from a convexity argument. Using this and (22.16), we get

$$\mathbf{P}^0(\pi(n)) \leq \exp\left(-\mu A^\beta TWn\epsilon^{-\beta}\right)\mathbf{E}^0(\mathcal{N}^n),$$

where $\mathcal{N}^n$ denotes the cardinality of $\mathcal{P}^n$. Using now Lemma 22.3.2, we get that

$$\mathbf{P}^0(\pi(n)) \leq \exp\left(n(\log(\xi)-K/\epsilon^\beta)\right),$$

where K is a positive constant. Hence for ϵ small enough, the series $\sum_n \mathbf{P}^0(\pi(n))$ converges and the Borel–Cantelli lemma implies that $\pi(n)$ holds for a finite number of integers n.

22.5.2 Poisson MANET Case

In this section we consider the $\frac{\text{GI}}{W+\text{M}/\text{GI}}$ model.

22.5.2.1 The Stationary Setting

In the $\frac{\text{GI}}{W+\text{M}/\text{GI}}$ model, or even in the $\frac{\text{M}}{W+\text{M}/\text{M}}$ model, the method used above (based on sub-additive ergodic theory) cannot be extended to assess the existence of a positive asymptotic velocity on the optimal path. The main problem is the lack of integrability of $\overline{|p^*(s,d,\widetilde{\Phi})|}$ in this Poisson MANET case:

Lemma 22.5.8. In $\frac{\text{M}}{W+\text{M}/\text{M}}$ model with fast fading and OPL 3, if W is positive and constant, for all s and d in $\mathbb{R}^2$, $\mathbf{E}[\overline{|p^*(s,d,\widetilde{\Phi})|}] = \infty$.

Proof. We have

$$|p^*(s,d,\widetilde{\Phi})| \geq \mathbf{L}^m(X(s)),$$

where $\mathbf{L}^m(X(s),\widetilde{\Phi})$ is the multicast local delay (as defined in § 17.5.6) from $X(s)$, the point of Φ which is the closest to s. In addition,

$$\mathbf{L}^m(X(s)) \geq \widehat{\mathbf{L}}^m(X(s),\widetilde{\Phi}),$$

where $\widehat{\mathbf{L}}^m(x(s),\widetilde{\Phi})$ is the multicast local delay in the noise limited case. Hence

$$\mathbf{E}[\overline{|p^*(s,d,\widetilde{\Phi})|}] = \mathbf{E}[|p^*(s,d,\widetilde{\Phi})|] \geq \mathbf{E}[\widehat{\mathbf{L}}^m(X(s),\widetilde{\Phi})].$$

But using the strong Markov property,

$$\mathbf{E}[\widehat{\mathbf{L}}^m(X(s),\widetilde{\Phi})] = \mathbf{E}^0[\widehat{\mathbf{L}}^m(0,\widetilde{\Phi}|_{\overline{B}})],$$

where $\mathbf{E}^0$ is the Palm probability of the Poisson p.p. $\widetilde{\Phi}$ and $\widetilde{\Phi}|_{\overline{B}}$) is the restriction of $\widetilde{\Phi}$ to the complement of the open ball $B = B_x(|x|)$, with $x \in \mathbb{R}^2$ independent of $\widetilde{\Phi}$ and having for density

$$\frac{\mathrm{d}\theta}{2\pi} 2\pi\lambda r \exp(-\lambda\pi r^2),$$

in polar coordinates. But since we consider here the noise limited case,

$$\mathbf{E}^0[\widehat{\mathbf{L}}^m(0, \widetilde{\Phi}|_{\overline{B}})] \geq \mathbf{E}^0[\widehat{\mathbf{L}}^m(0, \widetilde{\Phi})]$$

and since the last quantity is infinite when W is a positive constant (see § 17.5.6), this shows that $\mathbf{E}[|p^*(s, d, \widetilde{\Phi})|] = \infty$. □

22.5.2.2 The Palm Probability Setting

Here is another approach for assessing the progression of a priority packet on an optimal path. Let S and D be two points of $\mathbb{R}^2$. As reference probability space, we take $\mathbf{P}^2_{S,D}$, the Palm probability of order 2 of the i.m. Poisson p.p. $\widetilde{\Phi}$ at S, D. The difference between this setting and that of the last paragraph is that the latter considers optimal paths on Φ, from $X(s)$ to $X(d)$, namely from the random node which is the closest from s to the random node which is the closest to d, where s and d are arbitrary locations of the plane, whereas the former is the the optimal path on Φ when adding two nodes to Φ, one at S and one at D (see the interpretation of Palm probabilities of Poisson p.p.s in Chapter 9 in Volume I). Below, the optimal path from S to D is still denoted by $p^*(S, D, \widetilde{\Phi})$. This is consistent with the notation used so far as, under $\mathbf{P}^2_{S,D}$, $X(S) = S$ and $X(D) = D$.

Our main result on this Palm setting is that although the mean optimal delay is finite for a finite distance between source and destination, it scales *super linearly* with this distance in the following natural situation:

Proposition 22.5.9. In the $\frac{\mathrm{M}}{W+\mathrm{M}\,/\,\mathrm{M}}$ model with fast (Rayleigh) fading, for all S and D,

$$\mathbf{E}^2_{S,D}[|p^*(S, D, \widetilde{\Phi})|] < \infty\,. \tag{22.17}$$

However, if the thermal noise W is bounded from below by a positive constant and if OPL 3 is assumed, then

$$\lim_{|S-D|\to\infty} \frac{\mathbf{E}^2_{S,D}[|p^*(S, D, \widetilde{\Phi})|]}{|S - D|} = \infty\,. \tag{22.18}$$

Proof. The time $\mathbf{L}(S, D)$ it takes to go from S to D in one hop is equal to the local delay in the Poisson Bipolar model with the distance to the receiver $r = |D - S|$. The first statement of the lemma follows from Proposition 17.5.6 and from the inequality

$$\mathbf{E}^2_{S,D}[|p^*(S, D, \widetilde{\Phi})|] \leq \mathbf{E}^2_{S,D}[\mathbf{L}(S, D)] < \infty\,.$$

For the second statement, let $\mathbf{L}^m(S)$ denote the local delay at node S under the multicast mode (§ 17.5.6) and let $\widehat{\mathbf{L}}^m(S)$ denote this multicast local delay in the noise limited case. We have

$$\mathbf{E}^2_{S,D}[|p^*(S, D, \widetilde{\Phi})|] \geq \mathbf{E}^2_{S,D}[\mathbf{L}^m(S)] \geq \mathbf{E}^2_{S,D}[\widehat{\mathbf{L}}^m(S)]\,.$$

So it is enough to prove that

$$\lim_{|S-D|\to\infty} \frac{\mathbf{E}^2_{S,D}[\widehat{\mathbf{L}}^m(S)]}{|S-D|} = \infty$$

to conclude the proof of the second statement.

Using the methodology of § 17.5.6, we get that

$$E^2_{S,D}[\widehat{\mathbf{L}}^m] = \frac{1}{p}\sum_{q=1}^{\infty} \exp\left(-2\pi\lambda \int_{v>0} \left(1-(1-(1-p)\mathcal{L}_W(\mu l(v)T))^q\right) v\mathrm{d}v\right) \left(1-(1-p)\mathcal{L}_W(\mu l(r)T)\right)^q$$

with $r = |S-D|$ and $\mathbf{L}^m = \mathbf{L}^m(S)$. Let $w > 0$ be the constant lower bound on W. We have

$$E^2_{S,D}[\widehat{\mathbf{L}}^m] \quad \geq \quad \frac{1}{p}\sum_{q} \exp\left(-\pi\lambda \int_{u>0} \left(1-\left(1-(1-p)e^{-w\mu A^\beta u^{\beta/2}T}\right)^q\right) \mathrm{d}u\right) \left(1-(1-p)e^{-w\mu A^\beta r^\beta)T}\right)^q .$$

Let us show that for q large enough,

$$\exp\left(-\pi\lambda \int_{u>0} \left(1-\left(1-(1-p)e^{-w\mu A^\beta u^{\beta/2}T}\right)^q\right) \mathrm{d}u\right) > \frac{1}{q}.$$

Let

$$f(v) := (1-p)\exp(-w\mu T A^\beta v^{\beta/2}) .$$

and denote by v_q the unique solution of

$$f(v) = \frac{1}{q}.$$

We have

$$v_q = \frac{1}{A^2\left(\mu T w\right)^{2/\beta}} (\log(q(1-p)))^{2/\beta}.$$

It is clear that v_q tends to infinity as q tends to infinity. Therefore, for all $\alpha > 1$, there exists a Q such that for all $q \geq Q$ and for all $v \geq v_q$,

$$(1-f(v)) \geq \exp(-\alpha f(v)).$$

Hence, for all $q \geq Q$,

$$\begin{aligned}
\int_{v>0} \left(1-(1-f(v))^q\right) \mathrm{d}v \quad &\leq \quad v_q + \int_{v=v_q}^{\infty} \left(1-(1-f(v))^q\right) \mathrm{d}v \\
&\leq \quad v_q + \int_{v=v_q}^{\infty} \left(1-\exp(-\alpha q f(v))\right) \mathrm{d}v \\
&\leq \quad v_q + \int_{v=v_q}^{\infty} \alpha q f(v) \, \mathrm{d}v \\
&= \quad v_q + \int_{u=0}^{\infty} \alpha q f(u+v_q) \, \mathrm{d}u.
\end{aligned}$$

The third inequality follows from the fact that $1-\exp(-x) \leq x$. Using now the fact that $(u+v_q)^{\beta/2} \geq u + v_q^{\beta/2}$ (for q large enough) and denoting by K the constant $w\mu T A^\beta$, we get that

$$\begin{aligned}\int_{u=0}^{\infty} qf(u+v_q)\,\mathrm{d}u &= \int_{u=0}^{\infty} q(1-p)\exp(-K(u+v_q)^{\beta/2}))\,\mathrm{d}u \\ &\leq \int_{u=0}^{\infty} q(1-p)\exp(-Ku - Kv_q^{\beta/2})\,\mathrm{d}u = \frac{1}{K}\,,\end{aligned}$$

since $(1-p)\exp(-Kv_q^{\beta/2}) = 1/q$. Hence

$$\int_{v>0} \left(1-(1-f(v))^q\right)\,\mathrm{d}v \leq v_q + \frac{\alpha}{K}.$$

Also it is not difficult to see that, for all constants $0 < C < \infty$,

$$v_q < \log Cq\,, \tag{22.19}$$

for q large enough, so that

$$\begin{aligned}\exp\left(-\pi\lambda \int_{v>0}\left(1-\left(1-(1-p)e^{-w\mu A^\beta u^{\beta/2}T}\right)^q\right)\mathrm{d}u\right) &\geq C\exp(-\pi\lambda v_q) \\ &> \frac{1}{q}.\end{aligned}$$

Hence

$$\frac{E^{S,D}[\widehat{\mathbf{L}}^m]}{|S-D|} \geq \frac{1}{r}\sum_{q>0}\frac{\alpha^q}{q}\,,$$

where $\alpha = 1-(1-p)e^{-w\mu A^\beta T r^\beta}$. It is now easy to see that

$$\begin{aligned}\frac{1}{r}\sum_{q>0}\frac{\alpha^q}{q} &= \frac{\log(1-\alpha)}{r} \\ &= \frac{-\log\left((1-p)e^{-w\mu A^\beta T r^\beta}\right)}{r} \\ &= w\mu A^\beta T r^{\beta-1} + o(r) \quad r\to\infty\,.\end{aligned}$$

Thus $\lim_{r\to\infty} 1/r \sum_{q>0}\frac{\alpha^q}{q} = \infty$ which concludes the proof. □

22.6 Opportunistic Routing

As already mentioned, opportunistic routing is a short name for greedy routing on the time–space SINR graph. This belongs to the class of cross-layer routing schemes. Below, we define and analyze the most natural version which is of the best hop type. A few variants are considered in § 22.6.5.

The whole section focuses on the $\frac{\text{GI}}{W+\text{M}/\text{GI}}$ model.

22.6.1 Radial Opportunistic Routes

For $\widetilde{\Phi}$ as above, define the following family of time–space radial point maps, with destination D: for all n,

$$\mathcal{A}_n(X_i) = \mathcal{A}_n(X_i, \widetilde{\Phi}) = \arg\min\{|X_j - D| : X_j \in V(X_i, n)\}\,. \tag{22.20}$$

Note that given Φ, $\mathcal{A}_n(X_i)$ is a random variable, with possibly many different outcome nodes for different values of n (this contrasts with the layer-aware case of § 22.4.2 where the outcome node was either X_i or $\mathcal{A}(X_i)$). The above point maps are almost surely well defined because the probability of finding two or more points of the homogeneous Poisson p.p. which are equidistant to D is equal to 0.

Here are two sufficient conditions for this time–space point map to be a routing to D:

Lemma 22.6.1. Under either of the assumptions (a) and (b) of Lemma 22.4.3, the radial opportunistic point map originating from S is a routing to D with $\mathbf{P}^{S,D}$-probability one and it satisfies the ball property.

Proof. Without loss of generality, we assume that D is the origin of the plane. The fact that $X_i \in V(X_i, n)$ for all i and n implies that no node of norm larger than $|Y_n|$ will ever be selected as the next relay. Hence, for all n, $|Y_{n+1}| \le |Y_n|$, which proves the ball property.

In order to prove convergence, it is hence enough to show that the probability that $Y_{n+l} = Y_n$ for all $l \ge 1$ and for some $n \ge k$ is 0 when $Y_n \neq O$.

We consider first case (a). Denote by $\mathcal{G}$ the σ-algebra generated by Φ. Using the fast fading assumption, we get that conditionally on $\mathcal{G}$ and on the event $Y_n = X_i \neq O$ for a given $X_i \in \Phi \cup \{S\}$,

$$\begin{aligned}\mathbf{P}^{S,O}\Big\{\, Y_n = Y_{n+1} = \cdots = Y_{n+l} \;\mid\; \mathcal{G}, Y_n = X_i \neq O \,\Big\} &= \prod_{i=0}^{l-1} \mathbf{P}^{S,O}\{\, Y_{n+i} = Y_{n+i+1} \,|\, \mathcal{G}, Y_{n+i} = X_i \neq O \,\} \\ &= \Big(\mathbf{P}^{S,O}\{\, Y_n = Y_{n+1} \,|\, \mathcal{G}, Y_n = X_i \neq O \,\}\Big)^l\,,\end{aligned}$$

so that it is enough to prove that

$$\mathbf{P}^{S,O}\{\, Y_{n+1} = Y_n \,|\, \mathcal{G}, Y_n = X_i \neq O \,\} < 1$$

to conclude the proof. The rest of the proof is then as in Lemma 22.4.3.

Consider now case (b). Let $\mathcal{H}$ denote the σ-algebra generated by Φ and the fading variables Using the same argument as before, it is enough to prove that

$$\mathbf{P}^{S,O}\{\, Y_{n+1} = Y_n \,|\, \mathcal{H}, Y_n = X_i \neq O \,\} < 1\,.$$

The proof then follows from the fact that the $\mathcal{H}$-conditional law of the Poisson SN process $I_{\Phi_1^n \setminus \{X_i\}}(O)$ puts a positive mass on the interval $[0, z]$ for all positive z. □

Remark: Note that the result of Lemma 22.6.1 cannot be immediately concluded from the fact that at any time and current location of the packet, there is a positive probability of delivering it directly to the destination. In fact, opportunistic routing is not allowed to wait for such an event.

Remark: Another important remark is that if $W > 0$ and if there is either no fading or some slow fading, then there is a positive probability that the packet be trapped forever at some isolated node.

We conclude this section by simulations aiming at the comparison of the performance of radial opportunistic routing and layer-aware routing.

22.6.2 Simulation of Radial Opportunistic Routes

Simulation Setup The MANET nodes are sampled according to some Poisson p.p. with intensity $\lambda = 10^{-3}$ nodes /m^2 on the square domain $[0, 1000]$ m $\times [0, 1000]$ m. One S-D pair is added, with S and D in opposite parts of the domain, as shown in Figure 22.2, with a distance of about 1130 m from S to D (this represents approx. 9 hops for a transmission range of 140 m).

All nodes are assumed to always have packets to transmit and they always transmit whenever authorized by the MAC; these transmissions allow us to take the background traffic into account through the interference created at each time slot. The power used by all the transmitters is assumed to be equal to 1. We use the OPL 3 attenuation model with $A = 1$ and $\beta = 3$ and Rayleigh fading with mean 1. The default option for the thermal noise is $W = 0$ and that for the capture threshold is $T = 10$.

A basic simulation experiment allows one to get a sample of the end-to-end delay of one packet of the tagged S-D pair flow. For this, we track the time–space route selected for this packet, the transmission attempts and the selection of the next relay at each relay node. The tagged packet is treated as a higher priority packet at each node.

We repeat a large number of such basic experiments to evaluate means. Some means are for the same sample of the Poisson node p.p. These correspond to the conditional mean values given the Poisson p.p. Others are based on a resampling of the Poisson p.p. and are to be interpreted as mean values w.r.t. the Palm probability $\mathbf{P}^{S,D}$.

Layer-Aware Routing Scenario We consider the layer-aware time–space routing scheme associated with the following static routing: MWR (and more precisely minimal number of hops i.e. Dijkstra's algorithm) on the random geometric graph with transmission range r. Here we take r such that the graph of the finite window used for the simulation is connected with high probability (see § 3.2.1 in Volume I and below to learn how the tuning of r is done).

Opportunistic Routing The opportunistic routing algorithm is best described by the code for the motion of a tagged packet of the S-D pair flow located at some current node A.

Until A is the destination D do:

1. Until A is selected by the MAC to transmit, end-to-end delay++;
2. When A is selected by the MAC to transmit do:
   - 2.1. All the nodes which are selected by the MAC to transmit are transmitters, the remaining nodes are receivers;
   - 2.2. The set of transmitters together with the fading variables at that time slot determine the interference everywhere at this time slot;
   - 2.3. The set of receivers $\mathcal{S}$ which satisfy the SINR capture condition at this time slot receive the tagged packet successfully;
   - 2.4. Among the nodes of $\mathcal{S} \cup \{A\}$, the nearest to the destination, say B, is the next relay;
   - 2.5. The other nodes of $\mathcal{S}$ discard the tagged packet;
   - 2.6. end-to-end delay++;
   - 2.7. if $A \neq B$ then number-of-hops++;
3. $A := B$.

Paths Figure 22.2 gives three examples of radial paths obtained by simulation for different radio channel models. The path which is the closest to the segment joining the source to the destination node is obtained with the layer-aware routing algorithm. The latter is that associated with the MWR static point map on the random geometric graph. The second path moving farther away from this segment corresponds to opportunistic routing in the absence of fading. The third path, which allows one to search for relays very far away from the transmitter corresponds to opportunistic routing in the presence of fast Rayleigh fading.

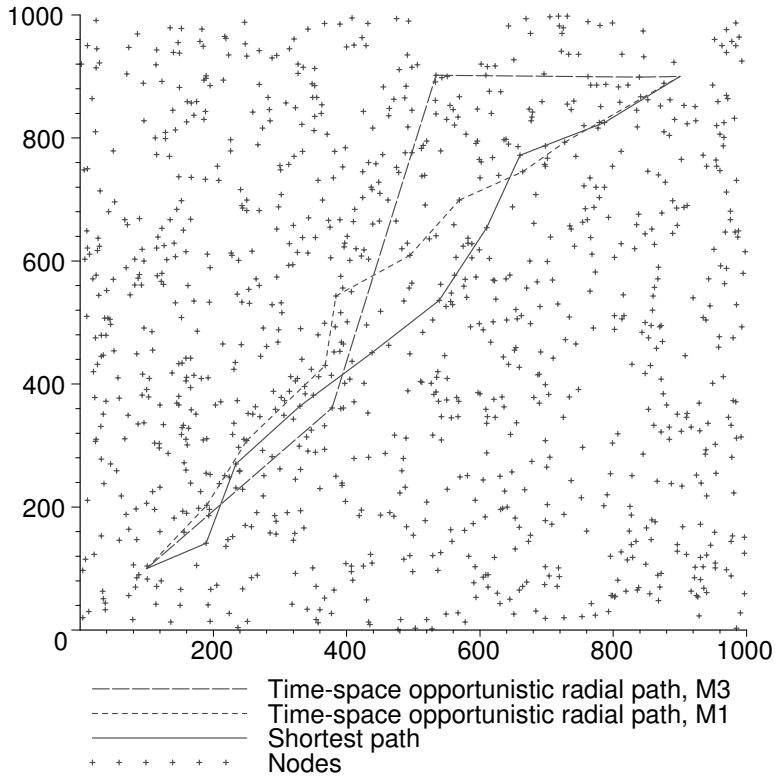

Fig. 22.2 Samples of packet paths with opportunistic radial routing (with and without fading) and of a MWR algorithm. M1 is the no fading case; M3 is fast Rayleigh fading.

Three other examples of paths obtained by simulation are given in Figure 22.3. The path which is the closest to the segment joining the source to the destination node is the layer aware case described above. The second path moving farther away from this segment corresponds to opportunistic routing when all nodes have perfect knowledge of their positions. The third path, which is a path on the right of the direct line between the source node and the destination node, corresponds to the case where only 10% of the network nodes having perfect knowledge of their position. The other nodes compute their positions using the simple localization algorithm which consists in estimating one's position as the barycenter of the one's neighbors having a perfect knowledge of their position.

Averaging and Confidence Intervals In order to calculate the means values of the performance characteristics of interest, we average over 80 different networks connecting a given S-D pair and for each network

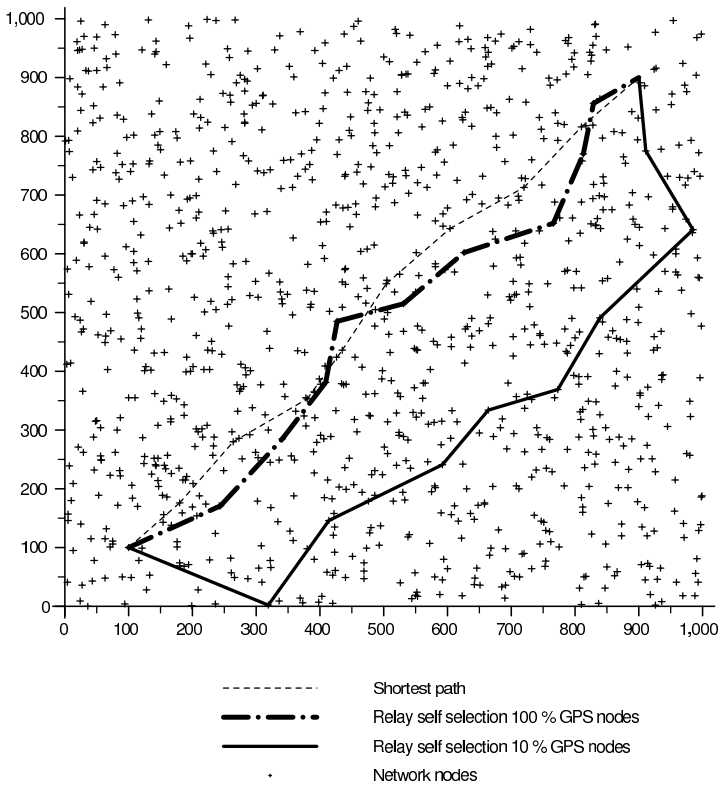

Fig. 22.3 Samples of packet paths with layer-aware routing and opportunistic radial routing under different assumptions for node positioning assumptions.

we average over 5 packets for the S-D pair. The results are presented with confidence intervals corresponding to a confidence level of 95%. Note that some of these confidence intervals are small and can only be seen when zooming in on the corresponding plots.

Tuning of the Layer-Aware Case The end-to-end delays for various values of r and of the transmission probability p are presented in Figure 22.4. We see that the best delay is obtained with $p = 0.003$ and with $r = 140$ m. This value, which is our default value for layer-aware MWR in what follows, is actually the smallest value of the transmission range which connects the network with high probability in this case.

Comparison of End-to-End Delays In Figure 22.5, we compare the MWR algorithm and opportunistic routing. In this figure we give the mean end-to-end delay as a function of p under different fading scenarios. We observe that opportunistic routing significantly outperforms the layer-aware MWR strategy in all cases: the average end-to-end delay of a packet is at least 2.5 times larger for the latter than for the former. We also see that the discrepancy between the two becomes much larger for a large p. Moreover, the performance of opportunistic routing is much less sensitive to a suboptimal choice of p.

Figure 22.6, which refines Figure 22.5 for opportunistic routing, shows that the presence of fading is beneficial in terms of mean end-to-end delays: in terms of end-to-end delays, opportunistic routing performs roughly four times better in the presence of fading than in the no fading case. Long simulations (not presented here) show that fast fading leads to slightly shorter delays than slow fading.

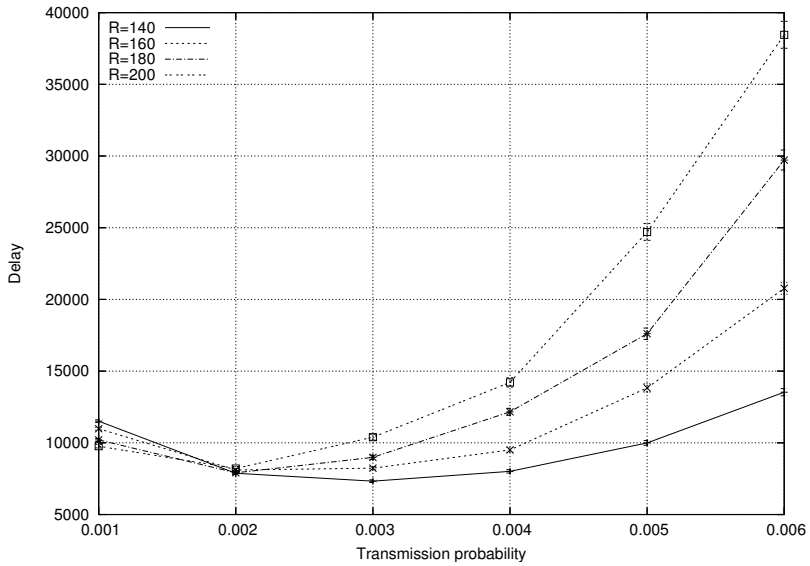

Fig. 22.4 Layer-Aware MWR: end-to-end delay versus p for various transmission ranges.

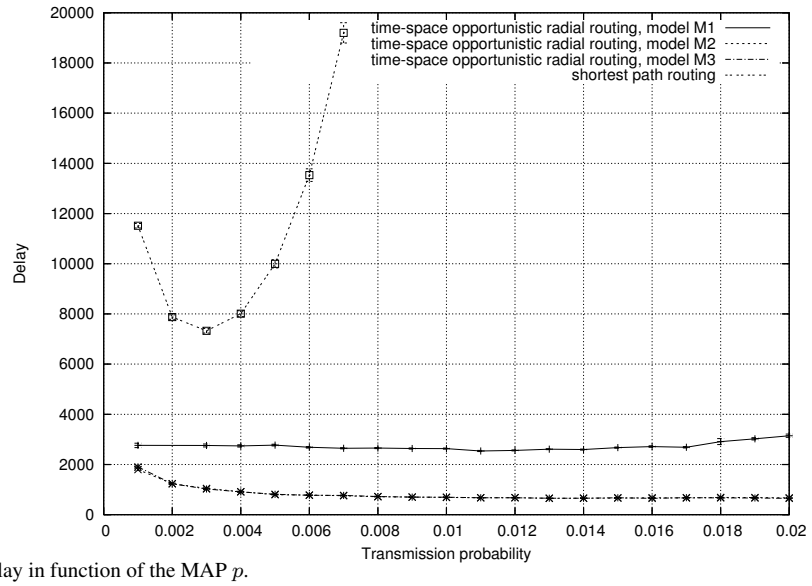

Fig. 22.5 End-to-end delay in function of the MAP p.

Comparison of Mean Number of Hops and Mean Local Delays Figure 22.7 gives the average number of hops to reach the destination for the two routing strategies with p varying from 0.001 to 0.02. In the case without fading, for small values of p, the opportunistic path is shorter (has a smaller mean number of hops) than the Dijkstra path, whereas it is longer for large values of p. In the presence of fading, opportunistic routing offers shorter paths than Dijkstra for $p \leq 0.014$ and slightly longer paths than Dijkstra for $p > 0.014$. We also observe that for opportunistic routing, the mean number of hops to reach the destination increases with p. This can be easily understood since when p increases, the time–space diversity decreases and thus the number of hops to reach the destination tends to increase.

Figure 22.8 studies the mean local delay for the same three scenarios as above. We see that in routing, for each p, the mean delay per hop is much smaller than that for the layer-aware algorithm. This explains why the average delay is smaller for opportunistic routing than for Dijkstra's algorithm even though the mean number of hops may be larger.

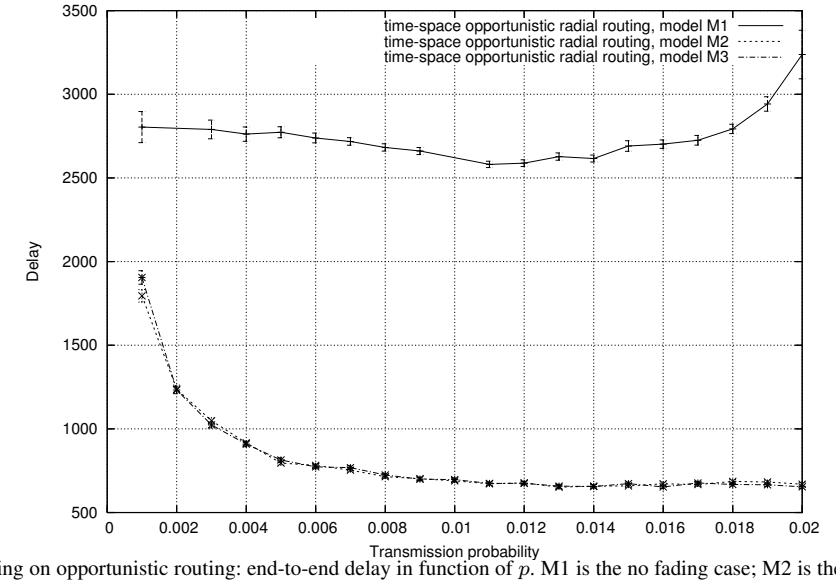

Fig. 22.6 Effect of fading on opportunistic routing: end-to-end delay in function of p. M1 is the no fading case; M2 is the slow fading and M3 the fast fading Rayleigh case.

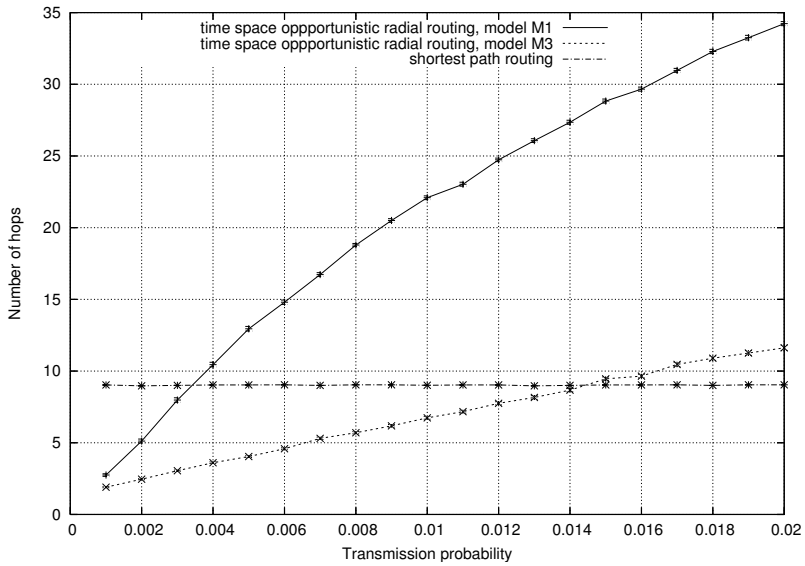

Fig. 22.7 Mean number of hops from S to D for opportunistic radial routing (with and without fading) and for the layer-aware MWR algorithm.

22.6.3 Directional Routes

Consider the Palm probability $\mathbf{P}^X$ (with associated expectation $\mathbf{E}^X$), corresponding to the addition of a node at X endowed with an independent MAC sequence $\mathbf{e}_X$ and fading sequence $\mathbf{F}_X$. For all vectors $\mathrm{d} \in \mathbb{R}^2$ with $|\mathrm{d}| = 1$, define the time–space point map

$$\mathcal{A}_{\mathrm{d},n}(X_i) = \arg\max\{\langle X_j, \mathrm{d}\rangle : X_j \in V(X_i, n)\}\,. \tag{22.21}$$

Since the probability of finding two or more points of a homogeneous Poisson p.p. on a line with a given direction is equal to 0, if all sets $V(X_i, n)$ are finite, then the point maps $\mathcal{A}_{\mathrm{d},n}$ are well defined. Let $\{Z_n = Z_n(X)\}_{n\geq 0}$ denote the associated d-directional route with initial condition $(X, 0)$. We say that the directional routing algorithm *converges* if this route is such that the progress in n hops:

$$D_n = \langle Z_n, \mathrm{d}\rangle$$

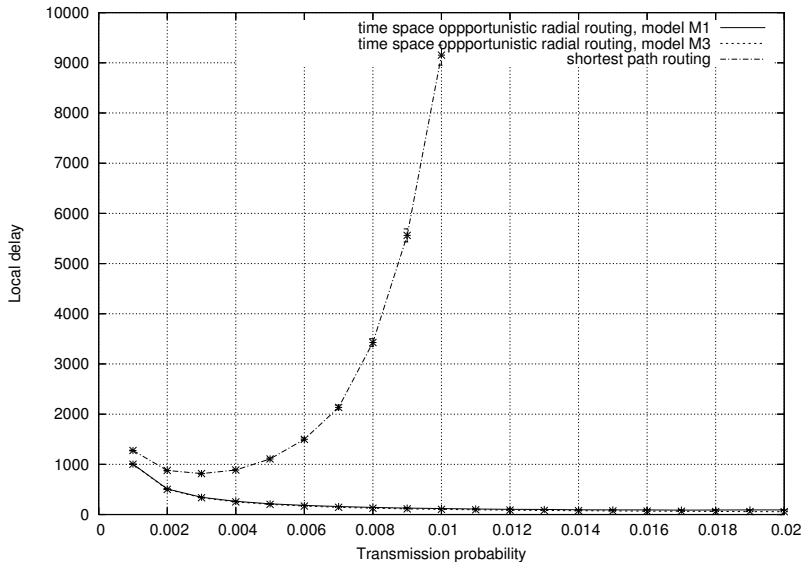

Fig. 22.8 Mean local delay for opportunistic radial routing (with and without fading) and for the layer-aware MWR algorithm.

tends to ∞ when $n \to \infty$. Note that $D_{n+1} \geq D_n$, for all $n \geq 0$.

We say that the directional routing algorithm *progresses* if its route is such that $|Z_n| \to \infty$ when $n \to \infty$.

Lemma 22.6.2. Assume that either $W \equiv 0$ or fading is fast. Then the opportunistic directional routing algorithm progresses with probability $\mathbf{P}^X$ one.

Proof. The proof is similar to that of the last lemma and is just sketched.

Poisson configurations of points Φ^X are locally finite and it is enough to prove that conditionally on $Y_n = X_i \in \Phi^X$ and some appropriate σ-algebra, the event $\{ Z_{n+1} = Z_n \}$ has a probability strictly less than 1. For this, one considers the event that node $x(= x(X_i)$, the closest to X_i with $\langle x(, \mathrm{d}\rangle > \langle X_i, \mathrm{d}\rangle$, receives the packet transmitted by X_i and one shows that this event has a positive conditional probability. □

22.6.4 Scaling Properties of Directional Routes

In the following result $\mathbf{P}^0_\lambda$ denotes the Palm probability of a Poisson p.p. of intensity λ.

Proposition 22.6.3. Assume OPL 3 and $W \equiv 0$. Then for any of the fading variation models, the law of the sequence $\{Z_n = Z_n(0)\}_n$ under $\mathbf{P}^0_\lambda$ is the same as that of $\{Z_n/\sqrt{\lambda}\}_n$ under $\mathbf{P}^0_1$.

Proof. Note that the distribution of the underlying Poisson p.p. $\Phi = \{X_i)\}_i$ under $\mathbf{P}^0_\lambda$ is the same as the distribution of $\Phi(\lambda) = \{(X_i/\sqrt{\lambda})\}_i$ under $\mathbf{P}^0_1$. Moreover, under our assumptions on l and W, the SINR (in fact the SIR) is invariant with respect to the scaling $\Phi(\lambda)$ of the p.p. Indeed,

$$l(|X_i/\sqrt{\lambda} - X_j/\sqrt{\lambda}|) = \lambda^{\beta/2} l(|X_i - X_j|)$$

and

$$I_{\Phi^n_1(\lambda)\setminus\{X_i/\sqrt{\lambda}\}}(X_j/\sqrt{\lambda}) = \lambda^{\beta/2} I_{\Phi^n_1\setminus\{X_i\}}(X_j).$$

Moreover, the dilation (our scaling) is a conformal mapping (preserves angles). Consequently, the directional point map $\mathcal{A}_{\mathrm{d},n}(X_i/\sqrt{\lambda})$ acting on $\Phi^0(\lambda)$ is equal to $1/\sqrt{\lambda}\mathcal{A}_{\mathrm{d},n}(X_i)$ acting on Φ^0_1. □

It is immediate to extend this to the iterates of order k of the point map. We deduce from this that the distribution of the Euclidean length of the segments of the directional route scales like $1/\sqrt{\lambda}$ in this case.

Remark 22.6.4. When λ grows large, the network is interference limited and the thermal noise is negligible and the last scaling law is asymptotically valid. We deduce from this that the number of time steps to progress of some distance r in the direction d asymptotically scales like $Cr\sqrt{\lambda}$ at least, where C is a positive constant. This is of course compatible with the Gupta and Kumar scaling law.

22.6.5 Related Directional Greedy Point Maps

In connection with (22.21), here are some related time–space directional point maps.

- **Largest progress and probability of success**:

$$\widetilde{\mathcal{A}}_{\mathrm{d},n}(X) = \underset{X_j \in \Phi^0(n)}{\arg\max} \{\langle X_j - X, \mathrm{d}\rangle p_X(X_j)\}, \tag{22.22}$$

  where $p_x(y) = \mathbf{E}^{x,y}[\delta(x,y,0) \mid e_x^0 = 1, e_y^0 = 0]$ is the probability of successful transmission from a transmitter at x to a receiver at $y \in \mathbb{R}^2$, which can be evaluated using the results of §16.2.2. This point map selects the receiver which maximizes the product of the progress in direction d and of the probability of success.
- **Largest progress and conditional probability of success**: this point map maximizes the product of the progress and of the conditional probability of success given the points of Φ:

$$\overline{\mathcal{A}}_{\mathrm{d},n}(X) = \underset{X_j \in \Phi^0(n)}{\arg\max} \{\langle X_j - X, \mathrm{d}\rangle \mathbf{E}^X[\delta(X,X_j,0) \mid \mathcal{G}, e_X = 1, e_{X_j} = 0]\}, \tag{22.23}$$

  where $\mathcal{G}$ is the σ-algebra generated by Φ.
- **Largest progress and throughput**:

$$\widehat{\mathcal{A}}_{\mathrm{d},n}(X) = \underset{X_j \in \Phi^0(n)}{\arg\max} \left\{ \langle X_j - X, \mathrm{d}\rangle \log\left(1 + \frac{F_0^j(n)/l(|X_j - X|)}{W + I_{\Phi_1^n/\{X\}}(X_j)}\right)\right\}, \tag{22.24}$$

  where the last term is the throughput of the wireless link from X to X_j.
- **Smallest hop in a cone**:

$$\mathcal{A}_{\mathrm{d},n}^{(\alpha)}(X) = \underset{X_j \in \Phi^0(n) \cap C(X,\alpha,\mathrm{d})}{\arg\min} \{|X_j - X|\}, \tag{22.25}$$

  where

$$C(x,\alpha,\mathrm{d}) = \{y \in \mathbb{R}^2, |\arg(y-x) - \arg(\mathrm{d})| \le \alpha/2\}$$

  denotes the cone of apex X, direction d and angle α. If $\alpha = \pi$, this boils down to smallest hop directional routing as defined in (21.13), Chapter 21.

The scaling properties of § 22.6.4 are easily extended to these point maps whenever $W \equiv 0$. ok?

22.6.6 Route Averages on Radial Time–Space Routes

We conclude with a negative result on the scaling of the delay on all radial time–space routes (and in particular opportunistic routes) on a Poisson MANET Φ. Let $\mathbf{P}^{S,D}$ denote the Palm probability of order 2 of Φ at (S,D). Let $\{\mathcal{A}_n\}_n$ by any radial time–space routing to D and let $\Delta(S,D)$ denote the end-to-end delay of the associated route from S to D under $\mathbf{P}^{S,D}$.

Corollary 22.6.5. In the $\frac{\mathrm{M}}{W+\mathrm{M}\,/\,\mathrm{M}}$ model with fast fading and with OPL 3, if the thermal noise W is bounded from below by a positive constant, then then for all radial time–space point map to D,

$$\lim_{|S-D|\to\infty} \frac{\mathbf{E}^{S,D}[\Delta(S,D,\widetilde{\Phi})]}{|S-D|} = \infty\,, \tag{22.26}$$

or equivalently the end-to-end delay of a priority packet scales super linearly with distance.

Proof. Optimality implies that

$$\Delta(S,D) \geq \Delta^*(S,D)\,,$$

with $\Delta^*(S,D)$ the optimal number of steps. The result then follows from the second statement of Proposition 22.5.9. □

22.7 Conclusion

Here are a few conclusions of practical nature on the packet model over Poisson MANETs.

- Greedy routing on the time–space SINR graph takes information theoretic limitations into account and leverages the physical characteristics of wireless communications. We showed that this greedy scheme works well at finite distance, in the sense that it drives a priority packet from source to destination in finite time under rather natural conditions.
- In contrast, because of the dead end problem, greedy routing on the static random geometric graph ignores the physical characteristics of wireless links and does not work at finite distance, even in the case where the associated Boolean model percolates and where the source and destination nodes belong to the infinite component. Models ignoring these key characteristics may hence lead to more difficulties than actually needed....
- The fact that greedy schemes work well at finite distance should be put in perspective as the mean end-to-end delays scale super linearly with distance in many practical cases. In a sense, the dead end problem hits back in the greedy time–space scenario: the fact that the mean local delays scale in a more than linear way with distance is again primarily due to the very large number of time steps that the packet needs to progress from certain relay nodes along the route.

This chapter opens many questions on the packet model. For instance, we are currently working on the following problems:

- In the case of a Poisson MANET with an added periodic infrastructure, does there exist greedy routing schemes on the time–space SINR graph with delays scaling linearly with distance or with a positive asymptotic velocity?
- In the Poisson MANET case, what is the rate at which delays grows to infinity with distance?
- How can one integrate packet contention and queueing disciplines (other than preemptive priority)?

The chapter was centered on the packet model but it should be clear that most of the above questions (optimal routes, greedy schemes) have natural counter parts in the Shannon capacity model.

Let us conclude by stressing that, more generally, SINR routes on a p.p., both optimal and suboptimal, form fascinating new objects of stochastic geometry which generate a large number of questions at the interface between communications and probability theory.

Bibliographical Notes on Part V

The ergodic properties of MWR in Chapter 20 are directly related to first-passage percolation, an issue extensively studied in the mathematical literature. For instance, first passage percolation on the complete Poisson p.p. graph, with weights $w(x, y) = |x - y|^\alpha$, for $\alpha > 1$ was studied in (Howard and Newman 1997). The existence of the Euclidean minimal spanning tree for infinite Poisson point patterns is considered in (Aldous and Steele 1992). See also (Howard and Newman 1997).

Geographic routing is discussed in (Karp 2000). To the best of our knowledge, the first paper on the performance evaluation of routing algorithms using spatial p.p. is (Takagi and Kleinrock 1984), where what we call directional routing was analyzed. Protocols where one minimizes the remaining distance to destination are considered in (Stojmenovic and Lin 2001a; Stojmenovic and Lin 2001b). The analysis of greedy geographic routing in Chapter 21 is based on (Baccelli and Bordenave 2007) and on (Bordenave 2006). The routing paradox was first observed in (Baccelli and Bordenave 2007) within the context of smallest hop routing.

To the best of the authors' knowledge, the studies presented in (Blum, He, Son, and Stankovic 2003) and (Baccelli, Blaszczyszyn, and Mühlethaler 2003) were the first papers where geographic routing was used in combination with a MAC protocol and where an opportunistic self election of relays was proposed for packets traveling from an origin to a destination node. (Biswas and Morris 2005) also uses this idea. Both protocols presented in (Blum, He, Son, and Stankovic 2003) and (Biswas and Morris 2005) use 802.11 like MAC access solution where the acknowledgement scheme is modified to allow the selection of the relay. Chapter 22 is primarily based on (Baccelli, Błaszczyszyn, and Mirsadeghi 2009) and (Baccelli, Blaszczyszyn, and Mühlethaler 2009b). In relation with the variants considered in § 22.6.5, let us quote (Weber, Jindal, Ganti, and Haenggi 2008), where a routing scheme based on the the longest outgoing edge in the SINR graph is studied.

The question of the speed of the delivery of information in large wireless ad-hoc networks was studied recently in (Ganti and Haenggi 2009; Jacquet, Mans, Mühlethaler, and Rodolakis 2009). In these papers the so called delay-tolerant networks are considered and modeled by a spatial SINR or SNR graph with no time dimension. In these models, the time constant (defined there as the asymptotic ratio of the graph distance to the Euclidean distance) is announced to be finite, even in the pure Poisson case. The reason for

the (apparently) different performance of these models lays in the fact that they do not take into account the time required for a successful transmission from a given node in the evaluation of the end-to-end delay. The heavy-tailness of this time (cf. Section 17.5.6) makes the time constant infinite in the space-time Poisson scenario. This is not so surprising observation in view of (Jelenković and Tan 2007a; Jelenković and Tan 2007b), although the physical phenomena at hand are quite different there; in our model the spatial irregularities in the ad-hoc network play a role similar to that of the file size variability in papers cited above.

Part VI

Appendix: Wireless Protocols and Architectures

The aim of this part is to give a compact survey on the statistical properties of channels which are commonly used in the analysis of wireless networks. The main focus will be on the principles and most of the fine points associated with technological aspects will not be discussed here.

In Chapter 23, we describe scattering and fading channels; this can be seen as the very first level of statistical modeling within this context. The presence of scatterers and the resulting multipath propagation together with the mobility of the source or the destination lead to the definition of a variety of fading channels including the Rayleigh and Rician models.

Chapter 24 will then outline the theory of detection for such channels with a main emphasis on point to point channels in scenarios involving a collection of simultaneous transmissions taking place in some domain. The case of direct-sequence spread-spectrum, where the interference created by other transmissions can be seen as noise for any given point to point channel, will be discussed, again at the level of principles. This discussion will in particular lead to a comprehensive explanation of the key role played by the SINR in such a scenario.

The aim of Chapter 25 is to provide a bestiary of classical network architectures and protocols which will be used as simple illustrating examples in Part I in Volume I and to which we will return in more details in the parts which follow. We will in particular survey the basic medium access control protocols used to organize the competition between such a collection of transmissions and on multi-hop routing within this context. Among the examples of network architectures which will be outlined, let us quote mobile ad hoc networks, wifi mesh networks and cellular access networks.

These chapters rely on a variety of scientific domains: physics, with questions pertaining to propagation, the Doppler effect, scattering etc.; information theory, with questions bearing on additive white Gaussian noise channels, detection theory etc. and finally networking, with routing algorithms or protocols for the organization of concurrent transmissions sharing a common medium.

All these ingredients are necessary for a full understanding of the main findings concerning SINR, which are the basis of most of the models of the monograph.

23

Radio Wave Propagation

In this chapter we will be interested in the propagation of an electromagnetic signal in space, where it is absorbed and reflected by many, possibly moving, obstacles. In such a context, solving and even establishing the detailed electromagnetic field equations is not feasible. However, for wireless communication engineering, it is often enough to use some macroscopic model that predicts the relationship between transmitted and received signals in a statistical way. In such a model, the impact of the unknown locations of various objects which absorb and reflect the signal is represented by some random transformation of the signal. Most macroscopic models just give the mean signal power attenuation for a given distance. They describe the average signal power attenuation for different environments (e.g. an urban environment, the countryside, etc.). Refined statistical models also give the fluctuations of the signal power attenuation around this mean profile. These models will be used in the analysis of the higher layers (detection, MAC, routing, etc).

23.1 Mean Power Attenuation

Mean power attenuation is concerned with the macroscopic description of the decrease of the signal power with the distance between the transmitter and receiver. We will first give two motivating examples and then introduce a few simple parametric models.

23.1.1 Motivating Examples

Digital radio communications are based on electromagnetic waves. Assume that the electric signal transmitted at time t by an antenna located at the origin of the three dimensional Euclidean space is of the form $S(t) = \cos(2\pi f t)$. If f is equal to 1 GHz, the wavelength is $\lambda = c/f$, where c is the speed of light, that is $\lambda \sim 30$ cm.

Example 23.1.1 (Free Space Propagation). The simplest propagation model is the free space model which states that the signal received at the point (r, θ, ψ) at time t is

$$R_{r,\theta,\psi}(t) = \frac{\alpha(\theta,\psi)}{r}\cos(2\pi f(t - r/c)) = \frac{\alpha(\theta,\psi)}{r}\cos(2\pi f t - \phi), \tag{23.1}$$

where $\alpha = \alpha(\theta, \psi)$ denotes the gain of the antenna in the (θ, ψ) direction and where the signal phase ϕ is $2\pi r/\lambda$. The $1/r$ term in the amplitude stems from a simple energy conservation law. Hence the power received at distance r is proportional to $1/r^2$. In the particular case of omni-directional antennas, $\alpha(\theta, \psi)$ is constant.

In the free space model, the power of the signal is attenuated proportionally to $1/r^2$. In practice however, when the traversed space is not empty, power decreases much faster. We will explain this in the following example, where we take into account the reflection of the signal on the ground, and where power decreases in $1/r^4$.

Example 23.1.2 (Ground Reflection). If the transmitter and the receiver are above the ground, then one should both consider the direct path with length r_1 and the reflected path with length r_2. Let r denote the ground distance between the transmitter and the receiver. Then for r large, $r_2 - r_1 \approx b/r$ where b is a constant that depends on the heights of the transmitter and the receiver. The received signal is then

$$R_r(t) \approx \alpha(\theta, \psi) \left(\frac{1}{r_1} \cos(2\pi f(t - r_1/c)) - \frac{1}{r_2} \cos(2\pi f(t - r_2/c)) \right), \tag{23.2}$$

which is easily seen to be of the order of $1/r^2$ in the far-field, namely when r is large. Hence the power is proportional to $1/r^4$. The minus sign in the second term of the last equation stems from the fact that the sign of the electric field is reversed by the ground reflection; this explains why the two waves interact here in a destructive way.

In view of the two simple scenarios described above, it should be clear that an exact analysis of the propagation of the signal in a "real" scenario with many obstacles and reflections would be extremely complicated. Fortunately this is not necessary as some statistical models of the attenuation of power are often sufficient for the purpose of radio communication engineering.

23.1.2 Mean Power Attenuation Models

Linked to the two models described above, it is customary to consider the following general macroscopic distance-and-angle dependent *path-gain model* according to which the power of the signal received at distance r and in the direction θ, ψ (respectively referred to as the azimuth and the tilt) is equal to

$$\sigma^2 = \sigma^2(r, \theta, \psi) = \frac{\bar{\alpha}^2(\theta, \psi)}{l(r)}, \tag{23.3}$$

where

- l is the *omni-directional (isotropic) path loss function* [1] (OPL),
- $\bar{\alpha}^2(\theta, \psi)$ denotes the value of the *mean normalized radiation pattern* (RP) in the direction θ, ψ; it takes into account the transmitter and receiver antenna gains.

[1] This definition of path loss is natural: if the path loss is large, the received signal has a low power.

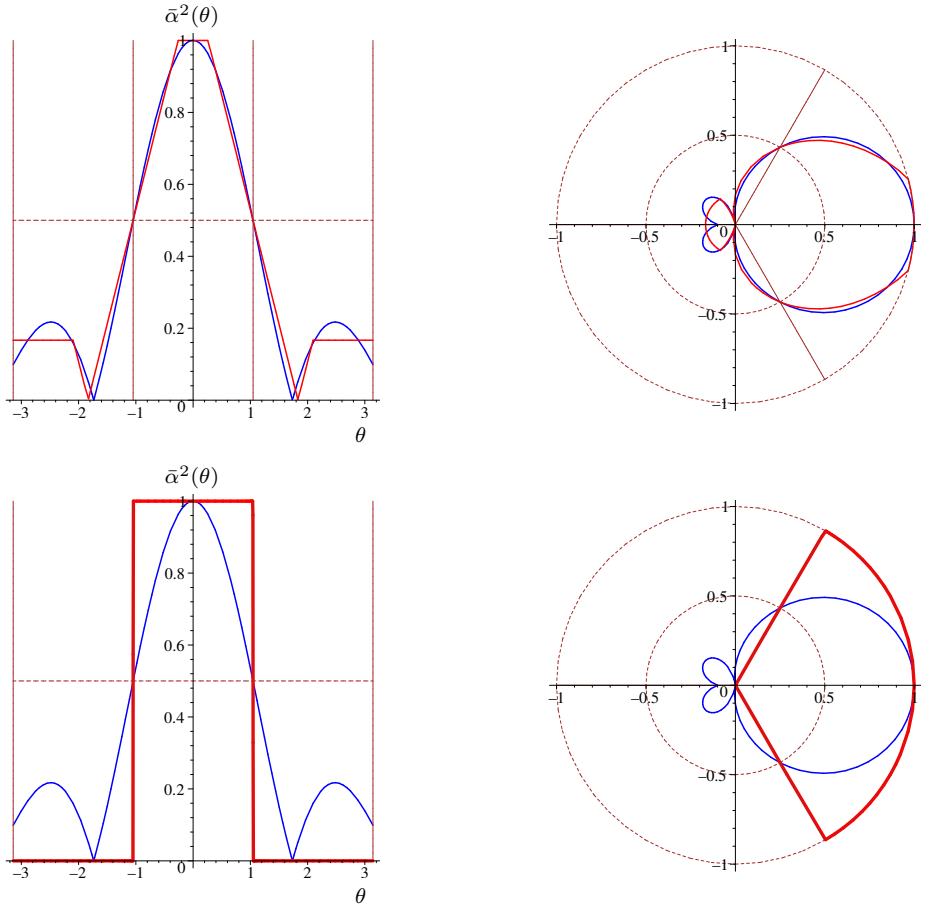

Fig. 23.1 Top: approximation of RP1 by RP2 with $\theta_1 = \frac{1}{12}\pi, \theta_2 = \frac{2}{3}\pi$; Cartesian and polar plots. Bottom: in boldface/red, perfect RP modeled by RP2 with $\theta_1 \to \pi/3-$ and $\theta_2 \to \pi/3+$; Cartesian and polar plots.

Example 23.1.3 (Omni-directional path-loss function). The following examples of isotropic path-loss functions will be considered:

(OPL 1) $l(r) = (A \max(r_0, r))^\beta$,
(OPL 2) $l(r) = (1 + Ar)^\beta$,
(OPL 3) $l(r) = (Ar)^\beta$,

for some $A > 0$, $r_0 > 0$ and $\beta > 2$, where β is called the *path-loss exponent*. Note that OPL3 is a simplified model making no sense for r close to 0. However it is reasonable for r bounded away from 0. It is thus important to use it is with caution. All three cases OPL1–OPL3 give similar values for $r > r_0$ and/or when Ar is large.

Example 23.1.4 (Planar radiation patterns *). We will concentrate on *planar RPs*, namely RPs such that $\bar{\alpha}^2(\theta, \psi) = \bar{\alpha}^2(\theta)$. Apart from a few exceptions, we will use

(RP0) $\bar{\alpha}^2 \equiv 1$, which corresponds to perfect omni-directional radiation.

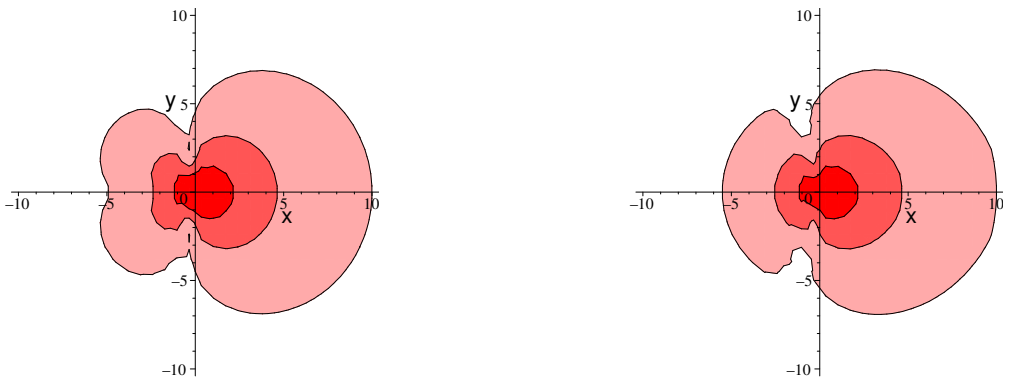

Fig. 23.2 Equal-strength power sets (path-loss level sets) for (23.3) with omni-directional attenuation OPL 2 with $A = 1000$, $\beta = 3$, and radiation patterns RP1 (left), RP2; $\theta_1 = \frac{1}{12}\pi, \theta_2 = \frac{2}{3}\pi$ (right). The contours represent the levels $t = \{100, 110, 120\}$dB.

As examples of truly directional RPs we will consider patterns with a 3dB *azimuth beam-width* of 120°. Here are two mathematical models with this property:

(RP1) is defined by

$$\bar{\alpha}^2(\theta) = \left| \frac{\sin(\omega\theta)}{\omega\theta} \right| \qquad |\theta| \leq \pi\,,$$

where $\omega = 1.81$ is chosen such that $\bar{\alpha}^2\left(\frac{1}{3}\pi\right) = \frac{1}{2} = 3$dB.

(RP2) is defined by

$$\bar{\alpha}^2(\theta) = \begin{cases} 1 & \text{for } |\theta| \leq \theta_1, \\ \left| 1 - \dfrac{|\theta| - \theta_1}{2(\pi/3 - \theta_1)} \right| & \text{for } \theta_1 < |\theta| \leq \theta_2, \\ \left| 1 - \dfrac{|\theta_2| - \theta_1}{2(\pi/3 - \theta_1)} \right| & \text{for } \theta_2 < |\theta| \leq \pi, \end{cases}$$

where $0 < \theta_1 < \frac{1}{3}\pi < \theta_2 < \pi$ and $\theta_1 + \theta_2 > \frac{2}{3}\pi$ are such that $\bar{\alpha}^2\left(\frac{1}{3}\pi\right) = \frac{1}{2} = 3$dB.

Figure 23.1 illustrates these RP models. Notice that in the above definitions,

- The main and the first secondary lobes can be taken into account.
- In RP2, if one lets $\theta_1 \to \pi/3-$ and $\theta_2 \to \pi/3+$ in such a way that $(\theta_2 - \pi/3)/(\pi/3 - \theta_1) \to 1+$, then RP2 tends to a perfect coverage of the sector $(-\pi/3, \pi/3)$.
- If $\theta_1 = \frac{1}{12}\pi$ and $\theta_2 = \frac{2}{3}\pi$, then RP2 is a piecewise linear approximation of RP1 (these parameters are chosen by "visual inspection").

Figure 23.2 depicts the *equal-signal-strength* set (or path-gain level-set) $\{y \in \mathbb{R}^2 : \sigma^2(|y|, \arg(y)) = t\}$ associated with a few levels t. The antenna has its main lobe in the direction $\theta = 0$ (one also says that its azimuth is equal to 0) and is located at $0 \in \mathbb{R}^2$. We consider both RP 1 and RP 2 and assume $l(r)$ is given by OPL 2. One sees that a piece-wise-linear radiation pattern RP 1 can be used to approximate RP 2.

23.2 Random Fading

The mean model of power attenuation described in the previous section does not capture the important phenomenon of the variation of the signal power over short distances (of the order of the wavelength) and in time. We will explain the nature of these variations in a few examples and then show a stochastic model which, in some cases, can capture this phenomenon.

23.2.1 Motivating Examples

When the transmitted signal propagates to the receiver, it may actually meet a collection of different objects (called *scatterers*) on its way, and they may reflect it. This leads to the situation where several different copies of the signal are received, each of them propagated along a specific path.

Example 23.2.1 (Scattering and Multipath Fading). Assume for simplicity that there are two paths: path 1 is the direct path with distance $r_1 = r$; path 2 stems from the reflection of the signal on a wall at distance $d > r$ from the transmitter and orthogonal to the direction of the direct path, so that $r_2 = 2d - r$. Hence the received signal is equal to

$$R(t) = \frac{\alpha}{r}\cos\left(2\pi f\left(t - \frac{r}{c}\right)\right) - \frac{\alpha}{2d-r}\cos\left(2\pi f\left(t - \frac{2d-r}{c}\right)\right).$$

The received signal is hence the superposition of two waves with the same frequency f but with a phase difference of $\Delta\phi = \pi + 4\pi f(d-r)/c = \pi + 4\pi(d-r)/\lambda$. When $\Delta\phi$ is an even (resp. odd) multiple integer of π, the two waves add constructively (resp. destructively). This means that *changing r by $\lambda/4$ can change the received signal strength from a local maximum to a local minimum.* Note however, that if the distance between two reception locations is significantly less than $\lambda/4$ the strength of the received signal is unchanged. This *coherence distance* $\Delta = \lambda/4$ is of the order of 10 cm when $f = 1$ GHz. Similarly, changing the frequency f by $c/(4(d-r))$ leads from a peak to a valley of the signal at a given location. However, if the frequency change is significantly smaller than this value, the signal strength does not vary too much. Thus the bandwidth $c/(2(d-r))$ is called the *coherence bandwidth*. The reciprocal of the coherence bandwidth is called the *delay spread*.

The following example shows how mobility (of transmitter, receiver or scatterers) impacts the variation of the signal strength in time.

Example 23.2.2 (Motion and Small Scale Fading). We assume that the receiver is moving at a speed v and in some direction which do not vary over the time interval considered. In the open space model the (direct) path length varies with time as

$$r(t) = r + vt\cos(\gamma),$$

where γ is the angle of the path and the receiver motion and where $r = r(0)$. Hence (23.1) should be replaced by

$$R(t) = \frac{\alpha(\theta(t), \psi(t))}{r(t)}\cos\left(2\pi f t - \phi(t)\right), \tag{23.4}$$

where

$$\phi(t) = \frac{2\pi r(t)}{\lambda} = \phi + \frac{v\cos(\gamma)}{c}2\pi f t.$$

with $\phi = 2\pi fr/c = 2\pi r/\lambda$. If we can assume that the path gain does not change significantly within the time intervals of interest, then

$$R(t) \sim \frac{\alpha(\theta,\psi)}{r}\cos\left(2\pi f\left(1-\frac{v\cos(\gamma)}{c}\right)t-\phi\right), \tag{23.5}$$

where we observe the classical *Doppler shift* $D = -vf\cos(\gamma)/c$, i.e. the change of the frequency from f to $f + D$.

Let us revisit now our simple wall reflection scenario of Example 23.2.1 with the receiver moving towards the wall. Path 1 is the direct path with $\gamma_1 = 0$ (the motion and the transmitter–receiver vectors are collinear) and $r_1(t) = r + vt$; path 2 stems from the reflection of the signal on the wall and $\gamma_2 = \pi$ and $r_2(t) = 2d - r - vt$. Then the time between a constructive and a destructive phase combination is $c/4vf$. More precisely,

$$R(t) = \frac{\alpha}{r+vt}\cos\left(2\pi f\left(\left(1-\frac{v}{c}\right)t-\frac{r}{c}\right)\right) - \frac{\alpha}{2d-r-vt}\cos\left(2\pi f\left(\left(1+\frac{v}{c}\right)t-\frac{2d-r}{c}\right)\right). \tag{23.6}$$

When the mobile is close to the wall, $r + vt$ and $2d - r - vt$ are of the same order (on a sufficiently small time interval) and

$$R(t) \sim \frac{2\alpha}{r+vt}\sin\left(2\pi f\left(t-\frac{d}{c}\right)\right)\sin\left(2\pi f\left(\frac{vt}{c}+\frac{r-d}{c}\right)\right).$$

We see that the received signal is the multiplication of some high frequency wave $\sin(2\pi f(t - d/c))$ (we recall that f is of the order of the GHz) by some low frequency (envelope) wave at fv/c. This means that the *strength of the signal received by this mobile antenna varies in time with the frequency* fv/c. The reciprocal of this value, c/vf, is called the *coherence time*. One can say that the power of the received signal remains constant in time intervals significantly smaller than this coherence time. For example if the velocity is of the order of 60 km/h, fv/c is of the order of 55Hz and the coherence time of the order of 18ms.

In cases with more reflectors, one observes several Doppler shifts of the frequency f. Denote by D_n that of path n. Then, the *Doppler spread* is defined as

$$D_s = \sup_n D_n - \inf_n D_n.$$

The envelope of $R(t)$ varies at a time scale of the order of $1/D_s$. On time intervals significantly smaller than the coherence time $T_c = 1/(4D_s)$, there is no sizable variation of the strength of the received signal. This time scale is small compared to that of the variations of the path gain induced by motion due to large scale fading. Hence the terminology of *small scale fading*.

It should also be clear that a similar phenomenon is also present when the transmitter and/or scatterers are mobile.

An exact analysis of the small time/space scale variations of the signal strength described in the above examples would be too complicated in a real life situation. The stochastic models described below are better suited for the description of these phenomena.

23.2.2 Random Scatterers

Consider many static or moving scatterers giving N different copies of the transmitted signal, each propagating along a specific path. A signal traveling on path n with length r_n arrives with some delay $\tau_n = r_n/c$.

Therefore the received signal is

$$R_N(t) \quad = \quad \sum_{n=1}^{N} \xi_n \cos\left(2\pi f(t-\tau_n)\right) = \sum_{n=1}^{N} \xi_n \cos\left(2\pi f t - \phi_n\right) \ , \tag{23.7}$$

where in the simplest case, $\phi_n = 2\pi f \tau_n$ and $\xi_n = b_n \frac{\alpha_n}{r_n}$, with α_n the antenna gain in the direction of path n and b_n the variable with value $+1$ or -1 depending on the number of reflections on path n. More complex scenarios can be considered like

- the case of mobility where ϕ_n depends on t via the Doppler shift D_n of path n: $\phi_n(t) = \phi_n + 2\pi D_n t$ (cf. (23.4));
- the case where each path is reflected on the ground so that when aggregating the effect of path n and its reflection, we get a formula of the form $\xi_n = b_n \frac{\alpha_n}{r_n^2}$.

Far-field Assumptions. In the case where transmitter, receiver and scatterers are fixed, the path parameters do not vary with time t and $\phi_n = 2\pi r_n/\lambda$. If we suppose now that $r_n \gg \lambda$, which corresponds to the so called *far-field model*, then it is reasonable to assume that

- $r_n/\lambda - \lfloor r_n/\lambda \rfloor$ is uniformly distributed in $[0,1)$, so that ϕ_n is uniformly distributed in $[0, 2\pi)$ and the phases $\{\phi_n\}$ are independent;
- the random variables ξ_n are i.i.d.; and
- the sequences $\{\phi_n\}$ and $\{\xi_n\}$ are independent.

Note that under these assumptions, variables b_n can be removed in (23.7) without altering the law of the received signal $R(t)$.

Claim 23.2.3. Under the above far-field assumptions, the received signal $\{R(t)\}$ is a centered stationary stochastic process with auto-correlation function

$$C\left(s\right) = \frac{1}{2} \sum_{n} \mathbf{E}\left[\xi_n^2\right] \cos\left(2\pi f s\right) \ . \tag{23.8}$$

Remark: Note that $\frac{1}{2} = 1/(2\pi) \int_0^{2\pi} \cos^2(t)\, \mathrm{d}t$ is the mean power of the transmitted signal and $\mathbf{E}[\xi_n^2] = a^2$ can be interpreted as the value of the mean path-gain function at a given location; cf. the model around Equation (23.3).

Proof. Stationarity stems from the fact that each term of the sum is stationary, which follows from the uniform phase assumption and the independence assumption. The first moment property is clear. Using the fact that the random phases are independent and uniform, one gets that the auto-correlation is

$$\begin{aligned}
\mathbf{E}[R(t+s)R(t)] &= \sum_{n,k} \mathbf{E}\left[\xi_n \cos\left(2\pi f\left(t+s\right) - \phi_n\right) \xi_k \cos\left(2\pi f t - \phi_k\right)\right] \\
&= \sum_{n} \mathbf{E}\left[\xi_n^2\right] \mathbf{E}\left[\cos\left(2\pi f\left(t+s\right) - \phi_n\right) \cos\left(2\pi f t - \phi_n\right)\right] \\
&= \frac{1}{2} \sum_{n} \mathbf{E}\left[\xi_n^2\right] \cos\left(2\pi f s\right) .
\end{aligned}$$

□

This property extends to the more complex settings considered so far, whenever the uniform phase and independence properties are satisfied.

Large Number of Random Scatterers in the Far-field. We now study what happens with the model (23.7) when the number of paths N is large. The setting is that of the far-field model. Moreover, we assume that

- $\xi_n = \xi_{N,n}$, $n = 1, \ldots, N$, $N \geq 1$ are such that the total power of the received signal

$$E[R(t)^2] = C(0) = \frac{1}{2} \sum_{n=1}^{N} \mathbf{E}\left[\xi_{N,n}^2\right] = a^2/2 \tag{23.9}$$

  is the same for all N.

A typical example is that where $\xi_{N,n} = \frac{1}{\sqrt{N}} Y_n$, where $\{Y_n\}_{n\in\mathbb{N}}$ is an i.i.d. sequence of positive random variables with finite second moment $a^2/2$. In this particular case, the central limit theorem implies that $R_N(t)$ converges in distribution to a centered Gaussian random variable when N tends to infinity. More generally, we have the following result when we assume that the path gains are independent but not necessarily identically distributed.

Claim 23.2.4. If the condition

$$\lim_{N\to\infty} \sum_{n=1}^{N} \mathbf{E}\left[\xi_{N,n}^2 \mathbb{1}\left\{\xi_{N,n} \geq \epsilon a\right\}\right] = 0, \quad \text{for all } \epsilon > 0 \tag{23.10}$$

is satisfied, then $R_N(t)$ converges in distribution to a Gaussian random variable $\mathcal{N}(0, a^2)$ when $N \to \infty$. Similarly, for all $k \geq 1$ and for all $t_1, \ldots, t_k$ and $\beta_1, \ldots, \beta_k \in \mathbb{R}$, the random variable $\sum_{j=1}^{k} \beta_j R(t_j)$ converges in distribution to a Gaussian random variable when $N \to \infty$.

Proof. We apply the Lindeberg version of the central limit theorem (Billingsley 1995, Theorem 27.1 p.359). Let

$$X_{N,n} = \xi_{N,n} \cos\left(2\pi f t - \phi_n\right).$$

Since

$$X_{N,n}^2 \mathbb{1}\left\{|[X_{N,n}| \geq \epsilon a\right\} \leq \xi_{N,n}^2 \mathbb{1}\left\{\xi_{N,n} \geq \epsilon a\right\}$$

and

$$\sum_{n=1}^{N} \mathbf{E}\left[X_{N,n}^2\right] = \frac{1}{2} \sum_{n=1}^{N} \mathbf{E}\left[\xi_{N,n}^2\right] = \frac{a^2}{2},$$

Condition (23.10) implies the Lindeberg condition

$$\lim_{N\to\infty} \sum_{n=1}^{N} \mathbf{E}\left[X_{N,n}^2 1\left\{X_{N,n} \geq \epsilon a\right\}\right] = 0, \quad \text{for all } \epsilon > 0$$

which allows one to apply Lindeberg's theorem (Billingsley 1995, Theorem 27.1 p.359).

□

23.2.3 Quadrature Amplitude Modulation (QAM)

Up to now we have considered radio transmission of a simple high frequency sinusoidal signal at the carrier frequency $f = f_c$. In reality, a low frequency signal $S^{(b)}(t)$ called *baseband* signal, to be communicated over the radio, is first transformed into some equivalent high frequency *passband* signal $S(t)$ which is then transmitted, propagated, received as $R(t)$ and transformed back to the low frequency baseband representation $R^{(b)}(t)$ of $R(t)$. This procedure is called *Quadrature Amplitude Modulation*. We now analyze the impact of our previous stochastic assumptions (large number of random scatterers, far-field) on the variation of the baseband representation of the signal at the receiver.

Denote by $S(t)$ the passband signal and by $S^{(b)}(t)$ the baseband signal. Denote by $\widehat{S}(f)$ the Fourier transform of $S(t)$ and by $\widehat{S}^{(b)}(f)$ that of $S^{(b)}(t)$, which we assume to exist. The one to one correspondence between the two signals is best described through the following relations between their Fourier transforms:

$$\widehat{S}(f) = \frac{1}{\sqrt{2}}\left[\widehat{S}^{(b)}(f - f_c) + \left(\widehat{S}^{(b)}\right)^*(-f - f_c)\right] \tag{23.11}$$

and

$$\widehat{S}^{(b)}(f) = \sqrt{2}\widehat{S}(f_c + f)\mathbb{1}\{f + f_c > 0\}. \tag{23.12}$$

The normalization by $\sqrt{2}$ is introduced so that S and $S^{(b)}$ have the same power. We assume that $\widehat{S}^{(b)}(f)$ vanishes for frequencies f outside the baseband $[-W/2, W/2]$ for some bandwidth $W/2 < f_c$, so that $\widehat{S}(f)$ vanishes for frequencies f outside the passband $[-W/2 + f_c, W/2 + f_c]$.

The fact that $\widehat{S}(-f) = \widehat{S}^*(f)$ shows that $S(t)$ is real, whereas the baseband signal is complex-valued:

$$S^{(b)}(t) = S_I^{(b)}(t) + iS_Q^{(b)}(t)$$

with $S_I^{(b)}(t)$ the in phase component and $S_Q^{(b)}(t)$ the quadrature component. This terminology stems from the following time domain up-conversion formula (which follows from (23.11)):

$$S(t) = \sqrt{2}S_I^{(b)}(t)\cos(2\pi f_c t) - \sqrt{2}S_Q^{(b)}(t)\sin(2\pi f_c t) = \sqrt{2}\mathcal{R}\left(S^{(b)}(t)e^{i2\pi f_c t}\right), \tag{23.13}$$

where $\mathcal{R}$ denotes the real part.

Assuming the channel model (23.7), if the passband signal $S(t)$ is transmitted, then the received signal is equal to

$$\begin{aligned} R(t) &= \sqrt{2}R_I^{(b)}(t)\cos(2\pi f_c t) - \sqrt{2}R_Q^{(b)}(t)\sin(2\pi f_c t) = \sum_{n=1}^{N}\xi_n S(t - \tau_n) \\ &= \sqrt{2}\left(\sum_{n=1}^{N}\xi_n\left(S_I^{(b)}(t - \tau_n)\cos(2\pi\tau_n) - S_Q^{(b)}(t - \tau_n)\sin(2\pi\tau_n)\right)\right)\cos(2\pi f_c t) \\ &\quad + \sqrt{2}\left(\sum_{n=1}^{N}\xi_n\left(S_I^{(b)}(t - \tau_n)\sin(2\pi\tau_n) + S_Q^{(b)}(t - \tau_n)\right)\cos(2\pi\tau_n)\right)\sin(2\pi f_c t), \end{aligned}$$

where we used (23.13). Simple trigonometry arguments show that the solution to this equation with a low frequency is

$$R_N^{(b)}(t) = \sum_{n=1}^{N}\xi_{n,N}e^{-i2\pi\tau_n}S^{(b)}(t - \tau_n). \tag{23.14}$$

One can prove a Central Limit Theorem for $R_N^{(b)}(t)$ under conditions similar to (23.10), namely one can show that when $N \to \infty$, the random variable $R_N^{(b)}(t)$ converges in distribution to a complex-valued Gaussian random variable $Z_I(t) + iZ_Q(t)$ (for more on complex-valued Gaussian random variables, see §24.1). It is beyond our scope to work out such conditions in detail. Instead, we exemplify this convergence in the following simple case:

Example 23.2.5. Since $S^{(b)}$ is a low frequency signal, it is reasonable to assume for simplicity that it is (piecewise) constant. Then $S^{(b)}(t-\tau_n) = S^{(b)}$. We recall that, under a far-field assumption, $\xi_n = \xi_{n,N}$ and $\phi_n = 2\pi\tau_n$ are independent and ϕ_n is uniformly distributed on $[0, 2\pi)$. Consequently $\mathbf{E}[\xi_n S^{(b)} e^{-i\phi_n}] = S^{(b)}\mathbf{E}[\xi_n]\mathbf{E}[e^{-i\phi_n}] = 0$. This shows that $\mathbf{E}[Z_I] = \mathbf{E}[Z_Q] = 0$. Let us now calculate the covariance of the real and imaginary parts of $R_N^{(b)}$. From (23.14) by independence of the paths

$$\mathbf{E}\big[\mathcal{R}(R_N^{(b)})\mathcal{I}(R_N^{(b)})\big] = \sum_{n=1}^{N} \mathbf{E}[\xi_{n,N}^2]\mathbf{E}\Big[\mathcal{R}\big(S^{(b)}e^{-i\phi_n}\big)\mathcal{I}\big(S^{(b)}e^{-i\phi_n}\big)\Big] = 0\,,$$

where $\mathcal{I}$ denotes the imaginary part, since

$$\begin{aligned}&\mathbf{E}\Big[\mathcal{R}\big(S^{(b)}e^{-i\phi_n}\big)\mathcal{I}\big(S^{(b)}e^{-i\phi_n}\big)\Big]\\ &= \Big((\mathcal{I}(S^{(b)}))^2 - (\mathcal{R}(S^{(b)}))^2\Big)\mathbf{E}\Big[\frac{\sin 2\phi_n}{2}\Big] + \mathcal{I}(S^{(b)})\mathcal{R}(S^{(b)})\mathbf{E}[\cos 2\phi_n] = 0\,.\end{aligned}$$

Hence Z_I and Z_Q are uncorrelated and thus independent, provided they form a Gaussian vector. Note also that under the assumption $\sum_{n=1}^{N}\xi_{n,N}^2 = a^2$, we have $\mathbf{E}[Z_I^2 + Z_Q^2] = |S^{(b)}|^2 a^2$, namely the mean power of the baseband signal is the product of $|S^{(b)}|^2$, the power of the baseband signal at the transmitter, and of a^2, the mean power attenuation.

Remark: Since Z_I and Z_Q are independent $\mathcal{N}(0, |S^{(b)}|^2\frac{a^2}{2})$ random variables (where $\mathcal{N}(\mu,\sigma^2)$ denotes the Gaussian law of mean μ and variance σ^2), the power $Z_I^2 + Z_Q^2$ of the received baseband signal has a χ_2^2 distribution (up to a multiplicative constant). More precisely it is an exponential random variable with mean $a^2|S^{(b)}|^2$ (and its square root has a Rayleigh distribution with parameter $a^2|S^{(b)}|^2$).

Inspired by the above remark we will introduce now a basic stochastic model for variations of the received power.

23.2.4 Rayleigh Fading and its Extensions

In Section 23.1.2 we have modeled the *mean* received signal power by some fraction $a^2 = a^2(r,\theta,\psi)$ of the emitted power. This mean fraction is a function of the distance between the transmitter and the receiver and of certain angles θ, ψ associated with antenna azimuths and tilts. The last examples lead to the following natural random model for the law of the received power.

Definition 23.2.6. We say that the wireless channel exhibits *Rayleigh fading* if the received power is equal to Pa^2F, where P is the power of the transmitted signal, a^2 is the mean attenuation function and F is exponential random variable with mean 1.

Note that this definition is only valid when QAM is used in the far-field and when there are many scatterers. In the situation where an important fraction of the power is received on the line-of-sight path, the following model is more pertinent:

Definition 23.2.7. We say that the wireless channel exhibits *Rician fading* if the received power is equal to $Pa^2\kappa/(\kappa+1) + F/(\kappa+1)$, where $\kappa/(\kappa+1)$ is the fraction of the mean power received on the line-of-sight path and P, a^2 and F are as for Rayleigh fading.

When several groups of paths can be distinguished, each group contributing to an exponential power with a different mean, one can use a *Nakagami* fading model (see (Stuber 2001)).

23.3 Conclusion

Note that the above stochastic models give the distribution of the fading F at a given location and at a given time with respect to some given transmitter. It is difficult to model the fading $F = F(t, x, f)$ in the time-space-frequency domain $x \in \mathbb{R}^3$, $t \in \mathbb{R}$, $f \in \mathbb{R}^+$. However, the following remarks will be useful:

- If $|x - y| \ll \Delta$, where Δ is the coherence distance (see Example 23.2.1), then one can assume that $F(t, x) = F(t, y)$.
- If $|t - s| \ll T_c$, where T_c is the coherence time (see Example 23.2.2), then one can assume that $F(t, x) = F(s, x)$.
- If $|t - s| \gg T_c$ or $|x - y| \gg \Delta$ then $F(t, x)$ and $F(s, y)$ can be considered as independent random variables. Since the scattering obstacles are different for (sufficiently separated) transmitter–receiver pairs, it makes sense to assume that these random variables are independent for all such pairs.
- Fading depends on the signal frequency. However if the change of frequency is significantly smaller than the coherence bandwidth (see Example 23.2.2) then the received power at a given location and time does not vary too much.

24

Signal Detection

The aim of this chapter is to show through a few basic examples how signal to noise and signal to noise and interference ratios determine error probability and hence throughput on the multipath wireless channels described in the preceding chapter. Detection will be considered in a discrete channel model based on the sampling theorem which is described first. We start with a few well known facts on complex–valued Gaussian vectors.

24.1 Complex Gaussian Vectors

A complex–valued random vector of dimension n is said to be Gaussian if its real and imaginary parts form a Gaussian vector of dimension $2n$. A complex–valued random vector X of dimension n is said to be

- circular-symmetric if $e^{i\theta}X$ has the same law as X for all θ;
- isotropic if for all unitary[1] transformations U of $\mathbb{C}^n$, UX has the same law as X.

A complex–valued Gaussian scalar is circular-symmetric iff its real and imaginary parts are i.i.d. and centered. We will denote by $\mathcal{N}^{\mathcal{C}}(0,\sigma^2)$ this distribution when the variance of the real (or imaginary) part is $\sigma^2/2$.

A vector of $\mathbb{C}^n$ with i.i.d. $\mathcal{N}^{\mathcal{C}}(0,\sigma^2)$ components is both circular-symmetric and isotropic.

24.2 Discrete Baseband Representation

24.2.1 Linear Model

Assume that the mapping which gives R from S is of the form

$$R(t) = \sum_n \xi_n(t) S\left(t - \frac{r_n(t)}{c}\right) \tag{24.1}$$

[1] U is unitary if $(U^t)^* U = I$ with U^t the transpose of U and U^* its complex conjugate.

with $\xi_n(t) = b_n\alpha_n(t)/r_n(t)$, which is a time dependent version of (23.7), Chapter 23. Let $S^{(b)}(t)$ and $R^{(b)}(t)$ denote the baseband representation of S and R respectively. By calculations similar to those made in § 23.2.2, we conclude that the mapping which gives $R^{(b)}$ from $S^{(b)}$ is

$$R^{(b)}(t) = \sum_n \beta_n(t) S^{(b)}\left(t - \frac{r_n(t)}{c}\right), \tag{24.2}$$

where

$$\beta_n(t) = \xi_n(t) e^{-2\pi i f_c \frac{r_n(t)}{c}}. \tag{24.3}$$

Assume now that $S^{(b)}(t)$ is integrable, continuous and band-limited to W. Since the Fourier transform of $S^{(b)}(t)$ vanishes outside $[-W/2, W/2]$, the sampling theorem (Brémaud 2002) states that there is no loss of information in sampling $S^{(b)}(t)$ every $1/W$ seconds and that

$$S^{(b)}(t) = \sum_{k\in\mathbb{Z}} S^{(b)}[k]\text{sinc}(Wt - k), \tag{24.4}$$

with $S^{(b)}[k] = S^{(b)}(k/W)$ the k-th sample and

$$\text{sinc}(t) = \frac{\sin(\pi t)}{\pi t}.$$

Hence (24.2) can be rewritten as

$$\begin{aligned} R^{(b)}(t) &= \sum_n \beta_n(t) \sum_k S^{(b)}[k]\text{sinc}(Wt - W\frac{r_n(t)}{c} - k) \\ &= \sum_k S^{(b)}[k] \sum_n \beta_n(t)\text{sinc}(Wt - W\frac{r_n(t)}{c} - k), \end{aligned} \tag{24.5}$$

provided the series is absolutely convergent. Thus, the m-th sample of $R^{(b)}(t)$ at multiples of $1/W$ is

$$R^{(b)}[m] = \sum_k S^{(b)}[k] \sum_n \beta_n(m/W)\ \text{sinc}\left(m - k - W\frac{r_n(m/W)}{c}\right).$$

Substituting $m - k = l$, we finally get the following discrete time filter:

$$R^{(b)}[m] = \sum_l H_l[m] S^{(b)}[m - l], \tag{24.6}$$

where

$$H_l[m] = \sum_n \beta_n(m/W)\ \text{sinc}\left(l - W\frac{r_n(m/W)}{c}\right). \tag{24.7}$$

This map from the sequence of complex *input symbols* $\{S^{(b)}[k]\}_k$ which are produced at rate W at the transmitter to the set of *output symbols* $\{R^{(b)}[k]\}_k$ at the receiver, takes into account both the modulation of the signal to its passband version at the transmitter, the propagation of the resulting signal from transmitter to receiver, the conversion back to the baseband at the receiver, and finally the sampling there.

A few important remarks are in order:

- If the functions $\xi_n(.)$ are constant (as in e.g. Example 23.2.1), then $H_l[m] \equiv H_l$ and the discrete linear filter is time-invariant.

- Using the shape of the sinc function, one sees from (24.7) that H_l predominantly selects the paths with a delay of the order of l/W.
- If the mapping which gives R from S is given by

$$R(t) = \sum_n b_n(t) \frac{\alpha_n(t)}{r_n(t)} S\left(t - \frac{r_n(t)}{c}\right) + W(t), \tag{24.8}$$

where $W(t)$ is a stationary 0-mean additive white Gaussian noise with variance σ^2, namely a Gaussian process such that $E(W(t)W(s)) = \frac{\sigma^2}{2}\mathbb{1}\{t = s\}$, then a similar construction gives the following input–output map:

$$R^{(b)}[m] = \sum_l H_l[m] S^{(b)}[m - l] + W[m], \tag{24.9}$$

where $W[m]$ is an i.i.d. sequence of $\mathcal{N}^{\mathcal{C}}(0, \sigma^2)$ random variables.

24.2.2 Time Coherence

From (24.2)–(24.3) and from the fact that $\xi_n(t)$ and $r_n(t)$ vary slowly, one gets that at time t, the linear map which gives $R^{(b)}$ from $S^{(b)}$ is approximately time invariant on time scales significantly smaller than the coherence time $T_c = 1/(4D_s)$, where D_s is the Doppler spread at time t, which is defined as

$$D_s = \frac{f_c}{c} \max_{n,n'} |\dot{r}_n(t) - \dot{r}_{n'}(t)|,$$

where the maximum bears on all pairs of paths (cf. Example 23.2.1). Similarly, one gets from (24.7) that for all l, the function $H_l[m]$ is approximately a constant in m when m varies over an interval of length less than WT_c.

24.2.3 Frequency Coherence

Let

$$T_d = \max_{n,n'} 2\pi \frac{1}{c} |r_n(t) - r_{n'}(t)|$$

be the multipath delay spread at time t. It is natural to define the coherence bandwidth W_c at time t as $W_c = 1/T_d$. If the bandwidth of the input W is significantly less than the coherence bandwidth W_c, then the delay spread is significantly less than the symbol time $1/W$ so that only one term l_0 has to be considered in the sum (24.9). This case is called *flat fading*. In most applications, T_d is of the order of a microsecond. This gives an upper bound on the bandwidth of the input for flat fading to be an acceptable model. The simplest flat fading model is

$$R^{(b)}[m] = H_0[m] S^{(b)}[m] + W[m]. \tag{24.10}$$

24.2.4 Statistical Model

Consider now the far field of §23.2.2. Since $f_c r_n(t)/c$ is large, it makes sense to assume that the phase on path n, which is this quantity modulo 2π, is uniformly distributed on $(0, 2\pi)$ at any time t. Hence for all n, l and m, the random variable

$$X_n = \xi_n(m/W) e^{-2\pi i f_c \frac{r_n(m/W)}{c}} \operatorname{sinc}\left(l - W\frac{r_n(m/W)}{c}\right),$$

which occurs in the definition of $H_l[m]$ (24.7), is a circular symmetric complex–valued random variable. Assume that N, the number of scatterers, is large and that the contributions of all paths (path gains and phases) are independent and satisfy a condition of the Lindeberg type. Then for all l and m, the law $H_l[m] = \sum_{n=1}^{N} X_n$ is asymptotically Gaussian circular symmetric (and in particular centered). Hence $|H_l[m]|$ has a Rayleigh distribution with a parameter σ_l that depends on l but not on m, at least for time scales where the distances $r_n(.)$ do not vary significantly.

Not surprisingly, the autocorrelation of the $H_l[m]$ sequence:

$$R_l(n) = E(H_l[m]H_l[m+n])$$

can be shown to become small for values n such that n/W is significantly larger than K/D_s with D_s the Doppler shift of the channel and K some constant, which is a rephrasing of the notion of coherence time already discussed above.

24.3 Detection

24.3.1 Coherent Detection

Assume a flat fading scenario of the form

$$Y = HX + W,$$

where

- $X = X[m]$ and $Y = Y[m]$ are complex–valued;
- $W = W[m]$ is $\mathcal{N}^{\mathcal{C}}(0, \sigma^2)$;
- $H = H[m]$ (in the case of Rayleigh fading, H is $\mathcal{N}^{\mathcal{C}}(0, g^2)$).

Assume $H = H[m]$ to be known by the receiver (this is the coherent detection case). In practice, this can be implemented using some pilot signal and requires that $H[m]$ does not change too fast with m. More precisely this requires that WT_c be large compared to 1 (for instance due to a large coherence time).

Assume antipodal signaling, namely the signal to be transmitted is real and either $+a$ or $-a$ with probability $\frac{1}{2}$.

Remark: Here, and throughout this section, in order to take into account the effect of the distance between emitter and receiver, the value of a^2 should be interpreted as the *mean power of the signal at the receiver*. In general, it depends on the value of the emitted power, distance and antenna parameters; cf. the models discussed in Section 23.1. So one may see the result of this section as given for the emitted power $P = 1$, mean path-gain equal to a^2 and the random channel fading at time m equal to H.

Claim 24.3.1. Under the foregoing assumptions, the maximum likelihood estimator leads to error probability

$$Q\left(\sqrt{2\frac{a^2|H|^2}{\sigma^2}}\right), \tag{24.11}$$

where Q is the tail of the cumulative distribution function of the $\mathcal{N}(0,1)$ density.

Proof. Given that $H = h$, if the complex number y is received, the maximum likelihood estimator gives $+a$ if

$$|y - ah| < |y + ah|.$$

Let v denote the complex number $v = h/|h|$. The last inequality is equivalent to

$$|v^* y - a|h| \,| < |v^* y + a|h| \,|,$$

where v^* denotes the complex conjugate of v. Since $a|h|$ is a real number, this is equivalent to

$$|\mathcal{R}(v^* y) - a|h| \,| < |\mathcal{R}(v^* y) + a|h| \,|.$$

Since $w = \mathcal{R}(v^* W)$ is $\mathcal{N}(0, \sigma^2/2)$, the probability of error given that $+a$ is transmitted is hence

$$P(|\mathcal{R}(v^*(ha + W) - a|h|)| > |\mathcal{R}(v^*(ha + W) + a|h|)|) = P(|w| > |w + 2a|h||) = P(w < -a|h|).$$

□

Hence, in the flat Rayleigh fading scenario, coherent detection leads to a probability of error which is determined by $\mathrm{SNR}[m]$ through the relation $p^e[m] = Q(\sqrt{2\mathrm{SNR}[m]})$, where

$$\mathrm{SNR}[m] = \frac{a^2 |H[m]|^2}{\sigma^2}$$

is the ratio of the power of the received signal to that of the noise power at time m, and $|H[m]|^2$ is exponentially distributed with mean $1/g^2$.

Remark: Notice that (24.11) gives the conditional error probability given the fading. In many situations, its makes sense to decondition this by integration w.r.t. the law of H. However, for so-called *opportunistic algorithms* which try to take advantage of the fluctuations (and more precisely of peaks) of fading, we will need an evaluation of such a conditional error probability.

24.3.2 Repetition Coding

Consider the same flat Rayleigh fading scenario as above. Assume that in order to decrease the probability of error, we repeat the same symbol n times, so that the channel becomes

$$Y[m + k] = H[m + k]X[m] + W[m + k], \quad k = 0, \ldots n - 1$$

or equivalently

$$\mathbf{Y} = X\mathbf{H} + \mathbf{W},$$

where

- $\mathbf{Y}$ is a complex–valued vector of dimension n;
- X is a scalar with value $+a$ or $-a$;
- $\mathbf{H}$ is a complex vector of dimension n;
- $\mathbf{W}$ is a complex–valued vector of dimension n with i.i.d. $\mathcal{N}^{\mathcal{C}}(0, \sigma^2)$ components;

Claim 24.3.2. Assume $\mathbf{H}$ to be known by the receiver. Then the maximum likelihood estimator has the error probability

$$Q\left(\sqrt{2\frac{a^2||\mathbf{H}||^2}{\sigma^2}}\right). \tag{24.12}$$

Proof. The maximum likelihood detector states that $+a$ was transmitted if

$$||\mathbf{Y} - a\mathbf{H}|| < ||\mathbf{Y} + a\mathbf{H}||$$

Defining $\mathbf{v} = \mathbf{H}/||\mathbf{H}||$, this holds iff

$$||\mathbf{v}^* \cdot \mathbf{Y} - a||\mathbf{H}|| \,|| < ||\mathbf{v}^* \cdot \mathbf{Y} + a||\mathbf{H}|| \,||,$$

where $\mathbf{v}^*$ is the complex conjugate of the transpose of $\mathbf{v}$. This is in turn equivalent to

$$|\mathcal{R}(\mathbf{v}^* \cdot \mathbf{Y}) - a||\mathbf{H}|| \,| < |\mathcal{R}(\mathbf{v}^* \cdot \mathbf{Y}) + a||\mathbf{H}|| \,|.$$

Hence, if $+a$ was transmitted, $\mathbf{Y} = a\mathbf{H} + \mathbf{W}$ and the error probability is

$$P(|\mathcal{R}(\mathbf{v}^* \cdot \mathbf{W})| > |\mathcal{R}(\mathbf{v}^* \cdot \mathbf{W}) + 2a||\mathbf{H}|| \,|.$$

The conclusion follows from the fact that $\mathcal{R}(\mathbf{v}^* \cdot \mathbf{W})$ is $\mathcal{N}(0, \sigma^2/2)$ which follows from isotropy. □

If n/W is small compared to the coherence time of the channel, it makes sense to assume that for all $k = 1, \ldots, n$, $H[m+k] = H[m]$. In this case $||H|| = \sqrt{n}|H[m]|$ so that the error probability is now $p^e[m] = Q(\sqrt{2n\mathrm{SNR}[m]}\,)$. Of course, this improvement of the error probability comes with a reduction of the data rate which is now W/n bits per second.

24.3.3 Direct-Sequence Spread-Spectrum Coding

In direct-sequence spread-spectrum, one uses a bandwidth $\overline{W}$ which is larger than the rate W at which bits are produced. Each bit is encoded using a *signature sequence* $\mathbf{U}$ of length n (n is called the processing gain). One sends one element of this sequence (one *chip*) every $1/\overline{W}$ second, whereas the bit rate is $W = \overline{W}/n$ bits per second.

In the case of flat Rayleigh fading and whenever the channel changes slowly compared to $n/\overline{W}$, the discrete channel at the chip time scale can be rewritten as

$$\mathbf{Y} = H\mathbf{X} + \mathbf{W} \tag{24.13}$$

with

- $\mathbf{Y}$ the complex–valued vector $(Y[1], \ldots, Y[n])$ of dimension n;
- $\mathbf{X}$ the complex–valued vector $+a\mathbf{U}$ or $-a\mathbf{U}$ (we assume antipodal signaling with $a > 0$);
- $\mathbf{W}$ the complex–valued vector $(W[1], \ldots, W[n])$ of dimension n with i.i.d. $\mathcal{N}^{\mathcal{C}}(0, \sigma^2)$ components;
- H a complex scalar ($\mathcal{N}^{\mathcal{C}}(0, g^2)$ in the Rayleigh case).

Assume that H is known to the receiver (coherent detection) as well as $\mathbf{U}$. By the same arguments as above, defining $\mathbf{v} = H\mathbf{U}/||H\mathbf{U}||$, using a maximal likelihood argument implies that $+a$ was transmitted iff

$$||\mathbf{Y} - aH\mathbf{U}|| < ||\mathbf{Y} + aH\mathbf{U}|| \quad \Leftrightarrow \quad ||\mathbf{v}^* \cdot \mathbf{Y} - a||H\mathbf{U}||\,|| < ||\mathbf{v}^* \cdot \mathbf{Y} + a||H\mathbf{U}||\,||.$$

Since $w = \mathbf{v}^* \cdot \mathbf{W}$ is $\mathcal{N}^{\mathcal{C}}(0, \sigma^2)$, this is equivalent to the coherent detection of an antipodal signal of amplitude $a||H\mathbf{U}||$. Hence

---

Claim 24.3.3. For direct-sequence spread-spectrum based on pseudo noise sequence $\mathbf{U}$, the probability of error of (24.13) is

$$Q\left(\sqrt{2\frac{||\mathbf{U}||^2 a^2 |H|^2}{\sigma^2}}\right) = Q\left(\sqrt{2||\mathbf{U}||^2 \mathrm{SNR}}\right). \tag{24.14}$$

The projection on $\mathbf{v}$ and the reduction to a scalar problem is referred to as a *matched filter*.

Remark: If the bandwidth is W, the power of the noise σ^2 is equal to $N_0 W$ with N_0 the spectral density of the Gaussian white noise. In the three formulas given so far for the bit error probability, namely (24.11), (24.12) and (24.14), the argument of the square root is twice the so-called E_b/N_0 ratio, with E_b the energy per bit (i.e. either $a^2|H[m]|^2/W$ in (24.11) or $a^2||\mathbf{H}||^2/W$ in (24.12) or $a^2||\mathbf{U}||^2|H|^2/\overline{W}$ in (24.14)) and with N_0 the spectral density of the noise.

As already explained, the general aim of repetition coding is to decrease the error probability at the expense of a lower rate (compared to the setting of Claim 24.3.1). In the direct-sequence spread-spectrum case, we will consider below scenarios where $||\mathbf{U}||^2 \approx n$; since the noise power ought to be $N_0\overline{W} = N_0 nW$, it follows that E_b/N_0 has exactly the same value as in Claim 24.3.1, so that the bit error probability is the same. Since the bit rate is the same in both cases too (namely W), we gain nothing at all for one user. The interest of the method will only become apparent in the case where a collection of users share the same medium; this is considered next.

24.3.4 Interference as Noise

Consider now the scenario where K simultaneous transmissions take place. Transmission k is from transmitter k to receiver k.

Assume all transmissions use the same direct-sequence spread-spectrum technique with processing gain n. Let $\mathbf{U}_k$ denote the pseudo-noise signature sequence of transmitter k. Assume that the signal received by receiver k is of the form

$$\mathbf{Y}_k = H(k,k)\mathbf{X}_k + \sum_{j=1,\ldots,K, j\neq k} H(j,k)\mathbf{X}_j + \mathbf{W}_k \tag{24.15}$$

with

- $\mathbf{Y}_k$ the complex–valued vector $(Y_k[1], \ldots, Y_k[n])$ of dimension n;
- $\mathbf{X}_j$ the complex–valued vector $+a_j\mathbf{U}_j$ or $-a_j\mathbf{U}_j$ with a_j a positive real number;
- $\mathbf{W}_k$ the complex–valued vector $(W_k[1], \ldots, W_k[n])$ of dimension n with i.i.d. $\mathcal{N}^{\mathcal{C}}(0, \sigma_k^2)$ components;

- $H(j,k)$ the fading from transmitter j to receiver k. [2]

Assume that the coordinates of $\mathbf{U}_k$ are i.i.d. $\mathcal{N}^{\mathcal{C}}(0,1)$, and that the vectors $\mathbf{U}_k$ are independent. Assume also that the fading variables, the Gaussian noise and the signatures are independent.

Conditionally on the fading variables $H_{j,k}$, the random vector

$$\mathbf{V}_k = \sum_{j \neq k} H(j,k)\mathbf{X}_j + \mathbf{W}_k$$

has i.i.d. $\mathcal{N}^{\mathcal{C}}(0, \sigma_k^2 + \sum_{j\neq k} a_j^2 |H(j,k)|^2)$ components. Hence we get from (24.14) that:

Claim 24.3.4. Under the foregoing assumptions, the conditional error probability of the channel from transmitter k to receiver k, given the fading $H(k,k)$ and $\mathbf{U}_k$ is

$$Q\left(\sqrt{2||\mathbf{U}_k||^2 \text{SINR}_k}\right), \tag{24.16}$$

with

$$\text{SINR}_k = \frac{a_k^2 |H(k,k)|^2}{\sigma_k^2 + \sum_{j\neq k} a_j^2 |H(j,k)|^2} \tag{24.17}$$

the ratio of the power of the signal to the power of interference plus that of noise for this channel.

A few observations are in order:

- The strong law of large number shows that $||\mathbf{U}_k||^2 \approx n$. Hence,

$$p_k^e \approx Q\left(\sqrt{2n\text{SINR}_k}\right). \tag{24.18}$$

- If $\sigma_k^2 = \overline{W} N_0^k$, the argument of the square root is now twice the ratio of the energy per bit ($E_b \approx n a_k^2 |H(k,k)|^2 / \overline{W}$) and of the sum of the spectral density of the noise (N_0^k) and the energy of the interference per chip ($\sum_{j\neq k} a_j^2 |H(j,k)|^2 / \overline{W}$).
- In the case of Rayleigh fading, for all j and k, $|H(j,k)|^2$ is an exponential random variable with parameter $g_{j,k}^2$.

Remark: What we have described above is not what is done in practice. To show the robustness of the general idea, consider the case where the components of $\mathbf{U}_k$ are still i.i.d. but instead of being $\mathcal{N}^{\mathcal{C}}(0,1)$ they are of the form $e^{i\theta}$ with θ uniform on $[0, 2\pi]$; then the projection of (24.15) on $\mathbf{v}_k = H(k,k)\mathbf{U}_k / ||H(k,k)\mathbf{U}_k||$ leads to the equation

$$\mathbf{v}_k^* \cdot \mathbf{Y}_k = |H(k,k)| x_k ||\mathbf{U}_k|| + \sum_{j\neq k} H(j,k) x_j \frac{H(k,k)^* \mathbf{U}_k^* \cdot \mathbf{U}_j}{||H(k,k)\mathbf{U}_k||} + w_k, \tag{24.19}$$

where $w_k = \mathbf{v}_k^* \cdot \mathbf{W}_k$ is $\mathcal{N}^{\mathcal{C}}(0, \sigma_k^2)$ thanks to isotropy. The conditional law of the random variable

$$\frac{H(k,k)^* \mathbf{U}_k^* \cdot \mathbf{U}_j}{||H(k,k)\mathbf{U}_k||} = \frac{H(k,k)^*}{|H(k,k)|} \frac{\mathbf{U}_k^* \cdot \mathbf{U}_j}{\sqrt{n}}$$

[2] For instance $H(j,k)$ could be $\mathcal{N}^{\mathcal{C}}(0, g_{j,k}^2)$ with $g_{j,k}^2$ equal to $d(j,k)^{-\beta}$ where $d(j,k)$ is the distance between transmitter j and receiver k and β is the path loss exponent.

given $\mathbf{U}_k$ and $H(k,k)$ is circular symmetric (because it is a linear combination of independent circular-symmetric random variables) and approximately Gaussian provided n is large enough (because of the central limit theorem). This together with arguments similar to those given above lead to the same conclusion as in Claim 24.3.4 concerning the error probability.

One can go further along these lines and take the components of $\mathbf{U}_k$ i.i.d. and e.g. equal to $+1$ or -1.

Another variant consists in using orthogonal sequences rather than pseudo-noise sequences for the signatures. In this case the weight of the interference term in the definition of SINR is different.

Interference Cancellation Factor. Consider a collection of direct-sequence spread-spectrum systems where one increases the bandwidth $\overline{W}$ and the processing gain n while keeping the bit rate $W = \overline{W}/n$ constant. Since $\sigma_k^2 = \overline{W} N_0^k$, the error probability for channel k equals $Q(\sqrt{2A_k}\,)$, where

$$A_k = \frac{||\mathbf{U}_k||^2 a_k^2 |H(k,k)|^2}{\overline{W} N_0^k + \sum\limits_{j \neq k} a_j^2 |H(j,k)|^2} \approx \frac{n a_k^2 |H(k,k)|^2}{\overline{W} N_0^k + \sum\limits_{j \neq k} a_j^2 |H(j,k)|^2} = \frac{a_k^2 |H(k,k)|^2}{W N_0^k + \frac{1}{n} \sum\limits_{j \neq k} a_j^2 |H(j,k)|^2}\,. \quad (24.20)$$

So, within this setting, when changing the spread-spectrum bandwidth $\overline{W}$ and the processing gain n while keeping the bit rate $W = \overline{W}/n$ constant, we see that the relevant ratio for estimating the error probability (and hence guaranteeing some *goodput*, defined as the mean number of error-less bits transmitted per unit of time) is the ratio of two terms: the numerator is the power of the received signal; the denominator is a linear function of the spectral density of the noise and of the power of the interference, namely $\sum_{j \neq k} a_j^2 |H(j,k)|^2$. Within this framework, the factor $\frac{1}{n}$ multiplying the interference power decreases to 0 when n increases (in what follows, this factor will be referred to as the *interference cancellation factor*), whereas the factor multiplying the noise spectral density is a constant in n.

Rephrased differently, as long as the interference created by the other users is small compared to n (e.g. as long as there are fewer than n users in a scenario with appropriate symmetry), the system accommodates a rate of W and an error probability which is approximately that of the case of Claim 24.3.4 to each user. Hence this scheme does almost as well as a frequency division multiple access (FDMA) scenario where one would reserve a bandwidth of W per user.

24.4 Conclusion

We conclude this chapter by stating that whenever the coherence time is large enough for fading to remain constant over sufficiently many symbols, the error probability (and hence the goodput or the effective rate at which bits are successfully transmitted) at a given time is determined by the instantaneous SNR at that time. In the case of direct-sequence spread–spectrum, the error probability is determined by the SINR. These results were obtained in the flat Rayleigh channel case. However similar conclusions hold for more general situations, and in particular for non-flat channels of the form (24.9), provided the coherence time is large enough, and for other kinds of fading models. See e.g. Chapter 3 of (Tse and Viswanath 2005).

25

Wireless Network Architectures and Protocols

25.1 Medium Access Control

Consider a wireless medium shared by a collection of transmitter–receiver pairs, all located in some domain. Medium Access Control (MAC) is in charge of organizing the simultaneous access of these transmitter–receiver pairs over time and space. The need for such a control stems from the basic observation that when two (or more) neighboring transmissions access the shared medium simultaneously, they might jam each other. To give a precise definition of jamming, we ought to describe precisely the nature of the channel and of the detection procedure. Consider for example the setting of § 24.3.4 where the interference created by other transmitters can be seen as noise. If the SINR of each receiver is above some threshold T, then a sufficiently small probability of error can be guaranteed and we say that the two transmissions do not jam each other. If the SINR is below $T' < T$, then the probability of error is high and we say that the two transmissions jam each other or collide.

Within this context, one defines the *contention domain* of a reference receiver as the set of locations such that if one adds a transmitter there, then the transmission to the reference receiver is jammed (e.g. the signal to interference ratio and hence the SINR at the reference node is below T'). Note that with such a definition, it is possible for a receiver to have no transmitter in its contention domain and to be jammed nevertheless.

We now give a few examples of MAC used in this book. In these examples, time is slotted and the duration of the slot could for instance be that of the transmission of a fixed number of symbols that we will call a packet.

25.1.1 Time Division Multiple Access (TDMA)

TDMA is based on a division of time into slots and on an appropriate scheduling of the access of nodes to the shared medium. The role of the scheduling is to ensure that nodes which transmit in the same time slot do not jam each other. Note that this is compatible with some *spatial reuse* in that transmitters which are far away can use the same time slot provided the power of interference they create at each receiver is such that SINR is above T. The main drawback of TDMA is that the collision free schedule ought to be computed and then made known to all nodes. If nodes move or join and leave, this schedule has to be re-computed and

communicated and this may be quite inefficient.

25.1.2 Aloha

At each time slot, each node tosses a coin with bias p, independently of everything else. Only the nodes tossing heads transmit during this time slot; The idea is that for appropriate p, there will be at the same time a large enough random exclusion zone around any node (and in particular any receiver), and hence a small enough interference at the receiver. Because of the random nature of the algorithm, collisions may take place. Acknowledgments are used to cope with this problem. One of the main advantages of this scheme (also shared by the other schemes described below) is that it is fully decentralized. One can in particular add or delete transmitters or let nodes move without altering the access mechanism.

25.1.3 Carrier sense multiple access (CSMA)

Each node has a timer which indicates its back-off time, namely the number of time slots it should wait before transmission. Each node senses the medium continuously; if the medium is sensed busy, namely if the node detects a transmitter in its contention domain, the node freezes its timer until the medium becomes free. When the timer expires, the node starts its transmission and samples a new random back-off time. There are several variants depending on whether carrier sensing is performed at the receiver (which is best) or by the transmitter (which is simpler to implement). Nevertheless, collisions can occur (either because two nodes in the contention domain of each other have sampled timers that expire at the same time slot, or because the SINR at the receiver is smaller than T in spite of the fact that there is no transmitter in its contention domain. Again acknowledgements are used to face this situation.

25.1.4 Code Division Multiple Access (CDMA)

All nodes transmit simultaneously, so that SINR may be feared to be small. To alleviate this, each node uses a direct-sequence spread-spectrum mechanism with a signature of length n (see § 24.3.3). If the receiver of transmission k knows the signature U_k of transmitter k, then it can use the matched filter described in § 24.3.3 to detect the symbols sent by this transmitter by considering the other transmissions as noise. Taking as above a definition of collision based on the error probability, we see from (24.18) that it is enough for the SINR at the receiver to be more than T/n to have no collision. On the more practical side, note that the receiver has to know the signature of the sender.

25.2 Power Control

Consider K simultaneous transmissions under the setting of § 24.3.4. Assume that transmission k requires a probability of error p_k or equivalently a SINR of T_k with $p_k = Q(\sqrt{2nT_k})$ – see (24.18). Two natural questions arise:

(1) Is this vector of error probabilities feasible, namely do there exist transmission powers a_k, $k = 1, \ldots, K$, such that the probability of error is less than p_k for all $k = 1, \ldots, K$?
(2) If it is feasible, what are the minimal elements of the set of powers such that the probability of error is less than p_k for all $k = 1, \ldots, K$?

In view of (24.17) one can rephrase this question as follows: does the linear system

$$P_k \geq \frac{T_k \sigma_k^2}{n|H(k,k)|^2} + \sum_{j \neq k} P_j \frac{T_k |H(j,k)|^2}{n|H(k,k)|^2}, \quad k = 1, \ldots, K \tag{25.1}$$

admit a positive solution $P_k = a_k^2$, and if so what are the minimal elements of the set of solutions?

One can rewrite this system as

$$\mathbf{P} \geq \mathbf{A}\mathbf{P} + \mathbf{B},$$

where $\mathbf{A}$ is the square matrix of dimension K with entries $\mathbf{A}(k,j) = \frac{T_k |H(j,k)|^2}{n|H(k,k)|^2}$ for $j \neq k$ and 0 otherwise, and where $\mathbf{B}$ is the vector of dimension K with entries $\mathbf{B}(k) = \frac{T_k \sigma_k^2}{n|H(k,k)|^2}$.

Claim 25.2.1. Under the assumption that all the variables $|H(j,k)|$ are positive, there exists a finite positive solution to (25.1) if and only if the spectral radius ρ of $\mathbf{A}$ is strictly less than 1, in which case, all solutions are bounded from below by

$$\mathbf{P}_0 = \sum_{l=0}^{\infty} \mathbf{A}^l \mathbf{B}. \tag{25.2}$$

Proof. If $\rho < 1$, then the last series converges and

$$\mathbf{P}_0 \quad = \quad \sum_{l=0}^{\infty} \mathbf{A}^l \mathbf{B} = \mathbf{B} + \sum_{l=1}^{\infty} \mathbf{A}^l \mathbf{B} = \mathbf{B} + \mathbf{A} \sum_{l=0}^{\infty} \mathbf{A}^l \mathbf{B} = \mathbf{B} + \mathbf{A}\mathbf{P}_0,$$

so that $\mathbf{P}_0$ is a solution. If $\mathbf{P}$ is a solution, then $\mathbf{P} \geq \mathbf{B}$, so that $\mathbf{P} \geq \mathbf{B} + \mathbf{A}\mathbf{B}$, which in turn implies by induction that

$$\mathbf{P} \geq \mathbf{B} + \sum_{l=1}^{L} \mathbf{A}^l \mathbf{B},$$

for all L. □

In other words, once the path gains and the fading variables are given, certain error probabilities are jointly attainable (those leading to a matrix gain $\mathbf{A}$ with a spectral radius less than 1) and others are not. In the former case, there is a best choice for the amplitude (or the power) of the transmitted signals, and it is given by (25.2).

25.3 Examples of Network Architectures

25.3.1 Mobile Ad Hoc Networks

Mobile ad hoc networks (MANETs) are wireless networks made of only one type of nodes; each node can either transmit or receive on a common frequency band, and there is no fixed infrastructure at all. Such networks use multihop routing: the nodes located between the source and the destination are possibly used as relays: a relay can receive symbols, buffer them and transmit them to further nodes. Each node can hence at the same time be a terminal (namely either the source or the destination of some traffic) and a router (namely a relay for traffic between other source–destination pairs). An important consequence is that the success of each hop by hop transmission and hence the connectivity between some source and destination nodes depend on the presence and the location of intermediate relay nodes.

25.3.1.1 Medium Access Control

Aloha, along with TDMA, was one of the first MAC protocols used in such radio networks. Today CSMA is one of the most popular schemes within the context of the IEEE 802.11 norm (better known as WiFi).

25.3.1.2 Point-to-point Routing

A major question within the setting of MANETs is that of routing. Point to point routing protocols are distributed algorithms that compute a route between all pairs of source and destination nodes. Usually the computation of this route is based on the exchange of control packets containing topology information and sent by the routing protocol. Distance vector and link state routing protocols are the most common within this framework (see e.g. (Keshav 1997)). We will not discuss here the problem of building and maintaining routing state/tables but rather focus on the construction of routes in two types of routing protocols used in such networks.

Minimal Weight Routing. Consider a MANET with nodes located in the Euclidean plane. In minimal weight multihop routing, one first defines (i) a graph on the set of nodes where edges are potential wireless links, (ii) a weight for each edge of this graph. For each source–destination (S–D) pair, one selects the path(s) with minimal weight between S and D (if there are such paths). This path can be found by dynamic programming (see Djikstra's algorithm below). Here are a few examples:

- *transmission range graph, minimal number of hops*: there are edges between all pairs of nodes and the weight of the edge between nodes x and y is 1 if $|x-y| \leq R_{max}$ and ∞ otherwise; the parameter R_{max} is the *transmission range*. This model assumes that it is possible to maintain a wireless link to each node at distance less than or equal to R_{max}. Notice that with this definition, there may be no path with finite weight from certain sources.
- *transmission range graph, minimal Euclidean distance*: much the same as above except that the weight between nodes x and y is $|x-y|$ if $|x-y| \leq R_{max}$ and ∞ otherwise.
- *Delaunay graph, minimal number of hops*: there is an edge between all pairs of nodes and the weight of the edge between nodes x and y is 1 if they are neighbors in the Voronoi sense (see Chapter 4 in Volume I) and ∞ otherwise. Within this setting, there is a finite weight path for any S–D pair.
- *Delaunay graph, minimal Euclidean distance*: the same as above excepts that the weight of the edge between nodes x and y equals $|x-y|$ if they are Voronoi neighbors and ∞ otherwise.

This minimal weight path is then used for routing all packets of this S–D pair.

Dijkstra's Algorithm. The setting features a connected graph with a positive weight associated with each edge. Denote by $\mathcal{N}(x)$ the neighbors of node x in the graph. If for all $y \in \mathcal{N}(x)$, one knows a/the minimal weight path $p^*(y,D)$ from y to D and its total weight $|p^*(y,D)|$, then the next hop from x to D in the minimal weight path is any element z in the set

$$\arg\min_{y \in \mathcal{N}(x)} \left(w(x,y) + |p^*(y,D)|\right)$$

and the optimal path from y to D is the concatenation of (y,z) and $p^*(z,D)$.

Dijkstra's algorithm (Dijkstra 1959), which is recalled below, constructs optimal paths to D using this dynamic programming principle in an inductive way, starting from the neighbors $x \in \mathcal{N}(D)$ of D (for which $p^*(x, D) = (x, D)$ and $|p^*(x, D)| = w(x, D)$).

At each step $n \geq 0$ of the procedure, the nodes are subdivided into three sets:

$A = A(n)$ is the set of nodes for which a path of minimum weight to D is already known;
$B = B(n)$ is the set of nodes that are connected in one hop to at least one node of A but do not yet belong to A;
$C = C(n)$ is the set of nodes that do not belong to $A \cup B$.

The paths are also subdivided into three sets:

$\mathcal{P}_1 = \mathcal{P}_1(n)$ is the set of shortest paths $p^*(x, D)$ connecting the nodes $x \in A$ to D (one path per node);
$\mathcal{P}_2 = \mathcal{P}_2(n)$ a set of paths connecting the nodes of B to D (one path per node);
$\mathcal{P}_3 = \mathcal{P}_3(n)$ is the set of all paths to D not yet considered.

`INITIALISATION:` At step 1, $A(1) = \{D\}$, $B(1) = \mathcal{N}(D)$ and $C(1)$ the set of all other nodes, whereas $\mathcal{P}_2$ is the set of one hop paths (y, D), $y \in \mathcal{N}(D)$. Let $x_1 = \arg\min_{y \in \mathcal{N}(D)} w(x, D)$ (if there are multiple edges with the same weight, we choose one of them arbitrarily); node x_1 is moved to A and the edge (x_1, D) is added to $\mathcal{P}_1(1)$.

`LOOP:` Suppose we are given $A(n-1), B(n-1), C(n), \mathcal{P}_i(n)$ $(i = 1, 2, 3)$ and denote by x_n the node added to A in step n. At step $n+1$, one performs the following operations:

(1) For all $y \in \mathcal{N}(x_n) \setminus A(n)$:
- If y belongs to set $C(n)$, it is moved to B and the path p, made of the edge (y, x_{n-1}) concatenated to the path from x_n to D that belongs to $\mathcal{P}_1$, is added to $\mathcal{P}_2$.
- If y belongs to set $B(n)$, we check whether the use of the edge (y, x_n) gives a path from y to D with a weight smaller than that in $\mathcal{P}_2(n)$. If it is so then the former path replaces the path initially in $\mathcal{P}_2$. Otherwise nothing is done.

Note that this update is such that B now contains the 1-hop neighborhood of $A(n)$ and $\mathcal{P}_2$ now contains exactly one path to D for each node in B.

(2) Let x_{n+1} be the node in B with a path to D in $\mathcal{P}_2$ with minimal weight. Denote this path by p_{n+1}, with any tie-breaking rule. Move it from B to A and move the path p_{n+1} from $\mathcal{P}_2$ to $\mathcal{P}_1$. The sets of remaining nodes and paths are denoted by $C(n+1)$ and $\mathcal{P}_3(n+1)$ respectively.

The above procedure terminates when all the nodes in the connected component of D are placed in A.

The following result is proved by induction on n:

Proposition 25.3.1. For all $n \geq 1$,

- for all $x \in A(n)$, the path from x in $\mathcal{P}_1(n)$ is the/a minimal weight path from x to D.
- for all $x \in B(n)$, after operation (2), the path from x in $\mathcal{P}_2$ is the/a minimal weight path from x to D among the set of paths that only contain nodes of $A \cup B$;

- the minimal weight paths to D are discovered in order of their weights, starting from the smallest.

The last statement of Proposition 25.3.1 shows that:

Corollary 25.3.2. For graphs defined on point patterns in the Euclidean space, for weights equal to Euclidean distance, the Dijkstra algorithm places any x in A in a finite number of steps provided x belongs to the connected component of D and the point pattern is locally finite. The same holds true for the number of hops provided the graph of the connected component of D to which x belongs has locally finite degree.

Remark: Note that the search of the minimal weight path from x to D which was described above has to be initiated by the destination D and terminates when x is discovered. In fact by symmetry, this path is the reverse of the minimal weight path from D to x, so that x can find it by initiating Dijkstra's algorithm and waiting until D is discovered.

Typically, once this algorithm has been applied, one can construct routing tables to any destination D which tell each node which neighbor is the next hop to D. Once such routing tables are built, the routing algorithm is hence quite local. However, the construction of the routing table (and more generally the construction of solutions to the dynamic programming equations) is a non-local procedure.

Geographic Routing. In geographic routing, node positions are used to determine the route to the destination. Geographic routing is often thought of as a way to reduce the routing state of each node. A typical situation is that where one selects the next relay of a node n for a given packet as the node which is the nearest to the destination within a set which contains n. This set could be e.g. the set of nodes which receive the transmitted packets without error, or the set of nodes which are within some transmission range R_{max} of node n. The general principle of choosing the closest node to the destination as next relay among such a set is referred to as *radial routing* in this monograph.

25.3.1.3 Multicast Routing

In the *one-to-many setting*, multicasting consists in broadcasting some *common symbols* from a source node to a collection of destination nodes. Multicast routing then aims at building a tree rooted in the source node and spanning all destination nodes. Such a tree can be used to alleviate significantly the network load compared to the point-to-point setting: in the latter case, one establishes a point-to-point route from the source to each destination and one sends the symbols on each such route, whereas in the multicast setting, one sends the symbols once on each wireless link of the multicast tree: each node of the tree sends the symbols it receives from its parent node to each of its offspring nodes.

The simplest way of building a multicast spanning tree consists in taking the union of the point-to-point paths between the source and each destination.

Remark 25.3.3. Of course, such a spanning tree is also a central object for situations where a collection of nodes have to send information to a single sink node. This situation shows up in a variety of contexts:

- In sensor networks, terminal nodes have both sensing and relaying capacities. These nodes typically behave like a MANET for transferring information, but all send the information they sense

to some special node called a *cluster head* with enhanced communication capacity (say to a satellite).

- On the uplink of WiFi mesh networks where only a subset of the nodes have a wired Internet connection and where the other WiFi nodes have to send their uplink data to these wired nodes.

25.3.2 Third Generation Cellular Networks

Cellular architectures involve a collection of nodes that belong to two types: concentrator nodes and terminal nodes. Concentrator nodes are assumed to be interconnected by a wired network which will not be discussed here. Wireless links connect certain terminals to certain concentrators (uplink) and certain concentrators to certain terminals (downlink). There are no direct wireless links between terminals. In the simplest scenario, each terminal is served by one concentrator for both the uplink and the downlink - for instance the closest. More general situations can be considered where the uplink concentrator of a terminal differs from its downlink concentrator, or where several concentrators serve the same terminal.

In cellular networks of third generation (3G), concentrators are called base stations . The uplink and the downlink have separated channels and CDMA is used on both the uplink and the downlink.

25.3.3 Wavelans

Wavelan networks can be seen as some kind of cellular architectures which are made of a collection of IEEE 802.11 (better known as WIFI) access points which play the role of concentrators and to which users associate. These access points are assumed to have wired connections to the Internet. In such networks, the uplink and the downlink are not separated and all nodes (access point and users) access the channel according to a CSMA mechanism.

Bibliographical Notes on Part VI

Chapters 23 and 24 follow (Tse and Viswanath 2005). Chapter 25 borrows ideas from several sources among which (Keshav 1997). The vision of power control which is described there is due to (Hanly 1999). Prim's algorithm was discovered in (Jarník 1930) and later independently in (Prim 1957). The main idea was rediscovered in (Dijkstra 1959).

Bibliography

Aldous, D. and J. M. Steele (1992). Asymptotics for euclidean minimal spanning trees on random points. *Probab. Thery Relat. Fields 92*, 247–258. 163

Asmussen, S., P. Fiorini, L. Lipsky, T. Rolski, and R. Sheahan (2008). Asymptotic behavior of total times for jobs that must start over if a failure occurs. *Mathematics of Operations Research 33*(4), 932–944. 54

Audrey M. Viterbi and A. J. Viterbi (1993, 8). Erlang capacity of a power controlled CDMA system. *IEEE Journal on Selected Areas in Communications 11*(6), 892–899. 100

Baccelli, F. and B. Blaszczyszyn (2010). A new phase transitions for local delays in MANETs. In *Proc. of IEEE INFOCOM*, San Diego. to appear, see also `http://hal.inria.fr/inria-00435237`. 99

Baccelli, F., B. Błaszczyszyn, and M. Karray (2004, December). Up and downlink admission/congestion control and maximal load in large homogeneous CDMA networks. *MONET 9*(6), 605–617. 83, 91, 100

Baccelli, F., B. Błaszczyszyn, and M. Karray (2005, March). Blocking rates in large CDMA networks via a spatial Erlang formula. In *Proc. of IEEE INFOCOM*, Miami, FL, USA. 94, 95, 96, 100

Baccelli, F., B. Błaszczyszyn, and M. Karray (2007). A spatial markov qeueing process and its applications to wireless loss systems. INRIA, Tech. Rep. 00159330. 94

Baccelli, F., B. Błaszczyszyn, and O. Mirsadeghi (2009). Optimal paths on the space-time SINR random graphs. *submitted for publication*. 138, 144, 163

Baccelli, F., B. Blaszczyszyn, and P. Mühlethaler (2003, November). An Aloha protocol for multihop mobile wireless networks. In *Proceedings of the Allerton Conference*, Urbana Champaign, Illinois. and *IEEE Transactions on Information Theory*, 52(2):421–436, 2006. 99, 163

Baccelli, F., B. Blaszczyszyn, and P. Mühlethaler (2009a). A stochastic model for spatial and opportunistic aloha. *JSAC*. Special Issue on Stochastic Geometry and Random Graphs for Wireless Networks, to appear. 21, 99

Baccelli, F., B. Blaszczyszyn, and P. Mühlethaler (2009b, June). Time-space opportunistic routing in wireless ad hoc networks: Algorithms and performance optimization by stochastic geometry. *The*

Computer Journal. 163

Baccelli, F., B. Błaszczyszyn, and F. Tournois (2003). Downlink capacity and admission/congestion control in CDMA networks. In *Proc. of IEEE INFOCOM*, San Francisco. 100

Baccelli, F. and C. Bordenave (2007). The radial spanning tree of a poisson point process. *Annals of Applied Probab. 17*(1), 305–359. 127, 128, 129, 163

Billingsley, P. (1995). *Probability and Measure* (3rd ed.). Wiley. 174

Biswas, S. and R. Morris (2005). Exor: opportunistic multi-hop routing for wireless networks. In *Proceedings of SIGCOMM '05*, Philadelphia, Pennsylvania, USA, pp. 133–144. 163

Błaszczyszyn, B. and M. Karray (2008a). An efficient analytical method for dimensioning of cdma cellular networks serving streaming calls. In *Proc. of ACM/ICST VALUETOOLS*, Athens, Greece. 100

Błaszczyszyn, B. and M. Karray (2009). Dimensioning of the downlink in OFDMA cellular networks via an erlang's loss model. In *Proc. of European Wireless Conference*, Aalborg. 100

Błaszczyszyn, B. and M. K. Karray (2007, May). Performance evaluation of scalable congestion control schemes for elastic traffic in cellular networks with power control. In *Proc. of IEEE INFOCOM*. 98, 100

Błaszczyszyn, B. and M. K. Karray (2008b). An efficient analytical method for dimensioning of CDMA cellular networks serving streaming calls. In *Proc. of ValueTools*. 100

Błaszczyszyn, B. and P. Mühlethaler (2010). Stochastic analysis of non-slotted Aloha in wireless ad-hoc networks. In *Proc. of IEEE INFOCOM*, San Diego. to appear, see also `http://hal.inria.fr/inria-00435236`. 27, 99

Błaszczyszyn, B., P. Mühlethaler, and Y. Toor (2009). Maximizing throughput of Linear Vehicular Ad-hoc NETworks (VANETs) — a stochastic approach. In *Proc. of European Wireless Conference*, Aalborg. 99

Błaszczyszyn, B. and B. Radunović (2007). M/D/1/1 loss system with interference and applications to transmit-only sensor networks. In *Proceedings of IEEE Spaswin 2007*. 27

Błaszczyszyn, B. and B. Radunović (2008). Using transmit-only sensors to reduce deployment cost of wireless sensor networks. In *Proc. of IEEE INFOCOM*, Phoenix, AZ. 27

Blum, B., T. He, S. Son, and J. Stankovic (2003). Igf: A state-free robust communication protocol for wireless sensor networks. Technical Report CS-2003-1, University of Virginia CS Department. 163

Bordenave, C. (2006). Navigation on a Poisson point process. Technical Report RR-5790, INRIA. 163

Brémaud, P. (2002). *Mathematical Principles of Signal Processing*. New York: Springer. 9, 180

Dijkstra, E. W. (1959). A note on two problems in connexion with graphs. *Numerische Mathematik 1*, 269–271. 193, 197

Durvy, M., O. Dousse, and P. Thiran (2009, March). Self-organization properties of csma/ca systems and their consequences on fairness. *IEEE Transactions on Information Theory 55*(3). 78

Ehsan, N. and R. L. Cruz (2006). On the optimal sinr in random access networks with spatial reuse. In *Proceedings of the CISS 2006 Conference*, Princeton University, NJ, USA. 99

Evans, J. and D. Everitt (1999, January). On the teletraffic capacity of CDMA cellular networks. *IEEE Transactions on Vehicular Technology 48*. 100

Feller, W. (1971). *An Introduction to Probability Theory and its Applications, volume II*. Wiley. 9

Ganti, R. K. and M. Haenggi (2009). Bounds on information propagation delay in interference-limited ALOHA networks. In *Proc. of Workshop on Spatial Stochastic Models for Wireless Networks*. 163

Ganti, R. K. and H. M. (2009). Spatial and temporal correlation of the interference in aloha ad hoc networks. *IEEE Communications Letters*. To appear. 100

Gilbert, E. N. (1961). Random plane networks. *SIAM J. 9*, 533–543. iv

Gilbert, E. N. (1962). Random subdivisions of space into crystals. *The Annals of Mathematical Statistics 33-3*, 958–972. iv

Haenggi, M. (2005, July). On routing in random rayleigh fading networks. *IEEE Transactions on Wireless Communications 4*, 1553–1562. 99

Haenggi, M. (2009). Outage, local throughput, and capacity of random wireless networks. *IEEE Transactions on Wireless Communications*. To appear. 99

Haenggi, M., J. Andrews, F. Baccelli, O. Dousse, and M. Franceschetti (Eds.) (2009). *Stochastic Geometry and Random Graphs for Wireless Networks*. Special Issue of IEEE JSAC. v

Hanly, S. (1999). Congestion measures in DS-CDMA networks. *IEEE Trans. on Comm. 47*(3). 197

Howard, C. D. and C. M. Newman (1997). Euclidean models of first-passage percolation. *Probab. Theory Relat. Fields 108*, 153–170. 163

Hunter, A., J. Andrews, and S. Weber (2008). Capacity scaling of ad hoc networks with spatial diversity. *submitted for publication*. 99

Jacquet, P. (2008). Realistic wireless network model with explicit capacity evaluation. *submitted for publication*. Rapport de recherche INRIA RR-6407. 99

Jacquet, P., B. Mans, P. Mühlethaler, and G. Rodolakis (2009). Opportunistic routing in wireless ad hoc networks: Upper bounds for the packet propagation speed. *IEEE JSAC, special issue on Stochastic Geometry and Random Graphs for Wireless Networks 27*, 1192–1202. 163

Jarník, V. (1930). About a certain minimal problem. *Práce Moravské Přírodovědecké Společnosti 6*, 57–63. in Czech. 197

Jelenković, P. and J. Tan (2007a). Can retransmissions of superexponential documents cause subexponential delays? In *Proc. of INFOCOM*, Anchorage, AL, USA. IEEE. 100, 164

Jelenković, P. and J. Tan (2007b). Is aloha causing power law delays? In L. Mason, T. Drwiega, and J. Yan (Eds.), *Managing Traffic Performance in Converged Networks*. Berlin: Springer. 100, 164

Jindal, N., J. Andrews, and S. Weber (2008, Dec.). Fractional power control for decentralized wireless networks. *IEEE Trans. Wireless Communications 7*(12), 5482–5492. 100

Jindal, N., S. Weber, and J. Andrews (2008, Dec.). Bandwidth partitioning in decentralized wireless networks. *IEEE Trans. Wireless Communications 7*(12), 5408–5419. 100

Karp, B. (2000). Geographic routing for wireless networks. Phd thesis, Harvard University. 163

Karp, B. and H. T. Kung (2000, August). Gpsr: Greedy perimeter stateless routing for wireless networks. In *6th Annual International Conference on Mobile Computing and Networking, MobiCom 2000, August 6.-11., 2000, Boston, Massachusetts, USA*, pp. 243–254. ACM / IEEE. 116

Karray, M. K. (2007). *Analytic evaluation of wireless cellular networks performance by a spatial Markov process accounting for their geometry, dynamics and control schemes*. Ph. D. thesis, ENST. 97, 100

Kauffmann, B., F. Baccelli, F. Chaintreau, V. Mhatre, K. Papagiannaki, and C. Diot (2007). Measurement-based self organization of interfering 802.11 wireless access networks. In *Proceedings of IEEE INFOCOM'07*, pp. 1451–1459. 97

Keil, J. M. and C. Gutwin (1992). Classes of graphs which approximate the complete Euclidean graph. *Discrete Comput. Geom. 7*, 13–28. 111

Kelly, F. P. (1991). Loss networks; special invited paper. *Ann. Appl. Probab. 1*, 319–378. 93

Keshav, S. (1997). *An Engineering Approach to Computer Networking*. Addison-Wesley. 192, 197

Kingman, J. (1973). Subadditive ergodic theory. *Annals of Probab. 1*, 883–899. 108

Kitchens, B. (1998). *Symbolic Dynamics*. Springer Berlin. 81

Kleinrock, L. (1975). *Queueing Systems*. John Wiley & Sons. iv, 93

Liu, Z. and M. El Zarki (1994, May). Sir-based call admission control for DS-CDMA cellular systems. *Selected Areas in Communications, IEEE Journal on 12*, 638 –644. 100

Meyn, S. and R. Tweedie (1993). *Markov Chains and Stochastic Stability*. Springer-Verlag. 128

Møller, J. (1994). *Lectures on Random Voronoi Tessellations*, Volume 87 of *Lecture Notes in Statistics*. New York: Springer-Verlag. 118

Nguyen, H., F. Baccelli, and D. Kofman (2007). A stochastic geometry analysis of dense IEEE 802.11 networks. In *Proceedings of IEEE INFOCOM 2007*, pp. 1199–1207. 100

Pimentel, L. (2006). The time constant and critical probabilities in percolation models. *Elect. Comm. in Probab. 11*, 160–168. 110

Prim, R. C. (1957). Shortest connection networks and some generalizations. *Bell System Technical Journal 36*, 1389–1401. 197

Russo, L. (1987). A note on percolation. *Z. Wahr. verw. Geb. 43*, 39–48. 108

Serfozo, R. (1999). *Introduction to stochastic networks*. New York: Springer. 95

Sidi, M. and D. Starobinski (1997). New call blocking versus handoff blocking in cellular networks. *Wireless Networks 3*. 100

Stojmenovic, I. and X. Lin (2001a). Loop-free hybrid single-path/flooding routing algorithms with guaranteed delivery for wireless networks. *IEEE Transaction on Parallel and Distributed Systems 12*, 1023–1032. 163

Stojmenovic, I. and X. Lin (2001b). Power-aware localized routing in wireless networks. *IEEE Transaction on Parallel and Distributed Systems 12*(11), 1122–1133. 163

Stuber, G. L. (2001). *Principles of Mobile Communication*. Boston: Kluwer AP. 177

Takagi, H. and L. Kleinrock (1984). Optimal transmission ranges for randomly distributed packet radio networks. *IEEE Transactions on Communication 32*(3), 246–257. 163

Tse, D. and P. Viswanath (2005). *Foundamentals of Wireless Communication*. Cambridge University Press. 187, 197

Vahidi-Asl, M. Q. and J. C. Wierman (1990). First-passage percolation on the Voronoi tessellation and Delaunay trangulation. In M. Karoński, J. Jaworski, and A. Ruciński (Eds.), *Random Graphs'87; Based on Proceedings of the 3rd International Seminar on Random Graphs and Probabilistic Methods in Combinatorics, June 27 – July 3*, pp. 341–359. Chichester: John Wiley & sons. 108

Venkataraman, J. and M. Haenggi (2004, Oct.). Optimizing the throughput in random wireless ad hoc networks. In *Proceedings of the 42st Annual Allerton Conference on Communication, Control, and Computing*, Monticello, IL, USA. 99

Weber, S., J. Andrews, and N. Jindal (2007, Nov.). The effect of fading, channel inversion, and threshold scheduling on ad hoc networks. *IEEE Trans. Information Theory 53*(11), 4127–4149. 99

Weber, S., N. Jindal, R. K. Ganti, and M. Haenggi (2008, Dec.). Longest-edge routing on the spatial aloha graph. In *Proc. IEEE Global Communications Conference (GLOBECOM'08)*, New Orleans, LA, USA. 163

Table of Mathematical Notation and Abbreviations

$\|X\|$	Euclidean norm of vector X.
$\|B\|$	Lebesgue measure of set $B \in \mathcal{B}$.
$\setminus$	set difference.
$< X, Y >$	scalar product of vectors X and Y.
A	parameter of the OPL attenuation models.
a.s.	almost surely.
$\mathcal{A}(X)$ (resp. $\mathcal{A}_n(X)$)	radial point map at X (resp. time-space point map at X and at time n).
$\mathcal{A}_{\mathrm{d}}(X)$ (resp. $\mathcal{A}_{\mathrm{d},n}(X)$)	d-directional point map at X (resp. time-space point map at X and at time n).
$\mathcal{B}$	the Borel σ-algebra of the Euclidean space.
$B_X(r)$	ball of center X and radius r.
β	attenuation exponent of the OPL attenuation models.
$\mathcal{C}_X(\Phi)$	Voronoi cell of point X w.r.t. the p.p. Φ.
$C_{(X,M)}(\Phi)$	SINR cell of point X w.r.t. the marks (fading, threshold, power, etc.) M and the p.p. Φ.
D	the destination node (in routing context; Part V in Volume II).
e (resp. $e(n)$)	indicator of MAC channel access (resp. at time n).
$\mathbf{E}$	expectation.
$\mathbf{E}^0$	expectation w.r.t. the Palm probability.
ϵ_x	Dirac measure at x.
F (resp. $F(n)$)	fading variable (resp. at time n).
$\mathcal{G}_{\mathrm{SINR}}$	the SINR graph.
$\mathbb{G}_{\mathrm{SINR}}$	the time-space SINR graph.
GI	General fading.
$\frac{\mathrm{GI}}{\mathrm{W+GI/GI}}$	Kendall-like notation for a wireless cell or network.

iff	if and only if.
i.i.d.	independently and identically distributed.
I_Φ	shot noise field associated with the point process Φ.
$K(\beta)$	constant associated with Rayleigh fading SN. See (2.26 in Volume I) and (16.9 in Volume II)
$L(X)$	length to the next hop from point X in a routing algorithm.
$\mathbf{L}(X)$	local delay at node X.
$l(.)$	attenuation function of the OPL models.
$\mathcal{L}_\Phi$	Laplace functional of the p.p. Φ.
$\mathcal{L}_V$	Laplace transform of the random variable V.
λ	the intensity parameter of a homogeneous Poisson p.p.
$\Lambda(.)$	the intensity measure of a Poisson p.p.
L.H.S.	left hand side.
$\mathbf{M}$	exponential random variable (or Rayleigh fading).
$\mathbb{M}$	space of point measures.
μ	the mean fading is μ^{-1}.
$\mathbb{N}$	the non-negative integers.
$\mathcal{N}(\mu, \sigma^2)$	the Gaussian law of mean μ and variance σ^2 on $\mathbb{R}$.
$\mathcal{N}^{\mathcal{C}}(0, \sigma^2)$	the complex vauled Gaussian law.
O	the origin of the Euclidean plane (in routing context; Part V in Volume II).
p	medium access probability in Aloha.
$P(X)$	progress from point X towards destination in a routing algorithm.
$\mathbf{P}$	probability.
$\mathbf{P}^0$	Palm probability.
p_c	probability of coverage.
Φ	point process.
$\mathbb{R}^d$	Euclidean space of dimension d.
S	the source node (in routing context; Part V in Volume II).
R.H.S.	right hand side.
T	threshold for SINR.
Var	Variance.
$V(X)$ (resp. $V(X, n)$)	set of neighbors of X in $\mathcal{G}_{\text{SINR}}$ (resp. of (X, n) in $\mathbb{G}_{\text{SINR}}$).
W (resp. $W(n)$)	thermal noise (resp. at time n).
$\mathbb{Z}$	the relative integers.

Index